UCTEA Turkish Chamber of Civil Engineers
TMMOB İnşaat Mühendisleri Odası

Turkish Journal of Civil Engineering

formerly
Teknik Dergi

Volume 34
Issue 2
March 2023

Turkish Journal of Civil Engineering (formerly Teknik Dergi) Publication Principles

Turkish Journal of Civil Engineering (TJCE), a non-profit, open access scientific and technical periodical of UCTEA Chamber of Civil Engineers, publishes papers reporting original research work and major projects of interest in the area of civil engineering. TJCE annually publishes six issues and is open to papers in English and Turkish. It should be noted that TJCE (formerly, Teknik Dergi/ Technical Journal of Turkish Chamber of Civil Engineers) is being published regularly for more than 30 years since 1990. Main publication principles of TJCE are summarized below:

1. Articles reporting original scientific research and those reflecting interesting engineering applications are accepted for publication. To be classified as original, the work should either produce new scientific knowledge or add a genuinely new dimension to the existing knowledge or develop a totally new method or substantially improve an existing method.
2. Articles reporting preliminary results of scientific studies and those which do not qualify as full articles but provide useful information for the reader can be considered for publication as technical notes.
3. Discussions received from the readers of the published articles within three months from publication are reviewed by the Editorial Board and then published together with the closing remarks of the author.
4. Manuscripts submitted for publication are evaluated by two or three reviewers unknown to the authors. In the light of their reports, final decision to accept or decline is taken by the Editorial Board. General policy of the Board is to get the insufficient manuscripts improved in line with the reviewers' proposals. Articles that fail to reach the desired level are declined. Reasons behind decisions are not declared.
5. A signed statement is taken from the authors, declaring that the article has not been published as a "journal article or book chapter". In case the Editorial Board is in the opinion that the article has already been published elsewhere with minor changes or suspects plagiarism or a similar violation of ethics, then not only that article, but none of the articles of the same authors are published.
6. Papers reporting works presented as conference papers and developed further may be considered for publication. The conference it was presented to is given as a footnote in the first page.
7. Additionally, a document signed by all authors, transferring the copyright to UCTEA Chamber of Civil Engineers is submitted together with the manuscript.

UCTEA Turkish Chamber of Civil Engineers
TMMOB İnşaat Mühendisleri Odası

Turkish Journal of Civil Engineering

(formerly Teknik Dergi)

Volume 34 Issue 2 March 2023

UCTEA Turkish Chamber of Civil Engineers
TMMOB İnşaat Mühendisleri Odası
Necatibey St. No: 57, Kızılay 06440 Ankara, Turkey
Tel: +90.312.294 30 00 - Faks: +90.312.294 30 88
E-mail: imo@imo.org.tr - www.imo.org.tr

Publisher *(Sahibi)*:
Taner YÜZGEÇ
On behalf of UCTEA Turkish Chamber of Civil Engineers

Administrative Officer *(Yazı İşleri Müdürü)*:
Özer AKKUŞ

Volume 34 - Issue 2 - March 2023 *(Cilt 34 - Sayı 2 - Mart 2023)*
Published bi-monthly. Local periodical. *(İki ayda bir yayınlanır, yerel süreli yayın)*
Date of Print: March1, 2023 *(Baskı Tarihi: 1 Mart 2023)*
Number of copies: 800 *(800 adet basılmıştır)*

ISSN: 2822-6836

Turkish Journal of Civil Engineering (formerly Teknik Dergi) is indexed by
- Science Citation Index Expanded
- Scopus
- Journal Citation Reports / Science Edition
- Engineering Index
- Concrete Abstracts (American Concrete Institute)
- National Technical Information Service (US NTIS)
- CITIS
- Ulrich's International Periodical's Directory
- Google Scholar
- TR Index

Turkish Journal of Civil Engineering (formerly Teknik Dergi) is a peer reviewed open access periodical publishing papers of original research and interesting practice cases. It addresses both the research community and the practicing engineers.

Printed by *(Baskı)*:
Ziraat Gurup Matbaacılık Ambalaj San. Tic. A.Ş.
Bahçekapı Mah. 2534 Sok. No: 18 Şaşmaz, Etimesgut / Ankara
Tel: 0.312.384 73 44 - Faks: 0.312.384 73 46

Reviewers:

This list is renewed each year and includes reviewers who served in the last two years of publication.

Şükran AÇIKEL
Merve AÇIKGENÇ ULAŞ
Perviz AHMEDZADE
Bülent AKBAŞ
Şeref Doğuşcan AKBAŞ
Rıfat AKBIYIKLI
Özge AKBOĞA KALE
Sarven AKCELYAN
Burcu AKÇAY ALDANMAZ
Cihan Taylan AKDAĞ
Cem AKGÜNER
Çağlar AKKAYA
Fevziye AKÖZ
Erkan AKPINAR
Muhammet Vefa AKPINAR
Atakan AKSOY
Hafzullah AKSOY
Tülay AKSU ÖZKUL
Uğurhan AKYÜZ
Sadık ALASHAN
Cenk ALHAN
Ayşe Burcu ALTAN SAKARYA
Sinan ALTIN
Adlen ALTUNBAŞ
Ahmet Can ALTUNIŞIK
Yalçın ALVER
Bahadır ALYAVUZ
Özgür ANIL
Necati ARAS
Davit ARDİTİ
Yalın ARICI
Deniz ARTAN İLTER
Ali Osman ATAHAN
Hakan Nuri ATAHAN
Ali Osman ATEŞ
Bekir Özer AY
Gökçe AYDIN
Metin AYDOĞDU
Hakan AYGÖREN
Mustafa Tamer AYVAZ
Ülker Güner BACANLI
İhsan Engin BAL
Selim BARADAN
Eray BARAN
Özgür Uğraş BARAN
Türkay BARAN
Bekir Oğuz BARTIN
Mustafa Gökçe BAYDOĞAN
Cüneyt BAYKAL
Niyazi Özgür BEZGİN
Senem BİLİR MAHÇİÇEK
Gökçen BOMBAR
Burak BOYACI
İlknur BOZBEY
Ali BOZER
Zafer BOZKUŞ
Erdem CANBAY
Zekai CELEP
Cihan CENGİZ
Halim CEYLAN
Hüseyin CEYLAN
Ömer CİVALEK
Joao Ramoa CORREIA
Ayşe COŞKUN BEYAN
Ali Fırat ÇABALAR
Barlas Özden ÇAĞLAYAN
Melih ÇALAMAK
Gülben ÇALIŞ
Umut ÇALIŞKAN
Süheyla Pelin ÇALIŞKANELLİ
Mehmet Alper ÇANKAYA
Dilay ÇELEBİ
Tevfik Kutay ÇELEBİOĞLU
Ahmet Ozan ÇELİK
Oğuz Cem ÇELİK
Semet ÇELİK
Hilmi Berk ÇELİKOĞLU
Kemal Önder ÇETİN
Mahmut ÇETİN
Mecit ÇETİN
Erdal ÇOKÇA
Semra ÇOMU
İsmail DABANLI
Ömer DABANLI
Atilla DAMCI
Yakup DARAMA
Osama M.F. DAWOUD
Tayfun DEDE
Abdullah DEMİR
Cem DEMİR
Emre DEMİR
Uğur DEMİR (İTÜ)
Uğur DEMİR (İYTE)
Munise Didem DEMİRBAŞ
Ender DEMİREL
Mehmet Cüneyd DEMİREL
Seyyit Ümit DİKMEN
Ali Ersin DİNÇER
İsmail DURANYILDIZ
Selim DÜNDAR
Nurhan ECEMİŞ ZEREN
Volkan Ş. EDİGER
Özgür EKİNCİOĞLU
Murat Altuğ ERBERİK
Ali ERCAN
Sinan Turhan ERDOĞAN
Şakir ERDOĞDU
Ramazan Cüneyt ERENOĞLU
Esin ERGEN PEHLEVAN
Gökmen ERGÜN
Bülent ERKMEN
Barış ERKUŞ
Yusuf Çağtay ERŞAN
Kağan ERYÜRÜK
Tuğba ESKİŞAR TEFÇİ
Burak FELEKOĞLU
Mahmut FIRAT
Okan FISTIKOĞLU
Onur GEDİK
Abdullah GEDİKLİ
Ahmet Talha GEZGİN
Sadık Can GİRGİN
Zehra Canan GİRGİN
Ilgın GÖKAŞAR
Serdar GÖKTEPE
Rahmi GÜÇLÜ
Ali GÜL
Fazlı Erol GÜLER
Ilgın GÜLER
Hamza GÜLLÜ
Gürkan GÜNAY
Taylan GÜNAY
Murat GÜNAYDIN
Samet GÜNER
Oğuz GÜNEŞ
Mehmet Şükrü GÜNEY
Tuba GÜRBÜZ BÜYÜKKAYIKÇI
Aslı Pelin GÜRGÜN
Soner HALDENBİLEN
Murat HAMDERİ
Ingo A. HANSEN
Umut HASGÜL
Bo-Tao HUANG
Zeynep IŞIK
Sabriye Banu İKİZLER
Erol İSKENDER
Medine İSPİR ARSLAN
Recep İYİSAN
Nihat KABAY
Mehmet Sedat KABDAŞLI
Mehmet Rifat KAHYAOĞLU
Özkan KALE
Volkan KALPAKÇI
Elif Çağda KANDEMİR
Tanay KARADEMİR
Hüseyin Faruk KARADOĞAN
Ümit KARADOĞAN
Mustafa Erkan KARAGÜLER
Halil KARAHAN
Zülküf KAYA
Oğuz KAYABAŞI
Hasan Ahmed KAZMEE
Mustafa Kubilay KELEŞOĞLU
Elçin KENTEL
Hadi KHANBABAZADEH
Havvanur KILIÇ
Ufuk KIRBAŞ
Veysel Şadan Özgür KIRCA
Cem KIRLANGIÇOĞLU
Güven KIYMAZ
Gökhan KİRKİL
Esat Selim KOCAMAN
Kasım KOÇAK
Salih KOÇAK
Niyazi Uğur KOÇKAL
Baha Vural KÖK
Mete KÖKEN
Hasan KURTARAN
Murat KURUOĞLU
Akif KUTLU
Abdullah KÜRKÇÜ
Hilmi LUŞ
Kasım MERMERTAŞ
Mahmoud MIARI
Yetiş Şazi MURAT
Öcal NECMİOĞLU
Fuad OKAY
Umut OKKAN
Derviş Volkan OKUR
Mehmet Hakkı OMURTAG
Sezan ORAK
Engin ORAKDÖĞEN
Akın ÖNALP
Bihrat ÖNÖZ
Ali Hakan ÖREN
Ceyhun ÖZÇELİK
Yiğit ÖZÇELİK
Gökhan ÖZDEMİR
Murat ÖZEN
Pelin ÖZENER
Hasan ÖZER
Hakkı Oral ÖZHAN
Mehmet Fatih ÖZKAL
Zeynep Huri ÖZKUL BİRGÖREN
Ahmet ÖZTOPAL
Sadık ÖZTOPRAK
Turan ÖZTURAN
Mustafa ÖZUYSAL
Tolga Yılmaz ÖZÜDOĞRU
Atilla ÖZÜTOK
Nilüfer ÖZYURT ZİHNİOĞLU
Ahmet Onur PEHLİVAN
Seval PINARBAŞI ÇUHADAROĞLU
Elişan Filiz PİROĞLU
Selman SAĞLAM
Mehmet SALTAN
Metin SARIGÖL
Altuğ SAYGILI
Serdar SELAMET
Osman SİVRİKAYA
Behzad SOLTANBEIGI
Serdar SOYÖZ
Rifat SÖNMEZ
Tayfun Altuğ SÖYLEV
Erol ŞADOĞLU
Olcay ŞAHİN
Yuşa ŞAHİN
Zekai ŞEN
Burak ŞENGÖZ
Karin ŞEŞETYAN
Ali Ünal ŞORMAN
Gülüm TANIRCAN
Serhan TANYEL
Kerem TAŞTAN
Gökmen TAYFUR
Rasim TEMÜR
Serdal TERZİ
Berrak TEYMUR
Hüseyin Onur TEZCAN
Mesut TIĞDEMİR
Salih TİLEYLİOĞLU
Vedat TOĞAN
Onur Behzat TOKDEMİR
İrem Dikmen Toker TOKER
Ali TOPAL
Cem TOPKAYA
Kamile TOSUN FELEKOĞLU
Erkan TÖRE
Ülgen Mert TUĞSAL
Gürsoy TURAN
Ö. Tuğrul TURAN
Cüneyt TÜZÜN
Eren UÇKAN
Latif Onur UĞUR
Ergin ULUTAŞ
Dilay UNCU
Tayfun UYGUNOĞLU
Volkan Emre UZ
İbrahim Mert UZUN
Deniz ÜLGEN
Mehmet Barış Can ÜLKER
Yurdanur ÜNAL
Cüneyt VATANSEVER
Syed Tanvir WASTI
Ahmet YAKUT
Erkut YALÇIN
Mehmet Cem YALÇIN
Aslı YALÇIN DAYIOĞLU
Mustafa Sinan YARDIM
Mert Yücel YARDIMCI
Anıl YAZICI
Gökhan YAZICI
Halit YAZICI
Mehmet YETMEZ
Tahsin Alper YIKICI
İrem Zeynep YILDIRIM
Mehmet YILDIRIMOĞLU
Abdülazim YILDIZ
Mustafa Tolga YILMAZ
Berivan YILMAZER POLAT
İsmail YÜCEL
Yeliz YÜKSELEN AKSOY
Shaban Isamel Albrka Ali ZANGENA
Abdullah Can ZÜLFİKAR

Turkish Journal of Civil Engineering (formerly Teknik Dergi)

Volume 34 Issue 2 March 2023

CONTENTS

RESEARCH ARTICLE

Mesnetlerinden Farklı Yer Hareketi Etkisindeki Kablo Destekli Köprülerin Yapı-Zemin Etkileşim Analizi 1
Hüseyin KARTAL, Kurtuluş SOYLUK

Effects of Pore Fluid and Surface Roughness on Geomembrane - Soil Interface Behavior 35
Inci DEVELIOGLU, Hasan Firat PULAT

Identification of Dispute Sources in the Construction Industry via Court Files 57
Murat ÇEVİKBAŞ

Rheological Performance of ZycoTherm/Nano-Silica Composite Modified Binders at High and Low Temperatures 77
Dania ALOTHMAN, Hüseyin GÖKÇEKUŞ, Shaban Ismael Albrka ALI

Replacement of Stirrups by Steel Fibers in Shear Dominant UHPFRC Beams 103
Umut HASGÜL, Altuğ YAVAŞ, Tamer BİROL

Finite Element Analysis and Investigation of Critical Impact Point of Steel Guardrails Affecting Safety and Structural Performance 125
Sedat OZCANAN

Kohezyonsuz Zeminde Kazık Aralığının Belirlenmesi ve Temel Davranışının Deneysel İncelenmesi 145
Ercan Egemen BAŞAR, İlyas Devran ÇELİK, Münire FINDIK, Soner UZUNDURUKAN

Strengthening System Effects on the Out-Of-Plane Mechanisms Activation of Masonry Walls under Tsunami Loads 173
Stefano BELLIAZZI, Gian Piero LIGNOLA, Andrea PROTA

Turkish Journal of Civil Engineering, 2023 1-33, Yazı 723, ***Araştırma Makalesi***

Mesnetlerinden Farklı Yer Hareketi Etkisindeki Kablo Destekli Köprülerin Yapı-Zemin Etkileşim Analizi

Hüseyin KARTAL[1]
Kurtuluş SOYLUK[2]

ÖZ

Bu çalışmada eşit merkez açıklığa sahip asma ve eğik kablo askılı köprülerin dinamik davranışının karşılaştırılması amacıyla önce merkez açıklığı 1000 m olan bir eğik kablo askılı köprü ile bir asma köprü sistemi tasarlanmıştır. Tasarımı yapılan köprülerin dinamik davranışlarını incelemek için köprülere üniform ve mesnetlerinden farklı yer hareketi uygulanıp, yapı-zemin etkileşiminin dikkate alındığı ve ihmal edildiği durumlar için zaman-tanım alanında doğrusal olmayan analizler gerçekleştirilmiştir. Çalışma sonucunda, mesnetlerinden farklı yer hareketi uygulamasının ve yapı-zemin etkileşiminin her iki köprü modelinde de yapısal tepkileri genel olarak arttırdığı gözlenmiştir. Bunun yanında, üniform ve mesnetlerden farklı yer hareketi uygulanmasına bağlı olarak hangi köprü sisteminin daha fazla etkilendiğine ilişkin değerlendirmelerde bulunulmuştur.

Anahtar Kelimeler: Asma köprü, eğik kablo askılı köprü, mesnetlerinden farklı yer hareketi, yapı-zemin etkileşimi.

ABSTRACT

Soil-Structure Analyses of Cable-Supported Bridges under Multiple-Support Excitation

In this study, it is intended to compare the dynamic behavior of suspension and cable-stayed bridges for equal center span lengths. For this purpose, a suspension and a cable-stayed bridge with center spans of 1000 m are designed so that a realistic comparison can be made. Then, uniform and multiple-support ground motions are applied to the bridges to determine their dynamic responses. Nonlinear time history analyses are carried out for cases where the soil-structure interaction is taken into account and ignored. The results show that the multiple-support excitation as well as the soil-structure interaction generally increase the structural

Note:
- Yayın Kurulu'na 18 Kasım 2021 günü ulaşmıştır. 16 Aralık 2022 günü yayımlanmak üzere kabul edilmiştir.
- 31 Mayıs 2023 gününe kadar tartışmaya açıktır.

- https://doi.org/10.18400/tjce.1224420

1 Kartal Proje, Ankara, Türkiye
kartalhuseyin@hotmail.com - https://orcid.org/0000-0002-5132-1205

2 Gazi Üniversitesi, İnşaat Mühendisliği Bölümü, Ankara, Türkiye
ksoyluk@gazi.edu.tr - https://orcid.org/0000-0002-3039-0332

responses for both bridge models. On the other hand, depending on the uniform and multiple-support motions, the sensitivity of each bridge model is explored.

Keywords: Cable-stayed bridge, suspension bridge, multiple-support excitation, soil-structure interaction.

1. GİRİŞ

Son yıllara kadar eğik kablo askılı köprüler orta açıklıkları (400-700m) geçmek için tercih edilirken, asma köprüler uzun açıklıkları (>1000m) geçmek için tercih edilmekteydi. Fakat son zamanlarda köprü sektöründeki yapım teknolojilerindeki gelişmeler ve doğru analizler ile birlikte, eğik kablo askılı köprüler de daha uzun açıklıklar için tercih edilmeye başlanmıştır. Bu durumda uzun açıklıklı köprü sistemlerinde, köprü tipine karar vermek için asma ve eğik kablo askılı köprülerin dinamik davranışlarının detaylı incelenmesi büyük öneme sahiptir. Eğik kablo askılı köprüler ile asma köprülerin deprem esnasında dinamik davranışları farklılık gösterdiğinden eşit açıklıklara sahip bu köprülerin dinamik davranışlarının detaylı tanımlanması gereklidir. Uzun açıklıklı asma ve eğik kablo askılı köprülerin dinamik davranışının karşılaştırılması ile ilgili olarak günümüze kadar yapılmış olan çalışmalarda köprü merkez açıklıkları farklı uzunluklarda olduğundan, söz konusu köprü sistemlerinin dinamik davranışlarının daha gerçekçi bir karşılaştırmasının yapılabilmesi için bu çalışmada merkez açıklıkları 1000 m olan bir adet asma köprü ile bir adet eğik kablo askılı köprünün tasarımı yapılmış ve nümerik model olarak kullanılmıştır. Tasarımı tamamlanan eğik kablo askılı ve asma köprülerde kritik deprem yüklemelerini belirleyebilmek için, sert, orta ve yumuşak olmak üzere üç farklı zemin grubuna ait kayıtlar kullanılarak üniform ve mesnetlerinden farklı yer hareketleri tanımlanmış ve köprü sistemlerine uygulanmıştır. Köprü modellerine uygulanan yer hareketleri, rasgele titreşim teorisi esas alınarak üretilirken, üretilen her bir yer hareketi EC8'de tanımlanan B, C ve D zemin sınıflarına karşılık gelen sert, orta ve yumuşak zemin cinsleri ile uyumlu olacak şekilde elde edilmiştir. Köprülerin dinamik tepkisine yapı-zemin etkileşiminin etkisini belirlemek için yapı-zemin etkileşiminin dikkate alındığı ve ihmal edildiği durumlar her iki köprü için de ayrı ayrı ele alınıp karşılaştırmaları yapılmıştır. Yapı-zemin etkileşiminin dikkate alındığı köprü modellerinde, ana kulelerin ve kenar ayakların mesnetlendiği noktalardaki zeminler doğrusal elastik yaylar ile temsil edilmiştir. Mesnet noktalarında, her bir ötelenme ve dönme için eşdeğer Winkler yatak katsayısı (k) hesaplanmıştır. Yapı-zemin etkileşiminin ihmal edildiği köprü modellerinde ise ankastre mesnet uygulaması yapılmıştır. Geçmişte asma ve eğik kablo askılı köprülerde yapı zemin etkileşiminin köprülerin dinamik davranışına etkisini ayrı ayrı inceleyen çalışmalar olmasına rağmen eşit merkez açıklığa sahip asma ve eğik kablo askılı köprüler için yapı zemin etkileşiminin de dikkate alınarak dinamik tepkilerinin karşılaştırıldığı bir çalışmaya rastlanmamıştır. Saadeghvaziri vd. [1] çalışmalarında mevcut köprülerde yapı-zemin etkileşiminin dinamik davranışa olan etkisini incelemişlerdir. Temel altı zemin dönme ve ötelenme rijitliği olan yaylar ile temsil edilmiştir. Çalışmanın sonucunda, eğik kablo askılı köprülerin analizlerinde yapı–zemin etkileşiminin dikkate alınmasının büyük öneme sahip olduğu belirtilmiştir. Soneji ve Jangid [2] ana kaya üzerine rijit kazık temel gruplarıyla mesnetlenmiş eğik kablo askılı köprü sisteminin dinamik davranışına yapı-zemin etkileşiminin etkisini incelemişlerdir. Kazık temel etrafındaki zeminin köprü davranışını önemli ölçüde değiştirdiği görülmüştür. Liang vd. [3] çalışmalarında uzun açıklıklı bir eğik kablo askılı köprünün mesnetlendiği kazıklı temellerin

dinamik davranışını zemin-kazık-köprü etkileşimini dikkate alarak incelemişlerdir ve mesnetli kule sistemlerinde kazık başlarındaki maksimum eğilme momentlerinin azaldığı belirtilmiştir. Zheng ve Takeda [4] çalışmalarında bir eğik kablo askılı köprü için yapı-zemin etkileşiminin sistemin dinamik davranışı üzerindeki etkisini incelemişlerdir. Çalışmanın sonucunda, kütle yay modelinin zemini temsil etmek için uygun bir model olduğu belirtilmiştir. Siddharth vd. [5] çalışmalarında yapı-zemin etkileşimini dikkate alarak sert, orta sert ve yumuşak zemin sınıfları için eğik kablo askılı köprülerin dinamik davranışında temel derinliğinin etkisini incelemişlerdir. Çalışma sonucunda zemin sınıfının eğik kablo askılı köprülerin dinamik davranışında büyük etkisinin olduğu, özellikle yumuşak zeminlerin yapının hakim periyotlarını %30 arttırdığı belirtilmiştir. Lyngs vd. [6] İzmit Körfez Geçişi Asma Köprüsü'nün sismik analizleri için yapı-zemin etkileşiminin modellenmesi üzerine çalışmışlardır. Çalışmanın sonucunda, temel altı zeminin ve zemin ile temel arasında bulunan ara dolgu elemanlarının lineer olmayan elemanlar ile modellenerek yapılan analizlerin daha gerçekçi sonuçlar verdiği belirtilmiştir. Miao ve Tang [7] Dalian Gulf Asma Köprüsü'nün 3 boyutlu dinamik davranışına kazık-zemin etkileşiminin etkisini incelemişlerdir. Yapılan analizler sonucunda yapı zemin etkileşiminin yapısal deplasmanları ve kesit tesirlerini arttırdığı belirtilmiştir. Keshishian [8] çalışmasında köprü türü uzun açıklıklı yapıların rasgele titreşim analizi ile çözümünde yer hareketindeki değişim ve yapı-zemin etkileşiminin etkisini incelemiştir. Çalışmasının sonucunda yer hareketindeki değişimin köprü davranışı üzerinde daha etkili olduğu ve yapı-zemin etkileşiminin sonuçları küçültebileceği gibi, arttırabileceği de gözlenmiştir. Khan ve arkadaşları [9] çalışmalarında zeminin yaylar ve sönümleyiciler ile modellendiği eşdeğer modal enerji yöntemini kullanarak yapı-zemin etkileşiminin yelpaze tipi eğik kablo askılı köprülerin dinamik davranışı üzerindeki etkisini incelemişlerdir. Mesnetlerdeki yer hareketleri arasındaki korelasyon etkileri dikkate alınarak yapı-zemin etkisinin göz önünde bulundurulduğu ve ihmal edildiği durumlar için yapılan dinamik analizler neticesinde, yapı-zemin etkileşiminin dikkat alındığı durumlarda korelasyon etkisinin daha fazla olduğu belirtilmiştir. Soyluk ve Sıcacık [10] eğik kablo askılı köprülerde, değişen yer hareketi bileşenleri için yapı-zemin etkileşimi analizi gerçekleştirmişlerdir. Çalışmalarının sonucunda eğik kablo askılı köprülerin dinamik analizi için farklı yer hareketi ve zemin-yapı etkileşiminin dikkate alınması gerektiği vurgulanmıştır. Kuyumcu ve Ateş [11] çalışmalarında değişerek yayılan yer hareketleri etkisindeki köprülerde zemin–temel–köprü etkileşiminin etkisini incelemişlerdir. Zeminin rijitlikleri yaylar ve sönümleyiciler ile tarfilenmiş ve yapının dinamik davranışı sert, orta sert ve yumuşak olmak üzere üç ayrı zemin sınıfı için incelenmiştir. Çalışmanın neticesinde, yapı-zemin etkileşiminin, özellikle yumuşak zeminler için, köprünün dinamik davranışı üzerinde büyük önemi olduğu vurgulanmıştır. Ateş ve arkadaşları [12] mesnetlerinden farklı yer hareketinin ve yapı-zemin etkileşiminin kazıklı temelleri olan eğik kablo askılı köprülerin dinamik davranışı üzerindeki etkilerini incelemişlerdir. Yapı-zemin etkileşimi Winkler modeli tabanlı dinamik empedans fonksiyonları ile dikkate alınmıştır. Çalışmanın sonucunda yapı-zemin etkileşiminin ve mesnetlerinden farklı yer hareketlerinin eğik kablo askılı köprülerin dinamik davranışı üzerinde önemli etkileri olduğu ve birlikte düşünülmesi gerektiği belirtilmiştir. Shiravand ve Parvanehro [13] çalışmalarında yapı-zemin etkileşimini dikkate alarak eğik kablo askılı köprülerin lineer olmayan dinamik davranışına sismik yer hareketinin etkilerini incelemişlerdir. Çalışmanın sonucunda farklı zemin türlerinin yapısal tepkileri arttırdığı belirtilmiştir. Tochaei ve arkadaşları [14] çalışmalarında yakın fay yer hareketinin ve yapı-zemin etkileşimininin eğik kablo askılı köprülerin dinamik davranışına etkilerini incelemişlerdir. Yapı–zemin etkileşimi box-spring sistem ile temsil edilmiştir.

Çalışmanın sonucunda yakın fay etkisinde ve yumuşak zeminlerde yapısal tepkilerin arttığı belirtilmiştir. Kartal ve Soyluk [15] ve Soyluk ve arkadaşları [16] çalışmalarında sırasıyla homojen ve heterojen zemin durumları için farklı merkez açıklıklara sahip bir eğik kablo askılı köprü ile bir asma köprünün dinamik davranışını karşılaştırmışlardır. Yapı-zemin etkileşiminin dikkate alınmadığı çalışmaların sonucunda üniform yer hareketi etkisi için eğik kablo askılı köprünün daha duyarlı olduğu belirtilmiştir. Soyluk ve Karaca [17] çalışmalarında kablo destekli köprülerin dinamik davranışına yakın fay ve uzak fay yer hareketi etkilerini incelemişlerdir. Çalışmanın sonucunda yakın fay yer hareketinin eğik kablo askılı köprüye oranla asma köprünün dinamik davranışı üzerinde daha büyük bir etkisinin olduğu belirtilmiştir. Kartal ve Soyluk [18] çalışmalarında asma köprülerin dinamik davranışına yapı-zemin etkileşiminin etkisini incelemişlerdir. Çalışmaların sonucunda asma köprülerde yapı-zemin etkileşiminin dikkate alındığı durum için elde edilen yapısal tepkilerin daha büyük olduğu ve yapı-zemin etkileşimi etkisinin zemin sınıfına göre değişkenlik gösterdiği belirtilmiştir. Dumanoğlu ve Adanur [19] asma köprülerin antisinkronize dinamik analizi üzerine çalışmışlardır. Çalışmanın sonucunda, asma köprülerin dinamik analizleri yapılırken eş-fazlı yer hareketi yanında zıt fazlı yer hareketinin ve deprem dalgalarının bir mesnetten diğerlerine ulaşma zamanlarının, buna bağlı olarak farklı hızların dikkate alınması gerektiği belirtilmiştir. Kartal ve Soyluk [20] çalışmalarında eğik kablo askılı köprülerin dinamik davranışına yapı-zemin etkileşiminin etkisini incelemişlerdir. Çalışmaların sonucunda eğik kablo askılı köprülerin tasarımı yapılırken köprülerin inşaa edileceği bölgedeki zemin sınıfının köprünün deprem yükleri altındaki davranışı üzerinde büyük etkisinin olduğunu ve yapı-zemin etkileşiminin dikkate alınması gerektiği belirtilmiştir.

2. EĞİK KABLO ASKILI KÖPRÜ GENEL ÖZELLİKLERİ VE SONLU ELEMAN MODELİ

Tasarımı yapılan eğik kablo askılı köprünün toplam uzunluğu 1970 m'dir. Köprünün merkez açıklığı 1000 m olup kenar açıklık mesafeleri ise 485 m'dir. Orta açıklık ve kenar açıklık tabliyesi çelikten oluşmaktadır (Şekil 1). Ana kulelerin yüksekliği 340 m'dir ve ters Y şeklinde tasarlanmıştır. Kablo yerleşim şekli yelpaze sistem olarak düşünülmüştür. Ana kule temellerinin genişliği 40m, boyu 80m ve kalınlığı da 10 m'dir. Ana kulenin zemine mesnetlendiği nokta ile tabliye arasındaki düşey mesafe 60 m olup tabliye üstünden ana kule tepe noktasına olan düşey mesafe 280 m'dir. Ana kule ve tabliye en kesiti Şekil 2'de gösterilmiştir. Köprü ayakları temelleri yüzeysel temel olarak tasarlanmıştır ve kule ayakları temellere ankastre olarak bağlanmıştır. Kenar açıklıklarda ise 120 m ve 250 m'lik kısımlarda ilave ayaklar olup köprü tabliyesi bu noktalarda düşey yönde mesnetlenmiştir [21].

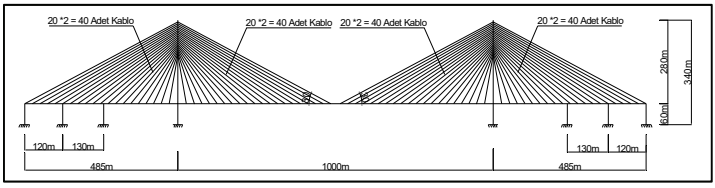

Şekil 1 - Eğik kablo askılı köprü genel görünümü

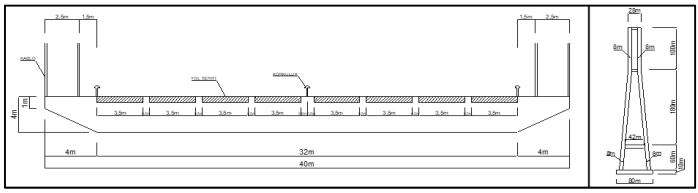

Şekil 2 - Eğik kablo askılı köprü ana kule ve tabliye en kesiti

Köprünün 3 boyutlu sonlu eleman modeli SAP 2000 Advanced 19.1.0 [22] sonlu eleman programı kullanılarak oluşturulmuştur. Ana kulelerin ve tabliyenin modellenmesinde çubuk elemanlar kullanılmıştır. Kabloların modellenmesinde SAP 2000 programının içinde mevcut bulunan özel kablo elemanları kullanılmıştır. Modelde toplam 384 düğüm noktası, 223 çubuk eleman, 160 adet kablo eleman ve 162 adet bağlantı elemanı kullanılmıştır. Şekil 3'de köprünün 3 boyutlu sonlu eleman modeli gösterilmiştir.

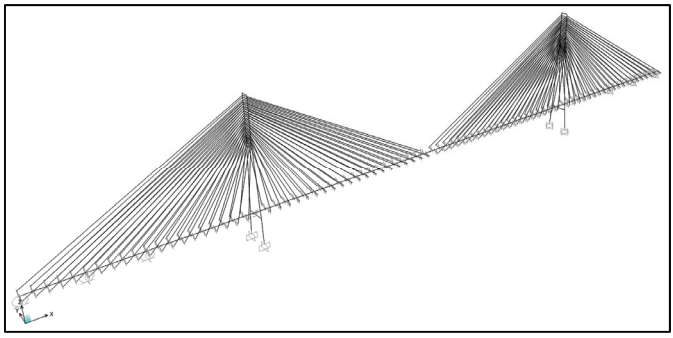

Şekil 3 - Eğik kablo askılı köprünün 3 boyutlu sonlu eleman modeli

Tablo 1 - Malzeme mekanik özellikleri

Yapısal Çelik Sınıfı (S 355)	Akma Gerilmesi (f_y) (N/mm²)	Kopma Gerilmesi (f_u) (N/mm²)	Elastisite Modülü (E) (N/mm²)	Kayma Modülü (G) (N/mm²)	Poisson (U)
	355	510	210000	80769	0,30
Kablo Çelik Sınıfı (EN 10138-3)	Akma Gerilmesi (f_y) (N/mm²)	Kopma Gerilmesi (f_u) (N/mm²)	Elastisite Modülü (E) (N/mm²)	Kayma Modülü (G) (N/mm²)	Poisson (U)
	1582	1860	195000	-	-
Beton Sınıfı (C 50)	Karakteristik Basınç Dayanımı (f_{ck}) (N/mm²)	Karakteristik Çekme Dayanımı (f_{ctk}) (N/mm²)	Elastisite Modülü (E) (N/mm²)	Kayma Modülü (G) (N/mm²)	Poisson (U)
	50	2,5	37000	15416	0,20

Orta açıklık ve kenar açıklık tabliyesi çelikten oluşmaktadır ve çelik kesitler köprü boyunca değişiklik göstermektedir. Tabliyede kullanılan çelik sınıfı S355 olarak seçilmiştir. Ana kule ve temellerde kullanılan betonarme donatı çeliği malzemesi ise S420 olarak seçilmiştir. Ana kule ve temeller için C50 beton sınıfı kullanılmıştır. Tabliye, ana kule ve kablolarda kullanılan malzemelerin mekanik özellikleri Tablo 1'de gösterilmiştir.

Ana kuleler 340 m yüksekliğinde ve ters Y şeklinde betonarme sistem olarak tasarlanmıştır. Ana kule ve ana kule ayaklarını birbirine bağlayan yatay kirişlerin en kesiti 8 m x 8 m'dir. Eğik kablo askılı köprü için sonlu eleman modelinde oluşturulan ana kule kesiti ve geometrik özellikleri de Şekil 4'de gösterilmiştir.

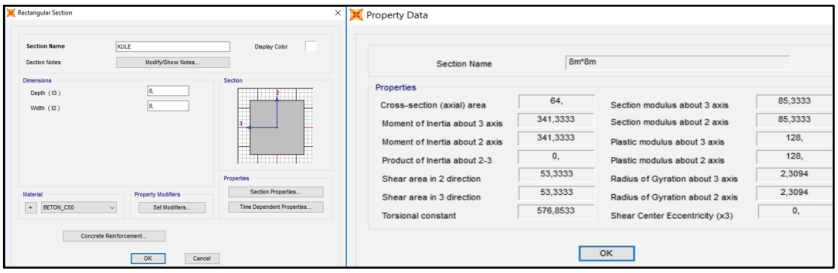

Şekil 4 - Eğik kablo askılı köprü ana kule kesiti ve geometrik özellikleri

Çelik malzemeden oluşan orta ve kanar açıklık tabliye kesitleri köprü boyunca değişkenlik göstermektedir. Eğik kablo askılı köprü için tabliye kesitleri bilgisayar modelinde Şekil 5'de gösterilen dağılıma göre tanımlanmıştır.

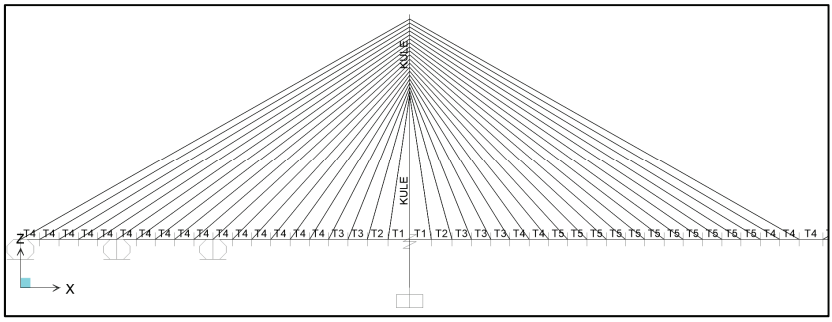

Şekil 5 - Eğik kablo askılı köprü için çelik tabliye kesitleri

Tabliye genişliği 40 m, tabliye yüksekliği de 4 m'dir. Kabloların tabliyeye bağlantı noktaları arası mesafe 24 m'dir. Ortotropik kutu kesitli tabliye aerodinamik bir enkesite sahiptir. Eğik kablo askılı köprü için bilgisayar modelinde oluşturulan çelik tabliye kesitlerin geometrik özellikleri Şekil 6'da gösterilmiştir.

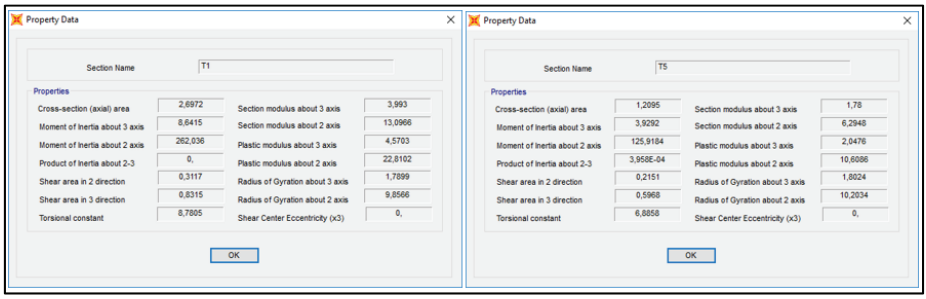

Şekil 6 - Eğik kablo askılı köprü tabliyesi T1 ve T5 kesiti geometrik özellikleri

Kablolarda oluşan sehim nedeniyle kablo elastisite modülü azalmaktadır. Yükün artmasıyla kablodaki sehimin azalması sonucu kablolarda ortaya çıkan lineer olmayan bu etkiyi dikkate almak için literatürde yaygın olarak kullanılan Ernst tarafından önerilen denklem ile hesaplanan eşdeğer elastisite modülü kullanılmıştır [23]. Kabloların yataydaki boyları ve çapları değişkenlik gösterdiğinden her bir kablo için eşdeğer elastisite modülü hesaplanmıştır. Kabloların genel yerleşimi Şekil 7'de, genel özellikleri de Tablo 2'de gösterilmiştir.

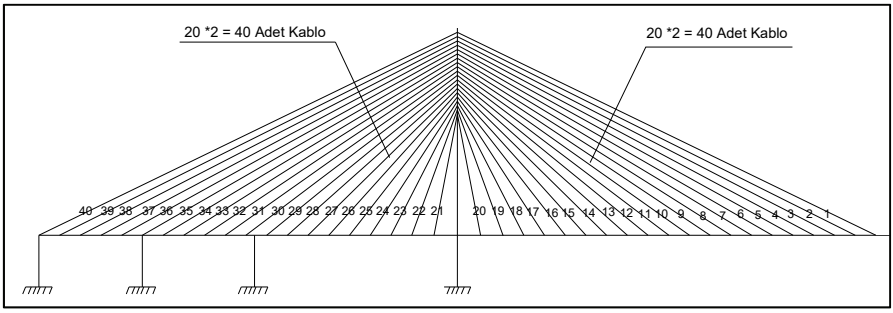

Şekil 7 - Eğik kablo askılı köprü kablo yerleşimi ve numaraları

Tabliyenin kütlesi tabliye kenar uçlarında kabloların bağlandığı noktalarda toplanmıştır [24]. Kütleler köprünün enine, boyuna ve düşey yönünde tanımlanmıştır. Tabliye çubuk elemanları ile ana kule çubuk elemanları birbirine bağlantı elemanları ile birleştirilmiştir. Bu bağlantı elemanları düşeyde ve enine yönde sabit olup, köprü boyuna yönünde 20000 kN/m'lik rijitliğe sahiptir. Ayrıca tabliye çubuk elemanları ile kablolar arasına rijit bağlantı elemanları tanımlanarak tabliye ile kablo bağlantısı gerçekçi bir şekilde sağlanmıştır. Şekil 8'de tabliyenin ana kuleye bağlantısı ve rijit bağlantı elemanları gösterilmiştir. Tabliyenin kenar ayaklar üzerindeki bağlantısı, köprünün boyuna yönünde kayar mesnet olarak diğer yönlerde ise sabit mesnet olarak düzenlenmiştir. Tabliyesinin ana kuleye mesnetlenme şartları Şekil 9'da gösterilmiştir [21].

Tablo 2 - Eğik kablo askılı köprü kablo özellikleri

ORTA AÇIKLIK KABLOLARI					KENAR AÇIKLIK KABLOLARI				
Kablo no	**Kablo Boyu (m)**	**Kablo yerleşimi**	**Kablo çapı (mm)**	**Kablo alanı (mm²)**	**Kablo no**	**Kablo Boyu (m)**	**Kablo yerleşimi**	**Kablo çapı (mm)**	**Kablo alanı (mm²)**
1	485	Ø7 * 400	174	15448	40	485	Ø7 * 400	174	15448
2	461	Ø7 * 400	174	15448	39	461	Ø7 * 400	174	15448
3	437	Ø7 * 400	174	15448	38	437	Ø7 * 400	174	15448
4	413	Ø7 * 400	174	15448	37	413	Ø7 * 400	174	15448
5	389	Ø7 * 400	174	15448	36	389	Ø7 * 400	174	15448
6	365	Ø7 * 400	174	15448	35	365	Ø7 * 400	174	15448
7	341	Ø7 * 400	174	15448	34	341	Ø7 * 400	174	15448
8	317	Ø7 * 330	160	13062	33	317	Ø7 * 330	160	13062
9	293	Ø7 * 330	160	13062	32	293	Ø7 * 330	160	13062
10	269	Ø7 * 330	160	13062	31	269	Ø7 * 330	160	13062
11	245	Ø7 * 330	160	13062	30	245	Ø7 * 330	160	13062
12	221	Ø7 * 330	160	13062	29	221	Ø7 * 330	160	13062
13	197	Ø7 * 220	136	9438	28	197	Ø7 * 330	160	13062
14	173	Ø7 * 220	136	9438	27	173	Ø7 * 330	160	13062
15	149	Ø7 * 220	136	9438	26	149	Ø7 * 330	160	13062
16	125	Ø7 * 220	136	9438	25	125	Ø7 * 220	136	9438
17	101	Ø7 * 220	136	9438	24	101	Ø7 * 220	136	9438
18	77	Ø7 * 180	119	7226	23	77	Ø7 * 180	119	7226
19	53	Ø7 * 180	119	7226	22	53	Ø7 * 180	119	7226
20	27	Ø7 * 180	119	7226	21	27	Ø7 * 180	119	7226

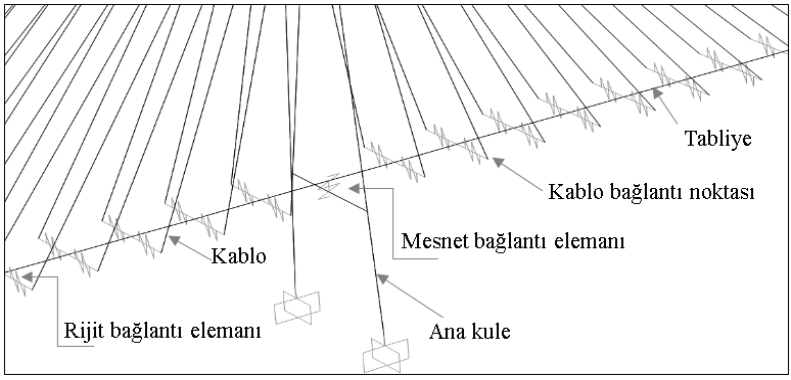

Şekil 8 - Köprü tabliyesinin ana kuleye bağlantısı ve rijit bağlantı elemanları

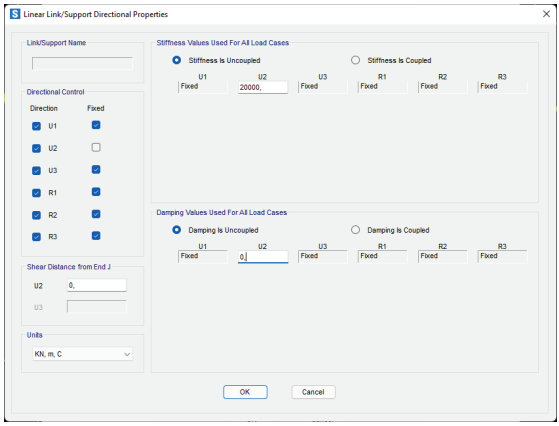

Şekil 9 - Eğik kablo askılı köprü tabliyesinin ana kuleye mesnetlenme şartları

3. ASMA KÖPRÜ GENEL ÖZELLİKLERİ VE SONLU ELEMAN MODELİ

Tasarımı yapılan asma köprünün toplam uzunluğu 1500 m'dir. Köprünün merkez açıklığı 1000 m olup kenar açıklık mesafeleri ise 250 m'dir (Şekil 10). 4 m yüksekliğindeki köprü tabliyesi 40 m toplam genişliğe sahip olup, çelikten oluşmaktadır ve çelik kesitler köprü boyunca değişkenlik göstermektedir. Asma köprü için tabliye kesitleri bilgisayar modelinde Şekil 11'de gösterilen dağılıma göre tanımlanmıştır. Ana kule 240 m yüksekliğinde ve H şeklinde betonarme olarak tasarlanmıştır (Şekil 12). Ana kule ve ana kule ayaklarını birbirine bağlayan yatay kirişlerin en kesiti 8 m x 8 m'dir. Asma köprü için sonlu eleman modelinde oluşturulan ana kule kesiti ve geometrik özellikleri ağık kablo askılı köprü ile aynı olup daha önce Şekil 4'de gösterilmiştir. Ana kablolar kuleden 250 m uzaklıkta beton bloklara ankre edilmiştir. Köprü ayak temelleri yüzeysel temel olarak tasarlanmıştır ve kuleler temellere ankastre olarak mesnetlenmiştir. Ana kule temellerinin genişliği 40 m, boyu 80 m ve kalınlığı da 10 m'dir [25].

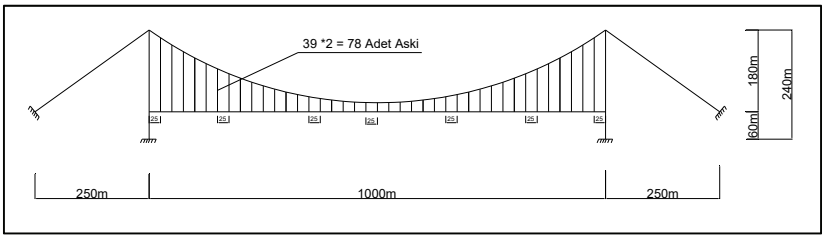

Şekil 10 - Asma köprü genel görünümü

Köprünün 3 boyutlu sonlu eleman modeli SAP 2000 Advanced 19.1.0 sonlu eleman programı kullanılarak oluşturulmuştur. Ana kulelerin ve tabliyenin modellenmesinde çubuk elemanlar kullanılmıştır. Asma köprü için oluşturulan çelik tabliye enkesiti ve enkesitlerin geometrik özellikleri eğik kablo askılı köprü ile aynı olup daha önce Şekil 6'da gösterilmiştir.

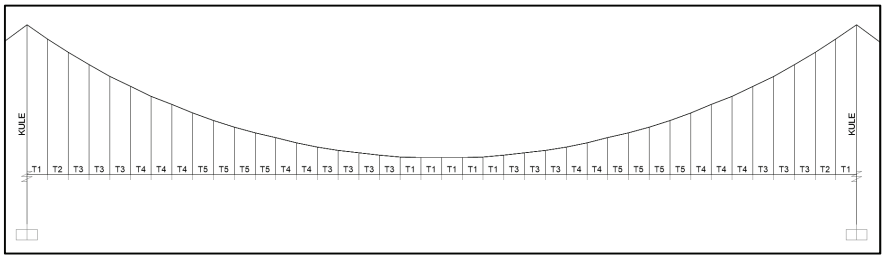

Şekil 11. Asma köprü çelik tabliye kesitleri

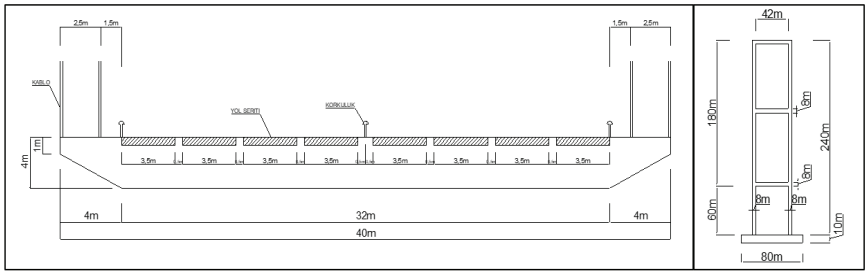

Şekil 12 - Asma köprü tabliye ve ana kule en kesiti

Askı halatlarının modellenmesinde SAP 2000 programının içinde mevcut bulunan özel kablo elemanları kullanılmıştır. Ana kablo ve askı halatları genel yerleşimi Şekil 13'de, genel özellikleri de Tablo 3'de gösterilmiştir.

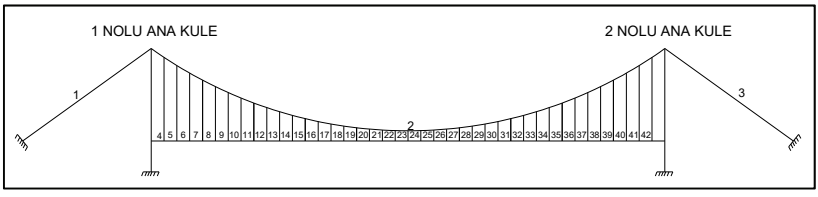

Şekil 13 - Asma köprü ana kablo ve askı halatları yerleşimi

Modelde toplam 271 düğüm noktası, 110 çubuk eleman, 162 adet kablo eleman ve 82 adet bağlantı elemanı kullanılmıştır. Şekil 14'de asma köprünün 3 boyutlu sonlu eleman modeli gösterilmiştir. Modelde tabliye çubuk elemanları ile askı halatları arasına rijit bağlantı elemanları tanımlanarak gerçek durumu yansıtacak şekilde tabliye ile askı halatı bağlantısı sağlanmıştır. Tabliyenin ana kuleye mesnetlendiği noktalarda, düşeyde ve enine yönde sabit olan ancak köprü ekseni boyunca 20000 kN/m'lik bir rijitliğe sahip olan bağlantı elemanları kullanılmıştır. Tabliyenin ana kuleye mesnetlenme şartları eğik kablo askılı köprü ile aynı olup daha önce Şekil 9'da gösterilmiştir. Tabliyenin kütlesi tabliye ile askı halatlarının bağlandığı noktalarda toplanmıştır [25].

Tablo 3 - Asma köprü ana kablo ve askı halat özellikleri

Kablo No	Kablo Boyu (m)	Kablo Çapı (mm)	Kablo Alanı (mm²)	Kablo No	Kablo Boyu (m)	Kablo Çapı (mm)	Kablo Alanı (mm²)
1	310	700	326952.5	21	21	160	13062.40
2	1067	700	326952.5	22	20.5	160	13062.40
3	310	700	326952.5	23	21	160	13062.40
4	163	160	13062.40	24	23	160	13062.40
5	147	160	13062.40	25	26	160	13062.40
6	132	160	13062.40	26	29	160	13062.40
7	118	160	13062.40	27	33	160	13062.40
8	106	160	13062.40	28	38	160	13062.40
9	94	160	13062.40	29	44	160	13062.40
10	84	160	13062.40	30	50	160	13062.40
20	23	160	13062.40	40	163	160	13062.40

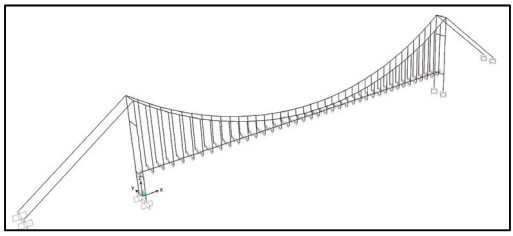

Şekil 14 - Asma köprü 3 boyutlu sonlu eleman modeli

4. KÖPRÜLERİN TASARIMINDA KULLANILAN YÜKLER

Köprü yapı elemanlarının zati yükü kesit tariflerine göre SAP 2000 programı tarafından hesaplanmıştır. Köprü tabliyesinde kullanılan ilave kaplama ve ekipman ağırlıkları ise Tablo 4'de gösterilmiştir.

Tablo 4 - Köprü tabliyesi ilave kaplama ve ekipman ağırlıkları

Yük Cinsi	Birim Ağırlık	Kalınlık	Yük Değeri
Asfalt	24.0 kN/m³	8 cm	1.92 kN/m²
İzolasyon	22.0 kN/m³	1 cm	0.22 kN/m²
Korkuluk	-	-	1.50 kN/m
Otokorkuluk	-	-	0.50 kN/m
Köprü üzeri aydınlatma	-	-	0.10 kN/m
Pilon Asansörü	-	-	0.15 kN/m

Trafik yüklemesi AASHTO- LRFD 2007 [26] Kısım 3.6.1.2.2'ye göre yapılmıştır. Yüklemede, köprünün tamamına üniform yayılı sabit trafik yükü uygulanırken, köprü boyunca 4 şeridin tamamının taşıt ile dolu olduğu durum incelenmiştir. Trafik yüklemesinde taşıt tipi olarak AASHTO'da tarifli tasarım kamyonu kullanılmıştır. Tasarım kamyonu ölçüleri ve yük değerleri Şekil 15'de gösterilmiştir.

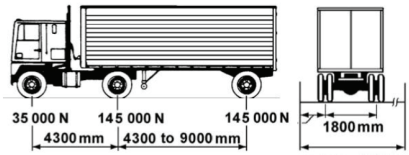

Şekil 15 - Tasarım kamyonu ölçüleri ve yük değerleri [24]

Yaya yüklemesi olarak AASHTO- LRFD 2007 Kısım 3.6.1.2.2'ye göre tabliye üzerinde 3,60 kN/m^2 yaya yükü alınmıştır. Yaya şeridi genişliği 2,50 m'dir. Toplam 18,00 kN/m değerindeki yaya yükü (2 x 3,60 kN/m^2 x 2,50 m) köprü tabliyesinin tamamına uygulanmıştır. Rüzgâr yüklemesi AASHTO- LRFD 2007 Kısım 3.8'e göre yapılmıştır. Tasarım rüzgâr hızı 160 km/sa olarak kabul edilmiştir ve elde edilen rüzgâr basıncı tabliye ve ana kulelere uygulanmıştır. Deprem yüklerinin hesabında AASHTO- LRFD 2007 Kısım 3.10 kullanılmıştır. Köprüye etki eden deprem yükü için davranış spektrum analizi yapılıp mod birleştirme yöntemi kullanılmıştır. Deprem bölgesi = 4, Ao = 0,40, Yapı önem katsayısı = 1.5 parametrelerine göre davranış spektrum grafiği oluşturulmuştur ve köprünün her iki yönünde deprem yükü uygulanmıştır.

5. DEPREM HAREKETİNİN TANIMLANMASI

Tasarımı yapılan eğik kablo askılı ve asma köprüde kritik deprem yüklemelerini belirleyebilmek için sert, orta ve yumuşak olmak üzere üç farklı zemin grubu için üretilen kayıtlar üniform ve farklı yer hareketleri şeklinde köprü sistemlerine uygulanmıştır. Yer hareketi kayıtları rasgele titreşim teorisi esas alınarak üretilirken, üretilen her bir yer hareketi EC8'de tanımlanan B, C ve D zemin sınıflarına karşılık gelen sert, orta ve yumuşak zemin cinsleri ile uyumlu olacak şekilde elde edilmiştir.

Yer hareketi üretmek üzere bu çalışmada Hao ve arkadaşları [27] tarafından önerilen simülasyon yöntemi esas alınıştır. Söz konusu yöntem, uygunluk fonksiyonu ile spektral yoğunluk fonksiyonlarına bağlı olarak farklı yer hareketlerinin üretilmesinde kullanılmaktadır. i ve j mesnet noktalarındaki ivmeler için uygunluk fonksiyonu,

$$\gamma_{ij}(iw) = \frac{S_{ij}(iw)}{\sqrt{S_{ii}(w) * S_{jj}(w)}} \tag{1}$$

Burada, $S_{ii}(w)$ ve $S_{jj}(w)$ sırasıyla, i ve j mesnetlerindeki yer hareket ivmelerine ait spektral yoğunluk fonksiyonlarını gösterirken, $S_{ij}(iw)$ i ve j mesnetlerindeki yer hareket ivmeleri

arasındaki karşıt-spektral yoğunluk fonksiyonunu göstermektedir. Uygunluk fonksiyonu ise aşağıdaki şekilde tanımlanmaktadır.

$$\gamma_{ij}(iw) = \left|\gamma_{ij}(w)\right|^{i} \gamma_{ij}(iw)^{w} \gamma_{ij}(iw)^{s} = \left|\gamma_{ij}(w)\right|^{i} \; exp\left[i\left(\theta_{ij}(w)^{w} + \theta_{ij}(w)^{s}\right)\right] \tag{2}$$

Burada $\gamma_{ij}(w)^{i}$ ve $\gamma_{ij}(iw)^{w}$, $\gamma_{ij}(iw)^{s}$ sırası ile korelasyon, dalga-yayılma ve zemin etkilerini ifade etmektedir. Zemindeki dalgaların yayılması esnasında yansıması ve kırılması sonucu oluşan korelasyon etkisi için, Harichandran ve Vanmarcke [28] tarafından önerilen ve yaygın olarak kullanılan model dikkate alınmıştır. Dalgaların mesnet noktalarına varış süreleri arasındaki farktan kaynaklanan dalga-yayılma etkisi,

$$\theta_{ij}(w)^{w} = \; -\frac{w d_{ij}^{L}}{v_{app}} \tag{3}$$

ifadesi ile tanımlanmaktadır. Burada v_{app} görünen dalga yayılma hızını ifade etmekte olup, d_{ij}^{L} dalga yayılma doğrultusunda mesnetler arasındaki yatay izdüşüm uzaklığını göstermektedir. Lokal zemin koşullarındaki farklılıklardan kaynaklanan zemin etkisi ise,

$$\theta_{ij}(w)^{s} = tan^{-1} \frac{Im\left[H_i(iw) H_j(-iw)\right]}{Re\left[H_i(iw) H_j(-iw)\right]} \tag{4}$$

ile tanımlanırken, burada $H_i(iw)$ zemin katmanlarındaki filtrasyonu temsil eden zemin frekans davranış fonksiyonudur.

Yer ivmesinin spektral yoğunluk fonksiyonu için, Clough ve Penzien [29] tarafından geliştirilen filtre edilmiş beyaz gürültü modeli kullanılmaktadır.

$$S_{ii}(w) = So \frac{w_g^4 + 4\zeta_g^2 w_g^2 w^2}{(w_g^2 - w^2)^2 + 4\zeta_g^2 w_g^2 w^2} \frac{w^4}{(w_f^2 - w^2)^2 + 4\zeta_f^2 w_f^2 w^2} \tag{5}$$

Burada S_0, spektral yoğunluk fonksiyonunun ordinat değerini gösterirken, w_g ve ζ_g, sırasıyla birinci filtreye ait doğal frekansı ve sönüm oranını, w_f ve ζ_f ise ikinci filtreye ait parametre değerlerini ifade etmektedir. Yer hareketi elde etmek için, ilk olarak belirtilen spektral yoğunluk fonksiyonları ile uyumlu stasyoner rasgele işlem örnekleri $\ddot{u}_1(t)$, $\ddot{u}_2(t)$, …, $\ddot{u}_n(t)$, oluşturulmaktadır (Hao ve arkadaşları [27]). Bu amaçla,

$$\ddot{u}_k(t) = \sum_{m=1}^{k} \sum_{l=1}^{N} A_{km}(w_l) \, cos[\, w_l t + \theta_{km}(w_l) + \phi_{ml}(w_l)] \tag{6}$$

kullanılmaktadır. Burada $w_l = l\Delta w$, $\Delta w = w_N/N$, w_N üst kesim frekansını, $\varphi_{ml}(w_l)$ 0-2π aralığında üniform dağılım gösteren rasgele faz açısını (φ_{ml} ve φ_{rs} m=r ve n=s olması dışında istatistiksel olarak bağımsız olmalıdır), k mesnet noktalarını ifade etmekte olup, $A_{km}(w_l)$ ve $\theta_{km}(w_l)$ ise oluşturulmuş kayıtların genlik ve faz açısını ifade etmektedir.

Deprem hareketinin stasyoner olmayan bir işlem olması nedeniyle farklı mesnet noktalarındaki stasyoner olmayan yer hareket ivmeleri, stasyoner olarak elde edilen yer

hareketlerinin stasyoner olmayan bir şekil fonksiyonu ile çarpılması sonucu elde edilmektedir.

$$a_k(t) = \xi(t)\ddot{u}_k(t) \tag{7}$$

Şekil fonksiyonu ξ(t) aşağıdaki gibi tanımlanmaktadır.

$$\xi(t) = \begin{cases} (t/t_0)^2 & 0 \le t \le t_0 \\ 1 & t_0 < t \le t_n \\ exp(-0.394(t-t_n) & t_n < t \end{cases} \tag{8}$$

Burada t_0 ve t_n dominant deprem titreşim bölgesindeki stasyoner bölümüm başlangıç ve bitiş sürelerini göstermektedir. Bu çalışmada t_0=4s ve t_n=10s değerleri kullanılmaktadır. Bu çalışmada oluşturulan tüm yer hareket ivme kayıtları, %5 sönüm oranı için ve 0.3g PSA'ya göre normalize edilmek suretiyle, Eurocode 8 [30] ile uyumlu olacak şekilde belirlenmiştir.

Üniform yer hareketi için köprü modelinin mesnetlerinde EC8'e göre sınıflandırılmış homojen sert (B), orta (C) ve yumuşak (D) zemin koşulları dikkate alınmıştır. B, C ve D sınıfı zemin için elde edilen ivme-zaman kayıtları kullanılarak köprülere enine, boyuna ve düşey doğrultuda olmak üzere üç yönlü üniform yer hareketleri uygulanmıştır. Düşey doğrultuda uygulanan yer hareketi, yatay bileşen 2/3 çarpılmak suretiyle elde edilmiştir. Köprü sistemlerine uygulanan üniform yer hareketleri Şekil 16'da gösterilmiştir.

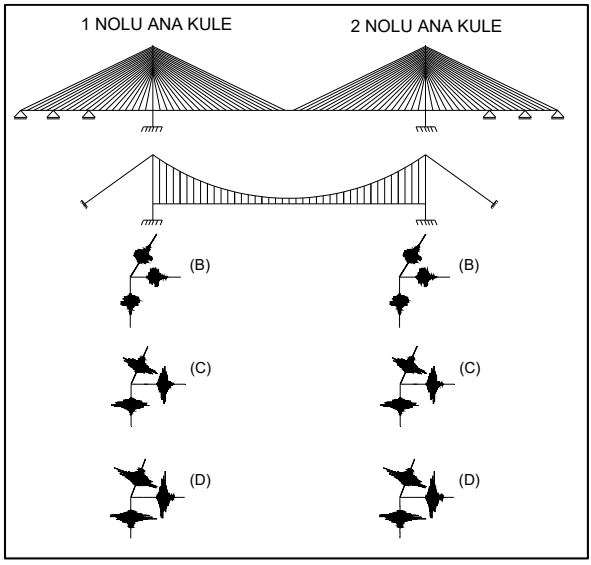

Şekil 16 - Köprü sistemlerine uygulanan üniform yer hareketleri

Üniform yer hareketi durumunda köprü sistemlerine uygulanmak üzere B, C ve D sınıfı zemin için elde edilen ivme–zaman kayıtları Şekil 17'de gösterilmiştir.

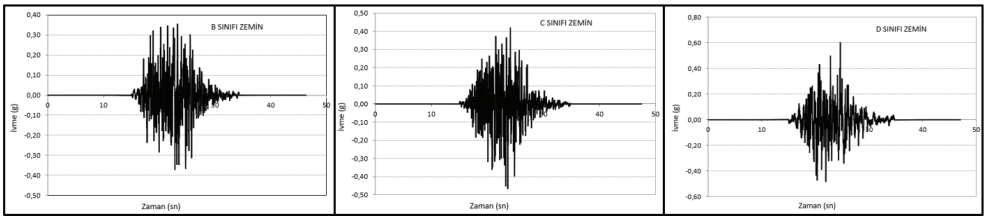

Şekil 17 - B,C ve D sınıfı zemin ivme-zaman kayıtları

SAP2000 programında yerdeğiştirme-zaman fonksiyonu kullanılarak farklı yer hareketi uygulanabildiğinden, üniform yer hareketi uygulamasından farklı olarak mesnetlerinden farklı yer hareketi uygulamasında yerdeğiştirme-zaman kayıtları kullanılmıştır. Yerdeğiştirme kayıtları ivme kayıtlarına bağlı olarak elde edilirken, DEEPSOIL v7.0 [31] yazılımı ile eksen düzeltmesi yapılmıştır. Farklı yer hareketi analizi için yer hareketi üretilirken önce zemin homojen alınmış olup, yer hareketi değişimi dalga-yayılma ve korelasyon etkisi ile dikkate alınmıştır. Bu durumda köprülerin 1 nolu ana kule mesnetlerine ve köprülerin bu yakasındaki diğer mesnetlere aynı yer hareketleri enine, boyuna ve düşey yönde olmak üzere üç doğrultuda uygulanırken, 2 nolu ana kule mesnetlerine ve köprülerin bu yakasındaki diğer mesnetlere dalga yayılma ve korelasyon etkisi dikkate alınarak belirlenen yer hareketleri yine üç doğrultuda uygulanmıştır. Dalga yayılma hızları B, C ve D zemin cinsi için sırasıyla 720 m/s, 360 m/s ve 180 m/s olarak dikkate alınmıştır.

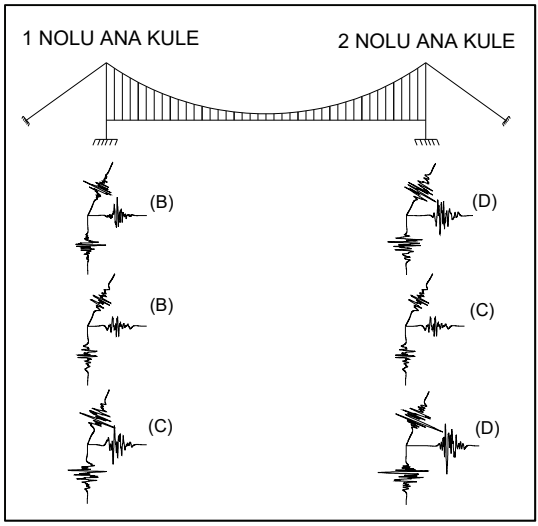

Şekil 18 - Asma köprüye uygulanan mesnetlerinden farklı yer hareketleri

Daha sonra 1 nolu ana kule mesnetleri ile köprülerin bu yakasındaki diğer mesnetlerdeki zemin cinsi aynı olmak üzere, 2 nolu ana kule mesnetleri ile köprülerin bu yakasındaki diğer mesnetlerdeki zemin cinsi farklı alınarak, iki yakadaki zemin cinsinin farklı olması durumu

için de farklı yer hareketi uygulaması yapılmıştır. Zemin cinsindeki farklılık yanında dalga-yayılma ve korelasyon etkisinden kaynaklanan yer hareketi değişimi de dikkate alınmıştır. Heterojen zemin cinsi olarak BC, BD ve CD durumları dikkate alınmıştır. BC kısaltması ile tanımlanan farklı yer hareketi için, köprü modellerinin 1 nolu ana kulesinin bulunduğu yakadaki mesnetlerin sert (B) zemin sınıfı üzerine inşa edildiği kabul edilirken, diğer yakasındaki mesnetlerin orta (C) zemin sınıfı üzerine inşa edildiği kabul edilmiştir. Köprü sistemlerine uygulanan mesnetlerinden farklı yer hareketleri Şekil 18'de gösterilmiştir.

Eğik kablo askılı köprüde ana kule mesnetleri harici diğer mesnetler köprünün boyuna yönde kayar mesnet olduklarından bu mesnetlere boyuna yönde yer hareketi uygulanmamıştır. Deprem yüklemeleri için zaman tanım alanında doğrusal olmayan analizler yapılmış olup söz konusu analizlerde köprülerin kendi ağırlıkları da göz önünde bulundurulmuştur. Asma köprüye uygulanan BC ve CD sınıfı zemin için üretilmiş farklı yer hareketine ait yerdeğiştirme–zaman kayıtları Şekil 19 ve Şekil 20'de gösterilmiştir.

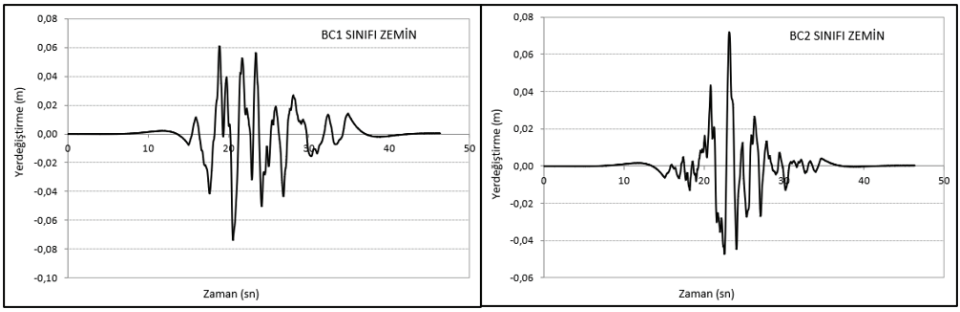

Şekil 19 - Asma köprü 1 ve 2 nolu yakada uygulanan BC sınıfı zemin yerdeğiştirme -zaman kayıtları

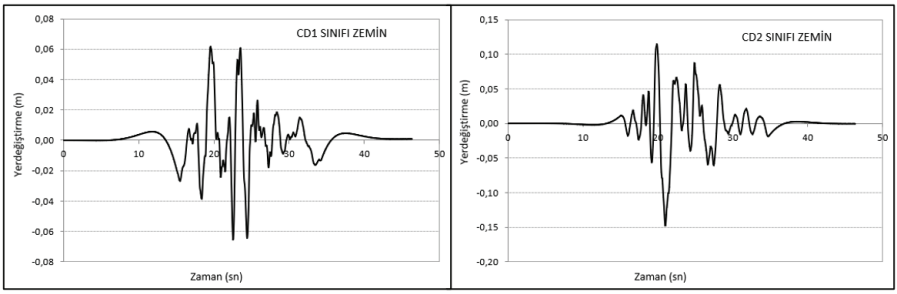

Şekil 20 - Asma köprü 1 ve 2 nolu yakada uygulanan CD sınıfı zemin yerdeğiştirme -zaman kayıtları

6. YAPI-ZEMİN ETKİLEŞİMİNİN TANIMLANMASI

Yapı-zemin etkileşiminin dikkate alındığı köprü modellerinde, ana kulelerin ve kenar ayakların mesnetlendiği noktalarda zeminler doğrusal elastik yaylar ile temsil edilmiştir. Mesnet noktalarında, her bir ötelenme ve dönme için eşdeğer Winkler yatak katsayısı (k)

hesaplanmıştır. Yatak katsayısı hesapları FEMA 356 [32] Bölüm 4'e göre yapılmıştır. Zemin sınıflarına göre zeminin dönme ve ötelenme rijitlikleri değiştiğinden her üç zemin sınıfı (B, C, D) için ayrı hesaplamalar yapılmıştır. Her iki köprü ana kule temellerinin de aynı boyutlarda olmasından dolayı her bir ana kule temeli için hesaplanan zemin rijitlikleri her iki köprü ana kule mesnet noktalarına da uygulanmıştır. Eğik kablo askılı köprünün kenar açıklık temelleri için de ayrıca yatak katsayısı hesabı yapılmıştır. Köprü temellerinin zemine mesnetlendiği noktalarda temellerin dönme ve ötelenme rijitlikleri için kullanılan formüller aşağıda verilmiştir. [32]

Temel enine yönde ötelenme rijitliği (Kx) = $[(G \times B) / (2 - \nu)] \times [3{,}4 \times (L/B)^{0{,}65} + 1{,}2]$

Temel boyuna yönde ötelenme rijitliği (Ky) = $[(G \times B) / (2 - \nu)] \times [3{,}4 \times (L/B)^{0{,}65} + 0{,}4 \times L / B + 0{,}8]$

Temel düşey yönde ötelenme rijitliği (Kz) = $[(G \times B) / (1 - \nu)] \times [1{,}55 \times (L/B)^{0{,}75} + 0{,}8]$

Temel boyuna yönde dönme rijitliği (Kxx) = $[(G \times B^3) / (1 - \nu)] \times [0{,}4 \times (L/B) + 0{,}1]$

Temel enine yönde dönme rijitliği (Kyy) = $[(G \times B^3) / (1 - \nu)] \times [0{,}47 \times (L/B)^{2{,}4} + 0{,}034]$

Temel düşey yönde dönme rijitliği (Kzz) = $(G \times B^3) \times [0{,}53 \times (L/B)^{2{,}45} + 0{,}51]$

Burada, "G" kayma modülünü, "B" temel genişliğini, "ν" poisson oranını, "L" de temel boyunu ifade etmektedir. Köprü temelleri için hesaplanan ötelenme ve dönme rijitlikleri köprü sonlu elamanlar modellerinde yay olarak her bir ana kulenin ve kenar ayakların mesnet noktalarında tariflenmiştir. Her üç zemin sınıfı için ana kule ve kenar açıklık temellerinin dönme ve ötelenme rijitlikleri Tablo 5 ve Tablo 6'da gösterilmiştir. Yapı-zemin etkileşiminin ihmal edildiği köprü modellerinde ise ankastre mesnet uygulaması yapılmıştır.

Tablo 5 - Asma ve eğik kablo askılı köprü ana kule temelleri dönme ve ötelenme rijitlikleri

Ana Kule Temelleri (B = 40m, L = 80m, v =0.5)						
Zemin Sınıfı	Kx (kN/m)	Ky (kN/m)	Kz (kN/m)	Kxx (kN.m)	Kyy (kN.m)	Kzz (kN.m)
B	501389577	532078262	784121731	3.31438E+11	9.26065E+11	6.27155E+11
C	75499776.91	80120911.8	118073886	49908256881	1.39448E+11	94437660923
D	15544071.72	16495481.84	24309329.47	10275229358	28709845636	19443047837

Tablo 6 - Eğik Kablo Askılı Köprü Kenar Ayak Temelleri Dönme ve Ötelenme Rijitlikleri

Kenar Ayak Temelleri (B = 10m, L = 40m, v =0.5)						
Zemin Sınıfı	Kx (kN/m)	Ky (kN/m)	Kz (kN/m)	Kxx (kN.m)	Kyy (kN.m)	Kzz (kN.m)
B	183590877	206607390.7	298297588.4	9782018349	75534907083	46994656134
C	27645309.92	31111161.09	44917968.78	1472986748	11374126811	7076505406
D	5691681.454	6405239.048	9247817.101	303261977.6	2341731990	1456927584

7. NÜMERİK ANALİZLER

Dikkate alınan köprü sistemlerin üniform ve farklı yer hareketleri etkisindeki analizleri hem yapı-zemin etkileşiminin dikkate alındığı hem de ihmal edildiği durumlar için yapılmış ve elde edilen bulgular karşılaştırılarak değerlendirilmiştir. Sert, orta ve yumuşak zemin cinsleri dikkate alınarak üretilen üniform ve farklı yer hareketleri için gerçekleştirilen dinamik analizler neticesinde ana kulelerde ve tabliyelerde elde edilen yer değiştirme ve kesit tesirlerinin karşılaştırmaları yapılmıştır. Yapı-zemin etkileşiminin dikkate alındığı durumlar "YZE" olarak, ihmal edildiği durumlar ise "ANKR" olarak adlandırılmıştır. Çalışmada dikkate alınan köprülerin geometri, kütle ve rijitlik özelliklerinin farklı olması nedeniyle, yapısal tepkilerin farklı olması beklenen bir durumdur. Burada yapılan karşılaştırmanın amacı, üniform ve mesnetlerinden farklı yer hareketi uygulaması durumları için söz konusu köprülerin performansını belirlemek ve deprem hareketinin üniform veya farklı olarak uygulanması durumunda, yapı-zemin etkileşimine de bağlı olarak, ne derece etkilendiklerini göreceli olarak karşılaştırmaktır. Böylelikle, bu çalışmanın amacına uygun olarak, merkez açıklığın 1000m'ye ulaştığı uzun açıklıklı kablo-destekli köprü sistemlerinde, deprem kuvvetleri açısından köprü tipinin seçimine karar verebilmek için bir değerlendirme yapılabilmesi hedeflenmiştir.

7.1. Modal Analiz Sonuçları

Eğik kablo askılı köprü analizlerinde 50 mod dikkate alınmış olup, kütle katılımı boyuna yönde %92, enine yönde %91 olarak gerçekleşmiştir. Köprünün modal analizi sonucunda elde edilen ilk üç mod şekilleri Şekil 21 ve Şekil 22'de gösterilmiştir. Köprünün 1. modu boyuna yöndeki salınım modudur ve 11.88 sn'lik doğal periyota sahiptir. 2. modu yatay yöndeki eğilme modudur ve 8,75 sn'lik periyota sahiptir. 3. modu düşey yöndeki eğilme modudur ve 5,97 sn'lik periyota sahiptir. Diğer modlar burulma modları olup periyodları da çok yakın olduğundan burada gösterilmemiştir.

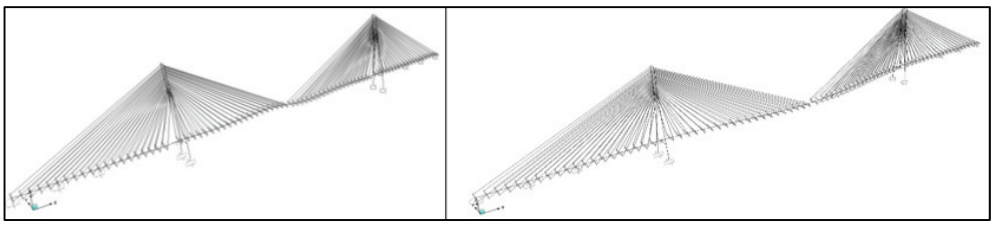

Şekil 21 - Eğik Kablo Askılı Köprü 1. ve 2. Mod Şekilleri

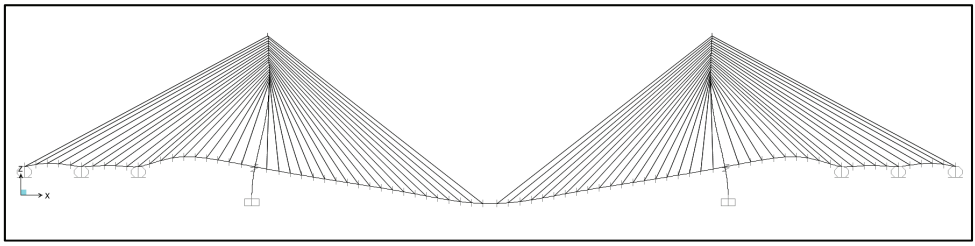

Şekil 22 - Eğik Kablo Askılı Köprü 3.Mod Şekili

Eğik kablo askılı köprü için düşey yöndeki eğilme frekansı hesabı Chinese Wind-resistant Design Specification for Highway Bridges [33] Bölüm 5'de yer alan ampirik formüller kullanılarak da hesaplanmıştır.

$f_b = 150 / L$ (9)

L = Köprü merkez açıklığı (Kenar açıklık mesnetli) = 1000 m

f_b = 0,15 Hz

Tb (Düşey Periyot)= $1/ f_b$ = 6,67 sn

Sonlu eleman yazılımı ile elde edilen düşey yöndeki eğilme modu 5,97 sn olup, yukarıdaki formulasyon ile elde edilen T = 6,67 sn değerine yakın olduğu görülmektedir.

Asma köprü analizlerinde 50 mod dikkate alınmış olup, kütle katılımı boyuna yönde % 93, enine yönde % 90 olarak gerçekleşmiştir. Köprünün modal analizi sonucunda elde edilen ilk üç mod şekilleri Şekil 23 ve Şekil 24'de gösterilmiştir. Köprünün 1. modu düşey yöndeki antisimetrik eğilme modudur ve 9,93 sn'lik doğal periyota sahiptir. 2. modu yatay yöndeki eğilme modudur ve 9,22 sn'lik periyota sahiptir. 3. modu düşey yöndeki eğilme modudur ve 7,01 sn'lik periyota sahiptir. Diğer modlar burulma modları olup periyodları da çok yakın olduğundan burada gösterilmemiştir.

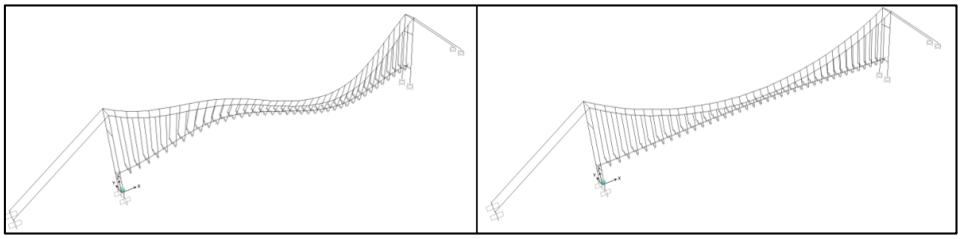

Şekil 23 - Asma Köprü 1. ve 2. Mod Şekilleri

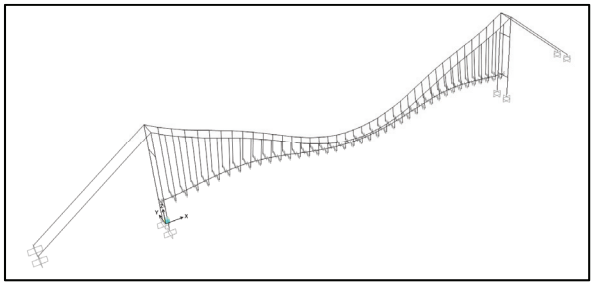

Şekil 24 - Asma Köprü 3.Mod Şekili

Dikkate alınan eğik kablo askılı ve asma köprü sistemlerinin kütle ve rijitlik özelliklerindeki farklılıklar yanında, mesnet koşullarındaki farklılığa da bağlı olarak modal davranışlarında

da farklılıklar ortaya çıkmıştır. Örneğin eğik kablo askılı köprü için ilk beş modun x ve y doğrultusundaki kütle katılım oranı %70 civarında iken, asma köprüde x doğrultusundaki katılım 19. modda, y doğrultusundaki katılım ise 8.modda %70'i geçmektedir. Söz konusu bu farklılıkların yapısal tepkiler üzerinde de etkili olduğu düşünülmektedir.

Asma köprü için düşey yöndeki simetrik ve antisimetrik eğilme frekansı hesapları da Chinese Wind-resistant Design Specification for Highway Bridges [33] Bölüm 5'de yer alan ampirik formüller kullanılarak hesaplanmıştır.

$$f_b = \frac{1}{L}\sqrt{\frac{EI\left(\frac{2\pi}{L}\right)^2 + 2H_g}{m}} \tag{10}$$

L = Köprü merkez açıklığı (Kenar açıklık mesnetli) = 1000 m

EI = Düşey eğilme rijitliği (1,73 x 10^{12} N/m^2)

Hg = Sabit yükler altında ana kabloda oluşan yatay çekme kuvveti (7,84 x 10^7 N)

m = Tabliye ve ana kablonun birim boy ağırlığı (25280 kg/m)

fb = 0,094 Hz

Tb (Düşey Periyot)= 1/ fb = 10,63 sn

Sonlu eleman yazılımı ile elde edilen düşey yöndeki antisimetrik eğilme modu 1. mod olup bu moda ait periyot değeri 9,93 sn'dir. Yukarıdaki formulasyon ile elde edilen T = 10,63 sn değerinin, sonlu eleman yazılımı ile elde edilen değere yakın olduğu görülmektedir. Asma köprü için düşey yöndeki simetrik eğilme frekansı da aşağıdaki formulasyon ile hesaplanmıştır.

$$f_b = \frac{0.1}{L}\sqrt{\frac{E_c A_c}{m}} \tag{11}$$

L = Köprü merkez açıklığı (Kenar açıklık mesnetli) = 1000 m

Ec = Ana kablo elastisite modulü (1,95 x 10^{11} N/m^2)

Ac = Ana kablo kesit alanı (0,33 m^2)

m = Tabliye ve ana kablonun birim boy ağırlığı (25280 kg/m)

fb = 0,159 Hz

Tb (Düşey Periyot)= 1/ fb = 6,29 sn

Sonlu eleman yazılımı ile elde edilen düşey yöndeki simetrik eğilme modu 3. mod olup bu moda ait periyot değeri 7,01 sn'dir. Yukarıdaki formulasyon ile elde edilen T = 6,29 sn değeri ile sonlu eleman yazılımı ile elde edilen değerin yine yakın olduğu görülmektedir.

7.2. Yer Değiştirmeler

Her üç zemin sınıfı için yapı-zemin etkileşiminin dikkate alındığı ve ihmal edildiği durumlar göz önünde bulundurularak uygulanan yer hareketleri neticesinde en fazla yer değiştirme değerlerinin elde edildiği eğik kablo askılı ve asma köprü sistemlerinin tabliye orta noktalarında ve eğik kablo askılı köprü sistemi ana kule tepe noktası ile asma köprü sistemi ana kule orta noktası için elde edilen yer değiştirme değerleri, merkez açıklık uzunluğuna ve kule yüksekliğine bölünmek suretiyle oransal olarak Tablo 7'de gösterilmiştir. Yer hareketlerinin asma ve eğik kablo askılı köprü üzerindeki göreceli etkilerini belirleyebilmek için, eğik kablo askılı köprü için elde edilen yer değiştirme oranları asma köprü için elde edilen yer değiştirme oranları ile normalize edilmiştir.

Hem yapı-zemin etkileşiminin dikkate alındığı hem de ihmal edildiği üniform yer hareketi uygulanması neticesinde eğik kablo askılı köprü tabliyesinde elde edilen düşey yer değiştirme değeri oranları asma köprü tabliyesinde elde edilen yer değiştirme değeri oranlarına göre her üç zemin sınıfı için de daha büyük çıkmış olup aradaki fark ortalama olarak %30 mertebesindedir. Yapı-zemin etkileşiminin ihmal edildiği mesnetlerinden farklı yer hareketi uygulaması neticesinde sert-yumuşak (BD) ile sert-orta (BC) heterojen zemin sınıfları için asma köprü tabliyesinde elde edilen düşey yerdeğiştirme değeri oranlarının eğik kablo askılı köprü tabliyesinde elde edilen yerdeğiştirme değeri oranlarına göre sırasıyla %44 ve %24 daha büyük olduğu, orta-yumuşak (CD) heterojen zemin sınıfı için elde edilen değerlerin ise oldukça yakın olduğu gözlenmiştir. Bunun yanında yapı-zemin etkileşiminin ihmal edildiği ve homojen zemin ortamının dikkate alındığı mesnetlerinden farklı yer hareketi uygulaması neticesinde homojen yumuşak (DD) zemin cinsi için eğik kablo askılı köprü tabliyesinde elde edilen düşey yerdeğiştirme değeri oranının asma köprü tabliyesinde elde edilen yerdeğiştirme değeri oranına göre %39 daha büyük olduğu, homojen sert (BB) ve homojen orta (CC) zemin sınıfları için elde edilen değerlerin ise oldukça yakın olduğu gözlenmiştir. Yapı-zemin etkileşiminin dikkate alındığı mesnetlerinden farklı yer hareketi uygulaması durumunda sert-yumuşak (BD) ile sert-orta (BC) heterojen zemin sınıfları için asma köprü tabliyesinde elde edilen düşey yerdeğiştirme değeri oranlarının eğik kablo askılı köprü tabliyesinde elde edilen yerdeğiştirme değeri oranlarına göre sırasıyla %39 ve %27 daha büyük olduğu, orta-yumuşak (CD) heterojen zemin sınıfı için elde edilen değerlerin ise yakın olduğu gözlenmiştir. Bunun yanında yapı-zemin etkileşiminin dikkate alındığı ve homojen zemin ortamının dikkate alındığı mesnetlerinden farklı yer hareketi uygulaması durumunda homojen orta (CC) zemin cinsi için asma köprü tabliyesinde elde edilen düşey yerdeğiştirme değeri oranının eğik kablo askılı köprü tabliyesinde elde edilen yerdeğiştirme değeri oranına göre %14 daha büyük olduğu, homojen sert (BB) ve homojen yumuşak (DD) zemin sınıfları için elde edilen değerlerin ise oldukça yakın olduğu gözlenmiştir.

Kule yatay yer değiştirme oranları incelendiğinde, hem yapı-zemin etkileşiminin dikkate alındığı hem de ihmal edildiği durumda üniform yer hareketinin uygulanması neticesinde her üç zemin sınıfı için de eğik kablo askılı köprüde elde edilen maksimum yatay yer değiştirme değeri oranlarının asma köprüde elde edilen maksimum yer değiştirme değeri oranlarına göre daha büyük olduğu gözlenmiştir. Orta (CC) zemin sınıfı için ankastre durumda söz konusu oran %93 mertebesindedir. Mesnetlerinden farklı yer hareketi uygulaması durumunda ise genel olarak asma köprüde elde edilen maksimum yatay yer değiştirme değeri oranları, eğik kablo askılı köprüde elde edilen maksimum yer değiştirme değeri oranlarına göre daha büyük çıkmıştır. Bunun yanında ankastre durumda sert-orta (BC) heterojen zemin sınıfı için eğik

kablo askılı köprü kule yatay yerdeğiştirme değeri oranının asma köprü kulesinde elde edilen yerdeğiştirme değeri oranına göre %30 mertebesinde daha büyük olduğu gözlenmiştir.

Tablo 7 - Tabliye ve ana kulelerde elde edilen maksimum yer değiştirme oranları

	Tabliye Orta Noktası Düşey Deplasman Oranları (u1/L)			Kule Yatay Deplasman Oranları (u2/h)		
Yer Hareketi	Kablo Askılı Köprü L=1000m (a)	Asma Köprü L=1000m (b)	Oran (a/b)	Kablo Askılı Köprü – Kule Tepe Noktası h=340m (a)	Asma Köprü - Kule Orta Noktası h=240m (b)	Oran (a/b)
Üniform Yer Hareketi BB (ANKR)	0.152	0.149	1,02	0.403	0.249	1.62
Üniform Yer Hareketi CC (ANKR)	0.221	0.162	1.36	0.724	0.375	1.93
Üniform Yer Hareketi DD (ANKR)	0.363	0.296	1.23	0.994	0.638	1.56
Üniform Yer Hareketi BB (YZE)	0.202	0.155	1.30	0.470	0.350	1.34
Üniform Yer Hareketi CC (YZE)	0.252	0.176	1.43	0.793	0.423	1.87
Üniform Yer Hareketi DD (YZE)	0.406	0.311	1.31	1.106	0.883	1.25
Farklı Yer Hareketi BD (ANKR)	0.398	0.711	0.56	0.653	0.933	0.70
Farklı Yer Hareketi BC (ANKR)	0.302	0.399	0.76	0.662	0.508	1.30
Farklı Yer Hareketi CD (ANKR)	0.485	0.477	1.02	0.797	1.121	0.71
Farklı Yer Hareketi BB (ANKR)	0.314	0.294	1.07	0.597	0.571	1.05
Farklı Yer Hareketi CC (ANKR)	0.328	0.314	1.04	0.756	0.714	1.06
Farklı Yer Hareketi DD (ANKR)	0.683	0.492	1.39	1.056	0.950	1.11
Farklı Yer Hareketi BD (YZE)	0.506	0.832	0.61	0.772	1.220	0.63
Farklı Yer Hareketi BC (YZE)	0.339	0.465	0.73	0.721	0.737	0.98
Farklı Yer Hareketi CD (YZE)	0.602	0.612	0.98	0.836	1.468	0.57
Farklı Yer Hareketi BB (YZE)	0.378	0.397	0.95	0.648	0.671	0.97
Farklı Yer Hareketi CC (YZE)	0.353	0.410	0.86	0.917	1.069	0.86
Farklı Yer Hareketi DD (YZE)	0.756	0.762	0.99	1.186	1.263	0.94

(u1 : Düşey Yerdeğiştirme (mm), u2 : Yatay Yerdeğiştirme (mm))

Yapı-zemin etkileşimi hem eğik kablo askılı köprüde hem de asma köprüde, üniform ve mesnetlerinden farklı yer hareketi uygulaması için tabliye düşey yer değiştirmelerini ve kule yatay yer değiştirmelerini arttırmıştır. Yapı-zemin etkileşiminden dolayı mesnetlerden farklı yer hareketi uygulanması durumunda eğik-kablo askılı köprü modeline ait kule ve tabliye yer

değiştirmelerinde gözlemlenen ortalama artış miktarı, üniform yer hareketi uygulaması için elde edilen artış miktarına yakın çıkarken, asma köprü modelinde mesnetlerden farklı yer hareketi uygulanması durumunda gözlemlenen ortalama artış miktarı, üniform yer hareketi uygulaması için elde edilen artış miktarından daha fazla olmuştur.

Tabliye düşey yerdeğiştirmeleri ile kule yatay yerdeğiştirmeleri için elde edilen sonuçlar, üniform yer hareketi etkisinde eğik kablo askılı köprünün asma köprüye oranla daha fazla etkilendiğini gösterirken, mesnetlerden farklı yer hareketi uygulaması durumunda asma köprünün genel olarak daha fazla etkilendiğini ortaya koymaktadır.

7.3. Eğilme Gerilmeleri

Eğik kablo askılı köprü tabliyesi için en büyük eğilme gerilmesi, maksimum momentin meydana geldiği tabliyenin ana kuleye mesnetlendiği noktalarda meydana gelmektedir. Bu nedenle eğik kablo askılı köprü tabliyesi için maksimum eğilme gerilmesi değeri (σ_{max}), tabliyenin ana kuleye mesnetlendiği noktalarda elde edilen eğilme momenti (M_{max}) değeri dikkate alınarak elde edilmiştir. Asma köprü tabliyesi için ise en büyük eğilme gerilmesi maksimum momentin meydana geldiği tabliyenin orta noktasında meydana geldiğinden, asma köprü tabliyesi için maksimum eğilme gerilmesi değeri (σ_{max}), tabliyenin orta noktasında elde edilen eğilme momenti (M_{max}) dikkate alınarak belirlenmiştir. Her iki köprü modelinde de en büyük eğilme gerilmesi maksimum momentin meydana geldiği ana kulelerin zemine mesnetlendiği noktalarda meydana gelmektedir. Bu nedenle her iki köprü sistemi ana kuleleri için maksimum eğilme gerilmesi değeri (σ_{max}), ana kulelerin zemine mesnetlendiği noktalarda elde edilen eğilme momenti (M_{max}) değerine bağlı olarak elde edilmiştir. Her üç zemin sınıfı için, yapı-zemin etkileşiminin dikkate alındığı ve ihmal edildiği durumlar da göz önünde bulundurularak uygulanan yer hareketleri neticesinde eğik kablo askılı ve asma köprülerin tabliyelerinde ve ana kulelerinde elde edilen maksimum eğilme gerilmesi değerleri ve oranları Tablo 8 ve Tablo 9'da gösterilmiştir.

Hem yapı-zemin etkileşiminin dikkate alındığı hem de ihmal edildiği durumda üniform ve farklı yer hareketi uygulanması için asma köprü tabliyesinde elde edilen eğilme gerilmeleri, eğik kablo askılı köprü tabliyesinde elde edilen eğilme gerilmelerinden daha büyük çıkmıştır. Üniform yer hareketi uygulaması için asma köprü tabliyesinde elde edilen eğilme gerilmeleri ortalama %10, farklı yer hareketi uygulaması için ise ortalama %15 daha büyük çıkmıştır.

Üniform ve mesnetlerinden farklı yer hareketi uygulaması için yapı-zemin etkileşimi her iki köprü modelinde de tabliye eğilme momentlerini arttırmıştır. Üniform yer hareketi durumunda eğik kablo askılı köprüde yapı-zemin etkileşimi tabliye eğilme momentlerini tüm zemin cinsleri dikkate alındığında ortalama %23,1 arttırırken, mesnetlerden farklı yer hareketi uygulaması durumunda ortalama %16,8 arttırmıştır. Asma köprü için elde edilen oranlar ise sırasıyla %25,2 ve %17,3'dir.

Tasarımı yapılan eğik kablo askılı köprü tabliyesinin mütemadi olmasından dolayı en büyük eğilme gerilmeleri tabliye ile köprü ayağının birleşim noktasında meydana gelmektedir. Asma köprü ise tek açıklıklı basit mesnetli sistem olarak çalıştığından en büyük eğilme gerilmeleri köprü açıklığı ortasında meydana gelmektedir. Söz konusu bu yapısal farklılığın, köprü tabliyelerinde eğilmeden kaynaklanan gerilmelerde gözlemlenen farklılığın nedeni olduğu düşünülmektedir.

Tablo 8 - Tabliyelerde elde edilen maksimum eğilme gerilmesi değerleri ve oranları

Yer Hareketi	Eğik Kablo Askılı Köprü Tabliyesinin Ana Kuleye Mesnetlendiği Noktada Elde Edilen Eğilme Gerilmesi (kN/m^2) (a)	Asma Köprü Tabliyesi Orta Noktasında Elde Edilen Eğilme Gerilmesi (kN/m^2) (b)	Oran (a/b)
Üniform Yer Hareketi BB (ANKR)	120681	129092	0.93
Üniform Yer Hareketi CC (ANKR)	125579	142872	0.88
Üniform Yer Hareketi DD (ANKR)	149694	164630	0.91
Üniform Yer Hareketi BB (YZE)	147825	165828	0.89
Üniform Yer Hareketi CC (YZE)	155491	178749	0.87
Üniform Yer Hareketi DD (YZE)	184005	200864	0.92
Farklı Yer Hareketi BD (ANKR)	183835	235204	0.78
Farklı Yer Hareketi BC (ANKR)	148164	190101	0.78
Farklı Yer Hareketi CD (ANKR)	165840	203951	0.81
Farklı Yer Hareketi BB (ANKR)	146672	166978	0.88
Farklı Yer Hareketi CC (ANKR)	173380	179103	0.97
Farklı Yer Hareketi DD (ANKR)	175956	195514	0.90
Farklı Yer Hareketi BD (YZE)	204994	262492	0.78
Farklı Yer Hareketi BC (YZE)	175607	228203	0.77
Farklı Yer Hareketi CD (YZE)	198796	235431	0.84
Farklı Yer Hareketi BB (YZE)	173492	204912	0.85
Farklı Yer Hareketi CC (YZE)	193736	204890	0.95
Farklı Yer Hareketi DD (YZE)	212820	233445	0.91

Kule eğilme gerilmelerine ait oranlar incelendiğinde, hem yapı-zemin etkileşiminin dikkate alındığı hem de ihmal edildiği durumda üniform yer hareketi uygulanması neticesinde eğik kablo askılı köprü kulesinin zemine mesnetlendiği noktada elde edilen eğilme gerilmelerinin, asma köprü kulesinde elde edilen eğilme gerilmelerine oranları genel olarak 1'e yakın çıkmıştır. Sonuçlar arasındaki en büyük farklılık DD yumuşak zemin sınıfı için gözlenmiş olup asma köprü kulesindeki eğilme gerilmesi değerleri eğik kablo askılı köprü kulesi eğilme gerilmesi değerlerinden %10 mertebesinde daha büyük çıkmıştır. Hem yapı-zemin etkileşiminin dikkate alındığı hem de ihmal edildiği durumda mesnetlerinden farklı yer hareketi uygulaması neticesinde her üç zemin sınıfı için de asma köprü kulesinde daha büyük eğilme gerilmesi değerinin ortaya çıktığı görülmektedir. Farklı yer hareketi uygulaması için asma köprü kulesinde elde edilen eğilme gerilmesi değerleri ortalama %19 daha büyük çıkmıştır.

Üniform ve mesnetlerinden farklı yer hareketi uygulaması için yapı-zemin etkileşimi her iki köprü modelinde de kule eğilme momentlerini arttırmıştır. Üniform yer hareketi durumunda eğik kablo askılı köprüde yapı-zemin etkileşimi kule eğilme momentlerini ortalama %12,7 arttırırken, mesnetlerden farklı yer hareketi uygulaması durumunda ortalama %13,4 arttırmıştır. Asma köprü için elde edilen oranlar ise sırasıyla %13,9 ve %14,7'dir.

Tablo 9 - Ana kulelerde elde edilen maksimum eğilme gerilmesi değerleri ve oranları

Yer Hareketi	Eğik Kablo Askılı Köprü Ana Kulesinin Zemine Mesnetlendiği Noktada Elde Edilen Eğilme Gerilmesi (kN/m^2) (a)	Asma Köprü Ana Kulesinin Zemine Mesnetlendiği Noktada Elde Edilen Eğilme Gerilmesi (kN/m^2) (b)	Oran (a/b)
Üniform Yer Hareketi BB (ANKR)	17433	17545	0.99
Üniform Yer Hareketi CC (ANKR)	20117	19489	1.03
Üniform Yer Hareketi DD (ANKR)	30555	33511	0.91
Üniform Yer Hareketi BB (YZE)	19693	20068	0.98
Üniform Yer Hareketi CC (YZE)	23061	21915	1.05
Üniform Yer Hareketi DD (YZE)	34408	38144	0.90
Farklı Yer Hareketi BD (ANKR)	29019	36971	0.78
Farklı Yer Hareketi BC (ANKR)	20275	32095	0.63
Farklı Yer Hareketi CD (ANKR)	32963	39294	0.84
Farklı Yer Hareketi BB (ANKR)	26461	31340	0.84
Farklı Yer Hareketi CC (ANKR)	32624	35173	0.93
Farklı Yer Hareketi DD (ANKR)	40793	42296	0.96
Farklı Yer Hareketi BD (YZE)	33651	43556	0.77
Farklı Yer Hareketi BC (YZE)	23319	37454	0.62
Farklı Yer Hareketi CD (YZE)	34046	44401	0.77
Farklı Yer Hareketi BB (YZE)	32307	39678	0.81
Farklı Yer Hareketi CC (YZE)	34713	41874	0.83
Farklı Yer Hareketi DD (YZE)	46450	49188	0.94

7.4. Eksenel Gerilmeler

Her iki köprü sistemi tabliyeleri için de en büyük eksenel gerilmeler maksimum eksenel kuvvetin meydana geldiği tabliyenin ana kuleye mesnetlendiği noktalarda meydana geldiğinden, her iki köprü tabliyesi için maksimum eksenel gerilme değeri (σ_{max}), tabliyenin

ana kuleye mesnetlendiği noktalarda elde edilen eksenel kuvvet (N_{max}) değerine bağlı olarak belirlenmiştir. Bunun yaninda, ana kulelerdeki maksimum eksenel gerilme değeri (σ_{max}), ana kulelerin zemine mesnetlendiği noktalarda elde edilen maksimum eksenel kuvvet (N_{max}) değerine bağlı olarak elde edilmiştir. Her üç zemin sınıfı için, yapı-zemin etkileşiminin dikkate alındığı ve ihmal edildiği durumlar da göz önünde bulundurularak uygulanan yer hareketleri neticesinde eğik kablo askılı ve asma köprü sistemlerinde tabliyenin ana kuleye mesnetlendiği noktalarda ve ana kulenin zemine mesnetlendiği noktalarda elde edilen eksenel gerilme değerleri ve oranları Tablo 10 ve Tablo 11'de gösterilmiştir. Üniform ve farklı yer hareketi uygulamasının asma ve eğik kablo askılı köprü üzerindeki etkilerini belirlemek için, eğik kablo askılı köprü için elde edilen maksimum eksenel gerilme değerleri ile asma köprü için elde edilen maksimum eksenel gerilme değerleri arasındaki oran verilmiştir. Her üç zemin sınıfı için hem yapı-zemin etkileşiminin dikkate alındığı hem de ihmal edildiği durumda üniform yer hareketi uygulanması neticesinde eğik kablo askılı köprü

Tablo 10 - Tabliyelerde elde edilen maksimum eksenel gerilme değerleri ve oranları

Yer Hareketi	Eğik Kablo Askılı Köprü Tabliyesinin Ana Kuleye Mesnetlendiği Noktada Elde Edilen Eksenel Gerilme (kN/m^2) (a)	Asma Köprü Tabliyesinin Ana Kuleye Mesnetlendiği Noktada Elde Edilen Eksenel Gerilme (kN/m^2) (b)	Oran (a/b)
Üniform Yer Hareketi BB (ANKR)	14120	1790	7.89
Üniform Yer Hareketi CC (ANKR)	14327	2473	5.79
Üniform Yer Hareketi DD (ANKR)	16041	3577	4.48
Üniform Yer Hareketi BB (YZE)	15723	2369	6.64
Üniform Yer Hareketi CC (YZE)	16006	2722	5.88
Üniform Yer Hareketi DD (YZE)	16980	3949	4.30
Farklı Yer Hareketi BD (ANKR)	16368	3408	4.80
Farklı Yer Hareketi BC (ANKR)	15079	2270	6.64
Farklı Yer Hareketi CD (ANKR)	16872	2971	5.68
Farklı Yer Hareketi BB (ANKR)	14582	2756	5.29
Farklı Yer Hareketi CC (ANKR)	15105	3780	4.00
Farklı Yer Hareketi DD (ANKR)	18303	4242	4.31
Farklı Yer Hareketi BD (YZE)	18787	3251	5.78
Farklı Yer Hareketi BC (YZE)	17475	2666	6.55
Farklı Yer Hareketi CD (YZE)	19811	3907	5.07
Farklı Yer Hareketi BB (YZE)	18444	3210	5.75
Farklı Yer Hareketi CC (YZE)	17279	3925	4.40
Farklı Yer Hareketi DD (YZE)	20703	4643	4.46

tabliyesinde elde edilen eksenel gerilmelerin asma köprü tabliyesinde elde edilen eksenel gerilmelere göre belirgin şekilde daha büyük olduğu gözlenmiştir. Sonuçlar arasındaki en büyük farklılık BB sert zemin sınıfı için gözlenmiş olup özellikle sert zemin (BB) sınıfı için eğik kablo askılı köprü tabliyesinde elde edilen eksenel gerilme değeri, asma köprü tabliyesinde elde edilen eksenel gerilmeye göre 7,89 kat daha fazla çıkmıştır. Benzer şekilde, hem yapı-zemin etkileşiminin dikkate alındığı hem de ihmal edildiği durumda mesnetlerinden farklı yer hareketi uygulanması neticesinde, üniform yer hareketi etkisinde olduğu gibi her üç zemin sınıfı için de eğik kablo askılı köprü tabliyesinde daha büyük eksenel gerilme değerlerinin ortaya çıktığı görülmektedir. Sonuçlar arasındaki en büyük farklılık sert-orta (BC) heterojen zemin sınıfı için gözlenmiş olup, söz konusu analiz durumu için köprüler arasında 6,64 kat mertebesinde farklılık gözlenmiştir.

Tablo 11 - Ana kulelerde elde edilen maksimum eksenel gerilme değerleri ve oranları

Yer Hareketi	Eğik Kablo Askılı Köprü Ana Kulesinin Zemine Mesnetlendiği Noktada Elde Edilen Eksenel Gerilme (kN/m^2) (a)	Asma Köprü Ana Kulesinin Zemine Mesnetlendiği Noktada Elde Edilen Eksenel Gerilme (kN/m^2) (b)	Oran (a/b)
Üniform Yer Hareketi BB (ANKR)	8346	6898	1.21
Üniform Yer Hareketi CC (ANKR)	7802	7138	1.09
Üniform Yer Hareketi DD (ANKR)	8399	7504	1.12
Üniform Yer Hareketi BB (YZE)	9149	8069	1.13
Üniform Yer Hareketi CC (YZE)	8850	7964	1.11
Üniform Yer Hareketi DD (YZE)	9492	8270	1.15
Farklı Yer Hareketi BD (ANKR)	9524	9436	1.01
Farklı Yer Hareketi BC (ANKR)	9342	8750	1.07
Farklı Yer Hareketi CD (ANKR)	10418	9653	1.08
Farklı Yer Hareketi BB (ANKR)	9325	9266	1.01
Farklı Yer Hareketi CC (ANKR)	10465	9784	1.07
Farklı Yer Hareketi DD (ANKR)	11581	10378	1.12
Farklı Yer Hareketi BD (YZE)	10302	10041	1.03
Farklı Yer Hareketi BC (YZE)	10975	9501	1.16
Farklı Yer Hareketi CD (YZE)	11034	10042	1.10
Farklı Yer Hareketi BB (YZE)	10150	9898	1.03
Farklı Yer Hareketi CC (YZE)	11860	10920	1.09
Farklı Yer Hareketi DD (YZE)	13078	11498	1.14

Kule eksenel gerilmeleri incelendiğinde, hem yapı-zemin etkileşiminin dikkate alındığı hem de ihmal edildiği durumda üniform ve farklı yer hareketi uygulanması neticesinde her üç zemin sınıfı için de eğik kablo askılı köprü kulesinin zemine mesnetlendiği noktada elde edilen eksenel gerilme değerlerinin, asma köprü kulesinde elde edilen eksenel gerilme değerlerine göre kısmen daha büyük olduğu görülmüştür. Sonuçlar arasındaki en büyük farklılık üniform yer hareketi durumunda BB (ANKR) yumuşak zemin sınıfı için gözlenmiş olup eğik kablo askılı köprü kulesindeki eğilme gerilmesi, asma köprü kulesindeki gerilmeden %21 daha büyük çıkmıştır.

Her iki köprü modeli arasındaki farklılık ortalama %10 mertebesindedir. En büyük eksenel yükler her iki köprü modeli için de tabliye ile köprü ayağının birleşim noktasında meydana gelmektedir. Eğik kablo askılı köprüde kenar açıklıklarda da tabliye olması nedeniyle dengeli konsol prensibinden dolayı tabliyeye ve kulelere aktarılan eksenel yük daha fazla olmaktadır. Bu nedenle eğik kablo askılı köprü kuleleri ve özellikle de tabliyesi eksenel gerilmelere karşı beklenildiği gibi daha hassastır.

7.5. Kesme Gerilmeleri

Eğik kablo askılı köprü tabliyesi için en büyük kesme gerilmesi, maksimum kesme kuvvetinin meydana geldiği tabliyenin ana kuleye mesnetlendiği noktalarda meydana geldiğinden, eğik kablo askılı köprü tabliyesi için maksimum kesme gerilmesi değeri (τ_{max}), tabliyenin ana kuleye mesnetlendiği noktalarda elde edilen kesme kuvveti (V_{max}) değeri dikkate alınarak elde edilmiştir. Asma köprü tabliyesi için ise en büyük kesme gerilmesi maksimum kesme kuvvetinin meydana geldiği tabliyenin orta noktasında meydana geldiğinden, asma köprü tabliyesi için maksimum kesme gerilmesi değeri (τ_{max}), tabliyenin orta noktasında elde edilen kesme kuvveti (V_{max}) dikkate alınarak belirlenmiştir.

Her iki köprü ana kuleleri için en büyük kesme gerilmesi maksimum kesme kuvvetinin meydana geldiği ana kulelerin zemine mesnetlendiği noktalarda meydana gelmektedir. Bu nedenle her iki köprü sistemi ana kuleleri için de maksimum kesme gerilmesi değeri (τ_{max}), ana kulelerin zemine mesnetlendiği noktalarda elde edilen kesme kuvveti (V_{max}) değerine bağlı olarak elde edilmiştir. Her üç zemin sınıfı için, yapı-zemin etkileşiminin dikkate alındığı ve ihmal edildiği durumlar da göz önünde bulundurularak uygulanan üniform ve farklı yer hareketi neticesinde köprü tabliyelerinde ve ana kulelerde elde edilen maksimum kesme gerilmesi değerleri ve oranları Tablo 12 ve Tablo 13'de gösterilmiştir.

Hem üniform hem de farklı yer hareketi uygulaması için eğik kablo askılı köprü tabliyesinin, kesme gerilmesi açısından asma köprü tabliyesine oranla daha fazla etkilendiği görülmüştür. Sonuçlar arasındaki en büyük farklılık, BB sert zemin sınıfının dikkate alındığı üniform yer hareketi uygulaması için %73 mertebesinde elde edilmiştir.

Kule kesme gerilmelerine ait oranlar incelendiğinde, hem yapı-zemin etkileşiminin dikkate alındığı hem de ihmal edildiği durumda üniform ve farklı yer hareketi uygulanması neticesinde her üç zemin sınıfı için de asma köprü kulesinin zemine mesnetlendiği noktada elde edilen kesme gerilmesi değerlerinin, eğik kablo askılı köprü kulesinde elde edilen kesme gerilmesi değerlerine göre daha büyük olduğu görülmüştür.

Tablo 12 - Tabliyelerde elde edilen maksimum kesme gerilmesi değerleri ve oranları

Yer Hareketi	Eğik Kablo Askılı Köprü Tabliyesinin Ana Kuleye Mesnetlendiği Noktada Elde Edilen Kesme Gerilmesi (kN/m^2) (a)	Asma Köprü Tabliyesinin Ana Kuleye Mesnetlendiği Noktada Elde Edilen Kesme Gerilmesi (kN/m^2) (b)	Oran (a/b)
ÜniformYer Hareketi BB (ANKR)	20141	11624	1.73
ÜniformYer Hareketi CC (ANKR)	20305	13332	1.52
ÜniformYer Hareketi DD (ANKR)	22351	16226	1.38
ÜniformYer Hareketi BB (YZE)	23005	14538	1.58
ÜniformYer Hareketi CC (YZE)	23138	15119	1.53
ÜniformYer Hareketi DD (YZE)	25470	19535	1.30
Farklı Yer Hareketi BD (ANKR)	22108	19897	1.11
Farklı Yer Hareketi BC (ANKR)	21393	14099	1.52
Farklı Yer Hareketi CD (ANKR)	21575	17620	1.22
Farklı Yer Hareketi BB (ANKR)	21580	14950	1.44
Farklı Yer Hareketi CC (ANKR)	22970	17242	1.33
Farklı Yer Hareketi DD (ANKR)	26983	21410	1.26
Farklı Yer Hareketi BD (YZE)	28772	26560	1.08
Farklı Yer Hareketi BC (YZE)	24852	18493	1.34
Farklı Yer Hareketi CD (YZE)	27884	19789	1.41
Farklı Yer Hareketi BB (YZE)	25663	16132	1.59
Farklı Yer Hareketi CC (YZE)	25892	19693	1.31
Farklı Yer Hareketi DD (YZE)	29984	24569	1.22

Tablo 13 - Ana kulelerde elde edilen maksimum kesme gerilmesi değerleri ve oranları

Yer Hareketi	Eğik Kablo Askılı Köprü Ana Kulesinin Zemine Mesnetlendiği Noktada Elde Edilen Kesme Gerilmesi (kN/m^2) (a)	Asma Köprü Ana Kulesinin Zemine Mesnetlendiği Noktada Elde Edilen Kesme Gerilmesi (kN/m^2) (b)	Oran (a/b)
ÜniformYer Hareketi BB (ANKR)	445	830	0.54
ÜniformYer Hareketi CC (ANKR)	526	954	0.55
ÜniformYer Hareketi DD (ANKR)	792	1416	0.56
ÜniformYer Hareketi BB (YZE)	470	872	0.54
ÜniformYer Hareketi CC (YZE)	576	1093	0.53

Tablo 13 - Ana kulelerde elde edilen maksimum kesme gerilmesi değerleri ve oranları (devam)

Yer Hareketi	Eğik Kablo Askılı Köprü Ana Kulesinin Zemine Mesnetlendiği Noktada Elde Edilen Kesme Gerilmesi (kN/m^2) (a)	Asma Köprü Ana Kulesinin Zemine Mesnetlendiği Noktada Elde Edilen Kesme Gerilmesi (kN/m^2) (b)	Oran (a/b)
ÜniformYer Hareketi DD (YZE)	890	1536	0.58
Farklı Yer Hareketi BD (ANKR)	1538	2315	0.66
Farklı Yer Hareketi BC (ANKR)	1407	2142	0.66
Farklı Yer Hareketi CD (ANKR)	1909	2035	0.94
Farklı Yer Hareketi BB (ANKR)	1499	2113	0.71
Farklı Yer Hareketi CC (ANKR)	1534	2322	0.66
Farklı Yer Hareketi DD (ANKR)	2257	2982	0.76
Farklı Yer Hareketi BD (YZE)	1771	2655	0.67
Farklı Yer Hareketi BC (YZE)	1630	2313	0.70
Farklı Yer Hareketi CD (YZE)	2245	2370	0.95
Farklı Yer Hareketi BB (YZE)	1649	2264	0.73
Farklı Yer Hareketi CC (YZE)	2012	2491	0.81
Farklı Yer Hareketi DD (YZE)	2451	3145	0.78

8. SONUÇLAR

Bu çalışmada merkez açıklıkları eşit (1000 m) olmakla birlikte, belirli bir geometriye sahip bir eğik kablo askılı köprü ile geometrik özelliklerinin farklı olduğu bir asma köprü sisteminin dinamik davranışı, köprülere üniform ve mesnetlerinden farklı yer hareketi uygulanmak suretiyle, yapı-zemin etkileşimi etkisi de dikkate alınarak belirlenmiş ve karşılaştırılmıştır.

Çalışma sonucunda, deprem hareketinin köprü mesnetlerine üniform veya farklı uygulanması durumunda eğik kablo askılı ve asma köprü sistemlerine ait yapısal tepkilerin farklılaştığı gözlenmiştir. Her iki köprü modeli için de maksimum yapısal tepkiler genel olarak mesnetlerinden farklı yer hareketi uygulanması neticesinde ortaya çıkmıştır. Dolayısıyla uzun açıklıklı kablo-destekli köprü sistemlerinin analizinde klasik bir yaklaşım olan üniform yer hareketi dikkate alınmasının yeterli olmayacağı, zemin cinsinde bağlı olarak deprem hareketi değişim etkisinin dikkate alınarak her bir köprü mesnedine farklı yer hareketi uygulanarak da analizlerin yapılması gerektiği görülmüştür.

Üniform ve mesnetlerinden farklı yer hareketi uygulanması durumunda, yapı zemin etkileşiminin dikkate alınması hem eğik kablo askılı köprüde hem de asma köprüde yapısal tepkileri arttırmıştır. Bunun yanında çalışmadan elde edilen sonuçlar, eğik kablo askılı ve asma köprülerin tasarımı yapılırken köprülerin inşa edileceği bölgedeki zemin sınıfının

köprünün deprem yükleri altındaki davranışı üzerinde büyük etkisinin olduğunu ve yapı-zemin etkileşiminin de dikkate alınması gerektiğini ortaya koymaktadır.

Dikkate alınan yapı elemanına, yapısal tepkiye ve uygulanan yer hareketine (üniform/farklı) bağlı olarak, bazen eğik kablo askılı köprünün bazen de asma köprünün daha fazla etkilendiği, sistematik bir değişimin olmadığı anlaşılmaktadır. Bununla birlikte, genel bir değerlendirme olarak, mesnetlerden farklı yer hareketi uygulanması durumunda asma köprünün eğik kablo askılı köprüye göre daha fazla etkilendiği, üniform yer hareketi uygulanması durumunda ise eğik kablo askılı köprünün daha fazla etkilendiği ifade edilebilir. Bu durum seçilecek köprü türüne karar verilirken, deprem hareketinin değişiminin dikkate alınarak yapı mesnetlerine farklı yer hareketinin uygulandığı mesnetlerden farklı yer hareketi uygulamasının da etkili olabileceğini göstermektedir.

Bu çalışma sonucunda deprem hareketinin yapı mesnetlerine üniform ve farklı olarak uygulanmasına bağlı olarak, uzun açıklıklar için köprü tipi seçimine yönelik değerlendirmelerde bulunulmuştur. Ancak nihai köprü tipi seçimine deprem kuvvetleri yanında köprü açıklığı, rüzgâr kuvveti, maliyet, inşaat aşamaları vb. etkenler de dikkate alınarak karar verilmelidir. Örneğin, köprü açıklığı arttıkça özellikle eğik-kablo askılı köprülerde kule yüksekliğinin oldukça artması, köprü seçimine etki edecek önemli etkenlerden bir tanesi olarak gözükmektedir. Diğer taraftan, eğik kablo askılı ve asma köprü modellerine ait kule tipinin, tabliye tipinin, kablo geometrisinin, mesnetlenme koşullarının, malzeme özelliklerinin vb. köprülerin dinamik davranışı üzerinde önemli etkisinin olacağı düşünülürse, bu çalışmada dikkate alınan ve belirli geometrik özelliklere sahip eğik kablo askılı ve asma köprü sistemleri için elde edilen sonuçlar genelleştirilmemelidir.

Kaynaklar

[1] Saadeghvaziri, M.A., Yazdani-Motlagh A.R., and Rashidi S., Effects of soil structure interaction on longitudinal seismic response of MSSS bridges. Soil Dynamics and Earthquake Engineering, 20 (1-4), 231-242, 2000.

[2] Soneji B.B., Jangid R.S., Influence of soil–structure interaction on the response of seismically isolated cable-stayed bridge. Soil Dynamics and Earthquake Engineering, 28 (4), 245-257, 2008.

[3] Liang F., Jia Y., Sun L., Xie W. and Chen H., Seismic response of pile groups supporting long span cable stayed bridge subjected to multi support excitations. Soil Dynamics and Earthquake Engineering, 101, 182-203, 2017.

[4] Zheng J. and Takeda, T., Effect of soil-structure interaction on seismic response of PC cable stayed bridge. Soil Dynamics and Earthquake Engineering, 14(6), 427-437, 1995.

[5] Siddharth G., Chandresh H. and Jatin D., Effect of foundation depth on seismic response of cable stayed bridge by considering soil-structure interaction. International Journal of Advanced Structural Engineering, 3(2), 121-132, 2011.

[6] Lyngs J., Kasper T., Bertelsen K., Modelling of soil-structure interaction for seismic anlyses of the İzmit Bay Bridge. A proceeding of the 18. International Conference on Soil Mechanics and Geotechnical Engineering, Paris-Fransa, 763-768, 2013.

[7] Miao F. and Tang D., 3-D seismic response of self-anchored cable-stayed suspension bridge under pile-soil-structure interaction. Electronic Journal of Geotechnical Engineering, (20), 6, 2015.

[8] Keshishian, P. G. Analysis of interconnected systems accounting for spatial variability of ground motions and soil-structure interaction. Doktora Tezi, Universty of California, Berkeley, 2001.

[9] Khan, R. A., Ahmad, S., and Datta, T. K., Effect of soil-structure interaction on seismic risk of FAN type cable stayed bridges. Journal of Seismology and Earthquake Engineering, 6(2), 47-56, 2004.

[10] Soyluk, K., and Sıcacık, E. A., Soil–structure interaction analysis of cable-stayed bridges for spatially varying ground motion components. Soil Dynamics and Earthquake Engineering, 35, 80-90, 2012.

[11] Kuyumcu Z., and Ateş Ş., Effect of soil – foundation – bridge interaction subjected to spatially varying earthquake ground motion. 2nd International Balkans Conference on Challenges of Civil Engineering, Tirana, 2013.

[12] Ateş Ş., Tonyalı Z., Soyluk K., Samberou S. M. A., Effectiveness of soil-structure ınteraction and dynamic characteristics on cable-stayed bridges subjected to multi support excitation. International Journal of Steel Structures**,** 18(2), 554-568, 2017.

[13] Shiravand M.R., Parvanehro P., Spatial variation of seismic ground motion effects on nonlinear responses of cable stayed bridges considering different soil types. Soil Dynamics and Earthquake Engineering, 119, 104-117, 2019.

[14] Tochaei E.N., Taylor T. and Ansari F., Effect of near-field ground motions and soil-structure interaction on dynamic response of a cable stayed bridge. Soil Dynamics and Earthquake Engineering, 133, 106-115, 2020.

[15] Kartal H. ve Soyluk K., Kablo destekli köprülerin dinamik davranışlarının karşılaştırılması. 2. Türkiye Deprem Mühendisliği ve Sismoloji Konferansı, Hatay-Türkiye, 1-13, 25-27 Eylül, 2013.

[16] Soyluk, K., Kartal, H. and Adanur, S. Comparison of Dynamic Behaviour of Long-Span Cable-Supported Bridges Vienna Congress on Recent Advances in Earthquake Engineering and Structural Dynamics (VEESD 2013), Paper No: 224, 28-30 August, Vienna, Austria, 2013.

[17] Soyluk K. ve Karaca H., Near-fault and far-fault ground motion effects on cable-supported bridges. X International Conference on Structural Dynamics, Rome-Italy, 3077-3082, 10-13 September, 2017.

[18] Kartal H. ve Soyluk K., Asma köprülerin dinamik davranışına yapı-zemin etkileşiminin etkisi. 8. Uluslararası Çelik Yapılar Sempozyumu, Konya-Türkiye, 96-107, 24-26 Ekim, 2019.

[19] Dumanoğlu, A. A., ve Adanur S., Asma köprülerin antisinkronize dinamik analizi. TMMOB İnşaat Mühendisleri Odası Teknik Dergi, 11(53), 2179-2197, 2000.

[20] Kartal H. ve Soyluk K., Eğik kablo askılı köprülerin dinamik davranışına yapı-zemin etkileşiminin etkisi. 4. Köprüler ve Viyadükler Sempozyumu, Ankara-Türkiye, 51, 01-02 Kasım, 2019.

[21] H. Kartal. Eşit merkez açıklığa sahip uzun açıklıklı asma ve eğik kablo askılı köprülerin dinamik davranışının karşılaştırılması. Doktora Tezi, Gazi Üniversitesi, Türkiye, 2018.

[22] SAP 2000 V19.1.0. Integrated finite elements analysis and design of structures, Computers and Structures, Inc, Berkeley, CA, 2015.

[23] Troitsky M.S., Cable-stayed Bridges : Theory and design, BSP Professional Books, 2nd edition, 1988.

[24] Wilson J.C., Gravelle W., Modelling of a cable-stayed bridge for dynamic analysis. Earthquake Engineering and Structural Dynamics, 20 (8), 707-721, 1991.

[25] Kartal H. and Soyluk K., Design of a suspension bridge having 1000m center span length. International Civil Engineering and Architecture Conference, Trabzon-Turkey, Vol.1, 1457-1490, 17-20 April, 2019.

[26] AASHTO LRFD Bridge Design Specifications. (2007). American Association of State Highway and Transportation Officals, 4.th Edition.

[27] Hao, H., Bolt, B.A. and Penzien, J. (1989). Effects of spatial variation of ground motions on large multiply-supported structures. Reprot No: UCB/EERC-89/06); Earthquake Engineering Research Center, College of Engineering, University of California, Berkeley, California.

[28] Harichandran, R.S. and Vanmarcke, E.H., Stochastic variation of earthquake ground motion in space and time. J. Eng. Mech. Div., ASCE **112**: 154-174, 1986.

[29] Clough, R.W. and Penzien, J., Dynamics of Structures. McGraw Hill, Inc., 1993.

[30] Eurocode8. Design of structures for earthquake resistance. General rules, seismic actions and rules for buildings. Brussels, 2004.

[31] Hashash Y., Musgrove M., Park D., Tsai C.C., Philips C., Groholski D.R. DEEPSOIL v7.0, 1-D Wave Propagation Program for Geotechnical Site Response, User Manual, University of Illinois at Urbana-Campaign, 2021.

[32] FEMA 356, Prestandard and Commentary for the Seismic Rehabilitation of Buildings, Federal Emergency Management Agency, 2000.

[33] Professional Recommendatory Standard of the People's Republic of China, Wind-resistant Design Specification for Highway, December, 2004.

Turkish Journal of Civil Engineering, 2023 35-56, Paper 724, ***Research Article***

Effects of Pore Fluid and Surface Roughness on Geomembrane - Soil Interface Behavior

Inci DEVELIOGLU[1]
Hasan Firat PULAT[2]

ABSTRACT

In this study, direct shear tests were conducted on soil - geomembrane interfaces. Sand/bentonite mixture and crushed sand were tested in contact with two geomembranes of the same type. To examine the effect of leachate on the mechanical properties of the geomembrane, acidic mine drainage, coal combustion product, and municipal solid waste leachates were prepared in the laboratory. The initial void ratio and internal friction angles of sand/bentonite and crushed sand were 0.34, 0.52, and 23º, 35º, respectively. In the smooth geomembrane - soil interface, the minimum interface friction angle (18^0) was obtained on acidic mine drainage cured geomembrane – sand/bentonite, while the maximum (31^0) interface friction angle was obtained on uncured geomembrane - crushed sand. In the textured geomembrane - soil interface, the minimum interface friction angle (17º) was obtained on acidic mine drainage cured geomembrane – sand/bentonite, while the maximum (43º) interface friction angle was obtained on uncured geomembrane - crushed sand. The friction angle of the crushed sand - geomembrane surface is higher than the friction angle of the sand/bentonite - geomembrane surface. While acidic mine drainage is the leachate that affects the shearing behavior of the geomembrane in the most negative way, coal combustion product is the leachate that has the least negative impact.

Keywords: Geomembrane, interface shear strength, leachate, direct shear test.

1. INTRODUCTION

Geosynthetics (GSs) are planar products made from polymers that have a widespread application in environmental and geotechnical engineering. Most parts of a modern landfill design are used as linings to prevent leachate from accumulating and leaking polluting the environment [1 – 3]. Storage of different solid waste (municipal, mine, coal, etc.) has become a common application in recent years [4 – 5]. However, disposal areas should be designed in

Note:
- This paper was received on May 19, 2022 and accepted for publication by the Editorial Board on December 16, 2022.
- Discussions on this paper will be accepted by May 31, 2023.
- https://doi.org/10.18400/tjce.1224424

1 Izmir Katip Celebi University, Department of Civil Engineering, Izmir, Türkiye
inci.develioglu@ikcu.edu.tr - https://orcid.org/0000-0001-6594-8095

2 Izmir Katip Celebi University, Department of Civil Engineering, Izmir, Türkiye
hfirat.pulat@ikcu.edu.tr - https://orcid.org/0000-0002-8298-7106

such a way that they do not pose a problem for the environment and human health [6 – 8]. Specially produced cover composite and lining systems should be placed on the base of the landfill and over the waste. These systems usually consist of multiple hydraulic barriers made up of layers of geomembrane (GM) or geosynthetic clay liner (GCL). Two kinds of GCL are generally used in geosynthetic composite systems in landfills; the unreinforced GCL containing a thin layer of bentonite bonded to high-density polyethylene (HDPE) GM, and the reinforced GCL containing a stitched or needle punched geotextile encapsulated bentonite to bond the support geotextiles [9 – 10]. Generally, textured HDPE geomembrane is preferred in systems used with geotextiles. On these barriers, sand or gravel is laid as the last layer [11 – 12].

Lateral shear stresses that can occur under the influence of lateral forces such as earthquake winds, etc., were not taken into account in the designs, which led to various construction errors, such as the shearing of the storage facility in Kettleman Hills, California [13]. Landfill covers (protection covers) used today effectively fulfill their duties. However, how long these systems can maintain their efficiency should be examined in detail. For this reason, it is necessary to elaborate examine its mechanical properties in detail. Although there are many studies on permeability, puncture, and tearing in the literature, studies examining mechanical properties under the influence of lateral stresses are quite limited [14 – 16]. As a result of the studies, it was determined that this disaster occurred due to the shear failure at the soil – GM interface. Due to limited references, engineers usually reduce the internal friction angle by a little (1/2 or 2/3) when obtaining the interface friction angle as recommended in textbooks [17]. Some researchers have determined that these coefficients may be less than 2/3 or even less than 1/2 in their studies, so the interface behavior between different soils and different geomembranes needs to be examined in detail [18 – 19].

In the literature, some studies examined the effect of only soil type or only geomembrane type on the interface shear behavior. Chai and Saito [20] determined the geomembrane – clay interface shear strength behavior with a large-scale direct shear device. Bentonite powder and quartz (30%) were mixed with clayey soil (70%). The types of geomembranes used in the study are polyvinyl chloride (PVC), polyethylene (PE), and high-density polyethylene (HDPE). Direct shear tests were conducted under the 50, 80, and 100 kPa normal stresses. The test results showed that the clayey soil – PVC interface had a maximum adhesion value. The interface friction angle between bentonite and all other geomembranes was quite small (3^{o} - 4^{o}). Since the water coming out of the bentonite accumulates at the interface during the shear test, a water layer is formed between the geomembrane and the bentonite particles, and therefore the interface friction angle is lower than it should be. Besides, the shear strength of the soil was achieved approximately 55% bigger than the interface shear strength. Effendi [18] studied the interface shear strength behaviors of different types of geomembranes (smooth HDPE, very smooth LDPE, PVC) and Ottawa sand. The geomembrane thicknesses were 2.03, 1.52, and 1.52 mm, respectively. The interface shear strength parameters were determined by the ring shear test, the normal stresses ranged from 50 kPa to 200 kPa, and the shear rate was 2.4 mm/min. The productivity ratio [E] ($\tan\delta/\tan\phi$) was derived to evaluate the results obtained. The HDPE with a very stiff and smooth surface had the lowest from 34 to 45% (E = 0.34 to 0.45). A higher between 44 to 59% of that of the Ottawa sand was mobilized in the tests with the relatively softer surface VLDPE geomembrane. For PVC geomembrane the productivity ratio ranged between 70 to 97% of the Ottawa sand at normal stress from 50 kPa to 223 kPa. In conclusion, the interface strength of these smooth

geomembranes was found to be dependent on normal stress levels: the PVC was the most dependent, and the smooth HDPE was the least dependent. Feng and Cheng [9] conducted laboratory tests to obtain the interface shear strength behaviors between geomembrane – soil and geomembrane – geotextile. These experiments were repeated more than once under different normal stresses. A 1.5 mm thick textured HDPE geomembrane and nonwoven geotextile with a mass per unit area of 400 g/m^2 were used. The soil was classified as silty clay with silty sand according to USCS. The shear strength experiments were conducted with a large-scale direct shear and the shear rate was 1 mm/min. For the geomembrane – geotextile interface, one sample was tested under increasing normal stress with the order of 50, 100, and 200 kPa. For geomembrane – soil interface experiments, five specimens were examined three times under constant normal stress of 20, 50, 100, 200, and 300 kPa. One sample was sheared three times at increasing normal stress from 50 to 100 and 200 kPa. The geomembrane – geotextile interface friction angle values were found 19.8º, 18.07º, and 17.45º for the 1st, 2nd, and 3rd repeat, respectively. The geomembrane – soil interface friction angle values were found 10.67º, 9.07º, and 9.00º for the 1st, 2nd, and 3rd repeat, respectively. Geomembranes are exposed to various leachates in storage facilities. These leachates damage the geomembranes over time due to the chemicals they contain. In the literature, there are studies examining the damage of leachates on geomembranes. Stark and Santoyo [21] investigated the interface shear strength behavior between ten geomembranes and two soils. Seven geomembranes are smooth, three are textured and their thickness varies between 0.75 and 1.5 mm. The types of geomembrane used are PVC, HDPE, LLDPE, coated woven polyethylene and polyolefin. The types of soil used were clayey glacial till and Ottawa fine sand. The interface shear strength parameters were measured with a torsional ring shear apparatus and the shear rate was 0.015 mm/min. The results of the experimental study showed that textured geomembranes have a larger interface friction angle than smooth geomembranes. According to clayey glacial till soil tests, the maximum interface friction angle (46º) was obtained tenth GM (textured, 1.5 mm, HDPE). The minimum interface friction angle (14º) was obtained ninth GM (smooth, 1.5 mm, HDPE). According to Ottawa sand soil tests, the maximum interface friction angle (31º) was obtained tenth GM (textured, 1.5 mm, HDPE). The minimum interface friction angle (15º) was obtained second GM (smooth, 1.5 mm, LLDPE). Also, the glacial till/geomembrane interfaces exhibited higher interface friction angles than the Ottawa Sand/geomembrane interfaces. Abdelaal et al. [22] investigated the effect of leachate constituents on the oxidation induction time (OIT) and physical properties of geomembrane. The leachate was obtained by mixing various chemicals in the laboratory to represent municipal solid waste leachate. The geomembranes were kept in glass pools containing these leachates for about 108 months at different temperatures (22, 40, 55, 70, and 85 ºC). Melt index, stress-crack resistance, and OIT tests were performed on the samples that completed the curing period. At the end of 4 months, the OIT value decreased by 98% at 85 ºC and by 40% at 55 ºC. There was a decrease in melting index at 55 ºC to reach almost 0.8 (from 1.0) after 25 months and then the values increase with time to the initial values after 75 months of incubation. Similar trends were obtained at other temperatures. On the other hand, a sharp decrease was observed in the stress-crack resistance at the end of 80 months at 55 ºC, 40 months at 70 ºC, and 12 months at 85 ºC. Gulec et al. [23] examined the effect of acidic mine drainage (AMD) leachate on the mechanical properties of the HDPE geomembrane. The geosynthetic materials were immersed in tanks containing synthetic AMD at 20, 40, or 60 °C over 22 months. According to mechanical test results, that is no temporal changes in wide-strip tensile, puncture, and tear strength are

evident, regardless of the temperature or leachate. Similar results have been reported by Mitchell [24] and Grubb et al. [25] for other geomembranes exposed to AMD.

In this study, the friction angle between the soil and the geomembrane was determined using a medium-scaled direct shear device. Smooth and textured HDPE GM with a thickness of 1.5 mm was used as the GM type. Crushed sand and sand/bentonite mixture (80/20) were used because they are generally used in landfills. In addition, GMs were cured in three different synthetic leachate fluids in a laboratory environment for four months to represent the environment formed in solid waste landfills more meaningfully. These fluids were leachates of municipal solid waste (MSW), coal combustion product (CCP), and acidic mine drainage (AMD). First of all, the geotechnical index parameters and internal friction angles (ϕ) of the soils were determined. Then, the friction angles (δ) of the interfaces formed between the uncured and cured geomembranes and the soils were determined. This study investigated soils and geomembranes with different properties in combination under the influence of various leachates. Shear strength mechanisms were determined and material behavior was evaluated. In addition, laboratory studies were supported by microscopic image analysis. In terms of content, it is thought that study will contribute to the development of both practice and academic studies.

2. MATERIALS

2.1. Soils

Two different soils were used in this study, namely, sand/bentonite (80/20) mixture (SB: particle size 2.0 mm – 0.0 mm) and crushed sand (CS: particle size 2.0 mm – 0.075 mm). The reason why these soils were preferred was that they were frequently used in waste storage areas [26 – 27]. In addition, the effect of grain size was investigated by using such soils. The geotechnical index properties of soils have been listed in Table 1. Image analysis was

Table 1 - Some geotechnical index properties of soils used in this study

Property	Sand/bentonite (SB)	Crushed sand (CS)
Specific gravity, G_s	2.46	2.68
Liquid limit, LL (%)	60.7	-
Plastic limit, PL (%)	30.2	NP
Max. dry unit weight, $\gamma_{dry,max}$ (kN/m^3)	17.0	17.3
Opt. moisture content, w_{opt} (%)	13.2	11.2
D_{10}	-	0.19
D_{30}	0.2	0.69
D_{60}	1.5	1.70
Coefficient of uniformity, C_u	-	8.95
Coefficient of curvature, C_c	-	1.47
USCS	SC	SW

performed with soil particles using the ImageJ software (Figure 1). As a result of the particle analysis, the roundness of the CS soil was obtained as 0.57, while the roundness of the SB soil was obtained as 0.71 (between 0-1).

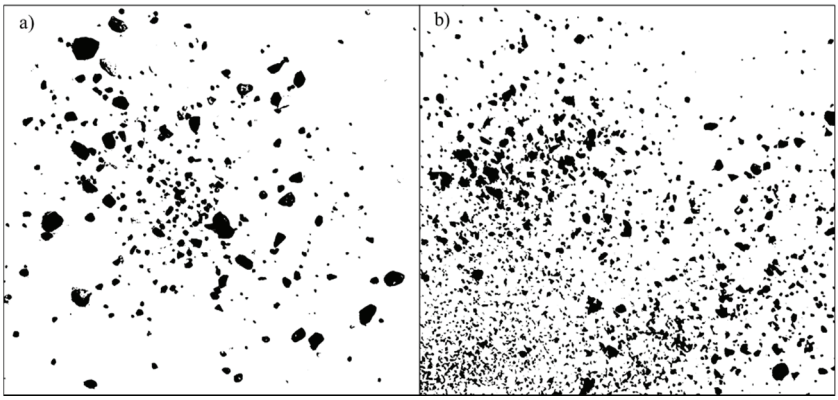

Figure 1 - Image analysis of a) CS, b) SB

2.2. Geomembranes

In this study, smooth (HDPE) and textured (HDPE/T) high-density polyethylenes, which are commercially available, were used. These types of GMs have a high tensile strength at low stresses, low-cost assembly, and long-term weather resistance so they are frequently preferred in applications. Polyethylene (PE) is the name of ethylene in monomer form. Ethylene turns into Polyethylene with several polymerization methods. HDPE geomembrane is a geosynthetic liner formed as a result of the extrusion of high-density polyethylene and shaped homogeneously. HDPE GMs are used for sealing in projects such as mine waste landfills, tank fields, municipal solid waste landfills, acid tanks, ponds, and irrigation canals. The properties and physical appearance of these GMs given by the manufacturer have been listed in Table 2.

Table 2 - Some characteristics of geomembranes used in this study

Essential characteristics	Unit	HDPE	HDPE/T
Thickness	mm	1.5	1.5
Stress crack resistance	h	>200	>200
Elongation at yield	%	>12	>12
Tensile stress at break	N/mm^2	>26	>26
Elongation at break	%	>700	>700
Water permeability	$m^3/m^2.d$	$<10^{-6}$	$<10^{-6}$
Resistance to weathering	%	<25	<25
Oxidation strength	%	<25	<25
Yield strength	N/mm^2	>16	>16
Static puncture resistance	N	3700	7200

2.3. Synthetic Leachates

The synthetic leachates used in this study were produced by mixing various chemical compounds in distilled water, as suggested by Hrapovic [28], Gulec et al. [23], Rowe et al. [29], and Benson et al. [30]. Three different leachates were created synthetically in the laboratory to represent solid waste landfills. These were leachates of municipal solid waste (MSW), coal combustion product (CCP), and acidic mine drainage (AMD). The MSW leachate was a suitable medium for the growth and maintenance of acetogenic, methanogenic, and sulfidogenic bacteria involved in the mineralization stage of anaerobic degradation. Also, the mixture containing only three volatile fatty acids, adjusted to pH = 3.45, was used as a possible variation of landfill leachate [31-34]. The chemical contents of the MSW leachate have been listed in Table 3.

Table 3 - Composition of MSW leachate (Hrapovic [28])

Chemical name	Chemical formula	Amount (per 1 L)
Acetic acid	CH_3COOH	7 mL
Propionic acid	$CH_3CH_2CO_2H$	5 mL
Butyric acid	$C_4H_8O_2$	1 mL
Dipotassium phosphate	K_2HPO_4	30 mg
Potassium bicarbonate	$KHCO_3$	312 mg
Potassium carbonate	K_2CO_3	324 mg
Sodium chloride	NaCl	1440 mg
Sodium nitrate	$NaNO_3$	50 mg
Bicarbonate of Soda	$NaHCO_3$	3012 mg
Calcium chloride	$CaCl_2$	2882 mg
Magnesium chloride hexahydrate	$MgCl_2.6H_2O$	3114 mg
Magnesium sulfate	$MgSO_4$	156 mg
Ammonium bicarbonate	NH_4HCO_3	2439 mg
Urea	$CO(NH_2)_2$	695 mg
Trace metal solution	-	1 mL
Sodium sulfide nonahydrate	$Na_2S.9H_2O$	Titrate to an E_h-120-180 mV
Sodium hydroxide	NaOH	Titrate to a pH 5.8-6.0
Distilled water	H_2O	To make 1 L

The CCP leachates used in this study were identified through analysis of a database containing leachate data from 33 CCP disposal sites compiled by the Electric Power Research Institute (EPRI) [30]. The database included concentrations of major cations and anions, ionic strength, the relative abundance of monovalent and polyvalent cations, pH, and electrical conductivity (EC). It was determined that CCP leachate was slightly alkaline (pH 7.65) as a result of pH measurements. The chemical contents of the CCP leachate have been listed in Table 4.

Table 4 - Composition of CCP leachate (Benson et al. [30])

Chemical name	Chemical formula	Amount (mg)
Potassium sulfate	K_2SO_4	161
Sodium chloride	NaCl	51
Calcium chloride	$CaCl_2$	58
Sodium sulfate	Na_2SO_4	722
Calcium sulfate	$CaSO_4$	987
Magnesium sulfate	$MgSO_4$	146

The composition of AMD was selected by reviewing the composition of 12 AMD for metallic mine waste reported in the literature [33]. In this mixture, the most common metals (Fe, Zn, Cu, and Ca) in AMD, their concentrations and types were determined, relative. Fe, Zn, and Cu are also three of the five most abundant metals extracted from sulfide ores (Fe, Ni, Cu, Pb, and Zn). It was determined that AMD leachate was quite acidic (pH 0.95) as a result of pH measurements. The concentrations of these metals obtained from the literature have been shown in Table 5.

Table 5 - Composition of AMD leachate (Gulec et al. [33])

Chemical name	Chemical formula	Amount (mg)
Copper (II) sulfate	$CuSO_4$	88
Zinc Sulphate Heptahydrate	$ZnSO_4.7H_2O$	864
Sulfuric Acid	H_2SO_4	886
Iron (II) sulfate heptahydrate	$FeSO_4.H_2O$	4076
Calcium sulfate	$CaSO_4$	681

They were replaced by fresh leachate every 2–4 weeks [33]. Direct shear tests were carried out with geomembranes that completed their curing period. When the studies in the literature were examined, it has been shown that there was a change in the mechanical properties of GMs even after 4 months of curing [35].

3. METHODS

3.1. Direct Shear Tests

In the first phase of the laboratory experiments, the internal friction angles of the soils were determined using a medium-scale direct shear box with dimensions of 100 x 100 mm using the conventional direct shear test method according to ASTM D30808 [36], [37 – 40]. The interface friction angle (δ) of the soil – GM interfaces were obtained according to ASTM D5321 [41] using a medium-scale direct shear apparatus, and the test setup is shown in Figure 2.

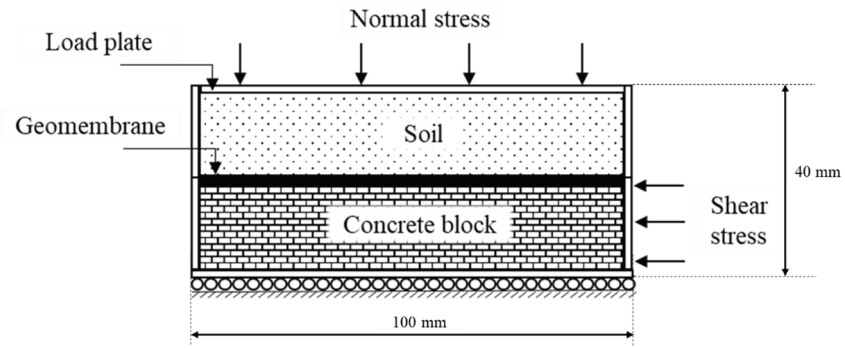

Figure 2 - Test setup of soil – GM interface direct shear test

Concrete blocks were produced in the dimensions of the lower box of the direct shear device, and this concrete block was placed in the lower box since if the soil was placed both above and below the direct shear box, the underlying soil would settle during the experiment and the geomembrane would not remain stable on the shearing surface. The geomembrane was attached to the concrete block with a strong adhesive (Mitreapel instant adhesive) to prevent the geomembrane from moving during the direct shear test. The soil was placed in the upper box of the direct shear device (Figure 3).

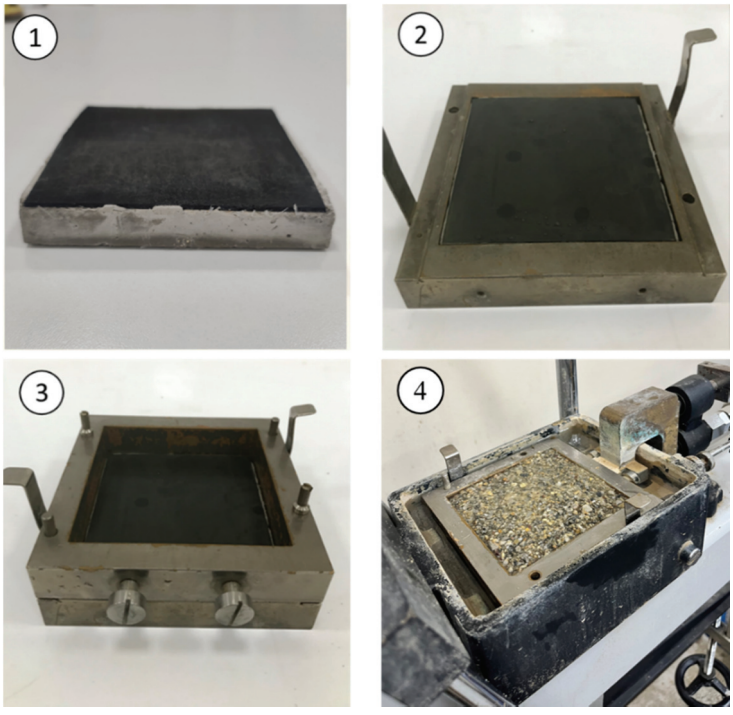

Figure 3 - Sample preparation steps for interface direct shear tests

Samples prepared at optimum water content were placed in the shear box at maximum dry unit weight density. The samples were kept in pore fluid for about two hours to achieve 100% saturation (After the experiments, the saturation degrees of the samples were almost 1). In stage I of the direct shear experiments, uncured geomembranes and tap water (TW) as pore fluid were used. In stage II, the geomembranes were kept in different leachate for 4 months, and then in the direct shear tests, these geomembranes were used. Medium-scale direct shear tests were carried out under the normal stress values of 49, 98, and 196 kPa. The experiments were carried out with a shear rate of 0.5 mm/min due to the very high permeability of CS, and 0.1 mm/min due to the low permeability of SB [20, 42].

3.2. Surface Roughness Measurement

First, Koerner [43] indicated that surface roughness measurements can be used as a textural index or a textural descriptor for manufacturing quality control and construction quality assurance. However, today, high-precision measurement techniques have proven that surface roughness measurements of geomembranes are not only quality descriptors for geomembranes but may be related to various soil-geosynthetic interaction mechanisms. The Optical Profilometer method (OPM) used to measure geomembrane surface roughness is based on the theoretical developments of Gokhale and Underwood [44] and the experimental work of Gokhale and Drury [45]. The surface roughness of the samples was measured with

an optical profilometer (OPM) after direct shear tests to determine the damage caused by the leachates on the surface of the geomembranes. A profilometer is a measuring instrument used to measure a surface's profile, to quantify its roughness. Critical dimensions such as step, curvature, and flatness are computed from the surface topography. The OPM analysis was conducted in Totomak A.Ş. with a profilometer device (Figure 4). Measurements were made from an area of 4 cm^2 in the middle of the geomembrane, both in the shear direction and perpendicular to the shear direction. The R_{max} value was calculated by taking the average of the two measurements.

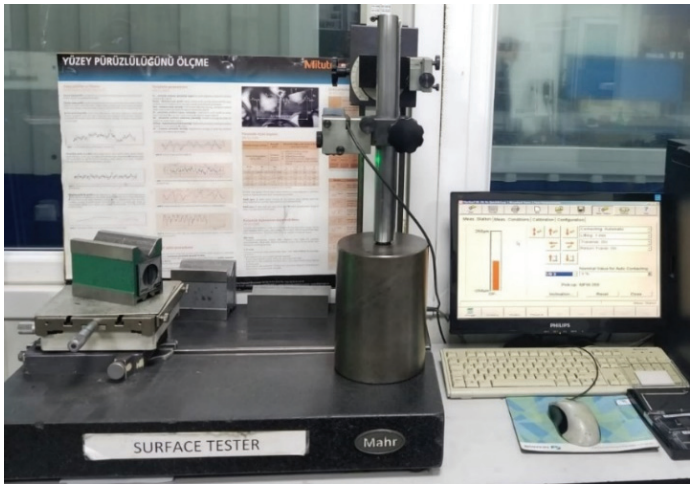

Figure 4 - Profilometer device

4. RESULTS AND DISCUSSION

4.1. Direct Shear Test

In order to determine the shear strength behavior, a conventional direct shear test (soil – soil interface) was carried out with two soils (SB, CS) prepared at the maximum dry unit weight and optimum moisture content under three normal stresses (49, 98, 196 kPa). The initial void ratio and internal friction angles of SB and CS were 0.339, 0.517, and 22.8, 34.7º, respectively. The interface friction angle values of the coarse soils were obtained higher. In the literature, as the particle size increased, the internal friction angle also increased because larger particles would require more frictional force to reach the sliding state and roll after being released at the lock peak [9, 46 – 47].

4.2. Interface Direct Shear Test

Interface direct shear tests were carried out to determine the effect of the particle size, the roughness of GM, and pore fluid on the interface shear behavior between soil – GM. The preparation steps and applied normal stresses of the samples are the same as for the traditional direct shear test. The repeatability of the laboratory experimental results in direct shear and interface direct shear tests was ensured by running two to three trials from multiple tests. The shear stress-strain graphs of soil – HDPE GM and soil – HDPE/T GM have been shown in Figure 5.

In Figure 5, shear stresses at the SB-HDPE interface, all curves up to 1% strain reaches the maximum and at the same time the final value. And there was an increase in shear stress parallel to the increase in normal stress. Shear stresses at the SB-HDPE/T and CS-HDPE/T, the effect of the surface roughness of the geomembrane was seen. The curves increased up to much larger strains, notably the final value for SB was not obtained. This situation can be explained as follows, the notches of the textured GM and the soil particles are interlocked during shearing so that the shear stresses increase for a long time and then take a constant value. On the other hand, in a smooth geomembrane, the soil particles adhere to the GM surface for a while and then slide on the smooth surface, causing shear stresses to increase and then fixate [1, 18, 48]. Also, for two soil types, the soil – HDPE/T shear strength has been determined greater than the soil – HDPE shear strength. This is already an expected result because the roughness on the GM surface increases the friction force and therefore the interface friction angle also increases. The same results were obtained by Vaid and Rinne [49] and Monteiro et al. [50]. The behavior of the smooth HDPE GM was an appearance of little or no hook-and-loop interaction between the soil – smooth HDPE GM. Conversely, at the soil – textured HDPE GM interface there was a significant hook-and-loop interaction and as the roughness increased, additional passive resistances were activated [51]. Envelopes of soil – HDPE and soil – HDPE/T interfaces obtained from shear stress-strain graphs have been presented in Figure 6.

While the interface shear strengths of SB and CS were almost the same at low normal stresses, it is seen that CS had greater shear strengths than SB as the normal stress increased. The shearing resistance of the interface is caused by the sliding, and rolling of soil particles, adhesion, interlocking of soil particles with the GM surface, or embedding of soil particles into the GM. For granular soil-GM, the cohesive force corresponds to the force required to

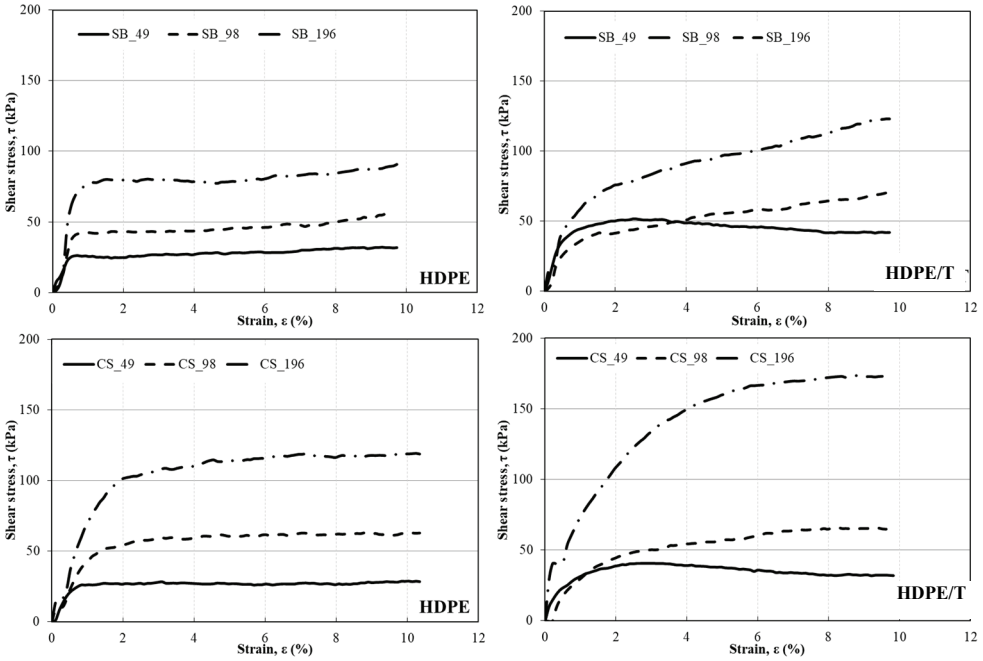

Figure 5 - Shear stress-strain graphs of soil – geomembrane interfaces

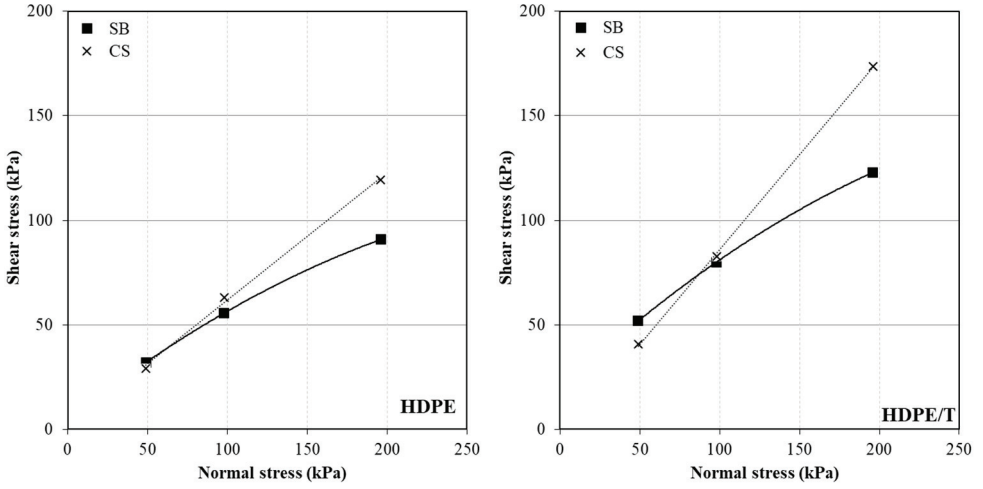

Figure 6 - Mohr-Coulomb failure envelopes of soil – geomembrane interfaces a) HDPE, b) HDPE/T

allow soil particles to slide across the interface. As the normal stress increases, so does the ability of soil particles to plow the GM. Therefore, both sliding and plowing can contribute to the overall frictional force when shearing granular soil-GM. However, the same is not true

for cohesive soils. Even under high normal stresses, they only slide, not plow [52]. This is an explanatory feature for CS with angular particles to have high shear strength. This also explains why the SB-HDPE interface has a parabolic envelope while the CS-HDPE interface has a linear envelope. In the literature, while drawing Mohr-Coulomb failure envelopes, researchers have used linear failure envelopes [53 – 54], while other researchers have to plot curved failure envelopes for cohesive soil-GM interfaces [55 – 56]. Markou and Evangelou [57] obtained the failure envelopes of the cohesive soil-GM as parabolic, while the failure envelopes of the granular soil-GM were linear.

4.3. Effect of Pore Fluid

Geomembranes were stored in different leachates for 4 months in order to examine the effects of leachate generated in landfills on the shear strength parameters of the geomembranes. Interface direct shear tests were performed without curing samples in tap water (TW) and 4 months cured samples in leachates (AMD, CCP, MSW). In addition, the surface roughness of the samples was measured with a profilometer after direct shear tests to determine the damage caused by the leachates on the surface of the geomembranes. R_{max} value, which is a surface roughness coefficient, was obtained from profilometer measurements. A comparison of the interface friction angles and R_{max} values for different pore fluids has been shown in Figure 7.

From Figure 7, it is seen that there is no general trend between the leachate and friction angles. However, in general, AMD was the leachate that most negatively affected the friction angles, while CCP was the leachate that had the least effect. The reason why **AMD** damages the geomembrane is that chemical degradation begins with a change in polymer structure and ends with a change in engineering properties [58]. Diffuse changes in the polymer; a decrease or increase in molecular weight, embrittlement, loss of additives and plasticizers, formation of free radicals, and deterioration of transparency [59]. The reason why **MSW** damages the geomembrane is that oxidative degradation begins. Viebke et al. [60] and Hsuan and Koerner [58] described oxidative degradation as a three-step process. In stage 1, there is no significant change in the engineering properties. Stage 2 is an induction time for degradation to begin and begins after the antioxidants are depleted. In stage 3, there are significant changes in physical and mechanical properties due to oxidation. In this study, it is seen that stage 2 started after a 4-month curing period. The reason **CCP** is less harmful than others is that CCP leachates are inorganic and may have more polyvalent cations and higher ionic strength than MSW [61-62]. It also has a much higher pH than AMD. Therefore, the effect of CCP to damage the mechanical properties of the geomembrane is very low compared to AMD and MSW.

Also from Figure 7, it has been determined that the interface friction angle is inversely proportional to the scratches and grooves formed on the surface during the experiment. In order to see these scratches and grooves more clearly, microscopic images of the geomembranes were obtained after the experiment (Figure 8). While there were no scratches on the geomembrane surface before the experiment, the scratches on the surface were observed after the experiment. In addition, it was determined that the geomembrane at the HDPE-CS interface had deeper and more numerous scratches than the geomembrane at the HDPE-SB interface.

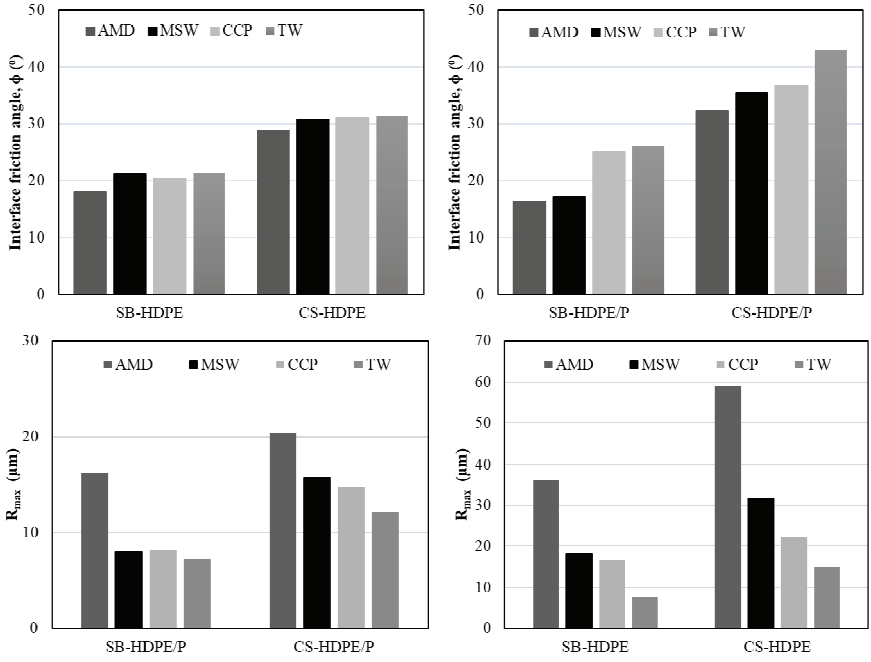

Figure 7 - Interface friction angles and R_{max} values of cured samples

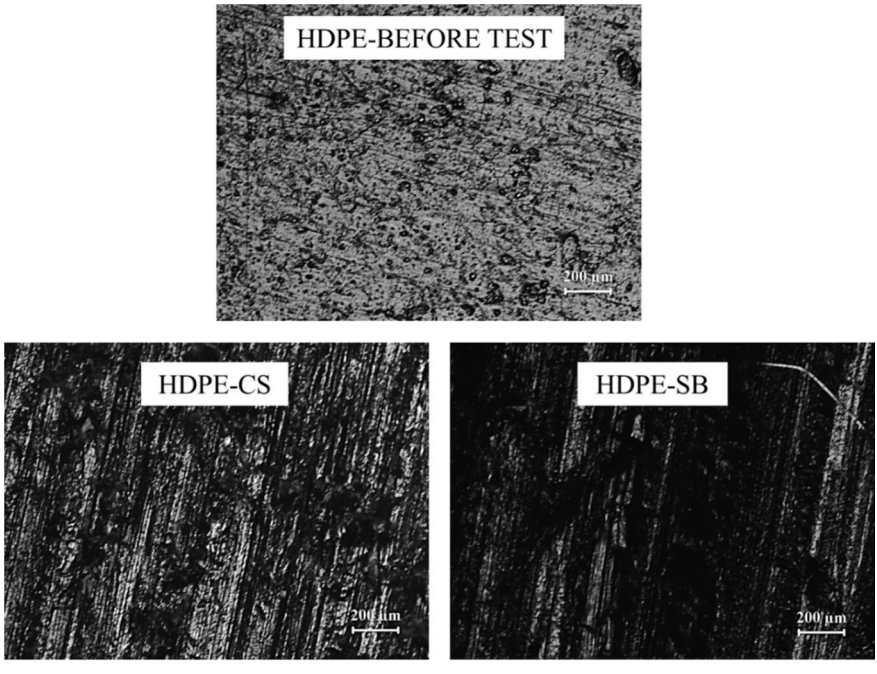

Figure 8 - Microscopic images of HDPE – soil interface

4.4. Effect of Particle Size

The interface friction angle values of soil – HDPE, and soil – HDPE/T GMs have been given in Figure 9. It was found that the interface friction angles of the SB were lower than the CS. Because relatively larger particles need more frictional force to reach sliding conditions and to roll after the release of interlocking [36]. CS is less spherical, less rounded, and less regular compared to SB. These angular sand particles can form deeper grooves and plow to afford a higher interface friction angle [46, 52, 63 – 64]. It has also been reported in studies that higher interfacial friction angle values are obtained at higher dry densities by Fleming et al. [48], Adamska [65], and Khilnani et al. [66],. This is because more soil grains are in contact with the surface of the GM, resulting in increased contact area and accordingly increased interface shear strength. Also, the same conclusion was reached as a result of this study.

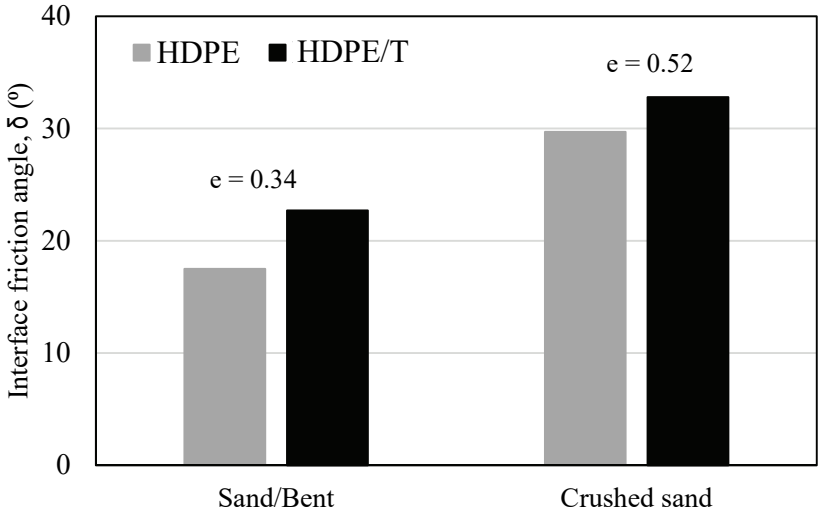

Figure 9 - The interface friction angle values of soil-HDPE and soil-HDPE/P in TW

4.5. Comparison with the Literature Studies

Isaev and Sharafutdinov (2020) investigated the interface shear behavior between clayey and sandy soils and concrete, steel (polished and rough) and polymer surfaces. The R_{int} coefficient was determined by dividing the interface shear strength to the internal shear strength. The coefficients in sandy soil were 0.47-0.78, 0.47, and 0.93 for steel (polished-rough), concrete and polymer, respectively. The coefficients in clayey soil were 0.65, 0.53, and 1.0 for steel (polished), concrete and polymer, respectively [67]. In the present study, the interface-to-internal friction angle ratio of SB-HDPE and CS-HDPE was 0.94 and 0.96 in uncured experiments. The interface-to-internal friction angle ratio of SB-HDPE/T and CS-HDPE/T was 1.17 and 1.19. When compared with the results obtained from this study, it is seen that the closest result is with polymer interfaces. Considering that HDPE GM is a polymer-based material, the results obtained in this study were found to be compatible with the literature. In another study, Cen et al. (2020) investigated the dynamic shear behavior of pure sand and textured and smooth HDPE geomembrane interface. The interface peak shear

strength/internal peak shear strength ratios are 0.61 and 0.89 for smooth and rough GM, respectively [68]. When compared with the results obtained from this study, it is seen that the ratios are lower. This is because the particles of the pure sand used are more rounded and also because the GMs have lower roughness. Cabalar (2016) obtained the interface friction angles between two different sands (Trakya sand [TS] and crushed stone sand [CSS]) and steel, concrete, and wood. The ratio of the interface friction angle to the internal friction angle in TS was obtained as 0.38, 1.06, and 0.81 for steel, concrete, and wood, respectively. The ratio of the interface friction angle to the internal friction angle in CSS was obtained as 0.34, 1.14, and 0.86 for steel, concrete, and wood, respectively [69]. Compared to the results obtained from this study, the concrete interface coefficient is compatible with HDPE/T, while wood is compatible with HDPE.

5. CONCLUSION

In this study the interface shear strength parameters of the soil – geomembrane were investigated. The interface friction angles of the soil – geomembrane interface were obtained with a medium-scale direct shear device. Two types of soils (sand/bentonite mixture, and crushed sand) were used in the tests to investigate the effect of particle size and angularity on the interface friction angle. Smooth and textured HDPE GMs of the same thickness were used to determine the effect of the geomembrane roughness on the interface friction angle. In addition, the interface direct shear tests were also performed with 4 months cured samples in different leachates (AMD, CCP, MSW) to determine the effect of the chemical content of the leachates. As a result of the study:

- The initial void ratio and internal friction angles of SB and CS were 0.34, 0.52, and 23, 35º, respectively.
- In HDPE-soil interface, the minimum interface friction angle (18º) was obtained on AMD cured GM-SB, while the maximum (31º) interface friction angle was obtained on uncured GM-CS.
- In HDPE/P-soil interface, the minimum interface friction angle (17º) was obtained on AMD cured GM-SB, while the maximum (43º) interface friction angle was obtained on uncured GM-CS.
- It was determined that shear stress increased with increasing horizontal displacement in textured HDPE-GM interfaces, but shear stress increased up to a certain horizontal displacement and then remained constant in smooth HDPE-GM interfaces.
- Soils with larger and more angular particles have higher **interface friction angles**.
- While granular soil-geomembrane interfaces have linear Mohr-Coulomb failure envelopes, cohesive soil-geomembrane interfaces have parabolic Mohr-Coulomb failure envelopes.
- In general, it has been determined that the leachate that affects the geomembranes most **adversely** is **AMD**, and the one that affects the geomembranes the **least** is **CCP**.
- It is recommended to avoid the use of smooth and textured HDPE GMs in mine tailing storage facilities using SB and CS.
- It is recommended to use smooth HDPE GMs in coal combustion waste storages and textured HDPE GMs in municipal solid waste storages.

Symbols

AMD	Acidic mine drainage
C_c	Coefficient of curvature
CCP	Coal combustion product
CS	Crushed sand
C_u	Coefficient of uniformity
E	Productivity ratio
EC	Electrical conductivity
GCL	Geosynthetic clay liner
GM	Geomembrane
GS	Geosynthetic
G_s	Specific gravity
HDPE	Smooth high density polyethylene
HDPE/T	Textured high density polyethylene
LDPE	Low density polyethylene
LL	Liquid limit
MSW	Municipal solid waste
OIT	Oxidation induction time
OPM	Optical profilometer
PE	Polyethylene
PL	Plastic limit
PVC	Polyvinyl chloride
SB	Sand/Bentonite mixture
TW	Tap water
USCS	Unified soil classification system
VLDPE	Very low density polyethylene
w_{opt}	Optimum water content
$\gamma_{dry,max}$	Maximum dry density
δ	Interface friction angle
ϕ	Internal friction angle

Acknowledgments

We gratefully thank the companies of Geoplas Plastik Zemin Teknikleri Ve Kimya San.Tic.Ltd.Şti. and Totomak Makina ve Yedek Parça Sanayi ve Ticaret A.Ş.

Funding

This work was supported by the TUBITAK 2211-A education scholarship program.

References

[1] Bonnour, H., Barral, C., Touze-Foltz, N. Altered geosynthetic clay liners: effect on the hydraulic performance of composite liners. Europ. J.. Environ. Civ. Eng., 19(9), 1155 – 1176, 2015. https://doi.org/10.1080/19648189.2015.1005161.

[2] Sabiri ,N.E., Caylet, A., Montillet, A., Le Coq, L., Durkheim, Y. Performance of nonwoven geotextiles on soil drainage and filtration. Europ. J.. Environ. Civ. Eng., 24(5), 670 – 688, 2020. https://doi.org/10.1080/19648189.2017.1415982.

[3] Chen, W., Xu, T., Zhou, W. Microanalysis of smooth Geomembrane–Sand interface using FDM–DEM coupling simulation" Geotext. Geomembr., 49, 276 – 288, 2021. https://doi.org/10.1016/j.geotexmem.2020.10.022.

[4] Pivato, A. Landfill Liner Failure: An Open Question for Landfill Risk Analysis. J. Environ. Protect., 2, 287 – 297, 2017. https://doi.org/10.4236/jep.2011.23032.

[5] Koda, E., Grzyb, M., Osiński, P., Vaverková, M.D. Analysis of failure in landfill and Hydraulic Properties of Three Geosynthetics. J. Geotech. Geoenviron. Eng., 131(8), 937 – 950, 2019.

[6] Pulat, H.F., Yukselen-Aksoy, Y. Compaction behavior of synthetic and natural MSW samples in different compositions. Waste. Manag. Res.: J. Sustain. Circ. Econo, 31(12), 1255 – 1261, 2013. https://doi.org/10.1177/0734242X13507967.

[7] Pulat, H.F., Yukselen-Aksoy, Y. Factors affecting the shear strength behavior of municipal solid wastes. Waste. Manag., 69, 215 – 224, 2017. https://doi.org/10.1016/j.wasman.2017.08.030.

[8] Pulat, H.F., Yukselen-Aksoy, Y. Compressibility and shear strength behaviour of fresh and aged municipal solid wastes. Environ. Geotech., 9(1), 55 – 63, 2022. https://doi.org/10.1680/jenge.18.00019.

[9] Feng, S.J., Cheng, D. Shear strength between soil/geomembrane and geotextile/geomembrane interfaces. Tunneling and Underground Construction, Shanghai, China, 26 – 28 May, 558 – 569, 2014.

[10] Oren, A.H., Ozturk, M., Ozdamar Kul, T., Nart, Z. Barrier performance of geosynthetic clay liners to copper (II) chloride solutions. Environ. Geotech., 7(7), 491 – 500, 2020. https://doi.org/10.1680/jenge.18.00024.

[11] Zhou, L., Zhu, Z., Yu, Z., Zhang, C. Shear Testing of the Interfacial Friction Between an HDPE Geomembrane and Solid Waste. Mater., 13, 1 – 16, 2020. https://doi.org/10.3390/ma13071672.

[12] Ghazizadeh, S., Bareither, C. A. Failure mechanism of geosynthetics clay liner and textured geomembrane composite systems. Geotext. Geomembr., 49, 789 – 803, 2021. https://doi.org/10.1016/j.geotexmem.2020.12.009.

[13] Seed, R. B., Mitchell, J. K., Seed, H. B. Slope Stability Failure Investigation: Kettleman Hills Repository Landfill Unit B-19, Phase IA. Berkeley, California: University of California, 1988.

[14] Brachman, R. W. I., Sabir, A. Geomembrane puncture and strains from stones in an underlying clay layer. Geotext. Geomembr., 28(4), 335-343, 2010.

[15] Noval, A. M., Blanco, M., Castillo, F., Leiro, A., Mateo, B., Zornberg, J. G., Aguiar, E., Torregrosa, J. B., Redon, M. Long-term Performance of the HDPE Geomembrane at the "San Isidro" Reservoir. In Proc. 10th Int. Conf. Geosynth., Berlin, Germany, 2014.

[16] Lambert, S., Touze-Foltz, N. A test for measuring permeability of geomembranes. In Proc. 2nd Europ. Geosynth. Conf., Berlin, Germany, 2000.

[17] Das B. M. 2007. Principles of foundation engineering. Sixth edition. Canada: Thomson, 1997.

[18] Effendi, R. Interface friction of smooth geomembranes and Ottawa sand. Info Teknik, 12 (1), 61 – 72, 2011.

[19] Punetha, P., Mohanty, P., Samanta, M. Microstructural investigation on mechanical behavior of soil – geosynthetic interface in direct shear test. Geotext. Geomembr., 45, 197 – 210, 2017. https://doi.org/10.1016/j.geotexmem.2017.02.001.

[20] Chai, J. C., Saito, A. Interface shear strengths between geosynthetics and clayey soils. Int. J. Geosyn. Groun. Eng., 2 (19), 3 – 9, 2016. https://doi.org/10.1007/s40891-016-0060-8.

[21] Stark, T. D., Santoyo, R. F. Soil/Geosynthetic Interface Strengths from Torsional Ring Shear Tests. In Proc. Geotech. Front., Orlando, Florida, 2017.

[22] Abdelaal, F., Rowe, R. K., Brachman, R. W. I. Brittle rupture of an aged HDPE geomembrane at local gravel indentation under simulated field conditions. Geosynt. Int., 21(1), 2014. https://doi.org/ 10.1680/gein.13.00031.

[23] Gulec, B. S., Benson, C. H., Edil, T. B. Effect of Acidic Mine Drainage on the Mechanical construction elements. MATEC Web of Conferences, 284, 2005. https://doi.org/10.1051/matecconf.

[24] Mitchell, J. K., Seed, R. B., Seed, H. B. Kettleman Hills waste landfill slope failure. I: Liner-System Properties. J. Geotech. Eng., 116 (4): 647 – 668, 1990. https://doi.org/10.1061/(ASCE)0733-9410(1990)116:4(647).

[25] Grubb, D., Cheng, S., Diesing, W. High altitude exposure testing of geotextiles in the Peruvian Andes. Geosynthet. Int., 6(2), 119 – 144, 1999.

[26] Ozdamar Kul, T., Oren, A.H. Geosentetik Kil Örtü Hidrasyon Yönteminin Alt Zemin Koşullarına Bağlı Olarak Değerlendirilmesi. Tek. Der., 504, 8385 – 8409, 2018. https://doi.org/10.18400/tekderg.378245.

[27] Polat, F., Ozdamar Kul, T., Oren, A.H. Influence of Mass Per Unit Area on the Hydraulic Conductivity of Geosynthetic Clay Liners (GCLs). Eur. J. Sci. Tech., 28, 1269 – 1273, 2021. https://doi.org/10.31590/ejosat.1013103.

[28] Hrapovic, L. Laboratory Study of Intrinsic Degradation of Organic Pollutants in Compacted Clayey Soil. PhD thesis, The University of Western Ontario, 300, 2001.

[29] Rowe, R. K. Rimal, S. Aging of HDPE Geomembrane in Three Composite Landfill Liner Configurations. J. Geotech. Geoenviron. Eng., 134(7), 906 – 916, 2008.

[30] Benson, C., Chen, J., Likos, W., Edil, T. Hydraulic Conductivity of Compacted Soil Liners Permeated with Coal Combustion Product Leachates. J. Geotech. Geoenviron. Eng., 144(4), 2018.

[31] Rowe, R.K., Rimal, S., Sangam, H. Ageing of HDPE geomembrane exposed to air, water and leachate at different temperatures. Geotext. Geomembr., 27(2), 137 – 151, 2009. https://doi.org/10.1016/j.geotexmem.2008.09.007.

[32] Xie, H., Lou, Z., Chen, Y., Jin, A., Zhan, T.L., Tang, X. An analytical solution to organic contaminant diffusion through composite liners considering the effect of degradation. Geotext. Geomembr., 36, 10 – 18, 2013. https://doi.org/10.1016/j.geotexmem.2012.10.007.

[33] Gulec, S. Effect of acid mine drainage on the properties of geosynthetics." PhD dissertation, Univ. of Wisconsin-Madison., Madison, Wis, 2003.

[34] Rowe, R. K., Islam, M. Z., Hsuan, Y. G. Effects of Thickness on the Aging of HDPE Geomembranes. J. Geotech. Geoenviron. Eng., 136 (2): 299-309, 2010. https://doi.org/10.1061/(ASCE)GT.1943-5606.0000207.

[35] Maisonneuve, C., Person, P., Duquenno, C., Morin A. Accelerated aging tests for geomembranes used in landfills. Sixth International Landfill Symposium, 207 – 216, 1997.

[36] ASTM (American Society for Testing and Materials). 2011. Standard Test Method for Direct Shear Test of Soils Under Consolidated Drained Conditions. ASTM D 3080/3080M – 11. West Conshohocken, PA: ASTM.

[37] Dadkhah, R., Ghafoori, M., Ajalloeian, R., Lashkaripou,r G. R. The effect of scale direct shear test on the strength parameters of clayey sand in Isfahan City, Iran. J. App. Sci., 10 (18), 2027 – 2033, 2010. https://doi.org/10.3923/jas.2010.2027.2033.

[38] Sobol, E., Sas, W., Szymanski, A. Scale effect in direct shear tests on recycled concrete aggregate. Stud. Geotech. Mech., 37 (2), 45 – 49, 2015. https://doi.org/10.1515/sgem-2015-0019.

[39] Mohapatra, S. R., Mishra, S. R., Nithin, S., Rajagobal, K. Effect of Box Size on Dilative Behaviour of Sand in Direct Shear Test. In Proc. Ind. Geotech. Conf., 16, 111 – 118: Chennai, India, 2016. https://doi.org/10.1007/978-981-13-0899-4_14.

[40] Zahran, K., El Naggar, H. Effect of Sample Size on TDA Shear Strength Parameters in Direct Shear Tests. Trans. Res. Rec., 2674 (9), 1110 – 1119, 2020. https://doi.org/10.1177/0361198120934482.

[41] ASTM (American Society for Testing and Materials). 2020. Standard Test Method for Determining the Shear Strength of Soil – Geosynthetic and Geosynthetic – Geosynthetic Interfaces by Direct Shear. ASTM D 5321/5321M – 20. West Conshohocken, PA: ASTM.

[42] Shi, J., Shu, S., Qian, X., Wang, Y. Shear strength of landfill liner interface in the case of varying normal stress. Geotext. Geomembr., 48, 713 – 723, 2020. https://doi.org/10.1016/j.geotexmem.2020.05.004.

[43] Koerner, R. M., Martin, J. P., Koerner, G. R. Shear strength parameters between geomembranes and cohesive soils. Geotext. Geomembr., 4(1), 21 – 30, 1986. https://doi.org/10.1016/0266-1144(86)90034-8.

[44] Gokhale, A. M. Underwood, E. E. A General Method for Estimation of Fracture Surface Roughness: Part 1. Theoretical Aspects. Metal. Trans. A, 21A, 1193 – 1199, 1990.

[45] Gokhale, A. M. Drury, W. J. A General Method for Estimation of Fracture Surface Roughness: Part II. Practical Considerations. Metal. Trans. A., 21A, 1201 – 1207, 1990.

[46] Vangla, P., Gali, M. L. Shear behavior of sand – smooth geomembrane interfaces through micro – topographical analysis. Geotext. Geomembr., 44, 592 – 603, 2016. https://doi.org/10.1016/j.geotexmem.2016.04.001.

[47] Marcotte, B. A., Fleming, I. R. Direct measurement of geomembrane strain from aggregate indentations. Geosynt. Int., 0 (0), 1 – 54, 2021. https://doi.org/10.1680/jgein.21.00027.

[48] Liu, F., Ying, M., Yuan, G., Wang, J., Gao, Z., Ni, J. Particle shape effects on cyclic shear behaviour of the soil-geogrid interface. Geotext. Geomembr., 49, 991 – 1003, 2021. https://doi.org/10.1016/j.geotexmem.2021.01.008.

[49] Vaid, Y. P., Rinne, N. Geomembrane coefficients of interface friction. Geosynt. Int., 2(1), 309 – 325, 1995.

[50] Monteiro, C. B., Araújo, G. L. S., Palmeira, E. M., Cordão Neto, M. P. Soil-geosynthetic interface strength on smooth and texturized geomembranes under different test conditions. In Proc. Int. Conf. Soil Mech. Geotech. Eng., 3053 – 3056, Paris, France, 2013.

[51] Adeleke D., Kalumba D., Nolutshungu L., Oriokot J., Martinez A. The Influence of Asperities and Surface Roughness on Geomembrane/Geotextile Interface Friction Angle. Int. J. Geosynth. Ground Eng., 7(20), 1 – 12, 2021.

[52] Zettler, T. E., Frost, J. D., DeJong, J. T. Shear-induced changes in smooth HDPE geomembrane surface topography. Geosynt. Int., 7(3), 243 – 267, 2000. https://doi.org/10.1680/gein.7.0174.

[53] Ling, H. I., Pamuk, A., Dechasakulsom, M., Mohri, Y., Burke, C. Interactions between PVC geomembranes and compacted clays. J. Geotech. Geoenviron. Eng., 127, 950 – 954, 2001. https://doi.org/10.1061/(ASCE)1090-0241(2001)127:11(950).

[54] Yamsani, S. K., Sreedeep, S., Rakesh, R. R. Frictional and interface frictional characteristics of multi-layer cover system materials and its impact on overall stability. Int. J. Geosynth. Gro. Eng., 2(23), 2 – 9, 2016. https://doi.org/10.1007/s40891-016-0063-5.

[55] Esterhuizen, J. J. B., Filz, G. M., Duncan, J. M. Constitutive behavior of geosynthetic interfaces." J. Geotech. Geoenviron. Eng., 127, 834 – 840, 2001. https://doi.org/10.1061/(ASCE)1090-0241(2001)127:10(834).

[56] Stark, T. D., Niazi, F. S., Keuscher, T. C. Strength envelopes from single and multigeosynthetic interface tests. Geotech. Geo. Eng., 33, 1351 – 1367, 2015. https://doi.org/10.1007/s10706-015-9906-4.

[57] Markou, I. N., Evangelou, E. D. Shear Resistance Characteristics of Soil–Geomembrane Interfaces. Int. J. Geosynth. Gro. Eng., 4(29), 1 – 16, 2018. https://doi.org/10.1007/s40891-018-0146-6.

[58] Hsuan, Y., Koerner, R. Antioxidant depletion lifetime in high density polyethylene geomembranes. J. Geotech. Geoenviron. Eng., 124(6), 532 – 541, 1998. https://doi.org/10.1061/(ASCE)1090-0241(1998)124:6(532).

[59] Kulshreshtha, A. Chemical degradation. Handbook of polymer degradation, Dekker, New York, 55–95, 1992.

[60] Viebke, J., Elble, E., Ifwarson, M., Gedde, U. W. Degradation of unstabilized medium-density polyethylene pipes in hot-water applications. Polymer Eng. Sci., 34(17), 1354 – 1361, 1994. https://doi.org/10.1002/PEN.760341708.

[61] Benson, C., Chen, J., Edil, T. Engineering properties of geosynthetic clay liners permeated with coal combustion product leachates. Rep. No. 3002003770, Electric Power Research Institute, Palo Alto, CA, 2014.

[62] Salihoglu, H., Chen, J., Likos, W., Benson, C. Hydraulic conductivity of bentonite-polymer geosynthetic clay liners in coal combustion product leachates. Proc., Geo-Chicago 2016: Sustainable Geoenvironmental Systems, ASCE, Reston, VA, 438–448, 2016.

[63] Frost, J. D., Kim, D., Lee, S. W. Microscale geomembrane-granular material interactions. KSCE J. Civ. Eng, 16 (1), 79 – 92, 2012. https://doi.org/10.1007/s12205-012-1476-x.

[64] Cen, W. J., Wang, H., Fe, Y. J. Laboratory investigation of shear behavior of high – density polyethylene geomembrane interfaces. Polymers, 10, 1 – 14, 2018. https://doi.org/10.3390/polym10070734.

[65] Adamska, K. Z. Water content – density criteria for determining geomembrane – fly ash interface shear strength. In Proc. MATEC Web of Conferences, 262, 1 – 8, 2018. https://doi.org/10.1051/matecconf/201926204005.

[66] Khilnani, K., Stark, T. D., Bahadori, T. M. Comparison of Single and Multi Layer Interface Strengths for Geosynthetic/Geosynthetic and Soil/Geosynthetic Interfaces. Geotech. Front., 276, 2017. https://doi.org/10.1061/9780784480434.005.

[67] Isaev, O. N., Sharafutdinov, R. F. Soil Shear Strength at the Structure Interface. Soil Mech. Found. Eng., 57(2), 139 – 146, 2020.

[68] Cen, W. J., Wang, H., Yu, L., Rahman, M. S. Response of High-Density Polyethylene Geomembrane–Sand Interfaces under Cyclic Shear Loading: Laboratory Investigation. Int. J. Geomech., 20(2), 1 – 15, 2020.

[69] Cabalar, A. F. Cyclic Behavior of Various Sands and Structural Materials Interfaces. Geomech. Geoeng., 10(1), 1 – 19, 2016.

Turkish Journal of Civil Engineering, 2023 57-75, Paper 725, ***Research Article***

Identification of Dispute Sources in the Construction Industry via Court Files

Murat ÇEVİKBAŞ[1]

ABSTRACT

Contracting parties generally tend to resolve their disputes through the litigation process. The lengthy litigation process reduces the belief among the parties that the disputes are resolved peacefully, and this destabilizes the sustainable structure of the construction industry where disputes are very common. Determining the most common sources of disputes in construction lawsuits is very important in terms of taking necessary precautions beforehand. Additionally, increasing the competency levels of construction and judicial actors regarding construction processes is extremely important in terms of making the judicial process more efficient and faster. Therefore, this study aims to reveal the most frequent dispute sources in the construction industry, the competency levels of judicial actors including expert witnesses and the average duration of the construction-related litigation process for the superior courts. Hence, 346 construction-related lawsuits conducted between 2018 and 2021 were examined via content analysis to classify the common themes. Lawsuits were investigated via the official websites of Courts of Cassation and National Judicial Network Information System (UYAP). Next, the frequency analysis was conducted to detect the significance of each theme via SPSS software. It is highly believed that this study will enable the decision-makers to take necessary precautions before the dispute occurs as well as improve the dispute resolution process in the construction industry. Projects related to superstructure works constituted the majority of the disputes ending up with the judicial process. Additionally, the majority of the disputes detected from lawsuits resulted from "Debit and Credit" related issues. Moreover, the litigation process was also detected as a very lengthy process. Furthermore, it is detected that majority of the lawsuits were rejected by the Courts of Cassation due to inadequacies of the competency levels of the judicial actors.

Keywords: Dispute, dispute resolution, contract, construction.

1. INTRODUCTION

Involving numerous stakeholders, construction projects aim to achieve desired quality, cost and time in accordance with the project contract with the help of limited resources [1]. Having

Note:
- This paper was received on July 2, 2022 and accepted for publication by the Editorial Board on December 16, 2022.
- Discussions on this paper will be accepted by May 31, 2023.
- https://doi.org/10.18400/tjce.1224425

1 Isparta University of Applied Science, Department of Civil Engineering, Isparta, Türkiye
muratcevikbas@isparta.edu.tr - https://orcid.org/0000-0002-8421-6591

commercial relations carried out by over 200 industries, the construction sector [2] has played a significant role in the economic growth of countries [3]. However, due to the complicated nature of construction projects, change is inevitable [4], [5]; thus, the relationship that commences positively between the parties is likely to deteriorate over time [6]. As a result of this, most of the projects end up with disputes for which contracting parties are liable to settle in a timely manner in order not to undermine their commercial relationships [7]. The contracting parties generally tend to resolve their disputes through litigation process which takes a long time as a result of many factors, and thus projects may lose both time and money [8]. The lengthy litigation process reduces the belief in resolving the dispute peacefully in the eyes of the contracting parties [9] and this destabilizes the sustainable structure of the construction industry where disagreements are very common.

Increasing the efficiency and competency levels of the construction and judicial actors related to construction proceedings are extremely essential for the judicial process to be more effective and rapid [10]. Additionally, developing solutions for dispute prevention is very vital to take the necessary precautions beforehand. Notwithstanding the popularity of the dispute resolution process, studies with respect to the investigation of the litigation process in conjunction with the construction industry in Turkey have been found out as insufficient. Investigating the proceedings until 2007, a study was conducted to spot the frequency of dispute types as per the provisions of Contract of Work in Turkish Code of Obligations, [11]. Later, the competency levels of actors taking part in the judicial process were investigated via semi-structured interviews conducted with 10 expert witnesses [10]. Moreover, the competency levels of judicial actors taking the role in construction-related lawsuits in Turkey were also revealed through semi-structured interviews conducted with judicial actors [12]. Furthermore, in the previous study [13], problematic areas concerning the litigation process were investigated by analysing the leading cases conducted by only Courts of Cassation until 2017. Since 2017, new regulations have been released to improve the judicial process, which has dramatically changed the jurisdiction system as well as the competency levels of judicial actors in Turkey. The main changes being intended to improve litigation process in Turkey have been enacted with respect to Expert Witness [14], establishment of the Regional Courts which started their duty on 20th July 2016 for Building Audit [15]. Since there have been the abovementioned major changes in the litigation process, a comprehensive reinvestigation of the litigation process is extremely crucial to detect the main dispute sources of the construction industry as well as the competency levels of construction and litigation actors. Additionally, awareness of practitioners in the construction industry in terms of the average duration of the litigation process is very vital so as to enable decision-makers in the construction project to compare the litigation process with the other alternative dispute resolution methods. This aids the decision-makers to form the project contract by considering alternative dispute resolution processes. Therefore, in order to lead the construction to take the necessary precautions during the course of the construction projects and improve the competency levels of litigation actors, this study aims to detect the average duration of the litigation process for the superior courts, the most frequent dispute sources in the construction industry and the competency levels of judicial actors. For this reason, 346 appealed construction-related cases conducted between 2018 and 2021 were examined through content analysis in order to categorize the common themes as per the average duration of the lawsuits, the types of projects, the source of disputes and the decisions of the upper courts. Then, the frequency analysis was conducted via SPSS program to determine the magnitude of each

theme under the categorizations. The cases were gathered from the websites of Courts of Cassation and UYAP in which leading cases are provided. It is explicitly believed that spotting the most frequent dispute sources may enable the decision-makers to take necessary precautions in the construction projects in advance. Additionally, judicial actors and lawmakers may take advantage of this research so as to improve the bottlenecks of the litigation process. Moreover, it is believed that this study revealing the average duration of litigation process will definitely rise the success of the dispute resolution process by enabling the practitioners to seek their rights with the help of alternative dispute resolution processes. Furthermore, international construction organizations seeking to make investment in Turkey can benefit from the outputs of this study in terms of the litigation process and its possible outcomes. To evaluate the outputs of this study provided in the section of Conclusions and Recommendations, it is highly believed that foreknowledge concerning the litigation process in Turkey is to be illustrated; hence, a summary of the literature reviews is provided in sections 2 and 3.

2. DISPUTE RESOLUTION PROCESS IN CONSTRUCTION INDUSTRY

Organizations of the jurisdiction system and their roles differ from country to country. In Turkey, there are two main justices, namely judicial and administrative. In addition to this, there are three levels of the justice system, namely, Courts of First Instance, Regional Courts and Supreme Courts. Courts of Cassation and Presidency of the Council of State are authorized as Supreme Courts for civil and administrative cases respectively. The Regional Courts (Courts of Appeal) may conduct a new investigation and a legal audit by collecting evidence that has not been collected by the concerned Court of First Instance and may hear witnesses again as well as may conduct a site survey in order to make a determination.

Courts of First Instance under Judicial Justice have two main divisions which are Civil Courts and Criminal Courts. Civil Courts contain Civil Courts of Peace, Civil Courts of General Jurisdiction and Specialized Courts. If the concerned Specialized Courts are not available in a district, Civil Court of General Jurisdiction is authorized. Courts of First Instance concerning administrative justice - which are regulated via Legislations # 4576 [16] and 4577 [17] - are categorized under three main courts which are “Administrative Court”, “Presidency of the Council of State - Chamber Number 1” and “Tax Court”. Most of the decisions given by the Courts of First Instance are rejected by the Regional Courts or Courts of Cassation due to the fact that the boundaries of authority concerning Courts of First Instance are not well known by the construction and judicial actors, and this further extends the duration of the litigation process unnecessarily [10]. Even though appealing brings justice, the prolongation of the process contradicts with Judicial Economy [25] (Article 141), [26] (Article 6), which results in time and money consumption for the dispute parties. The recognition of the boundaries concerning the authority and structure of civil and administrative courts prevents the prolongation of the construction-related cases, thus the organizational structure of courts is comprehensively illustrated in Figure 1, and later their authorizations – which are to be known to interpret the outputs of this study provided in the section of Conclusions and Recommendations - are defined in this chapter.

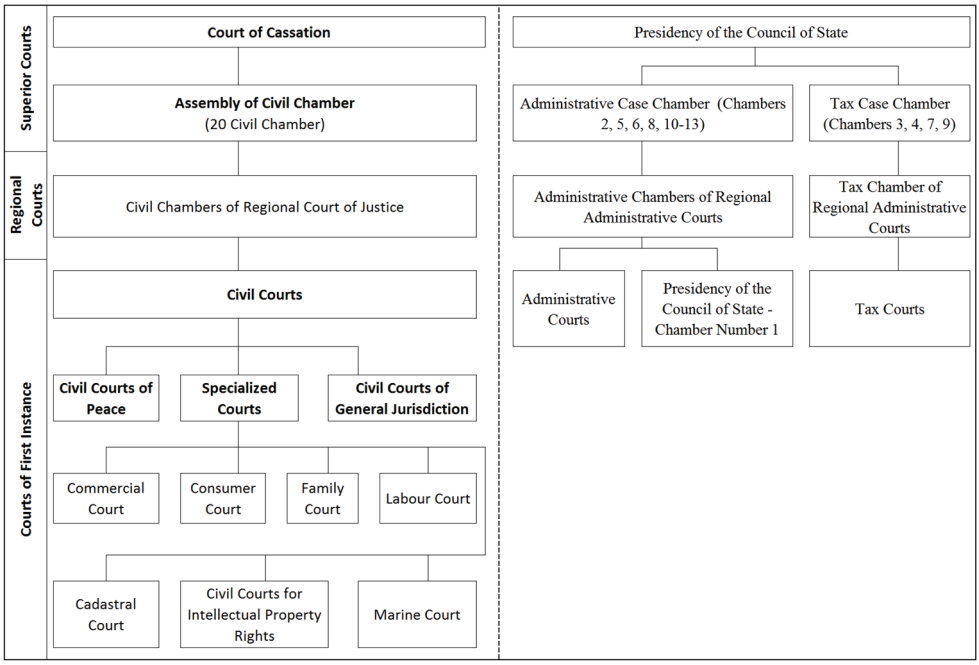

Figure 1 - Organization of Civil and Administrative Justice in Turkey

Administrative Court is authorized in disputes arising between the contracting parties due to administrative contracts made for the execution of one of the public services except for contracts referring to arbitration. Cases related to the tendering processes made by public services and claims concerning misinterpretation and misapplication of the legislation by the public services are conducted by the Administrative Courts. Tax Courts are authorized for the cases concerning tax issues of the organizations. According to articles 1 and 2 in Administrative Trial Procedure Law [18], disputing parties are not invited to the court in the cases conducted by Council of State, District Administrative Courts, Administrative Courts and Tax Courts. Thus, the determination is made as per case documents by the concerning courts. This procedure is also called "Written Trial Procedure". Different opinions have been put forward in the doctrine about whether the written trial procedure applied in our administrative judicial system is fair or not. Some jurists strongly argue that arrangements for the implementation of the oral proceedings should be made in order to demand justice by the concerning parties [19], [20]. Civil courts are empowered to deal with cases concerning property rights and personal property cases that are outside the duties of the peace courts and private law [21]. The Commercial Courts are responsible for conducting all commercial lawsuits, regardless of the value or amount of the subject matter [22]. Mediation is a compulsory process before suing in Commercial Courts. Courts of Peace are authorized in cases such as lawsuits for the sharing of movable and immovable property or rights, ending the partnership, debt of arising from the rental, and mediation issues [23]. Mediation is the prerequisite for suing in commercial courts and labour law [24]; therefore, the majority of

construction-related cases are coordinated in terms of the mediation process by Courts of Peace. According to Article 25/1 of the Cadastral Law No. 3402 [25], The Cadastral Court is authorized for the cases related to property ownership of immovable, land registry, deed annotation, border disputes of lands, and the works imposed by the private laws. The power of Consumer Court granted by consumer rights protection and their duties cover cases regarding disputes that may arise from practices for the consumers [26]. Mostly construction-related cases caused by the selling of the land, dwelling, material and equipment are heard in Consumer Courts. The Labour Courts are empowered to deal with legal disputes such as compensation, employee receivables between workers and the employer or the representative of the employer according to the Labour Courts Law No. 7036 [24]. Mediation is a mandatory process in advance of suing in Labour Courts. The rights of the craftsman are protected under Articles 1 to 3 of the Law of Intellectual Property Rights Number 5846. The utilization and any change of the work produced by a craftsman are subject to the craftsman's permission. In disputes such as the verbal or written form of the works, computer programs, photographs, maps, plans, projects, sketches, all kinds of architectural, urban designs, projects and models arising from this issue, Civil Courts for Intellectual Property are authorized [27].

Majority of the Turkish contract in the construction industry refer directly to the litigation process before applying to an alternative dispute resolution process (ADR) [10]. However, in some special cases such as labour [28], commercial [22] and consumer [26] related cases, mediation is a prerequisite of the application to the litigation process. By the same token, mediation as an ADR method is dictated by law in some special cases in Turkish Construction Industry. In other countries such as Europe and USA, ADR methods are part of the standard form of contracts. In FIDIC contract which is adopted all over the world as well as in Europe, Dispute Adjudication Board (DAB) and arbitration are referred to settle the dispute respectively [29]. In the UK, in New Engineering Contract 4 (NEC4), any dispute is to be referred to adjudication first, before applying to arbitration or litigation, as appropriate [30]. In the USA, The American Institute of Architects (AIA) contract pinpoints Dispute Review Board (DRB) which is known as DAB in FIDIC contract, mediation, arbitration and Initial Decision Maker (IDM) to settle the dispute between the contracting parties [31].

With regard to neutral dispute resolution, court types and their authorizations differ from country to country. Litigation is one of the most common and reliable processes to resolve disputes within the construction industry. In the UK, Technology and Construction Court (TCC) deals with construction dispute cases (e.g., buildings, engineering and surveying). TCC is part of the Queen's Bench Division of the High Court of Justice under the Civil Deviation of the Court of Appeal under the Supreme Court of the United Kingdom. TCC accepts disputes which are over the value of £250,000. The amount which is under this is dealt at the County Court [32]. The fact that there is a court for construction cases is the biggest feature that distinguishes the English court system from the Turkish court system.

In the USA, the federal court structure consists of three main levels which are district courts, also called as trial courts, circuit courts which are the first level of appeal, and the Supreme Court which is the final level of appeal. In the USA, a small percentage of the construction disputes filed end up going to litigation because the majority of the cases are resolved before the litigation process or assigned over to arbitration; therefore, 1 or 2 percent of the cases are carried to the litigation statistically. In the USA, decision-makers in the construction industry

do not elect to have a jury trial. The litigation system in the USA is similar to the Turkish litigation system in terms of having 3 levels of the court hierarchy.

3. TURKISH JUDICIAL SYSTEM

Filing a lawsuit and responding to the filed lawsuit are conducted with a petition. The time for the defendant to respond to the petition begins with the petition of the lawsuit notified to the defendant, and this period is two weeks (HMK m. 127). However, if the defendant party does not submit the rebuttal petition to the court, it is deemed to disclaim all claims of the plaintiff in the petition (HMK m.128). If there is a reply petition by the defendant, 2 weeks is allowed for the claimant to give a rejoinder petition (HMK m.136). The petitions must be written clearly, and evidence and the defence are proved thoroughly to the concerned court (HMK m.129). The claimant should apply to the authorized courts; otherwise, the prerequisite of the case is not fulfilled. Due to missing knowledge concerning the authorization of the courts by construction practitioners as well as judicial actors, numerous numbers of construction-related cases have been rejected by superior courts [13]. These interminable inappropriate acts prolong the hearings and conclude with the time and cost overrun as well as deteriorate the relationships of the contracting parties. In cases of hesitation in the understanding of the court's authority regarding the subject of the case, Regional Courts authorize the relevant Court of First Instance and the Courts of Cassation authorize the relevant Regional Courts (HMK m. 22). If a lawsuit is not filed to the authorized court, the court which is applied gives a decision of rejection of the venue. Plaintiff should apply to the court to take the case to the authorized court within the following two weeks; otherwise, the case is deemed as have not been opened (HMK m.20). The process of Courts of First Instance is illustrated in Figure 2 below.

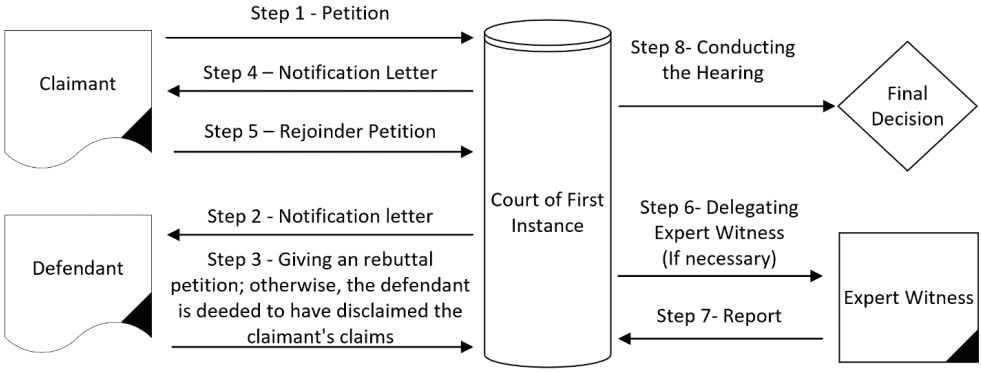

Figure 2 - Process of Courts of First Instance

Courts of First Instance concerning judicial justice consist of Civil Courts of Peace, Civil Courts of General Jurisdiction, and Specialized Courts [21]. Commercial Court, Consumer Court, Family Court, Labour Court, Cadastral Court, Civil Courts for Intellectual Property Rights and Marine Court are categorized under Specialized Courts. Civil Courts of General Jurisdiction are authorized in the case of the absence of Specialized Courts.

Regional Courts of Justice were established for appeal with the law numbered 5235 in 2004 and started their duties in 2016, and thus, judicial justice has become a three-level judicial system [33]. There are 191 Law offices and 177 criminal offices in the Regional Courts of Justice [34]. If the case amount is over the monetary limit which is defined by Article 341 in the Law of Civil Procedure, the parties can apply to Regional Court for an appeal within 2 weeks following the decision of the Courts of First Instance (Hukuk Muhakemeleri Kanunu m.345) [22]. This monetary limit is increased every year by the General Notification of the Tax Procedure Law (HMK Ek Mad. 1) [22]. If the due date of application to the superior court falls into the judicial vacation, the periods are deemed to be extended by one week from the end day of the judicial vacation, without the need for a separate decision (HMK m. 104) [22].

The Courts of Cassation, which is the last review authority in judicial justice, is in charge of reviewing the decisions of Regional Court (Yargıtay Kanunu m.1) [35]. There are twenty-three legal departments in the Courts of Cassation charged with reviewing civil cases, and this number has been changed to twelve in 2016 with the law numbered 6723 [36]; however, this change hasn't come into force. One of the parties can apply to Court of Cassation for an appeal within 2 weeks following the decision of the Regional Court (Hukuk Muhakemeleri Kanunu m.361) [22] as long as the case price is over the monetary limit which is defined by articles 362 and 369 in the Law of Civil Procedure. This price is increased every year by the General Notification of the Tax Procedure Law (HMK Ek Mad. 1) [22]. The case is examined at the General Assembly of Civil Chamber when the Courts of First Instance resist the reversion decision given by the Courts of Cassation. Additionally, General Assembly of Law is authorized when there is a conflict concerning jurisprudence between the civil chambers of courts of cassation and when one of the chambers intends to change a jurisprudence (Yargıtay Kanunu m.15) [35].

During the judicial process, actors such as judges, lawyers and expert witnesses play crucial roles to conduct the hearing most effectively. In Judicial Justice, being a judge requires graduation from an accredited law school, succeeding in a judgeship exam and interview, and being less than thirty-five years old [37], [38]. Justice Academy of Turkey (TAA) established in 2019 [39] provides training programs for judges, judge candidates, notaries and lawyers. Lawyers advocate for their clients in the court and in the other judicial bodies like arbitration, and thus a successful defence is vital for the triumphant hearing [40]. Also, certified lawyers can act as mediators during the mediation process [41]. Being a lawyer entails having an accredited law degree, completing a legal internship and registering in a Bar [40]. In addition to this, the candidates of lawyers, judges and notaries who graduated from law school after 1999 should pass the Entrance Exam for Legal Professions [42]. An expert witness is a natural person who is consulted for an expert report in order to provide technical information about the cases [43]. To be an expert witness, 24 hours of training concerning the proficiency of expert witness requires to be completed by the experts who are experienced in the concerning area for a minimum of 5 years. Every 3 years, 6 hours of theoretical and practical training is to be completed to renew the license of the expert witness.

4. METHODOLOGY

To thwart the negative consequences of the dispute, in this study, it was aimed to determine the average duration of the litigation process in higher courts, the most common disputed areas in the construction industry and the competency levels of judicial actors. Therefore, of 346 construction related lawsuits conducted between 2018 and 2021, 133 Regional Court decisions and 213 Court of Cassation decisions regarding the construction projects were reviewed. The cases were obtained from the official websites of Courts of Cassation and UYAP. To achieve the objective of this study, the reviewed cases were categorized according to the dispute subjects and project types with the help of content analysis. Later, the frequencies of the following comparisons were computed and average duration of the litigation process in higher courts was determined by using frequency analysis with SPSS software: "Project Types versus the number of cases conducted by regional courts and courts of cassation", "The subject of the lawsuits versus the number of cases conducted by regional courts and courts of cassation", "Decision of Appellate Court versus the number of cases conducted by regional courts and courts of cassation", "Decision of Appellate Court versus Subjects of Lawsuits", "Project Types versus Subjects of Lawsuits", "Durations of Proceedings Conducted by Courts of Cassation". The summary of the methodology is illustrated in Figure 3 below.

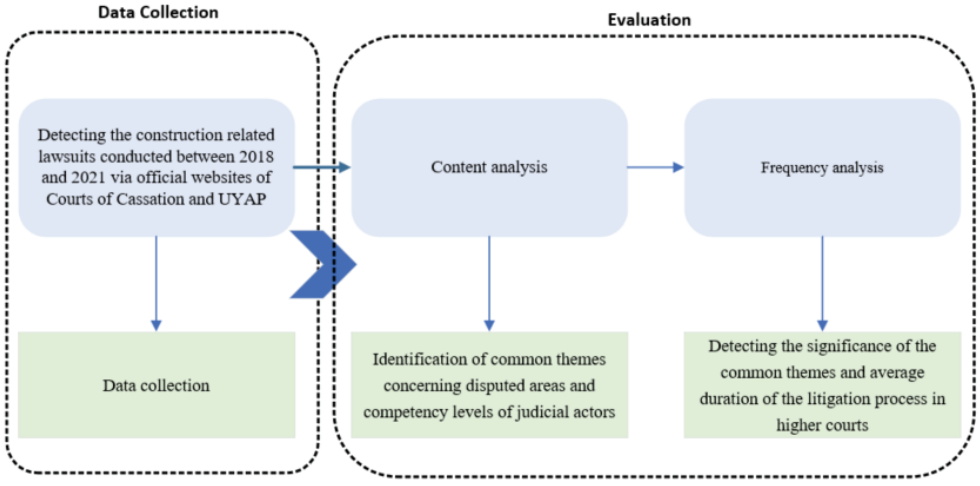

Figure 3 - Summary of Methodology

5. FINDINGS

In the wake of investigating the 346 construction-related cases conducted between 2018 and 2021 with the help of content analysis and frequency analysis, the categorizations of Project Types of the cases and their frequencies as per the number of cases conducted by Regional Courts and Courts of Cassation are depicted in Table 1 below.

Table 1 - Frequencies of Project Types of the Cases Conducted by Regional Courts and Courts of Cassation

Project Types	Number and Frequency of Cases			Average Duration (Year)
	Regional Court	Courts of Cassation	Frequency	Courts of Cassation
Superstructure Works	68	191	75%	1.81
Finishing Works	21	5	8%	2.20
Electrical Works	5	3	2%	2.33
Building Audit Works	1	6	2%	2.67
Infrastructure Works	25	7	9%	1.71
Electrical/Mechanical Works	5	1	2%	1.00
Mechanical Works	3	-	1%	-
Design Works	5	-	1%	-
Total/Average	**133**	**213**	**100%**	**1.84**

At the first glance of Table 1, in construction-related cases, the average duration of Courts of Cassation is 1.84 years. It turns out that the projects with the highest number of disputes are related to the superstructure works which constitute 75% of the total lawsuits. This is followed by Infrastructure works and finishing works with 9% and 8% respectively. Cases related to the "Building Audit Works" were resolved with the longest period of 2.67 years by the Courts of Cassation. The minimum duration of the case conducted by Courts of Cassation was related to Electrical/Mechanical Works, which is 1 year. Comparisons of the subjects of the lawsuits with the number of lawsuits conducted by Regional Courts and Courts of Cassation are tabulated in Table 2 below.

Table 2 - Frequencies of Subjects of the Lawsuits Conducted by Regional Courts and Courts of Cassation

Subjects of the Lawsuits	Number and Frequency of Cases			Average Duration (Year)
	Regional Court	Courts of Cassation	Frequency	Courts of Cassation
Registration and Nullification for Deed and Title	18	62	23%	1.98
Occupational Accident	3	4	2%	2.00
Debit and Credit	79	77	45%	1.70
Termination of Contract	10	21	9%	1.81
Project Delay	12	36	14%	1.89
Defective Products	11	13	7%	1.85
Total/Average	**133**	**213**	**100%**	**1.84**

It is beyond the question that the biggest number of cases was related to monetary issues, which constitute 45% of the total cases. It is followed by Registration and Nullification for Deed and Title (23%) and Project Delay (14%), Termination of Contract (9%), Defective Products (7%) and Occupational Accident (2%). Additionally, while the minimum duration of the cases conducted by Courts of Cassation is higher than 1.7 years, dispute resulting from occupational accidents has a maximum duration of 2 years. Frequency analysis of the decisions made by Regional Courts and Courts of Cassation is given in Table 3 below.

Table 3 - Frequencies of the Decisions made by Regional Courts and Courts of Cassation

Final Decisions of Appellate Courts	**Number and Frequency of Cases**			**Average Duration (Year)**
	Regional Court	**Courts of Cassation**	**Frequency**	**Courts of Cassation**
Reassessment - Unsuitable Case Condition	7	20	8%	2.30
Reassessment - Needs for Expert Judgment	1	2	1%	2.00
Approving the Verdict	31	40	21%	2.75
Reassessment - Decision of Rejection of Venue	51	72	36%	1.03
Reassessment - Missing Review and Wrong Assessment	38	67	30%	1.99
Approving Verdict with a Correction	0	5	1%	2.20
Reassessment - Defective Expert Judgment Report	4	6	3%	1.83
Reassessment - Not Offering Taking an Oath	1	1	1%	3.00
Total/Average	**125**	**191**	**100%**	**1.84**

The reassessment decision concerning the rejection of the venue – which results from the application to the wrong courts by plaintiffs and their lawyers - constitutes the biggest number of lawsuits by 36%. In addition to inadequacy of the knowledge of the lawyers regarding the authorizations of the courts, Judges in the Courts of First Instance heard these cases without rejecting them. It can be inferred from this study that the competency levels of the judicial actors such as lawyers and judges are not adequate in terms of authorizations of the courts. It is followed by the reassessment decisions resulting from Missing Review and Wrong Assessment by 30% due to inadequacies of the judges in terms of construction related cases. Next, Unsuitable Case Condition constitutes 8% of the total cases which also implies the inadequacies of the lawyers and judges in terms of construction related cases. It is followed by Defective Expert Judgment Report by 3%. Not Offering Taking an Oath by 1% and Needs for Expert Judgment by 1%. Only 22.5% of the cases were approved by the Appellate Courts.

Comparing the cases depicted in Table 3, while lawsuits resulting in reassessment decisions due to rejection of venue took a minimum duration which is 1.03 years, lawsuits resulting in reassessment decisions due to not offering to take an oath took a maximum duration which is 3 years. Decisions of Regional Courts and Courts of Cassation are compared with the case subjects as depicted in Table 4 below.

Table 4 - Comparison of the Decisions of Regional Courts and Courts of Cassation with Case Subjects

	Subjects of Lawsuits						
Final Decisions of Appellate Courts	**Debit and Credit**	**Defective Products**	**Project Delay**	**Occupational Accident**	**Termination of Contract**	**Registration and Nullification for Deed and Title**	**Total**
Reassessment - Needs for Expert Judgment	0.3%	0.0%	0.0%	0.3%	0.3%	0.0%	0.9%
Reassessment - Unsuitable Case Condition	3.8%	0.3%	0.3%	0.3%	0.9%	2.3%	7.8%
Reassessment - Missing Review and Wrong Assessment	12.1%	3.2%	5.5%	1.2%	3.8%	4.6%	30.3%
Reassessment - Decision of Rejection of Venue	19.4%	1.2%	4.3%	0.0%	2.0%	9.0%	35.8%
Approving Verdict with a Correction	0.3%	0.0%	0.3%	0.0%	0.0%	0.6%	1.2%
Approving the Verdict	9.0%	0.9%	3.2%	0.3%	1.2%	6.1%	20.5%
Reassessment - Defective Expert Judgment Report	1.4%	0.6%	0.0%	0.0%	0.9%	0.0%	2.9%
Reassessment - Not Offering Taking an Oath	0.0%	0.0%	0.0%	0.0%	0.0%	0.6%	0.6%
Total	46.2%	6.1%	13.6 %	2.0%	9.0%	23.1%	100%

Reassessment decisions were made by Regional Courts and Courts of Cassation for 78.3% of the cases. By the same token, Courts of First Instance made the wrong determination by 78.3%. It is clearly revealed that the competency levels of the actors taking part in the Courts of First Instance have to be improved. The most problematic area is the authorization of courts concerning Debit and Credit related issues, which constitutes 19% of the total cases. Secondly, decisions of Courts of First Instance were rejected by Appellate Courts by 12% for the cases concerning Debit and Credit issues. 9% of the cases related to Registration and

Nullification for Deed and Title were rejected by Appellate Courts due to filing the lawsuit to the unauthorized courts**.** A comparison between the project types and the subject of the lawsuits is illustrated in Table 5 below.

Table 5 - Comparison of the Decisions of Regional Courts and Courts of Cassation with Project Types

Project Types	**Subjects of Lawsuits**						**Total**
	Debit and Credit	**Defective Products**	**Project Delay**	**Occupational Accident**	**Termination of Contract**	**Registration and Nullification for Deed and Title**	
Infrastructure	5.5%	1.4%	1.7%	0.0%	0.3%	0.3%	9.2%
Electrical Works	1.4%	0.3%	0.0%	0.6%	0.0%	0.0%	2.3%
Finishing Works	5.5%	1.2%	0.3%	0.0%	0.0%	0.3%	7.2%
Building Audit Works	0.3%	0.3%	0.9%	0.0%	0.6%	0.0%	2.0%
Superstructure	30.1%	2.9%	10.1%	1.4%	8.1%	22.5%	75.1%
Electrical/Mechanical Works	1.4%	0.0%	0.3%	0.0%	0.0%	0.0%	1.7%
Mechanical Works	0.6%	0.0%	0.3%	0.0%	0.0%	0.0%	0.9%
Design	1.4%	0.0%	0.0%	0.0%	0.0%	0.0%	1.4%
Total	46.2%	6.1%	13.6%	2.0%	9.0%	23.1%	100.0%

30% of the debit and credit-related cases are related to superstructure projects. Also, 23% of the superstructure project related cases were associated with nullification for deed and title. In addition to this, 10% of the cases concerning project delay resulted from superstructure projects. Furthermore, 8% of the total cases related to superstructure works were about the termination of the project contract. When the remaining remarkable figures are examined, 5.5% of the cases relate to debit and credit and finishing works, and 5.5% of the cases are related to debit and credit and infrastructure work. Durations concerning the lawsuits conducted by Courts of Cassation are depicted in Table 6 below.

Table 6 - Durations of Proceedings Conducted by Courts of Cassation

Courts	**Case Duration (Year)**		
	Minimum	**Mean**	**Maximum**
Courts of Cassation	1	1.84	3

As is derived from the study, the cases of the third degree of appellate courts named Courts of Cassation took 1.84 years as average while the longest period of the cases is 3 years and the shortest period of the cases is 1year.

6. DISCUSSIONS

Since project contract is one of the major sources of dispute, the first step to be taken for the prevention of disputes is to form the project contracts thoroughly, correctly and understandably [44], [45]. In the UK, construction actors are also of the opinion that an improved project contract better governs the project management which enables the decision makers to settle the disputes [46]. As is defined in the "Freedom of Form Principle" defined in the Law of Obligations, the contract is not subject to any form unless otherwise stated in the law. However, as is derived from the reviewed lawsuits, most of the contracts of the cases subject to Contract of Work were formed verbally, which ended up with time consumption due to lack of proof.

It is derived from this study that litigation is a long-lasting process and may deteriorate business relationships. This very long process of litigation also contradicts the basic law principle, namely the necessity of concluding cases within a reasonable time, which is also called judicial economy [47], [48].

Superstructure works, finishing works and infrastructure works are the most sensitive projects in terms of the disputes related to monetary issues; therefore, the contracts of these projects are to be clear concerning the debt and credit-related issues [8]. The majority of the disputes in superstructure projects are related to the subjects concerning the nullification for deed and title, project delays and termination of the project contract. Preparation of the project contracts of superstructure projects by considering these subjects is very vital in terms of clarity and covering all project scopes. In addition to contract preparation, managing the contract with the adoption of BIM in construction projects may also enable the practitioners to manage all project scopes thoroughly [49].

One of the most imperative project deliverables to be considered when making a construction contract is project duration; however, it is difficult to accomplish a construction project in which many construction activities are beyond the control of the contractor [50], [51]. It was also detected in this study that most of the projects end up with disputes due to delays in projects. Despite the efforts made by construction practitioners and a great deal of empirical research, construction projects still suffer from delays and the risks of construction delay are global issues, with more than 40% of projects in the construction industry being delayed worldwide [52], [53].

Also, some of the disputes concerning the design work detected in this study were related to intellectual property rights, and these cases were conducted by Civil Courts for Intellectual Property. Concerning the issue of intellectual property rights, most project contract forms do not fully define it although the issue is of interest to project stakeholders [49].

Defective expert witness report is one of the major causes of rejection of the cases by Courts of Cassations, which undermine the litigation process. One of the biggest reasons can be shown as the lack of qualifications of expert witnesses. The experience in lawsuits reveals that numerous expert witnesses are very inadequate to improve themselves in terms of

technology changing rapidly [54]. Secondly, expert witnesses in the construction industry tend to accept all kinds of cases without considering their expertise areas [10].

As is derived from this study, one of the most problematic areas in construction-related cases is the lack of knowledge of construction and law actors concerning the authorizations of the Court of First Instance. Enough law lectures concerning law are not provided in engineering and architectural departments, and availability of little if any lawyers - who specialized in a certain domain - is very problematic. These issues may cause the application of unauthorized courts which can delay the litigation processes further. Also, since construction actors have limited knowledge about the litigation process, the majority of the disputes occurring in the construction projects tend to be carried to the litigation without considering the drawbacks of the litigation process.

The majority of the lawsuits were related to the disputes resulting from debit and credit issues for which Commercial Courts and Civil Courts are authorized. Firstly, the inadequate definitions of the contract terms related to payment may result in dispute among contracting parties. Additionally, inefficiency and ineffectiveness of the mediation process related to commercial cases also increase the number of the debit and credit related lawsuits [13]. It is also asserted in the literature that changes in projects can be overwhelming and have a significant impact on project success and profitability ending up debit and credit related disputes [55]; therefore, changes in construction projects are also to be managed thoroughly.

It was detected that reassessment decisions concerning the rejection of the venue were made by the superior courts due to selecting the wrong courts by plaintiffs resulting from the inadequacies of the knowledge of the lawyers to the authorizations of the courts. Later, substantial numbers of the lawsuits were declined by the superior courts due to missing reviews and wrong assessments performed by the judges. In addition to this, judges in the Courts of First Instance heard these cases without rejecting them. These drawbacks stand for that the competency levels of the judges are also not adequate. Also, reassessment decisions due to unsuitable case conditions imply the inadequacies of the lawyers and judges in terms of construction related cases. Furthermore, a great number of the lawsuits were declined due to the defects in the expert witness reports, which indicate the disqualifications of expert witnesses.

7. CONCLUSIONS AND RECOMMENDATIONS

Having sophisticated nature and involving a high number of stakeholders, construction projects mostly end up with disputes resulting in the litigation process. An in-depth investigation of construction-related lawsuits is extremely important for diminishing the disputes in the construction industry as well as reveal the drawbacks concerning the litigation process related to the construction industry. Hence, this study aimed to divulge the most common dispute causes in the construction industry, the competency levels of judicial actors including expert witnesses and the average duration of the litigation process for the superior courts.

Regional Courts and Courts of Cassation gave reassessment decisions by 78.3% of the cases. Reassessment decision due to rejection of venue constitutes the majority of the rejected lawsuits by superior courts. It is followed by “Missing Review and Wrong Assessment”,

"Unsuitable Case Condition", "Defective Expert Judgment Report", "Needs for Expert Judgment" and "Not Offering Taking an Oath" respectively. To reduce the number of the reassessment decisions, competency levels of judicial actors concerning debit and credit related lawsuits are to be improved in Commercial Courts and Civil Courts. Additionally, participating in the cases conducted by Courts of First Instance, judicial actors' competency levels related to project delay and registration and nullification for deed and title also have to be increased in order to diminish wrong determination of the cases as well as reduce the duration of the litigation process. Next, petitions, rebuttal petitions rejoinder petitions - whose processes are also defined in Figure 2 - have to be written by lawyers whose experiences are closely related to the case subject in order to diminish the number of unsuccessful lawsuits resulting from rejection of venue. Later, the expertise areas of expert witnesses in the construction industry have to be more specific to reduce defective expert witness reports. Also, the qualifications of expert witnesses can be improved by accelerating the training duration and including a final exam in the training program.

The vast majority of construction-related cases arise from projects with superstructure works. It is followed by Infrastructure Works, Finishing Works, Building Audit Works, Electrical Works, Mechanical Works and Design Works. Additionally, with regards to superstructure projects, "Debit and Credit" related disputes constitute the majority of the lawsuits. Furthermore, it is detected that Courts of Cassation rejected majority of the lawsuits related to "Debit and Credit". To improve the dispute resolution process in the construction industry in Turkey, contract terms should be improved in accordance with the subjects concerning debit and credit. Other sources of the disputes - which are Registration and "Nullification for Deed and Title", "Project Delay", "Termination of Contract", "Defective Products" and "Occupational Accident" respectively - are relatively less compared to the debit and credit related cases; however, they are significant and also require to be controlled and monitored closely in construction projects.

Since project contract is one of the sources of the dispute, standard forms of contracts for Turkish construction industry can be formed to reduce contract-related disputes. Also, since construction projects are complex in nature, all contracts in the construction industry should be formed in written or official forms rather than verbal ones to diminish misapprehensions.

Moreover, the litigation process was detected as a very lengthy process. Average duration of litigation process conducted by Courts of Cassations was detected as 1.84 years. As is detected in this study, the dispute resolution process is long; therefore, being defined by Law of Civil Procedure, the monetary limits concerning carrying the cases to the upper courts can be increased in order to reduce the duration of the litigation process. By considering the lengthy litigation process, contracting parties are recommended to consider alternative dispute resolution processes in their contract before seeking their rights through litigation. By the same token, the project contract should refer to the reasonable dispute resolution process to which contracting parties can apply in case of any dispute between the contracting parties instead of directly referring to the litigation process whose prolongation may result in monetary loss and deterioration of relationships. Furthermore, it is also highly suggested that alternative dispute resolution processes such as arbitration, mediation, dispute adjudication process, expert determination and negotiation can be part of the lectures for the Bachelor's Degree in engineering and architecture departments.

To diminish the number of disputes carried to the litigation, it is also recommended that construction law lectures are to be included in the bachelor's degrees of engineering, architecture and law departments. Since delay is one of the major sources of the dispute, employing a scheduler may also contribute to lowering the number of disputes related to project delays by informing the possible delays in advance. Additionally, disputes related to the design work resulted from intellectual property rights which were conducted by Civil Courts for Intellectual Property. To diminish the number of lawsuits, the awareness of construction actors in terms of property rights can be risen by involving this subject in the bachelor's degree in engineering and architecture departments.

This study is unique by investigating dispute domains in the construction industry from law point of view. It is believed that this study will pave the way for improving the constructional dispute resolution process with the help of the outputs of this study. Moreover, this study is also believed to shed light on the improvement of the litigation process by illuminating the possible inadequacies encountered during the course of construction-related proceedings. Furthermore, this study may enable the legislative to improve the legislation concerning Contract of Works in Code of Obligation numbered 6098 in Turkey by considering the abovementioned outputs.

References

[1] E. Taş and Ö. Fırtına, "The use of dispute review boards in construction projects: A comparison of Turkey, UK and US," *A|Z ITU J. Fac. Archit.*, vol. 12, no. 2, pp. 187–204, 2015, [Online]. Available: https://www.journalagent.com/itujfa/pdfs/ITUJFA-74745-THEORY_ARTICLES-TAS.pdf.

[2] V. Kaya, Ö. Yalçınkaya, and İ. Hüseyni, "Ekonomik Büyümede İnşaat Sektörünün Rolü:Türkiye Örneği (1987-2010)," *Atatürk Üniversitesi İktisadi ve İdari Bilim. Derg.*, vol. 27, no. 4, pp. 148–167, 2013, [Online]. Available: https://dergipark.org.tr/tr/download/article-file/30518.

[3] Oxfordbusinessgroup, "Turkey's Construction Sector to Maintain Its Significant Role in the Economy, with Several Large Projects under Way," 2015. https://www.oxfordbusinessgroup.com/turkey-2015 (accessed Nov. 20, 2019).

[4] M. Cevikbas, O. Okudan, and Z. Işık, "Identification and assessment of disruption claim management risks in construction projects: a life cycle-based approach," *Eng. Constr. Archit. Manag.*, 2022, doi: 10.1108/ECAM-05-2022-0470.

[5] D. Artan Ilter and G. Bakioglu, "Modeling the Relationship between Risk and Dispute in Subcontractor Contracts," *J. Leg. Aff. Disput. Resolut. Eng. Constr.*, vol. 10, no. 1, p. 04517022, 2018, doi: 10.1061/(ASCE)LA.1943-4170.0000246.

[6] G. Başyiğit, "Kat Karşiliği İnşaat Sözleşmeleri ve Kat Karşiliği Standart İnşaat Sözleşme Maddeleri Önerisi," Yıldız Teknik Üniversitesi, 2012.

[7] D. Arditi and T. Pulket, "Predicting the Outcome of Construction Litigation Using Boosted Decision Trees," *J. Comput. Civ. Eng.*, vol. 19, no. 4, pp. 387–393, Oct. 2005, doi: 10.1061/(ASCE)0887-3801(2005)19:4(387).

[8] D. Ilter, "Identification of the relations between dispute factors and dispute categories in construction projects," *Int. J. Law Built Environ.*, vol. 4, no. 1, pp. 45–59, 2012, doi: 10.1108/17561451211211732.

[9] H. Hendek, "Adil Yargılanma Hakkının Bir Unsuru Olarak Yargılamaların Makul Sürede Bitirilmesi," Kocaeli Üniversitesi, Kocaeli, 2015.

[10] M. Çevikbaş and A. Köksal, "Evaluation of Litigation Process in Turkish Construction Industry from Expert Witnesses' Perspective," *Mühendislik Bilim. ve Tasarım Derg.*, vol. 6, no. 2, pp. 213–218, Apr. 2018, doi: 10.21923/jesd.403713.

[11] E. C. Apanoğlu and M. E. Öcal, "Türkiye'de inşaat sektöründe yargiya intikal eden süre ve özen borcu kaynaklı anlaşmazlıkların analizi," *Ç.Ü Fen Bilim. Enstitüsü*, vol. 19, no. 1, pp. 123–133, 2008.

[12] M. Çevikbaş and A. Köksal, "Evaluation of Litigation Process in Turkish Construction Industry from the Perspective of Judicial Actors," *Tamap J. Eng.*, vol. 2019, no. 1, pp. 1–7, 2019, doi: 10.29371/2019.3.76.

[13] M. Çevikbaş and A. Köksal, "An Investigation of Litigation Process in Construction Industry in Turkey," *Tek. Dergi*, vol. 29, no. 6, pp. 8715–8730, 2018, doi: 10.18400/tekderg.389757.

[14] Resmi Gazete, *Expert Witness Regulation*. 2017.

[15] Ministry of Environment and Urban Planning, *Yapi Denetimi Uygulama Yönetmeliğinde Değişiklik Yapilmasina Dair Yönetmelik*. Turkey, 2018.

[16] TBMM, *Bölge İdare Mahkemeleri, İdare Mahkemeleri ve Vergi Mahkemelerinin Kuruluşu ve Görevleri Hakkinda Kanun*. Turkey, 1982.

[17] TBMM, *Bölge İdare Mahkemeleri, İdare Mahkemeleri ve Vergi Mahkemelerinin Kuruluşu ve Görevleri Hakkında Kanun ile İdarî Yargılama Usulü Kanununda Değişiklik Yapılmasına Dair Kanun*. 2000.

[18] TBMM, *Administrative Procedure Law*. Türkiye: Resmi Gazete, 1982.

[19] M. Ocak, "İdari Yargıda Duruşmanın Adil Yargılanma Hakkı Açısından İncelenmesi," *TBB Derg.*, vol. 145, pp. 349–367, 2019, Accessed: May 20, 2020. [Online]. Available: http://tbbdergisi.barobirlik.org.tr/m2019-145-1886.

[20] A. Ayhan, "İdari Yargılama Hukukunda İvedi Yargılama Usulü," Dicle Üniversitesi, 2019.

[21] TBMM, *Adlî Yargı İlk Derece Mahkemeleri İle Bölge Adliye Mahkemelerinin Kuruluş, Görev ve Yetkileri Hakkında Kanun*, no. 1. Türkiye: Resmi Gazete, 2004.

[22] TBMM, *Code of Civil Procedure*. Türkiye: Resmi Gazete, 2011, pp. 1–51.

[23] TBMM, *Regulation on Mediation in Civil Disputes*. Türkiye, 2018.

[24] TBMM, *Labor Courts Law*. Türkiye, 2017.

[25] TBMM, *Cadastral Law*. Türkiye, 1987.

[26] TBMM, *Law on Consumer Protection*. Türkiye, 2013.

[27] TBMM, *5846 Sayılı Fikir ve Sanat Eserleri Kanununun Bazı Maddelerinin Değiştirilmesine İlişkin Kanun*. Türkiye, 1995.

[28] TBMM, *Labor Law*. Turkey, 2003.

[29] A.-V. Jaeger and G.-S. Hok, *FIDIC-A Guide for Practitioners*, vol. 3. Springer London, 2015.

[30] A. Garrett, "Latest legal publications," *Mills & Reeve*, 2017. https://www.mills-reeve.com/insights/publications/nec4-what-s-new-in-the-resolution-of-disputes (accessed Dec. 03, 2022).

[31] AIA, "Understanding Different Methods of Dispute Resolution," *AIA*, 2021. https://www.aia.org/articles/6456563-understanding-different-methods-of-dispute (accessed Dec. 03, 2022).

[32] HM Courts & Tribunals Service, "Technology and Construction Court," 2022. https://www.gov.uk/courts-tribunals/technology-and-construction-court (accessed Dec. 02, 2022).

[33] Adalet Bakanlığı, "Bölge Adliye Mahkemeleri ve Bölge İdare Mahkemelerinin Tüm Yurtta Göreve Başlayacakları Tarihe İlişkin Karar," 2015. [Online]. Available: https://www.resmigazete.gov.tr/eskiler/2015/11/20151107.htm.

[34] Hakimler ve Savcılar Kurulu, "Adli ve İdari Yargı Listesi," 2016. https://www.hsk.gov.tr/Adli-Idari-Yargi-Listesi.aspx (accessed Dec. 11, 2019).

[35] TBMM, *Courts of Cassation Law*, no. 1. Türkiye: Resmi Gazete, 1983, pp. 5579–5608.

[36] TBMM, *Law on the Amendment of the Law on the Council of State and Some Laws*. Türkiye: Resmi Gazete, 2016.

[37] TBMM, *Law on Judges and Prosecutors*. Türkiye, 1983.

[38] TBMM, *Law Amending the Law on Judges and Prosecutors and Some Laws and Decrees*. Türkiye, 2014.

[39] Cumhurbaşkanlığı Karranamesi, *Türkiye Adalet Akademisi Hakkında Cumhurbaşkanlığı Kararnamesi*. 2019.

[40] TBMM, *Attorneyship Law*. Türkiye, 1969.

[41] TBMM, *Mediation Law in Civil Disputes*. Türkiye: Resmi Gazete, 2012, pp. 1–11.

[42] N. Ömeroğlu, "Af Yasası(1. ve 2. Yargı Paketinde Ne Gibi Yasal Düzenlemeler Var)," *Hukiki Haber*, 2019. https://www.hukukihaber.net/af-yasasi-1-ve-2-yargi-paketinde-ne-gibi-yasal-duzenlemeler-var-makale,7115.html?fbclid=IwAR1uF8X9uCEc3mcnpqRwGJyp2AKx-It8CfyUi1tjktKAyriFxx-JSlOIAmk (accessed Nov. 05, 2019).

[43] TBMM, *Expert Witness Law*. Türkiye, 2016.

[44] Ç. Çamcı, "Kamu Inşaatlarında Ortaya Çıkan Uyuşmazlıklar: Örnek Kararlar Işığında Uyuşmazlık Nedenlerinin İncelenmesi," Anadolu Üniversitesi, 2008.

[45] O. Durrah, "Structural Equation Model of Construction Contract Dispute Potential," *J. Constr. Eng. Manag.*, vol. 35, no. March, pp. 359–372, 2018.

[46] R. M. Thompson, M. C. Vorster, and J. P. Groton, "Innovations to Manage Disputes: DRB and NEC," *J. Manag. Eng.*, vol. 16, no. 5, pp. 51–59, 2000, doi: 10.1061/(asce)0742-597x(2000)16:5(51).

[47] TBMM, *Constitution of the Republic of Turkey*, no. 1. Türkiye: Resmi Gazete, 1982.

[48] "Avrupa İnsan Hakları Sözleşmesi," 1950. [Online]. Available: https://www.danistay.gov.tr/upload/avrupainsanhaklarisozlesmesi.pdf.

[49] A. H. Abd Jamil and M. S. Fathi, "Enhancing BIM-Based Information Interoperability: Dispute Resolution from Legal and Contractual Perspectives," *J. Constr. Eng. Manag.*, vol. 146, no. 7, pp. 1–12, 2020, doi: 10.1061/(asce)co.1943-7862.0001868.

[50] C. A. Mikhail and E. Serag, "Quantifying the Delay from Lost Productivity," *J. Leg. Aff. Disput. Resolut. Eng. Constr.*, vol. 11, no. 4, pp. 05019005-1–10, 2019, doi: 10.1061/(asce)la.1943-4170.0000322.

[51] I. Ndekugri, N. Braimah, and R. Gameson, "Delay Analysis within Construction Contracting Organizations," *J. Constr. Eng. Manag.*, vol. 134, no. 9, pp. 692–700, 2008, doi: 10.1061/(ASCE)0733-9364(2008)134:9(692).

[52] H. Derakhshanfar, J. J. Ochoa, K. Kirytopoulos, W. Mayer, and C. Langston, "A cartography of delay risks in the Australian construction industry: impact, correlations and timing," *Eng. Constr. Archit. Manag.*, vol. 1992, 2020, doi: 10.1108/ECAM-04-2020-0230.

[53] M. Çevikbaş, O. Okudan, and Z. Işık, "New Delay-Analysis Method Using Modified Schedule and Modified Updated Schedule for Construction Projects," *J. Constr. Eng. Manag.*, vol. 148, no. 11, pp. 1–18, 2022, doi: 10.1061/(asce)co.1943-7862.0002394.

[54] M. Guévremont and A. Hammad, "Review and Survey of 4D Simulation Applications in Forensic Investigation of Delay Claims in Construction Projects," *J. Leg. Aff. Disput. Resolut. Eng. Constr.*, vol. 12, no. 3, pp. 04520017-1–9, 2020, doi: 10.1061/(ASCE)LA.1943-4170.0000391.

[55] Z. G. Al-Kofahi, A. Mahdavian, and A. Oloufa, "System dynamics modeling approach to quantify change orders impact on labor productivity 1: principles and model development comparative study," *Int. J. Constr. Manag.*, vol. 22, no. 7, pp. 1355–1366, 2020, doi: 10.1080/15623599.2020.1711494.

Turkish Journal of Civil Engineering, 2023 77-101, Paper 726, ***Research Article***

Rheological Performance of ZycoTherm/Nano-Silica Composite Modified Binders at High and Low Temperatures

Dania ALOTHMAN[1]
Hüseyin GÖKÇEKUŞ[2]
Shaban Ismael Albrka ALI[3]

ABSTRACT

This study aims to investigate the impact of control and warm mix binders modified with nano-silica on the asphalt binder functioning to resist rutting endurance and low-temperature cracking. The percentages of nano-silica employed in this research were 2%, 4%, and 6% of asphalt binder weight. The control and modified binders were evaluated by performing conventional and rheological tests. The rheological properties were examined by master curves, isochronal plots, multiple stress creep recovery (MSCR), Superpave rutting parameter, and bending beam rheometer. The outcomes implied that the performance of the asphalt binder (with or without ZycoTherm) improved when nano-silica was added concerning ($G^*/\sin\delta$) parameter. The MSCR test demonstrated that the recovery (R %) of the control and warm mix binders improved whereas the non-recoverable creep compliance (J_{nr}) dropped, implying that nano-silica boosted the rutting potential. Moreover, it was observed at different temperatures that the values for the complex shear modulus increased when the phase angle values were reduced. Furthermore, at low temperatures, it is presumed that the performance of nano-silica modified asphalt binders will have minimal performance as opposed to the binders prepared with ZycoTherm, which prevents low-temperature cracking.

Keywords: nano-silica, ZycoTherm, modified asphalt binders, rheological behavior, rutting resistance, MSCR, BBR.

Note:
- This paper was received on December 15, 2021 and accepted for publication by the Editorial Board on December 28, 2022.
- Discussions on this paper will be accepted by May 31, 2023.
- https://doi.org/10.18400/tjce.1239171

1 Near East University, Department of Civil Engineering, Nicosia, Cyprus
20177819@std.neu.edu.tr - https://orcid.org/0000-0003-4009-4489

2 Near East University, Department of Civil Engineering, Nicosia, Cyprus
huseyin.gokcekus@neu.edu.tr - https://orcid.org/0000-0001-5793-4937

3 Near East University, Department of Civil Engineering, Nicosia, Cyprus
shabanismael.albrka@neu.edu.tr - https://orcid.org/0000-0003-1938-9127

1. INTRODUCTION

Asphalt pavement must have the ability to withstand various loads during its service life to ensure optimal effectiveness for flexible pavements. Pavements are subjected to various forms of distress including high-level temperature rutting, middling-temperature fatigue, and minimal-level temperature cracking. A significant form of distress in asphalt pavements is known as rutting. Rutting is prevalent in elevated - temperatures areas owing to the asphalt's decreased stiffness as well as the materials flow caused by their viscoelastic characteristics [1]. Asphalt is the primary cause of rutting distress, especially in low and intensive traffic at elevated – temperatures [2]. The existence of shear deformation and increased density are the main causes of rutting within the asphalt pavement layers. Furthermore, the build-up of enduring strain in the various asphalt layers due to permanent deformation extensively influences rutting. On the other hand, thermal cracking is a serious problem that occurs in cold-weather asphalt pavements. Because of the thermal shrinkage of asphalt, thermal cracking generally develops in the asphalt pavement layer [3]. The asphalt layer is prevented from being moved by friction between both the asphalt and bottom layers, leading to tensile stresses in the asphalt layers. The levels of these stresses rise as the temperature falls. Once these stresses exceed the asphalt mixture's tensile strength, initial cracks appear at the base of the asphalt layer [4, 5].

The pavement performance is affected by the conventional physical and rheological features of the asphalt mixtures at elevated and reduced environmental temperatures, which influence the final function of the mixture. Therefore, it is crucial to discover the enhanced asphalt that offers exceptional road operation, easy construction and is cost-effective. The application of various nanomaterials such as nano-alumina, nano-tubes, and nano-clays has been studied for use as modifiers for asphalt binders [6-9]. Nano-silica is considered to be one of the most significant nano-materials that is effective for modifying the attributes of asphalt and asphalt mixtures. The important advantages of nano-silica are its high-performance features and its low production costs. It also has many advantageous properties including suitable dispersing capacity, high stability, elevated purity percentages, high specific area, and strong absorption [10].

Permanent deformation is one of the most common types of asphalt pavement deterioration. Previous studies have advocated for the use of nano-silica in asphalt binders to improve rutting resistance [11-13]. Many researchers have employed nano-silica to modify the asphalt features and observed that the asphalt modified with nano-silica had greater complex modulus (G^*) and lesser phase angle (δ) values [14-15]. Therefore, by adding nano-silica to improve binder properties, the permanent deformation and fatigue distress performance of asphalt can be enhanced [10]. Saltan *et al*., [16] applied nano-silica at three different percentages of 0.1%, 0.3%, and 0.5%. The results showed that the asphalt binder's elastic behavior improved, resulting in improved fatigue and rutting resistance. Shafabakhsh *et al.,* [11] discovered that the inclusion of 3% nano-silica did not affect the elevated temperature performance of asphalt binder while the inclusion of 5% and 7% nano-silica improved the asphalt binder's elevated temperature performance by one and two grades, respectively. Bhat and Mir [13] demonstrated that nano-silica modified binders displayed increased rutting resistance in comparison to unmodified binders. In their research, the rutting resistance was analyzed by utilizing various methods such as MSCR, $G^*/\sin\delta$, and creep assessments. All the methods revealed that the application of nano-silica improved the rutting resistance of the

neat binder. Arshad *et al.,* [17] incorporated nano-silica at various concentrations (1-5%), and the results revealed that 2% nano-silica was the optimal dose with greater effect in terms of non-recoverable creep compliance (J_{nr}) and percentage recovery (R %). At low temperatures, the performance of asphalt modified with nanoparticles may be a disadvantage. Onochie et *al.,* [15] tested the control asphalt with 2% and 4% nano-silica using a BBR and discovered that the modifications resulted in 6% and 14% greater creep stiffness, respectively. Nejad *et al.,* [14] reported the same findings, the incorporation of nano-silica into the asphalt caused higher creep stiffness and lowered the m-value, demonstrating the inefficiency of nano-silica on the low-temperature cracking resistance. Therefore, higher nano-silica doses may increase rutting resistance but have a negative impact on low-temperature performance [18].

Other than the utilization of nano-silica, the use of Nano-ZycoTherm as an additive for warm mix binder is a promising alternative. Warm mix asphalt (WMA) technologies are applied to decrease the asphalt production temperature to 120-135 ◦C and compaction temperature to 105-120 ◦C [19]. WMA is considered one of the ideal options for paving as it is eco-friendlier compared to conventional HMA. Warm mix additives lead to a reduction in fumes, while preserving the environment and the well-being of people. Recently, numerous studies have been conducted on warm mix asphalt technologies wherein the utilization of various forms of additives. For instance, nano-technology ZycoTherm was proposed as a silane-based anti-striping agent, which has the potential to minimize temperatures without negatively affecting the compaction at low-temperature levels [20]. Ziari *et al.,* [21] studied the features of ZycoTherm-modified binders through physical and rheological assessments of asphalt. The outcomes revealed that applying ZycoTherm did not significantly influence the elastic responses, fatigue, and rutting properties of the binder. However, Mirzababaei *et al*., [22] conducted a study using the MSCR test for asphalt binders of asphalt with 85/100 grade. The results gathered implied that ZycoTherm reduced the non-recoverable compliance values (J_{nr}), which indicates lower susceptibility against rutting distress for asphalt binders. According to the results obtained from the evaluations, the binder prepared with ZycoTherm (0.1%) was found to have the greatest effect on the asphalt binder's performance with 85/100 penetration grade facing permanent deformation. Raufi *et al.,* [23] studied the after-RTFO (short-term aging) performance of ZycoTherm modified binder. The ZycoTherm-modified binder showed an improvement in rutting property and led to increasing $G^*/\sin\delta$ rates in comparison to the control binders at various frequencies and temperature ranges. In addition, it was observed that an enhancement of the asphalt binder concerning the rutting performance was attained as a result of nano-ZycoTherm adjustments. Ibrahim and Mehan [24] conducted a study involving DSR and BBR assessments. The study revealed an increment in the rutting parameter ($G^*/\sin\delta$), fatigue parameter ($G^*.\sin\delta$), creep stiffness, and also the m-values for each ZycoTherm-modified asphalt binder, and when 0.5% of ZycoTherm was added, all these outcomes reflected higher values.

Individually, ZycoTherm and nano-silica are effective asphalt binder modifiers. However, their compatibility as a couple is an area of research that needs to be looked into more. The following research focuses on examining the rheological features of asphalt modified with ZycoTherm given that there have been few studies conducted on the MSCR and frequency sweep tests of ZycoTherm-modified binders. Furthermore, studies on nano-silica have been carried out in recent years, but the effect of ZycoTherm/nano-silica concerning the rutting resistance and low-temperature cracking has yet to be determined. Hence, it is decisive to

analyze the performance of ZycoTherm modified with several percentages of nano-silica utilizing these approaches.

2. THE STUDY'S OBJECTIVES

1. Examine the effects of ZycoTherm, nano-silica, and ZycoTherm / nano-silica on the viscosity of the asphalt binder at various temperature ranges.

2. Evaluate the effects of adding ZycoTherm, nano-silica, and ZycoTherm / nano-silica on various rheological characteristics of the asphalt binder using a frequency sweep test.

3. Assess the permanent deformation of ZycoTherm, nano-silica, and ZycoTherm / nano-silica modified binders utilizing Superpave rutting resistance parameter ($G^*/\sin\delta$) and MSCR.

4. Investigate the effect of adding ZycoTherm, nano-silica, and ZycoTherm/nano-silica on the low-temperature performance using BBR.

3. MATERIALS AND EXPERIMENTAL DESIGN

The examined materials' specifications are presented in this section. Fig. 1 shows a tree diagram displaying the experimental system applied to demonstrate the complete scope of this research study.

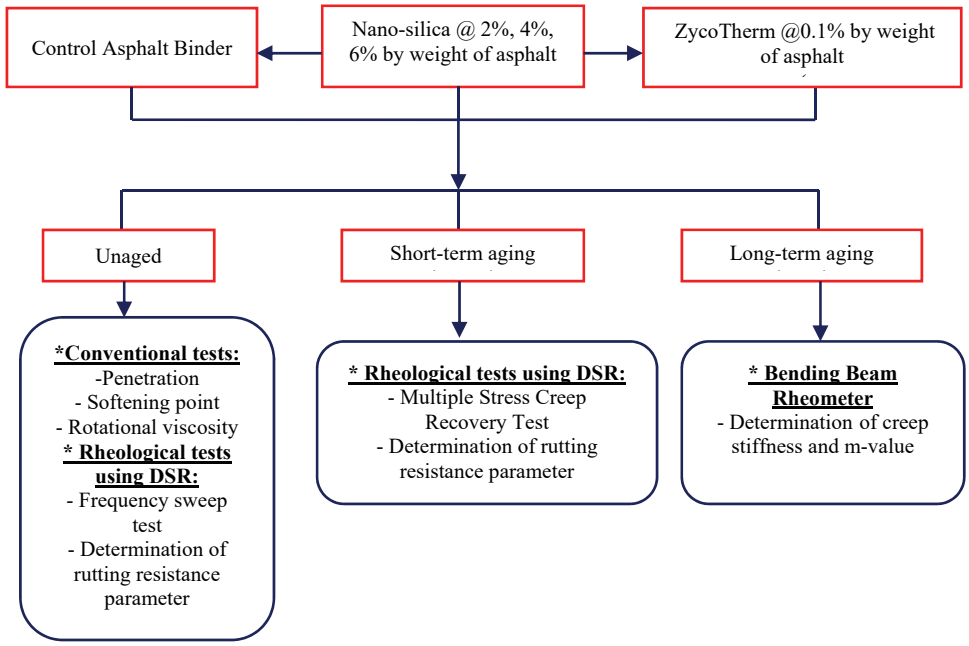

Figure 1 - The flowchart of the study

3.1. Asphalt Binder

The control asphalt binder utilized in this research was 60/70 grade. Table 1 below displays the characteristics of the asphalt binder.

Table 1 - Physical properties of control asphalt binder

Test	Test method	Unit	Result	Criteria
Penetration at 25°C	ASTM D5	0.1 mm	67	60-70
Softening point	ASTM D36	°C	50	48-56
Ductility at 25°C	ASTM D113	cm	100	100 minimum
Flash point	ASTM D92	°C	322	230 °C minimum
Rotational viscosity at 135 °C	ASTM D4402	Pa.s	0.5672	3 Pa s maximum

3.2. Nano-Silica

The silica composite is available globally and is applicable in the manufacturing of colloidal silica, silica gel, fumed silica, and other substances [25]. SiO_2 is the chemical compound for silica and is similar to the compound structure of diamonds. SiO_2 exists in nature in both crystalline and amorphous forms. Silica is white and has relatively high melting and boiling points [26]. There are various functional characteristics of nano-silica including high precise surface area, intense absorption, effective dispersal capability, high-level stability, and high chemical purity [10]. The addition of nano-materials offers various benefits including reduced manufacturing costs and increased performance [27]. The nano-silica features are shown in Table 2.

Table 2 - Physical properties of nano-silica

Property	Value
Appearance	Translucent liquid
pH	6.71
Viscosity (20 °C)	3.05mPa.s
Particle size	11 nm

3.3. ZycoTherm

ZycoTherm is a chemical warm mix additive that provides significant benefits as a result of WMA technologies. ZycoTherm lowers the mixing and compaction temperatures. ZycoTherm is considered to be an antistrip warm-mix chemical additive to stipulate moisture endurance for asphalt pavements. Moreover, it is also a scent-free substance. At room temperature, ZycoTherm has been identified as a warm mix additive that is integrated at 0.1% - 0.15% of the weight of the asphalt binder [28]. ZycoTherm, a silane-base technology, was

employed and is considered to be more efficient than other well-known chemical WMA additives that are amine-based due to the fact the silane-based additives produce a molecular level hydrophobic zone that is water-resistant. The characteristics of ZycoTherm are shown in Table 3.

Table 3 - Physical properties of ZycoTherm

Property	**Value**
Physical state	Liquid
Color	Pale yellow
Viscosity	1-5 Pa.s
Specific gravity (25°C)	0.97g/cm^3
Odor	Odorless
Flash point	>80 °C
pH	10 % solution in water neutral or slightly acidic

3.4. Preparing the Modified Binder

The asphalt binder was combined with 2-6% of nano-silica, using 2% increments of the original weight for the binder, to produce nano-silica modified asphalt binder. The asphalt binder was heated to 160 °C, while the asphalt binder was modified with the aid of a mechanical mixer. Approximately 400g of binder was placed in a cylinder-shaped container and set on a hot plate. To preserve the viscosity of the binder within the blending process, the hot plate was adjusted at 160 °C. The heated asphalt binder was progressively infused with nano-silica while the mixture was stirred with a mechanical mixer. The stirring speed was adjusted to 1800 rpm for 60 minutes. To ease the reference of each sample, the nano-silica modified asphalt binders were identified by utilizing the following acronyms: 2% NS, 4% NS, and 6% NS. According to the manufacturer's suggestion, the WMA binder was prepared by using an additive content set at 0.1% of the binder's weight. The mechanical stirrer was set up at a speed sufficient to create a 15-30 mm deep vortex within the liquefied asphalt. The ZycoTherm was then added to the center of the vortex in a drop-wise method, while the asphalt was stirred at 130 °C with a pace of 10 drops per minute with a 1 ml syringe. The stirring continued for 15 minutes to complete the mixing procedure. Furthermore, to prepare WMA modified with nano-silica (ZycoTherm/nano-silica), the control asphalt was blended first with 0.1% ZycoTherm as mentioned previously, and then the nano-silica was gradually added to the mix by 2, 4, and 6% and blended with asphalt binder at 1800 rpm. The modified binders were labeled as, 0.1%Z+2%NS, 0.1%Z+4%NS, and 0.1%Z+6%NS.

3.5. Aging Conditions of Asphalt Binder

The control asphalt and modified binders were conditioned under short and long-term aging phases. To simulate the conditions of the short-term aging, a rolling thin film oven (RTFO) was utilized. The standard assessment method ASTM D 2872 indicates that 35 grams of

asphalt must be set in open-mouthed cylinder bottles and then positioned into a heated carousel prepared oven at a temperature of 163 ˚C, which revolves beneath air- blown pressure at 15 rpm for 85 minutes. The test samples were utilized in the rheological evaluation of the RTFO-aged asphalt. According to ASTM D 6521, the asphalt binders were aged for 20 hours in a pressure aging vessel at 100 ˚C and a pressure of 2.1 MPa in terms of long-aging.

4. EXPERIMENTAL METHODS

4.1. Basic Physical Binder Tests

The fundamental properties of the control asphalt binder and the modified binders were identified by using the following tests: penetration test (ASTM D5), softening point test (ASTM D36), and viscosity test using a Brookfield Rotational Viscometer (ASTM D4402).

4.2. Temperature Susceptibility

Asphalt binder is composed of thermoplastic material, which means that when temperatures increase, it becomes softer, and when temperatures decrease, it hardens. This feature is one of the traits of asphalt binders known as temperature susceptibility. As the physical traits of asphalt transform at increased temperatures, the consistency and temperature susceptibility are specified by using the PI parameter, or penetration index. To compute the PI, the temperature susceptibility for binders is calculated by using the penetration at a temperature of 25 ˚C and softening point outcomes, as shown in Eq. 1 [29].

$$\mathrm{PI} = \frac{1952 - 500\log(Pen_{25}) - 20SP}{50\log(Pen_{25}) - SP - 120} \quad (1)$$

Where $\mathrm{Pen}(25)$ denotes the value of the penetration of the asphalt binder at 25 ˚C in 0.1mm and (SP) is the softening point value of the asphalt binder in ˚C.

4.3. Dynamic Shear Rheometer (DSR)

The rheological characteristics of asphalt have been identified through its vicious and elastic features at low, moderate, and elevated temperatures. The DSR was utilized to perform Superpave rutting resistance, frequency sweep, and multiple stress creep recovery (MSCR) consistent with ASTM D7175, AASHTO T315, and ASTM D7405, respectively. The assessments were carried out to analyze the rheological features of control asphalt and warm mix binder that were modified by using various degrees of nano-silica. A frequency sweep assessment was employed to analyze the linear rheological features of the control and modified binders. The rheological indicators that are frequently acquired from the DSR experiment are the complex modulus (G^*) and phase angle (δ). The following indicators were applied to analyze the binder's elasticity characteristics. Moreover, the MSCR test was employed to identify the recovery (R %) and the non-recoverable creep compliance (J_{nr}) for the control and warm mix binder modified with nano-silica in RTFO aged state.

4.3.1. Frequency Sweep Test

The asphalt pavement structures under traffic loads displayed a dynamic loading influence and the blacktop material demonstrated various viscoelastic attributes when placed under various load frequencies. The assessment of the frequency sweep was performed where the load frequency was changed from 1 Hz to 15 Hz. Moreover, the assessment was conducted under strain-regulated states and the temperatures ranged between 10 ◦C and 82 ◦C with a temperature gap of 6 ◦C. During the assessment, an 8 mm plate was applied for temperatures under 40 ◦C, while a 25 mm plate was utilized for temperatures higher than 40 ◦C. The G^* and δ results obtained from the frequency assessment were employed to establish master curves for the control and warm mix binder modified with nano-silica. Additionally, the isochronal plots were plotted to assess how the modification process affected the performance features of both the control and warm mix asphalt binder.

4.3.2. Multiple Stress Creep Recovery (MSCR) Test

On the RTFO-aged specimens, a DSR was utilized to perform the MSCR test. The test evaluates the rutting performance of a binder by assessing both the recovery percent ($R\ \%$) and the non-recoverable parameter of creep compliance (J_{nr}). At 0.1kPa and 3.2kPa levels of stress, the MSCR test comprises 10 cycles of stress creep with a 1-second duration and a 9-second recovery time. The samples were tested utilizing a 25 mm plate and a 1 mm spacing at a temperature of 64 ◦C. After releasing the imposed stress, the ($R\ \%$) denotes the binder's elastic recovery. An asphalt binder with a high elastic tendency may result in minimal lasting asphalt deformation. A high value of (J_{nr}) implies a binder's susceptibility to rutting and conversely is right. The (J_{nr}) values might show the stress dependency of both unmodified and modified binders. Eqs. 2 and 3 are used to quantify (J_{nr}) and ($R\ \%$), respectively.

$$J_{nr} = \frac{\varepsilon_{nr}}{\sigma} \tag{2}$$

Where J_{nr} represents the non-recoverable creep compliance (kPa^{-1}), ε_{nr} symbolizes the unrecoverable strain at the end of the recovery period, and σ symbolizes the stress (kPa) utilized during the loading period.

$$R\ \% = \frac{\varepsilon_1 - \varepsilon_{10}}{\varepsilon_1} \times 100 \tag{3}$$

Where $R\ \%$ is the percentage recovery, ε_1 symbolizes the value of the strain at the end of the creep stage, and ε_{10} denotes the strain rate at the end of the recovery stage.

4.3.3. Superpave Rutting Resistance Parameter

The Superpave rutting parameter ($G^*/\sin\delta$) was performed per ASTM D 7175-15 to measure the resistance to rutting of the control and modified binders. $G^*/\sin\delta$ parameter is used to determine whether asphalt binders fail when exposed to high temperatures. The binder deformation is avoided at loading as $G^*/\sin\delta$ rises. The $G^*/\sin\delta$ ratio for an unaged asphalt binder must be greater than 1kPa, whereas the $G^*/\sin\delta$ ratio for RTFO-aged binder must be

greater than 2.2kPa based on ASTM D 2872. On both unaged and RTFO- aged binders, the assessment was carried out utilizing a DSR and a 25-mm-diameter parallel plate shape and a spacing of 1 mm. The test procedure was done at a frequency of 10 rad/sec in a range of temperature of 58 ˚C to 76 ˚C, at temperature intervals of 6 ˚C.

4.4. Bending Beam Rheometer (BBR) Test

The BBR method was applied to evaluate the low-temperature function of asphalt binders under ASTM D6648. The creep stiffness and m-value were attained by applying the BBR method for 60 seconds at varying temperatures: 0 ˚C, - 6 ˚C, -12 ˚C, and -18 ˚C. As stated by the requirement sets for Superpave, the creep stiffness has an ultimate value of 300 MPa and at least 0.3 is required for the m-value. To compute the creep stiffness and m-value, the control asphalt and the modified binders were all evaluated. All binder samples were subject to short-term aging (RTFO) and long-term aging (PAV).

5. RESULTS AND DISCUSSION

5.1. Conventional Physical Properties

The softening point and penetration tests' findings are shown in Table 4. The penetration test was conducted to assess the consistency of the control asphalt and modified binders, and the softening point test was conducted to validate the asphalt binders' high-service temperature.

The effect of adding nano-silica to the control and ZycoTherm binders is illustrated in Table 4. The penetration diminishes and the softening point rises, as can be seen. In comparison to the control and ZycoTherm binders, each nano-modified asphalt binder sample had a lower penetration and a greater softening point. The decrease in penetration values reveals that the binder has a stiffening influence, with stiffening increasing in proportion to the rise in nano-silica concentration. The binder's softening point is also increased when nano-silica is added, which improves its temperature susceptibility. The higher the penetration index value is, the lower the temperature susceptibility for the asphalt binder. Table 4 shows the PI outcomes.

Table 4 - Physical properties of control asphalt and modified binders

Binder Type	Penetration at 25 ˚C (0.1mm)	Softening point (˚C)	PI
Control Binder	67	50	-0.495
2%NS	52.65	55.30	0.165
4%NS	49.36	57.85	0.555
6%NS	46.51	59.40	0.727
0.1% Z	55	52.82	-0.296
0.1% Z+ 2%NS	50.50	56.50	0.325
0.1% Z+ 4%NS	48.94	58.75	0.719
0.1% Z+ 6%NS	45.30	60.60	0.9003

The viscosity of the control and nano-modified binders was measured utilizing a Brookfield rotational viscometer (RV) at a range of high temperatures between 135 ˚C and 195 ˚C with 10 ˚C increments. According to Fig. 2, all of the samples of asphalt binder had low viscosity values at elevated temperatures. Typically, when the temperature increases, the viscosity values are reduced. The inclusion of nano-silica in the control binder leads to increased viscosity values for the nano-silica modified asphalt binders. Moreover, according to the Superpave criteria, at 135 ˚C the viscosity values were within the limits, and the nano-silica modified asphalt binders acquired lower viscosity values in comparison to the maximum limit at 3 Pa s. However, looking at 4% NS, one can infer from the mixing procedure of the nano-silica modified asphalt binders that chemical reactions and physical diffusions might occur in which a new structure may be developed because of the nano-silica's temperature resistance resulting in the reduction in viscosity value as compared to other percentages. Moreover, nano-silica can intensify the control binder and enhance the recovery capability upon applying stress. Conversely, the viscosity value was decreased when nano-silica was added to the warm mix binders, which is part of the warm mix additive ZycoTherm that greatly affects the reduction of viscosity. As a result, the ZycoTherm resulted in a reduction in viscosity values, for example; a viscosity reduction of roughly 11.5% and 15% at 135 and 165 ˚C, respectively, in the binder containing both 0.1% ZycoTherm and 6% NS. ZycoTherm is regarded as an advantageous attribute for an additive, especially when assessing its effectiveness, given that it minimizes the functional temperatures that assist in preparing potential cost-effective and sustainable pavements. When ZycoTherm is in a liquid condition, it is considered one of the elements that influence the reduction of viscosity [23].

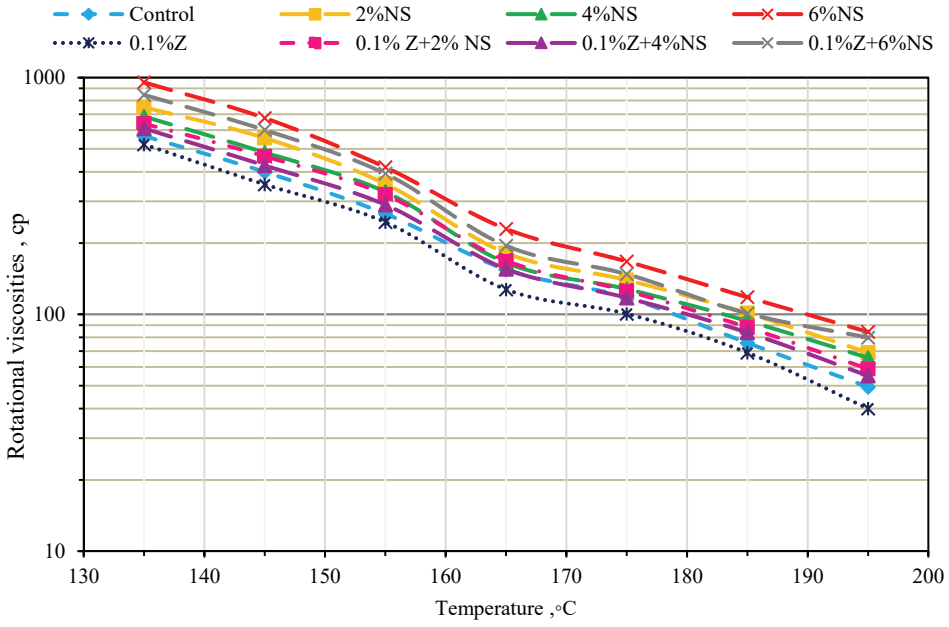

Figure 2 - Rotational viscosities for control and modified binders

5.2. Multiple Stress Creep Recovery (MSCR) Test

5.2.1. Cumulative Strain

The usual strain outputs from the MSCR assessment of control and modified asphalt at 64 °C with two levels of stress are displayed in Figs. 3a and 3b, respectively. In Fig. 3a, the low-stress level (100 Pa) for the first 100 seconds is displayed, while Fig. 3b shows the high-stress level (3200 Pa) for the next 100 seconds. The outcomes obtained from the MSCR consist of two stages, namely the creep stage and the recovery stage, to finish a cycle. It can be shown by analyzing the gathered strain and stress levels, the accumulated creep compliance at 100Pa is lesser than at 3200Pa, which signifies that when stress levels increase, the accumulated strain increases as well. Moreover, the addition of 0.1% ZycoTherm on the control asphalt led to a slight decrease in the gathered strain. However, when adding nano-silica to the binders, it can be observed that the gathered strain decreases considerably when compared to the control and ZycoTherm binders. As a result, the nano-silica can enhance the stiffness of the binder at elevated temperatures. From the outcomes gathered, it is shown that 6% NS has the lowest accumulated strain followed by a 0.1%Z +6%NS compared to the other percentages.

5.2.2. Recovery Percentage (R %)

The recovery percentage strain assists in identifying the elastic characteristic of the asphalt when subject to loading. The percentage recoverable strain is an essential constraint for assessing the recovery capability of the asphalt after it has deformed. The increase in the percentage of asphalt recovery (*R %*) represents minimal exposure to permanent deformation. This occurs during the 9-second rest period within each cycle, which allows more strain to return to its former condition. This constraint is crucial when analyzing the asphalt binder resistance to rutting as it denotes the hindered asphalt elasticity. As shown in Fig. 3c, the recovery percentage strain at 100 Pa and 3200 Pa stress levels for control asphalt and modified binders. According to the analysis of the outcomes obtained at each stress level, the value marginally declined at 3200 Pa as opposed to the value at 100 Pa.

The following results imply that by adding nano-silica to control asphalt, the elastic recovery and rutting resistance for the asphalt binder is improved. Adding nano-silica increases the recovery value and this is evident in the data gathered. By observing the data collected at 100 Pa stress level, the recovery of the control binder is 6.6% and it increases to 24.28%, 20.56%, and 27.72% once nano-silica was added at 2%, 4%, and 6%, respectively. While the warm mix binder (0.1% Z) shows a 7.84% recovery, and this recovery jumps to 20.54%, 15.14, and 25.99% when 2%, 4%, and 6% nano-silica were added, respectively. The same type of improvement was observed at the 3200 Pa stress level. As a consequence, the inclusion of nano-silica improves the asphalt binder's elasticity, resulting in a better recovery response.

5.2.3. Non-recoverable Creep Compliance (J_{nr})

The non-recoverable creep compliance (J_{nr}) constraint is used to determine the impact of the binder on rutting performance. When J_{nr} values are low, it represents improved rutting

resistance, and when J_{nr} values are high, it represents poor rutting resistance. In Fig. 3d, the J_{nr} outcomes are shown for the control and ZycoTherm binders, which have been modified with nano-silica at both 100 Pa and 3200 Pa stress levels. According to the data, the J_{nr} increases as the stress level transitions from 100 Pa to 3200 Pa, at 100 Pa results show the decline of J_{nr} for the control binder from 3.058 to 1.643, 1.76, and 1.319 when nano-silica was added at 2%, 4% and 6% of, respectively. The J_{nr} for warm mix binder (0.1%Z) is 2.644, with the addition of 2, 4, and 6% of nano-silica the J_{nr} values dropped to 1.791, 2.512, and 1.501, respectively.

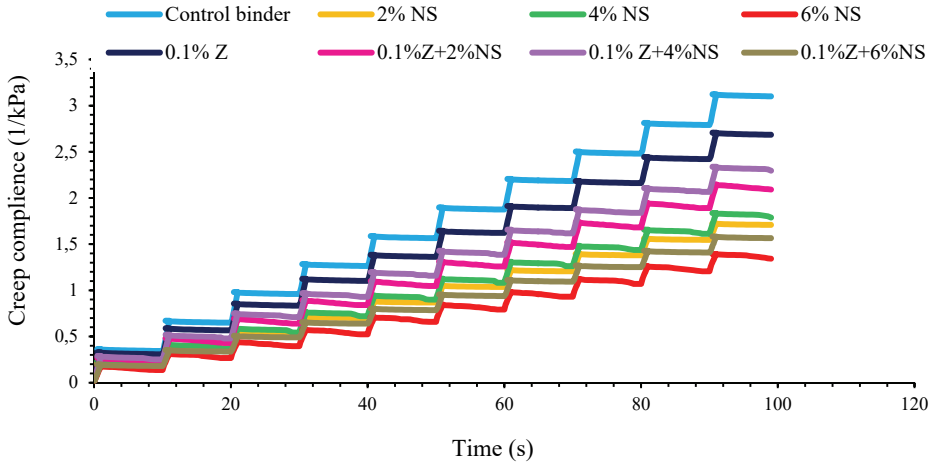

Figure 3a -The accumulated creep compliance at 100 Pa

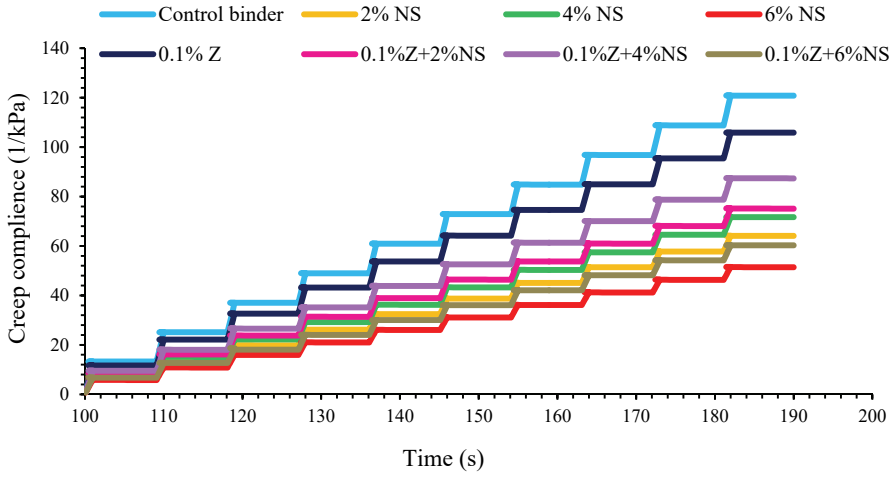

Figure 3b - The accumulated creep compliance at 3200 Pa

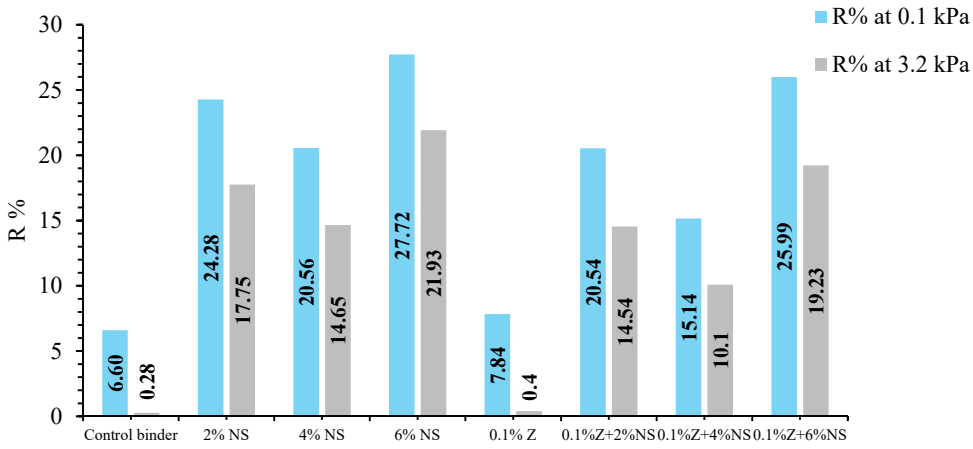

Figure 3c - R% at 100 Pa and 3200 Pa levels of stress

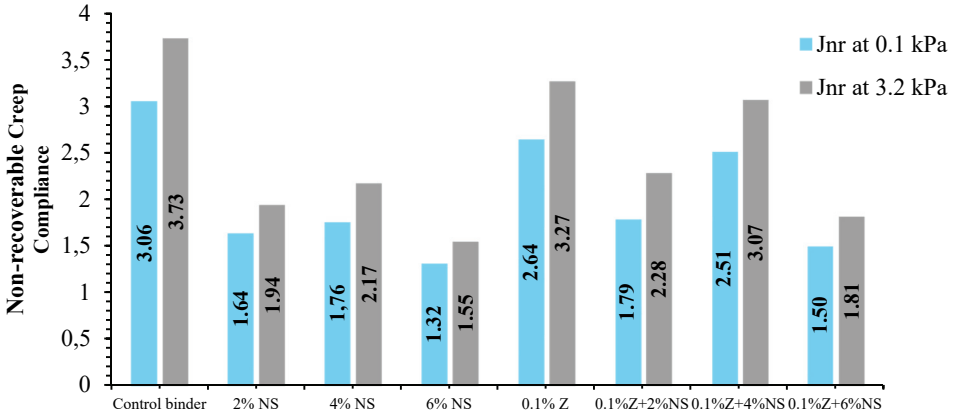

Figure 3d - J_{nr} at 100 Pa and 3200 Pa levels of stress

The higher stiffness of the modified binders might explain the drop in the J_{nr} value with the presence of nano-silica. The recovery strain percent (*R %*) revealed an inverse relation with non-recoverable creep compliance (J_{nr}). The reduction in non-recoverable creep compliance along with the increase in recovery values revealed that the modified binders with nano-silica have a greater impedance to permanent deformation.

According to AASHTO T350, J_{nr} at 3200 Pa is used as a criterion to categorize asphalt depending on a specified traffic volume and loading rate, as shown in Table 5. According to the J_{nr} results, control, 4%NS, 0.1%Z, 0.1%Z+2%NS, and 0.1%Z+4%NS modified binders were determined to be appropriate for standard loading (S), whereas 2%NS, 6%NS, and 0.1%Z+6%NS were determined to be suitable for heavy loading (H). As a result, the

inclusion of nano-silica improves the asphalt binder's traffic loading grade. Moreover, the decrease in J_{nr} values with the addition of nano-silica might be explained by the greater stiffness of the modified asphalt binders.

Table 5 - Grade category of Jnr at 3200Pa based on traffic loading

Grade Category	J_{nr} at 3200 (1/kPa)	Traffic loading level (ESALs)
E (Extremely loading)	0.0 < 0.5	> 30 million and speed of traffic<20Km/h
V (Very high loading)	0.5 < 1.0	> 30 million or speed of traffic<20Km/h
H (High loading)	1.0 <2.0	10-30 million or speed of traffic 20-70Km/h
S (Standard loading)	2.0 < 4.0	<10 million and speed of traffic >70Km/h

5.3. Frequency Sweep Test

5.3.1. Isochronal Plots

The use of isochronal plots allowed the viscoelastic attributes of the control and modified asphalt like the G^* and δ against temperature, to be illustrated at specific frequencies. Figs 4a-4d show the temperature ranges plotted against the phase angle and complex modulus for the unaged control binder, warm mix binder, and nano-silica modified binders at 1 Hz and 15 Hz. Figs.4a and 4b show the isochronal plots for the control asphalt modified with nano-silica at 1 and 15 Hz, respectively. The G^* value rises and the δ value reduces at all temperatures as a result of the addition of NS to the control binder for up to 6%. This implies that the dispersion of nano-silica within the mixture results in an improvement in the strength of the modified asphalt and considerably improves the asphalt's elevated-temperature performance. The complex modulus of nano-silica modified binders has increased significantly, enhancing the binders' rutting resistance. This increase becomes more pronounced at higher frequencies. Moreover, when temperature increases, the phase angle of the binders increases, and the modified binders with nano-silica exhibit lower phase angles than the control asphalt. The phase angle of the 6% NS decreases significantly at both low and high temperatures. Furthermore, the phase angle of nano-silica modified binders decreases at low (1 Hz) and high (15 Hz) frequencies, showing that the modified binders seem to be elastic [13,30].

Figs. 4c and 4d show the isochronal plots for the control, ZycoTherm, and ZycoTherm/nano-silica binders at 1 and 15 Hz, respectively. It is shown that asphalt modified with 0.1% ZycoTherm is capable of insignificantly increasing the G^* and reducing the δ values in comparison to the control binder, implying that its behavior at high temperatures is quite similar to that of control asphalt. However, when nano-silica was added to the warm mix binder at various proportions, this resulted in a significant increase in the G^* values and a

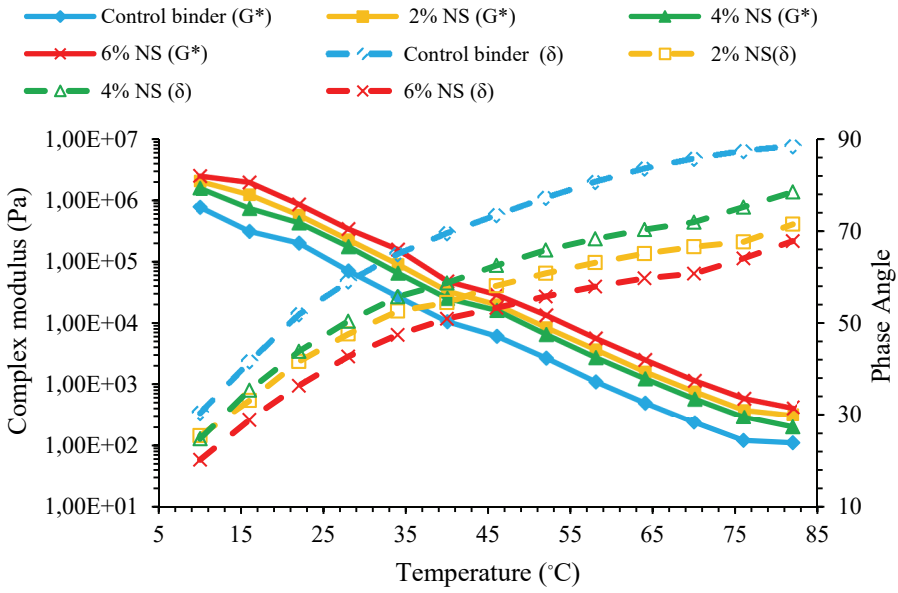

Figure 4a - Isochronal plot of G and δ of control binder modified with NS at 1 Hz*

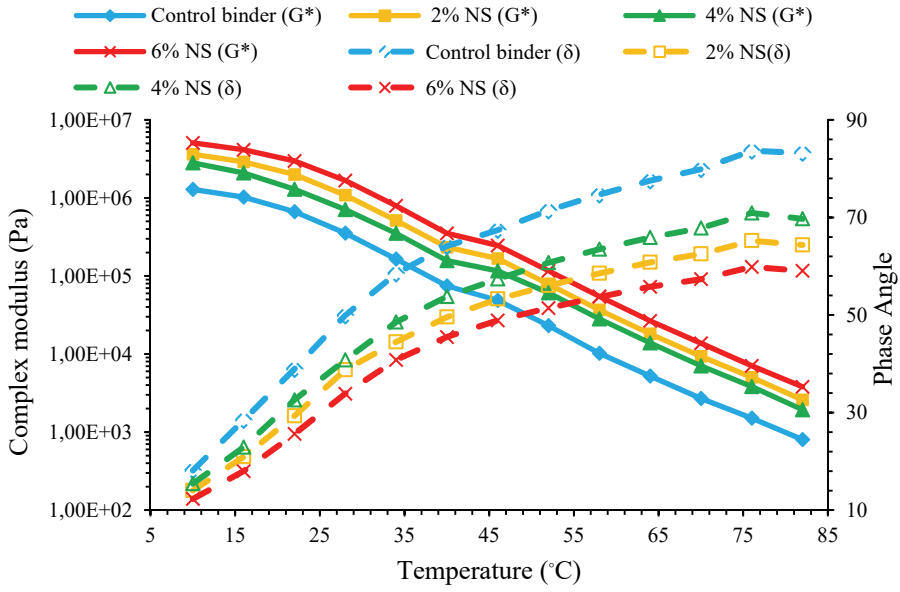

Figure 4b - Isochronal plot of G and δ of control binder modified with NS at 15 Hz*

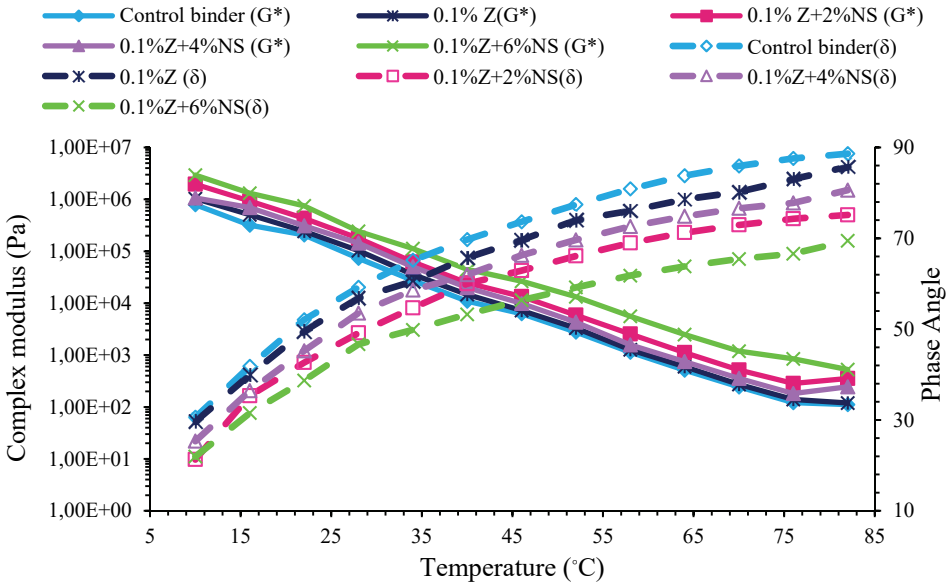

Figure 4c - Isochronal plot of G and δ of control binder, warm mix binder and warm mix binder modified with NS at 1 Hz*

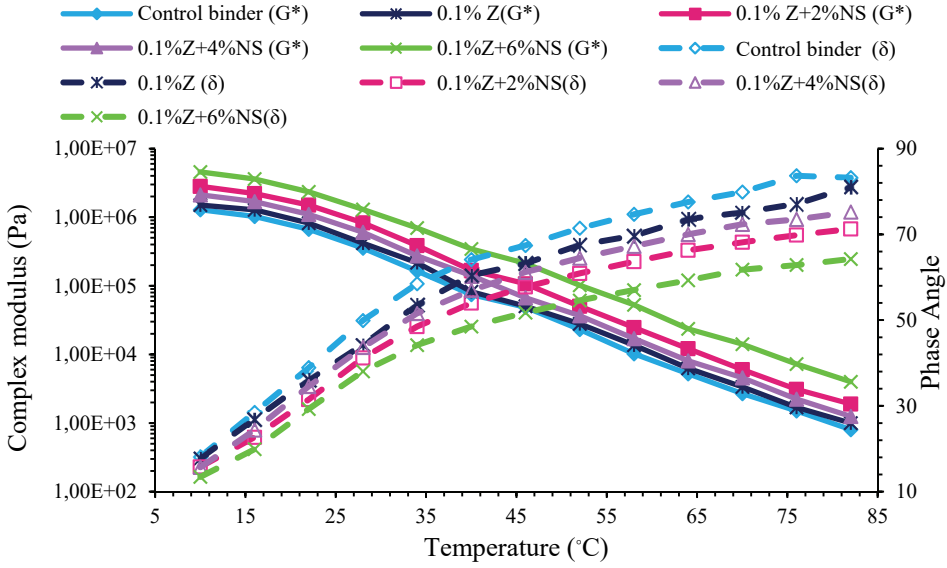

Figure 4d - Isochronal plot of G and δ of control binder, warm mix binder and warm mix binder modified with NS at 15 Hz*

decrease in the δ values. The variations found in the G^* and δ values at 15 Hz for the control, warm mix, and nano-silica modified binders at 2%, 4%, and 6% were much more significant than those at 1 Hz but followed the same pattern, demonstrating that the effect of additives was more pronounced at higher frequencies. Because all modified binders with nano-silica show higher stiffness at both high and low temperatures, it can be stated that nano-silica modified binders with or without ZycoTherm were able to enhance the performance of the elevated temperatures (resistance to rutting) of control asphalt but were ineffective in enhancing the performance of the low-medium temperature.

5.3.2. Master Curves

A master curve can be described as a curve that reflects the binder's time dependence by displaying rheological parameters, such as G^* and δ, across a selection of temperatures and frequencies. The established curve is capable of distinguishing the various assessed binders. Developing the master curve required a time-temperature superposition, where 22 °C was selected as the reference temperature. Furthermore, upon plotting a smooth curve at other temperatures, the rheological outcomes were shifted horizontally using related factors. Fig.5 shows the master curves for the G^* and δ of the control binder, warm mix binder, and nano-silica modified binders for the unaged samples. In Fig. 5a, the complex shear modulus, G^*, for the control asphalt modified with nano-silica modified is shown. It is demonstrated that adding nano-silica to the asphalt resulted in higher values of complex modulus over the whole range of frequency and temperature. Because of the presence of nano-silica, an increase in the complex modulus values indicates that the asphalt binder becomes stiffer and can considerably improve the asphalt's high-temperature performance. The degree of increase in complex modulus values for 6% NS is greater than for the other percentages. This tendency, however, is observed to be more evident at lower frequency ranges. Generally, lower frequencies indicate slower-moving vehicles, making the pavement more susceptible to rutting [31]. On the other hand, Fig. 5b illustrates the complex shear modulus, G^*, for the control asphalt binder, warm mix binder, and warm mix binder modified with nano-silica. It is evident that the complex modulus of ZycoTherm-asphalt was marginally higher than the control asphalt, but not significantly; however, when NS was added at any percentage to the ZycoTherm-asphalt binder, the G^* significantly increased. This might contribute to the stiffening effect of nano-silica particles. In Fig. 5c, the master curves for the phase angle of the control asphalt modified with various NS percentages are shown. As shown in the figure that the phase angle declines across all frequencies. In comparison, the phase angle of the control asphalt approaches 90°, meaning that the asphalt will lose its elasticity and enter the viscous flow phase. The nano-silica modified binders have a phase angle of no greater than 75°, guaranteeing that the asphalt is resistant to rutting. In Fig. 5d, the master curves of the phase angles for the control asphalt, warm mix binder, and warm mix modified with nano-silica are illustrated. It is shown that the control asphalt had the highest phase angle value; however, this parameter was slightly decreased when 0.1% of ZycoTherm was added; the drop-in phase angle values in the middle and low-frequency ranges are more noticeable. When NS was added to binders containing ZycoTherm, the phase angle values were significantly reduced in comparison to those of the control asphalt and warm mix asphalt. Logically, the nano-silica modified binders displayed the largest variation degrees in raising the complex modulus and lowering the phase angle.

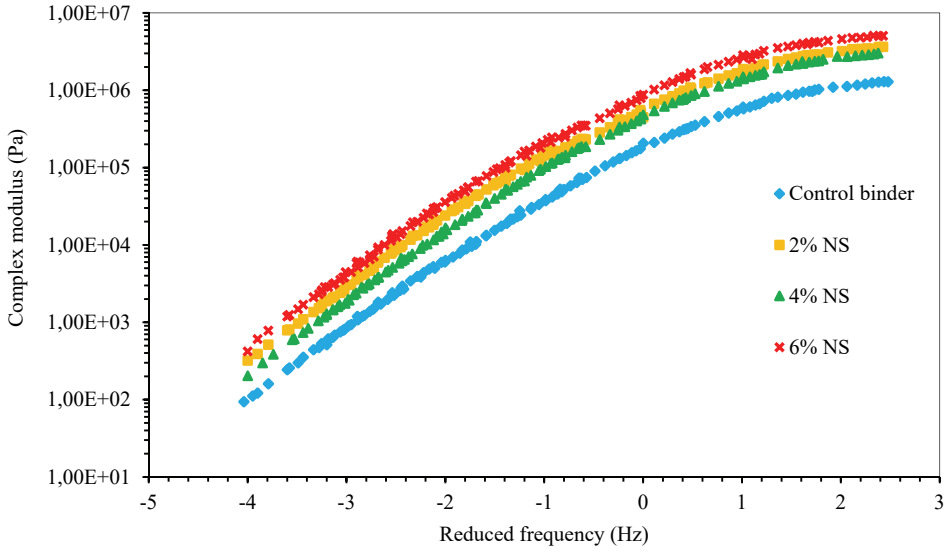

Figure 5a - G master curve of control binder modified with NS*

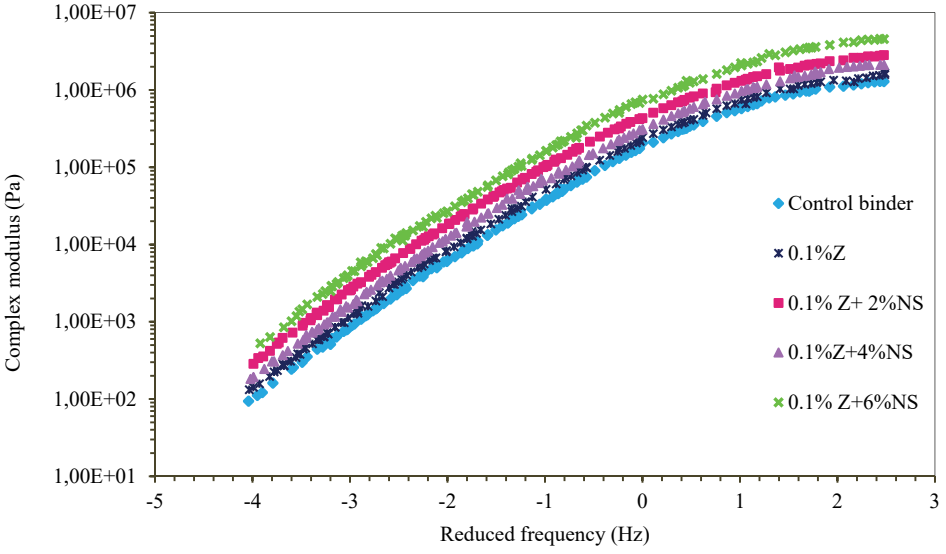

Figure 5b - G master curve of control binder, warm mix binder and warm mix binder modified with NS*

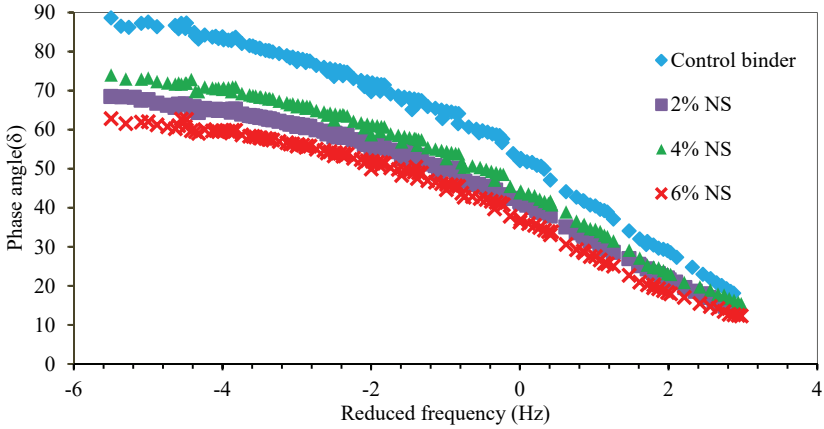

Figure 5c - δ master curve of control binder modified with NS

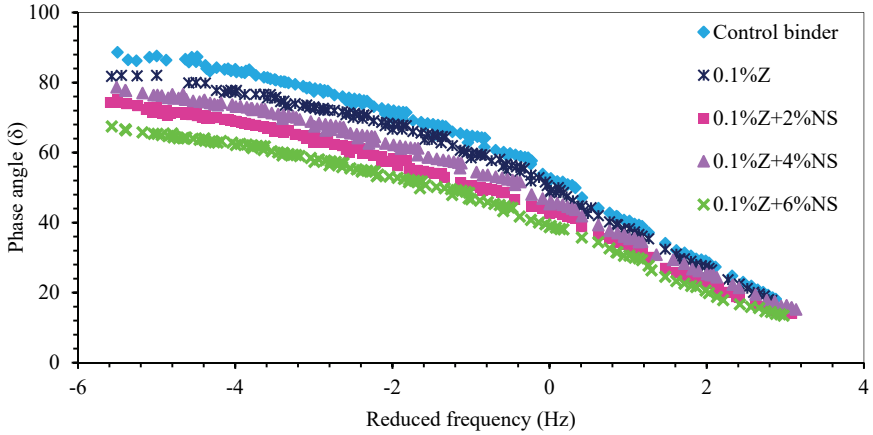

Figure 5d - δ master curve of control binder, warm mix binder and warm mix binder modified with NS

5.4. Superpave Rutting Parameter

Because the majority of the asphalt binder's permanent deformation occurs during the early phases of pavement construction, the Superpave standard mandates that the DSR test be performed on unaged and RTFO-aged asphalt at high -temperatures to determine rutting resistance. The Superpave rutting parameter ($G^*/\sin\delta$) is utilized to define the enhancement of the binder's rutting resistance when adding nano-silica to the control and warm mix binders at various temperatures, as depicted in Fig. 6. Fig. 6a shows that all the unaged nano-silica modified binders have higher $G^*/\sin\delta$ values than control and warm mix binders, while the ZycoTherm-modified binder revealed insignificant resistance towards potential rutting in

comparison to the control binder and that this resistance increased significantly following the inclusion of nano-silica. By observing the outcomes of the modified binders, the addition of nano-silica to control and warm mix binders the enhancement levels at all temperatures are significant. The rutting enhancement is the result of nano-silica dispersion within the asphalt binder, where the NS particles adhere to the binder's surface, forming a new network structure of NS-modified asphalt binder. Fig. 6b shows the *G*/sin δ* values for RTFO-aged binders. Despite this, all nano-silica modified binders have a higher *G*/sin δ* than the control and warm mix binders, which is identical to the unaged condition. Control and warm mix binders having up to 6% NS by weight of binder had the greatest *G*/ sin δ* value, followed by binders containing 2% NS, while binders containing 4% NS had the lowest *G*/ sin δ* value. The incorporation of nano-silica into asphalt binder improves rutting resistance at elevated - temperatures in general, with the effects of 6% NS being the most substantial.

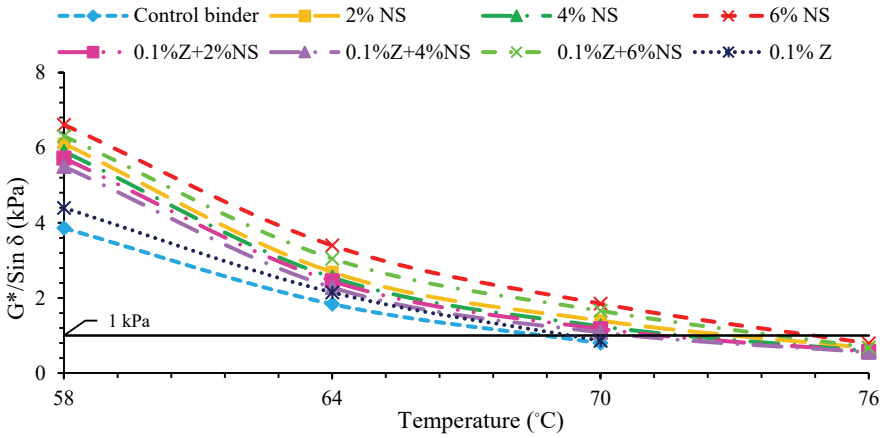

Figure 6a - G/sin δ for unaged control asphalt and modified binders*

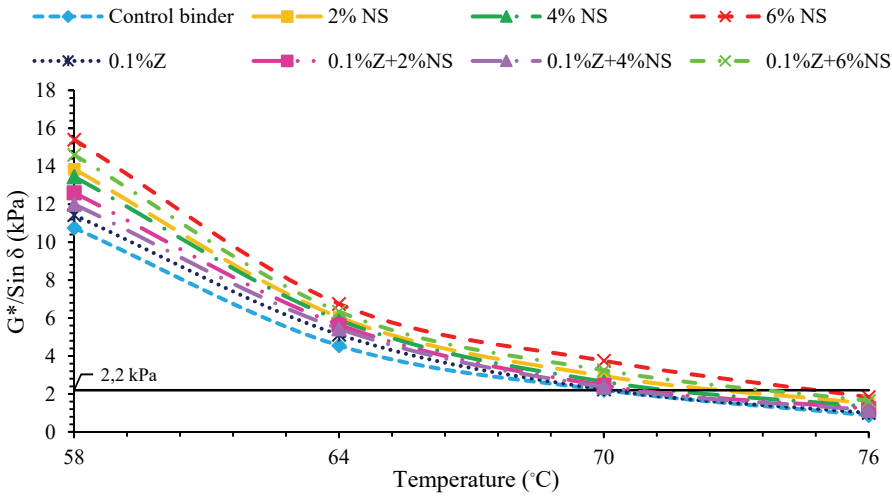

Figure 6b - G/sin δ after RTFO for control and modified binders*

5.5. Bending Beam Rheometer Test

The BBR test was utilized to assess the rheological features of the binders at low temperatures. As displayed in Fig. 7a and Fig.7b, at 60 seconds, all binders' creep stiffness and m-values were determined below 0 ˚C, -6 ˚C, -12 ˚C, and -18 ˚C. When the temperature was reduced from 0 ˚C to −18 ˚C for all asphalt binders, it is evident that the creep stiffness increased and the m-value decreased. Moreover, it is apparent that the creep stiffness of 2% NS, 4% NS, and 6% NS was higher than the control binder and the m-value for the binders was marginally less than that of the control binder. Nano-silica had a negative impact on binders' low-temperature performance, as evidenced by drop-in m- values and an increase in stiffness values. Additionally, the addition of nano-silica to the control asphalt in the absence of ZycoTherm did not effect on the control binder's low-temperature performance grade, despite changing the m-values and creep stiffness values. The insignificant influence of nano-silica on the low-temperature PG of binders was also documented in previous studies [10, 14, 32]. In comparison to the control binder, the creep stiffness is somewhat lower and the m-value higher for the warm mix binder containing 0.1% ZycoTherm. Furthermore, the ZycoTherm binder has a greater m-value as compared to control asphalt; a higher m-value indicates superior cracking resistance. The control asphalt met the low-temperature standards at -6 ˚C, whereas the ZycoTherm binder at -12 ˚C, as the m- value was more than 0.3. However, the creep stiffness increased and the m-values decreased when NS was added to the warm mix binder. As a result, adding nano-silica to the control asphalt does not effect on its low-temperature performance and is insufficient to change the low-temperature grade, whereas the ZycoTherm binder with or without nano-silica particles at low temperature is able of changing the performance grade for the control asphalt and cracking might be avoided. As a result of the findings, the control binder, warm mix binder, and nano-modified asphalt stiffnesses at 60 s were all below 300 MPa and the m-values for all the binders at the 60s were above 0.300. All the evaluated binders are within the Superpave™ specification.

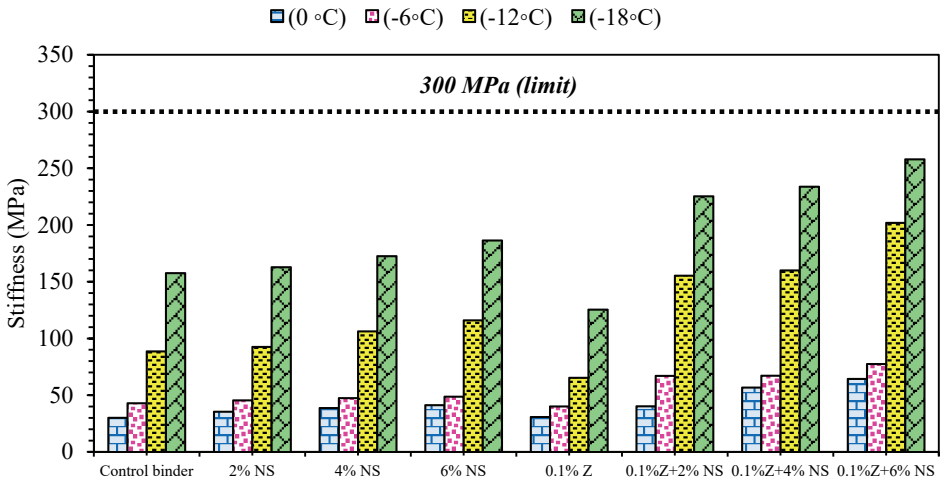

Figure 7a - Creep stiffness values for control and modified binders

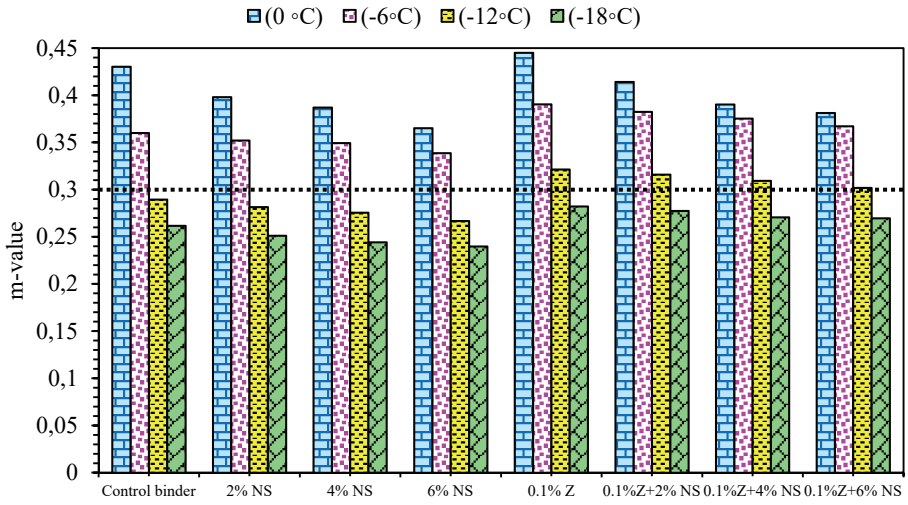

Figure 7b - m-values for control and modified binders

6. CONCLUSION

This research focused on analyzing the impacts of the various percentages of nano-silica (i.e., 2%, 4%, and 6%) on the basic physical features and the rheological features of the control and warm mix binders. Moreover, the research evaluated the impacts of various temperature and frequency ranges on complex modulus and phase angle values as well as the permanent deformation resistance by using the MSCR and Superpave rutting resistance parameter. The influence of low temperatures was utilized using the bending beam rheometer. The results obtained from this study are as follows.

The basic physical features reveal that by adding nano-silica to the control binder, the penetration values decreased while the softening point values increased. Additionally, the warm mix binders modified with nano-silica displayed better enhancement as opposed to the control binder and nano-silica modified binders without ZycoTherm.

By incorporating nano-silica into the control binder, the high-temperature susceptibility decreased and is better enhanced for warm mix binders modified with nano-silica.

The outcomes obtained from the rotational viscosity prove that nano-silica modified binders have higher values than warm mix binders modified with nano-silica. This implies that adding ZycoTherm decreases viscosity. The modified binders' viscosity values all fall within the Superpave specifications requirement at 135 ◦C.

The frequency sweep assessment reveals that the stiffness of the control and warm mix binders was enhanced with the inclusion of nano-silica, resulting in greater complex modulus (G*) values and lesser phase angle (δ) values and enhanced rutting resistance.

The MSCR evaluation displays the effect of nano-silica modified control and warm mix binders on improving the rutting resistance by boosting the recovery percentages and decreasing the J_{nr} values.

Based on the Superpave rutting resistance parameter $G^*/\sin\delta$, adding nano-silica to the control and warm mix binders increases the elasticity of the binder rendering it more resistant to rut.

The BBR test reveals that at low temperatures, applying nano-silica to the control asphalt increases creep stiffness, thus lowering the m-value. This demonstrates nano-silica's ineffectiveness at low temperatures, as well as its resistance to cracking. However, the inclusion of ZycoTherm material had a good influence on changing the grade from -16 ˚C to -22 ˚C, meaning that the ZycoTherm/ nano-silica modification had a greater effect on low-temp grade owing to the presence of ZycoTherm.

References

[1] Bastos, J.B., Babadopulos, L.F., Soares, J.B., Relationship between multiple stress creep recovery (MSCR) binder test results and asphalt concrete rutting resistance in Brazilian roadways, Construction and Building Materials, 145, 20-27, 2017.

[2] Santagata, E., Baglieri, O., Alam, M., Dalmazzo, D., novel procedure for the evaluation of anti-rutting potential of asphalt binders, International Journal of Pavement Engineering, 16(4), 287-296,2015.

[3] Deng, Y., Yang, Q., Rapid evaluation of a transverse crack on a semi-rigid pavement utilising deflection basin data, Road Materials and Pavement Design, 20(4), 929-942,2019.

[4] Kakar, M.R., Refaa, Z., Bueno, M., Worlitschek, J., Stamatiou, A., Partl, M.N., Investigating bitumen's direct interaction with Tetradecane as potential phase change material for low temperature applications, Road Materials and Pavement Design, 21(8), 2356-2363, 2020.

[5] Wang, T., Wang, J., Hou, X., Xiao, F., Effects of SARA fractions on low temperature properties of asphalt binders, Road Materials and Pavement Design, 22(3), 539-556, 2021.

[6] You, Z., Nanomaterials in asphalt pavements, International Journal of Pavement Research and Technology, 6(3), p.IV, 2013.

[7] Castillo Jr, L., State-of-the-art review of the applications of nanotechnology in pavement materials, Doctoral dissertation, Texas A&M University-Kingsville, 2014.

[8] Li, R., Xiao, F., Amirkhanian, S., You, Z., Huang, J., Developments of nano materials and technologies on asphalt materials–A review, Construction and Building Materials, 143, 633-648,2017.

[9] Martinho, F.C., Farinha, J.P.S., An overview of the use of nanoclay modified bitumen in asphalt mixtures for enhanced flexible pavement performances, Road Materials and Pavement Design, 20(3), 671-701,2019.

[10] Yao, H., You, Z., Li, L., Lee, C.H., Wingard, D., Yap, Y.K., Shi, X., Goh, S.W., Rheological properties and chemical bonding of asphalt modified with nanosilica, Journal of Materials in Civil Engineering, 25(11), 1619-1630,2013.

[11] Shafabakhsh, G., Motamedi, M., Firouznia, M., Isazadeh, M., Experimental investigation of the effect of asphalt binder modified with nanosilica on the rutting, fatigue and performance grade, Petroleum Science and Technology, 37(13), 1495-1500, 2019.

[12] Ghanoon, S. A., Tanzadeh, J., Laboratory evaluation of nano-silica modification on rutting resistance of asphalt Binder, Construction and Building Materials, 223, 1074-1082, 2019.

[13] Bhat, F.S., Mir, M.S., Rheological investigation of asphalt binder modified with nanosilica. International Journal of Pavement Research and Technology, 14(3), 276-287, 2021.

[14] Nejad, F.M., Nazari, H., Naderi, K., Karimiyan Khosroshahi, F., Hatefi Oskuei, M., Thermal and rheological properties of nanoparticle modified asphalt binder at low and intermediate temperature range, Petroleum Science and Technology, 35(7), 641-646,2017.

[15] Onochie, A., Fini, E., Yang, X., Mills-Beale, J., You, Z., Rheological characterization of nano-particle based bio-modified binder, In Transportation research board 9 2nd annual meeting, 125-131,2013.

[16] Saltan, M., Terzi, S., Karahancer, S., Examination of hot mix asphalt and binder performance modified with nano silica, Construction and Building Materials, 156, 976-984,2017.

[17] Arshad, A.K., Samsudin, M.S., Masri, K.A., Karim, M.R., Halim, A.A., Multiple stress creep and recovery of nanosilica modified asphalt binder, In MATEC Web of Conferences ,103, 09005, EDP Sciences, 2017.

[18] Moeini, A. R., Badiei, A., Rashidi, A. M., Effect of nanosilica morphology on modification of asphalt binder, Road Materials and Pavement Design, 21(8), 2230-2246, 2020.

[19] Ziari, H., Moniri, A., Imaninasab, R., Nakhaei, M., Effect of copper slag on performance of warm mix asphalt, International Journal of Pavement Engineering, 20(7), 775-781,2019.

[20] Behbahani, H., Ayazi, M.J., Moniri, A., Laboratory investigation of rutting performance of warm mix asphalt containing high content of reclaimed asphalt pavement, Petroleum Science and Technology, 35(15), 1556-1561,2017.

[21] Ziari, H., Mirzababaei, P., Babagoli, R., Properties of bituminous mixtures modified with a nano-organosilane additive, Petroleum Science and Technology, 34(4), 386-393,2016.

[22] Mirzababaei, P., Nejad, F.M., Vanaei, V., Investigation of rutting performance of asphalt binders containing warm additive, Petroleum Science and Technology, 35(1), 79-85,2017.

[23] Raufi, H., Topal, A., Sengoz, B., Kaya, D., Assessment of asphalt binders and Hot Mix asphalt modified with nanomaterials, Periodica Polytechnica Civil Engineering, 64(1), 1-13,2020.

[24] Ibrahim, I., Mehan, H.N.A., The effect of nano-materials on hot mixture "asphalt-concrete", *Open Journal of Civil Engineering*, *5*(04), 419, 2015.

[25] Yang, J., Tighe, S., A review of advances of nanotechnology in asphalt mixtures, Procedia-Social and Behavioral Sciences, 96, 1269-1276, 2013.

[26] Fernández, L.D., Lara, E., Mitchell, E.A., Checklist, diversity and distribution of testate amoebae in Chile, European Journal of Protistology, 51(5), 409-424,2015.

[27] Lazzara, G., Milioto, S., Dispersions of nanosilica in biocompatible copolymers, Polymer degradation and stability, 95(4), 610-617, 2010.

[28] Rohith, N., Ranjitha, J., A study on marshall stability properties of warm mix asphalt using zycotherm a chemical additive, International Journal of Engineering Research & Technology (IJERT). ISSN, 2278-0181, 2013.

[29] Read, J., Whiteoak, D. The Shell Bitumen Handbook, Thomas Telford, 2003

[30] Nazari, H., Naderi, K., Nejad, F. M., Improving aging resistance and fatigue performance of asphalt binders using inorganic nanoparticles, Construction and Building Materials, 170, 591-602, 2018.

[31] Sukhija, M., Saboo, N., Yadav, A. K., Rath, C., Laboratory study on the suitability of nano-silica as a modifier for asphalt binders, Construction and Building Materials, 302, 124406, 2021.

[32] Saed, S. A., Kamboozia, N., Mousavi Rad, S., Performance evaluation of stone matrix asphalt mixtures and low-temperature properties of asphalt binders containing reclaimed asphalt pavement materials modified with nanosilica, Journal of Materials in Civil Engineering, 34(1), 04021380, 2022.

Turkish Journal of Civil Engineering, 2023 103-124, Paper 727, ***Research Article***

Replacement of Stirrups by Steel Fibers in Shear Dominant UHPFRC Beams

Umut HASGÜL[1]
Altuğ YAVAŞ[2]
Tamer BİROL[3]

ABSTRACT

In the present study, the impacts of variety of fiber types and amounts on shear dominant Ultra High Performance Fiber Reinforced Concrete (UHPFRC) beams and the feasibility of fully replacement of stirrups by the steel fibers were investigated. Fifteen UHPFRC beams containing five different fiber types and three volume fractions were prepared without stirrup and were loaded under four-point loading. The influences of steel fiber were discussed in terms of the load-deflection behavior, cracking behavior, collapse modes, ultimate shear strength, nominal moment capacity and deflection ductility. The steel fiber use prominently increased the post-cracking stiffness and load capacity of the UHPFRC beams with the help of the fibers' crack-bridging ability. Conversely, the steel fibers in different types didn't have an importance on the collapse mode of the shear dominant UHPFRC beams. The use of straight steel fibers in the UHPFRC beams, even at very low volume fractions of 0.5 percent, changed the collapse condition from shear to flexure resulting in a ductile behavior. But the hooked fiber inclusion by 1.5 vol percent percent at least is needed to guarantee the flexural behavior regardless of hooked or multi hooked-end form.

Keywords: Ultra high performance fiber reinforced concrete, ultimate shear strength, moment capacity, fiber type, volume fraction.

1. INTRODUCTION

In recent years, the Ultra High Performance Fiber Reinforced Concrete (UHPFRC) has become one of the important products of concrete technology thanks to its many advantages. The UHPFRC use is a new option to fulfill the disadvantages of traditional normal strength

Note:
- This paper was received on March 22, 2022 and accepted for publication by the Editorial Board on January 11, 2023.
- Discussions on this paper will be accepted by May 31, 2023.
- https://doi.org/10.18400/tjce.1237663

1 Balikesir University, Department of Civil Engineering, Balıkesir, Türkiye
hasgul@balikesir.edu.tr - https://orcid.org/0000-0002-9358-3369

2 Balikesir University, Department of Civil Engineering, Balıkesir, Türkiye
ayavas@balikesir.edu.tr - https://orcid.org/0000-0002-2619-8671

3 Balikesir University, Department of Civil Engineering, Balıkesir, Türkiye
tbirol@balikesir.edu.tr - https://orcid.org/0000-0003-2428-6202

reinforced concrete in design and practical applications through its excellent compressive strength and considerably improved post-cracking tensile behavior. As widely used in the literature, when the concrete compressive strength exceeds the threshold of 130 MPa - 150 MPa and the tensile strain-hardening characterization is ensured by sufficient steel fiber content, this kind of special concrete mixture can be defined as the UHPFRC [1-6]. The compressive and tensile properties of UHPFRC are improved with optimization of the standard cement, silica fume, grand granulated blast slag, quartz flour and particular admixtures such as superplasticizer, air-entraining agent [1,7-10]. In addition, the steel fibers can be randomly dispersed in the UHPFRC mixture, which may be in straight, single, double or triple end-hooked, wavy or twisted forms, significantly improves the strength, stiffness and ductility of structural members. Compared to normal or high strength fibrous concrete, the UHPFRC has high level of compressive / tensile deformation capacities and durability through its high-density matrix and special curing techniques [2, 11, 12]. Thus, the superior mechanical properties of UHPFRC allow more economic and long-life structures in comparison to the traditional normal or high strength concrete usas [7, 13]. The above-mentioned advantages of the UHPFRC become much more evident in design applications of reinforced concrete beams [7, 13, 14].

Regarding the shear dominant UHPFRC beams, as in well-known structural behavior for the normal or high strength concrete, when the principal tensile stress exceeds the tensile stress of concrete, the diagonal inclined shear crack develops through the member's web region and thus the brittle collapse occurs in adverse manner. Owing to the superior mechanical properties of the UHPFRC, the steel fibers randomly added to the concrete mixture have a noteworthy potential to fully replace or partially reduce the stirrups or shear reinforcements or shear links which may lead to reinforcement congestion in slender cross-section members [7]. In the meantime, the inclusion of steel fibers considerably restricts the formation and propagation of shear cracks.

In earlier studies, the shear behavior of UHPFRC members with and without stirrups have been intensively investigated under two topics. The first one is the impact of fiber type and amount on the shear strength and failure pattern, and the second one is the feasibility of use of steel fibers in place of the stirrups or shear reinforcements. Some research studies by others widely reported that the addition of steel fibers to the UHPFRC beams enhanced their ultimate shear strength through the concrete's post-cracking strength, depending also upon the fiber geometry and volume fraction, compressive strength, tensile reinforcement characteristics, shear span-to-depth ratio [7, 15-25]. In this sense, Voo et al. [26] pointed out that the fiber type and amount didn't have a notable effect on the first cracking load, but they had a particular influence on the failure load and crack propagation. Baby et al. [15] revealed that the shear strength of UHPFRC beam not only depended on the compressive and tensile strengths, but also the cross-section shape, dispersion characteristics of fibers, level of applied pre-stressing load. Yang et al. [21] stated that the shear strength of a pre-stressed UHPFRC beams were larger than that of non-pre-stressed beam under same fiber content. Ciprian et al. [23] studied the impacts of mono and hybrid fiber usages to the shear behavior on I-shaped UHPFRC beams. For the considered fiber amounts of 1.5 vol percent, 2.0 vol percent and 2.55 vol percent, the hybrid fiber use was more effective than the mono use in point of the ultimate strength and cracking parameters. El-Dieb et al. [16] also noted that the ultimate strength of a UHPFRC beam containing the steel fibers of 1.2 vol percent was greater than that of beams with the stirrups. Qi et al. [17] obtained similar outcomes with respect to

these parameters in the shear dominant UHPFRC beams. They reported that the fiber type did not have a notable impact for same fiber volume fraction. At this point Yavas et al. [7] concluded that the steel fiber use in low volume fractions did not have significant effect on the first cracking levels regardless of fiber type. Nevertheless, the shear load exhibited an increasing trend for further fiber amounts. It was also noted that the UHPFRC members' collapse mode changed to flexure, indicating ductile behavior when the short-straight fibers of 1.5 vol percent were used. Lim and Hong [20] tested a series of rectangular shaped UHPFRC beams in shear. They reported for the cases with and without the shear reinforcement that the fiber use contributed positively to the shear strength and played an important role on restraining the cracks along with the shear reinforcement. It was also noted that the UHPFRC beams gained a significant strength even when the spacing of shear reinforcements was exceeded the stipulated limits in the ACI 318 design code. A similar study was conducted by Yavas and Goker [27] for four tensile reinforcement ratios ranging from 0.8 percent to 2.2 percent. Although the steel fibers were insufficient to prevent the shear failure at higher reinforcement ratios, the ultimate strength increased about 2 times in comparison to the non-fiber beam. However, the inclusion of hooked fibers to the concrete mixture changed the collapse mode to the ductile flexure failure for lower reinforcement ratios.

Another research issue for the shear dominant UHPFRC members is the feasibility of fully or partially replacement of stirrups by the steel fibers. Within this context, the partially use of steel fibers in place of the stirrups in the reinforced concrete members was included for the normal strength concrete in the ACI 318-19 [28]. But very limited information is available with regard to this challenge. Zagon et al. [29] studied the replacement of stirrups by steel fibers on the I-shaped UHPFRC beams exhibiting the shear behavior without steel fiber. They declared that the replacement of traditional stirrups by the steel fibers in particular volume fraction was feasible for moderate level of shear loads. The study recommended a combination of additional single diagonal rebar and steel fiber uses instead of fully stirrup use. Yoo et al. [30] investigated the elimination of minimum shear reinforcement in high-strength fibrous reinforced concrete beams. Based on the test results of five beams with and without the hooked fibers, the inclusion of steel fibers by 0.75 vol percent might correspond the minimum shear reinforcement stipulated in design codes. A similar outcome was presented in Lim and Hong [20] and they revealed that no shear reinforcement required for the UHPFRC beams including the fiber content of 1.5 vol percent. Qi et al. [17], on the other hand, recommended the use of moderate level stirrups to get better structural performance since the increasing fiber volume fraction did not ensure a notable contribution. Meszöly and Randl [31] discussed the importance of traditional stirrups and steel fiber usages on the shear behavior. The total of twenty I-shaped UHPFRC beams consisting of the non-fiber, short-straight fiber and different stirrup configurations was tested in the shear. The results showed that the steel fiber use, regardless of the volume fraction, provided notable contribution to the ultimate shear strength and ductility of UHPFRC beams compared to the configurations with the stirrup.

Various efforts were made on the shear response of UHPFRC beams, however, most of them focused on the short-straight fibers. In the existing studies, the feasibility of replacement of the stirrups in the reinforced concrete beams has not been examined for different fiber types. Thus, there is significant lack of knowledge about different fiber content (type and amount) on the shear behavior. In the experimental study presented here, the impact of various fiber

contents on the shear dominant UHPFRC beams as well as the best fiber content allowing the availability of steel fibers in place of the stirrups were investigated. In this context, a total of fifteen UHPFRC beams with five fiber types and three volume fractions were prepared without stirrup and they were loaded until collapse failure. In addition, two non-fiber reference beams were produced with/without the stirrups to represent pure effectiveness of steel fibers. The structural behaviors relation to the test beams were discussed in terms of the load-deflection behavior, cracking behavior and failure pattern, ultimate shear strength, nominal moment capacity and deflection ductility by referencing the non-fiber configurations.

2. EXPERIMENTAL PROGRAM

2.1. Mixture Design and Mechanical Properties

In the experimental program, the UHPFRC and non-fiber mixture compositions, which were previously developed in other studies by the authors, were used [6, 7]. So, the minimum concrete compressive strengths of 130-140 MPa and 110-120 MPa were targeted for the fibrous and non-fiber mixtures, respectively. The binder part of mixtures consisted of the standard cement CEM-I/42.5-R (C), silica fume (SF) and ground granulated blast-furnace slag (GGBFS). The aggregates consisted of two sizes of quartz sands, the particle sizes in the range of up to 0.8 mm (QS-1) and 1.0 to 3.0 mm (QS-2). In proportion to the traditional concrete mixtures, the water-to-binder ratio (W/B) for the designed concrete mixture was significantly reduced to 0.18 with the help of polycarboxylate ether-based superplasticizer (SP) which could provide adequate viscosity and workability. When the impacts of different fiber contents were investigated, two types of short-straight and two types of hooked and multi hooked-end steel fibers were used in the UHPFRC mixtures. However, the considered volume fractions of 0.5 percent, 1.0 percent and 1.5 percent comprised of the fiber use by 0.75 vol percent in place of the minimum shear reinforcement in the ACI 318-19 design code [28]. The mixture components and proportions, fiber dimensions, type and volume fractions,

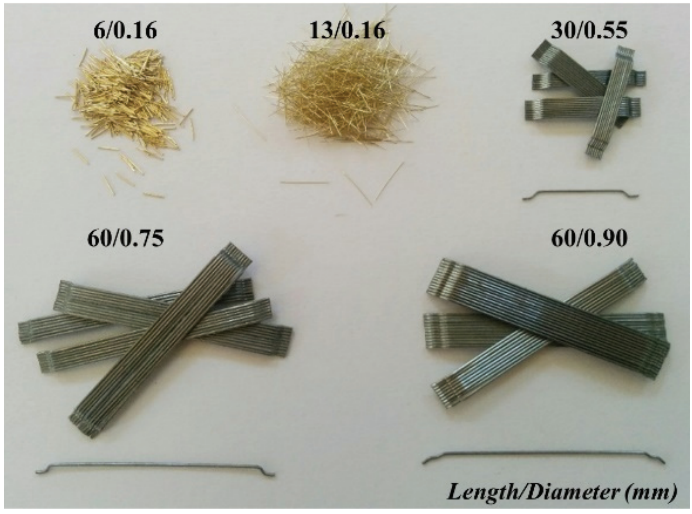

Figure 1 - The considered straight and hooked-end steel fiber types

characteristic strengths of tensile reinforcements are given in Figure 1 and Tables 1-2. The concrete compressive strength of each mixture was obtained from uniaxial compression tests using the cubic samples in the dimension of 100x100x100 mm^3 in accordance with the specifications of EN 12390-1 and EN 12390-3 [32-33]. Regarding the tensile strengths of mixtures, the dog bone-shaped samples having cross-sectional area of 30x30 mm^2 with the 68 mm overall width and 240 mm height were prepared. While the compression strengths of samples were measured by a hydraulic press with the 3000 kN loading capacity and rate of 1 MPa/s, the tensile strengths were determined through the universal testing machine with the displacement control by the loading speed of 0.1 mm/min. The samples were tested at 28 days.The average experimental strengths of cube and dog bone-shaped specimens corresponding to each beam configuration are summarized in Table 2. The test beams were coded by the fiber length, type and volume fraction (percent), respectively. Here, the *S*, *H* and *MH* denote the straight, hooked and multi hooked-end fibers, respectively. For instance, the code 13S_1.5 indicates the beam containing the straight fiber with the length of 13 mm by 1.5 vol percent (Table 2).

Table 1 - Material composition by weight (kg/m^3)

Mixture	Non-fiber	UHPFRC-1	UHPFRC-2	UHPFRC-3
C	690	690	690	690
SF	138	138	138	138
GGBFS	276	276	276	276
QS-1	542	535	530	525
QS-2	542	535	530	525
Water	199	199	199	199
SP	17.25	17.25	17.25	17.25
Steel fiber	-	0.5 vol percent	1.0 vol percent	1.5 vol percent

All UHPFRC mixtures showed higher compressive strength than the non-fiber mixture due its high-density matrix as well as the limitation of opening of micro cracks and further propagation by the steel fibers. Thus, the steel fiber use relatively improved the compressive strength in the percentages varying between 2 percent and 20 percent. It should be noted that the increases related to the mixtures containing the straight fibers of 13 mm were more apparent than those of other fiber types. However, the highest compressive strength was obtained for the mixture with 13 mm straight fiber by 1.5 vol percent. It can be deduced that, increasing fiber volume fraction enhanced the compressive strength, regardless of the fiber type, due to improvement in the mechanical bond strength, as shown in Table 2. Regarding this matter, the similar outcomes were pointed out in some research by others [6, 7, 9, 30, 34-36].

Table 2 - Steel fiber, reinforcement and concrete properties

Beam	Fiber					Rebar	Concrete	
	Type	L_f (mm)	L_f / D_f	f_t^{fib} (MPa)	percentvol	f_y and f_u (MPa)	f_c' (MPa)	f_t^{conc} (MPa)
NF	-	-	-	-	-	458 / 581	126	4.8
NF_OS							128	
6S_0.5	Straight	6	38	2500	0.5	466 / 570	132	5.8
6S_1.0					1.0		134	5.9
6S_1.5					1.5		139	7.9
13S_0.5	Straight	13	81	2500	0.5	469 / 593	144	5.9
13S_1.0					1.0		148	7.1
13S_1.5					1.5		152	10.2
30H_0.5	Hooked-end	30	55	1345	0.5	451 / 573	136	5.3
30H_1.0					1.0		142	5.6
30H_1.5					1.5		144	6.8
60H_0.5	Hooked-end	60	70	1225	0.5	484 / 597	131	4.7
60H_1.0					1.0		133	5.2
60H_1.5					1.5		137	6.1
60MH_0.5	Multi hooked-end	60	67	1500	0.5	488 / 607	130	4.3
60MH_1.0					1.0		132	6.4
60MH_1.5					1.5		135	7.7

L_f: fiber length, D_f: fiber diameter, f_t^{fib}: tensile strength of fiber, *percentvol* : fiber volume fraction,

f_y and f_u: yield and tensile strength, f_c': compressive strength, f_t^{conc}: tensile strength of concrete

As for the results of tensile strength, the inclusion of steel fibers ranged from 0.5 vol percent to 1.5 vol percent significantly improved the tensile strength by between 8 percent and 113 percent by depending also on the fiber geometry. It was also noted that when the fiber amount in the mixture increased from 0.5 vol percent to 1.0 vol percent, the tensile strength was more sensitively affected by the increase in fiber amount, as shown in Table 2. During the uniaxial sample tests, the brittle collapse occurred once the first cracking was observed on the non-fiber specimen, as expected. After this stage, the tensile strain-hardening behavior was achieved for the fibrous concrete mixtures above 1.0 vol percent except for the shortest straight fiber of 6 mm (Figure 2). This fiber type did not exhibit hardening response for the

overall volume fractions since the fiber length could not build a bridge on both sides of cracks. Beyond the peak load level, the fibers began to slide out because of the growing of cracks in the tensile region. Thus, the strength drops launched on axial force - deflection relationships of the samples.

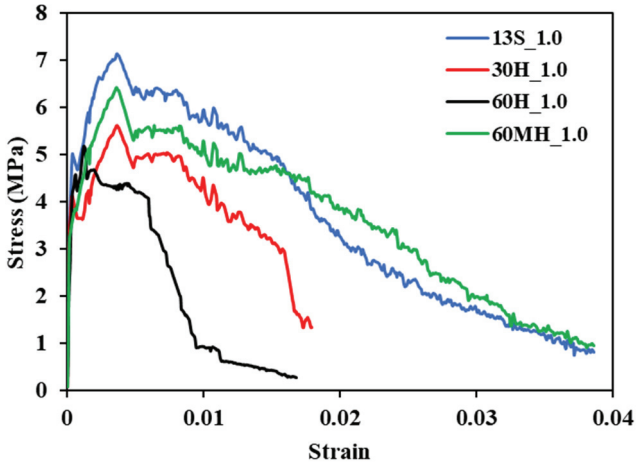

Figure 2 - Stress-strain relationships of specimens with fiber volume fraction of 1.0 percent showing strain hardening behavior

2.2. Preparation of UHPFRC Test Beams

In the framework of this study, a total of fifteen simply reinforced UHPFRC beams consisting of five fiber types were prepared for three volume fractions. In addition, two non-fiber reference beams were produced with (NF_OS) and without (NF) the stirrup to reveal the impacts of variety of fiber content (type and amount). The dimensions of the test beams are 100x150x1500 mm and clear span between the two supports is 1400 mm. The tensile reinforcement ratio was kept constant as 2.4 percent, which composed of two 14 mm steel rebars. Whereas the considered reinforcement ratio almost corresponds the upper limit (2.0 percent) in the Turkish Design Standard (TS 500) [37], the maximum ratio stipulated in the ACI 318 design code was modified by the strain equilibrium in the recent editions [28, 38, 39], in which the ratio was calculated as 6.3 percent.

The beam dimensions and reinforcement details are presented for a typical test beam in Figure 3. Three coupon samples related to the longitudinal reinforcements for each test group were tested under the direct tension. In this way, the average yield and tensile strengths of the samples are given in Table 2. The ends of longitudinal reinforcements were hooked to avoid the premature bond failure. Shear reinforcement was not provided in the shear span of UHPFRC beams to eliminate the influences of other components. While the beam NF was designed to fail by shear, the beam NF_OS was equipped with open stirrups with 8 mm diameter and the spacing of 65 mm, which almost corresponds to the minimum transverse spacing in the TS 500 and ACI 318-19 guidelines [37, 28], as shown in Figure 3. Overall, the preparation and casting procedures in regard to the test beams can be found in detail in Hasgul et al. and Yavas et al. [7, 13].

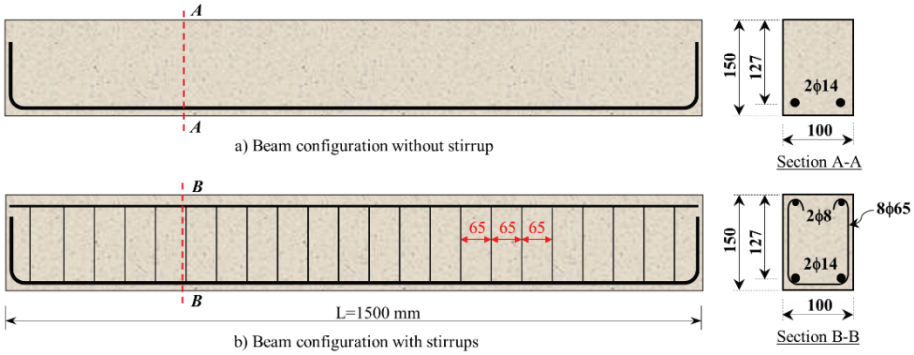

Figure 3 - Schematic representations of test beams

2.3. Test Setup

The four-point loading test setup is presented in Figure 4. In the study, the shear-span to depth ratio (a/d) was 3.9 for all beams, and the vertical loads were applied at a distance of 500 mm from both supports. Referring to Figure 4, a load cell was attached between the jack and spreader beam to measure the applied load. The load P was applied to the beams as two equal concentrated loads as $P/2$ and $P/2$ through a steel spreader beam. Later on, the load increments were monotonically applied to the beam by a hydraulic servo testing machine with the capacity of 500 kN. The whole tests were conducted under deflection control procedure at 0.2 mm/min.

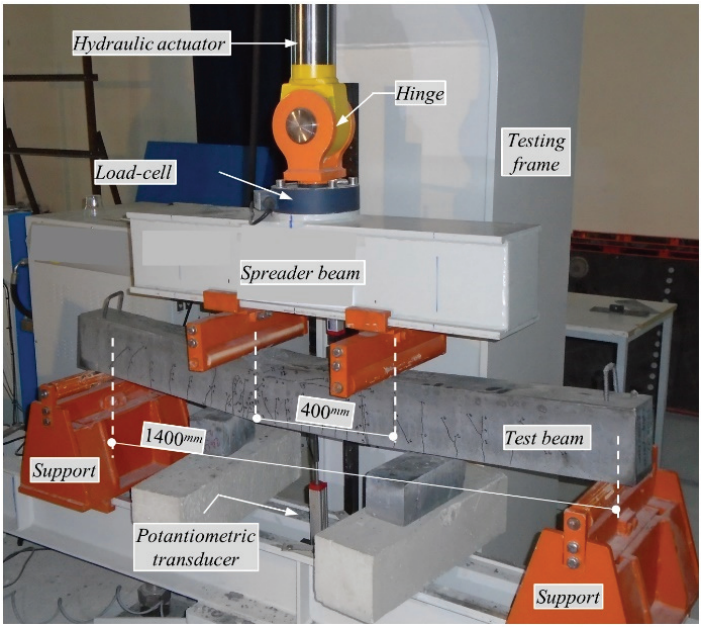

Figure 4 - The four-point loading system

It should be noted that the loading speed for the test beams changing to flexure was increased to 0.5 mm/min to reduce duration between the peak and ultimate deflections. A potentiometric transducer was mounted the bottom face of beam midpoint to measure vertical deflections. The applied load (P) and mid-span deflections (Δ) were recorded by use of 24-channel data acquisition system that had the data-recording frequency of 8 Hz per channel. At the certain deflection steps, the crack formations and propagations were highlighted over the test beams.

3. TEST RESULTS AND DISCUSSIONS

In the experimental program, the total of seventeen singly reinforced UHPFRC beams and non-fiber reference beams were loaded under the four-point loading scheme until collapse failure. Because of conducted various loadings, the parameters of P–Δ behavior, cracking pattern and collapse mode, ultimate shear strength, nominal moment capacity and deflection ductility were discussed by comparing them with the non-fiber reference configurations.

3.1. Load-Deflection Relationships

The test beams were subjected to the planned loading protocol until the collapse condition and their load (P) and mid-span deflection (Δ) behaviors were determined (Figure 5). The P–Δ relationships and corresponding crack patterns at the collapse conditions are given for each fiber type in Figure 5. In addition, the main quantitative features obtained from the loadings are summarized in Table 3. It should be noted at this point that the deflection and ductility responses beyond the peak load were determined for only the beams the structural behavior of which transformed from the shear to flexure after the steel fiber use. Firstly, the yield deflection Δ_y was calculated from the bi-linearized $P - \Delta$ relationship, which is one of the methods recommended in Park [40]. Here, the deflection point Δ_y corresponds to the deflection at the intersection of secant stiffness at the peak load P_p and $0.75P_p$ [2, 13]. Secondly, Park [40] also proposed some procedures to specify the ultimate deflection Δ_u of an experimental load-deflection relationship. One of these procedures, which is well-known as the load reduction method of 20 percent, was based on in the study [41-44].

Referring to Figure 5, all the P–Δ relationships showed linear elastic response until the first cracking point and stiffness degradations commenced on the beam responses. In the post cracking stage, the P-Δ relationships could be divided into two groups according to their collapse conditions as the shear or flexure. In the shear dominant beams, as shown in Figures 5c-5e, a dramatic load drop occurred without any significant increase in the deflection response as well as before the yielding of reinforcement.

When the stirrup or sufficient fiber content was provided, full flexural response was observed by reinforcement yielding following the deflection hardening as well as strength degradation after the peak load (Figures 5a-5e). The short-straight fibers considered each volume fraction prominently improved the post-cracking stiffness values and load-carrying capacities of the UHPFRC beams in comparison with the non-fiber configuration because of the crack-bridging ability of the fibers which allows smaller deflections even at higher load levels. In addition, the stiffness and load capacity showed an increasing trend with the increases in the

fiber amount. While the hooked and multi hooked-end fibers provide ductile flexural behavior for only 1.5 percent volumetric ratio, they significantly improved the capacity with respected to the reference beam NF_OS, especially beams with long hooked-end fibers of 60H_1.5 and 60MH_1.5 (Figures 5c-5e). However, these beams were limited in terms of deflection capacity compared with the beam NF_OS. These results are very compatible with the previous studies in relation to the structural behavior of UHPFRC beams [2, 7, 13, 17, 45-48].

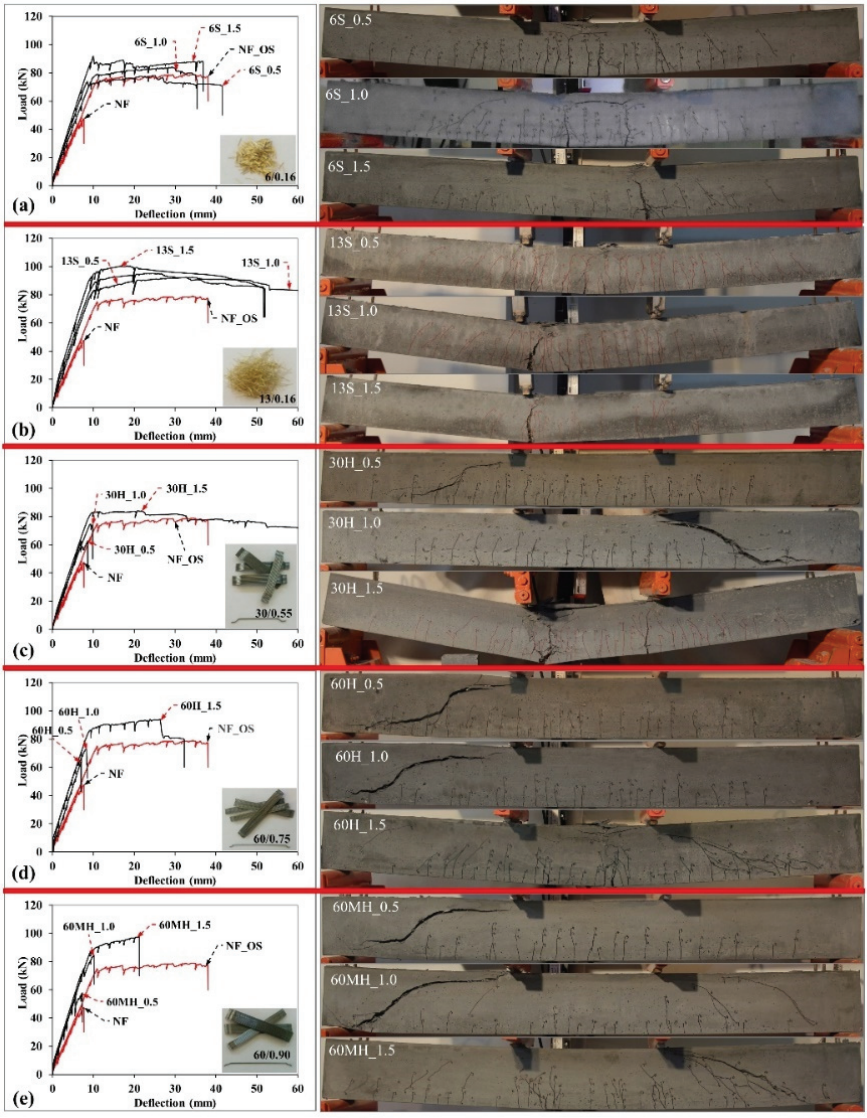

Figure 5 - P–Δ relationships and collapse modes of the test beams; a)6S, b)13S, c)30H, d)60H, e)60MH

Table 3 - Characteristic values of P–Δ relationships at various stages and collapse modes

Beam	Δ_y (mm)	P_y (kN)	Δ_p (mm)	P_p (kN)	Δ_u (mm)	P_u (kN)	Ductility index		Collapse mode
							Δ_p/Δ_y	Δ_u/Δ_y	
NF	-	-	7.57	47.41	-	-	-	-	DT
NF_OS	11.23	71.36	34.28	78.84	38.1	77.37	3.05	3.39	CC
6S_0.5	8.57	73.31	24.72	78.19	41.54	70.38	2.88	4.85	CC
6S_1.0	10.41	78.19	29.22	83.85	35.32	74.62	2.81	3.39	CC
6S_1.5	9.53	88.21	9.95	91.87	36.86	87.05	1.04	3.87	CC
13S_0.5	10.54	82.84	32.76	92.35	51.65	84.75	3.11	4.90	CC
13S_1.0	10.22	88.15	23.37	95.11	72.01	76.09	2.29	7.05	RR
13S_1.5	9.58	92.87	18.16	100.32	51.94	84.23	1.90	5.42	RR
30H_0.5	-	-	8.62	62.76	-	-	-	-	DT
30H_1.0	-	-	9.26	74.58	-	-	-	-	DT
30H_1.5	9.00	80.25	20.88	84.08	66.74	67.24	2.32	7.42	CC
60H_0.5	-	-	6.99	63.62	-	-	-	-	DT
60H_1.0	-	-	8.26	72.90	-	-	-	-	DT
60H_1.5	9.40	84.56	26.27	93.81	32.25	79.80	2.79	3.43	CC
60MH_0.5	-	-	7.26	57.78	-	-	-	-	DT
60MH_1.0	-	-	10.19	84.37	-	-	-	-	DT
60MH_1.5	-	-	21.16	97.60	-	-	-	-	F+DT

P_y: yield load, P_p: peak load, P_u: ultimate load, Δ_y: yield deflection, Δ_p: peak deflection, Δ_u: ultimate deflection, DT: diagonal tension, CC: concrete crushing, RR: reinforcement rupture, F: Flexure

3.2. Cracking Behavior and Collapse Modes

The collapse conditions of UHPFRC beams with respect to the studied fiber types are presented for three volume fractions in Figure 5. At the beginning of load steps, the vertical flexural cracks vertically commenced at the lowermost faces in the constant moment zone of the beams. Thereafter, additional vertical cracks formed alongside the existing cracks with the increasing loads, but the crack widths remained in a well-restricted level for the UHPFRC beams because the steel fibers built a bridge between both sides of the cracks. But it is not easy to see these cracks with naked eyes until the peak load in the $P - \Delta$ relationship. These cracks can be only seen with the help of crack width magnifier. As the load increased further, the member behavior and collapse modes separated depending on the fibers type and amount as shown in Figure 5.

For the reference beam (NF) without the fiber and stirrup, when the principal tensile stress reached the tensile strength of concrete, as in the conventional normal strength concrete, the beam failed suddenly as a consequence of formation of diagonal single crack initiated in the

shear span and propagated between the loading point and support, as shown in Figure 6a. This collapse mode points out the diagonal tension (DT) in the brittle manner. At this point, while the test beams containing the hooked or multi hooked-end fiber by 0.5 vol percent and 1.0 vol percent failed by the DT, the fibers significantly delayed the formation of shear cracks (Figure 6a). However, the beam 60MH_1.5 exhibited the flexure-shear failure by a splitting at the diagonal crack after the tensile reinforcement yielded. It can be deduced that the steel fiber type has an important influence on the collapse mode of the shear dominant UHPFRC beams.

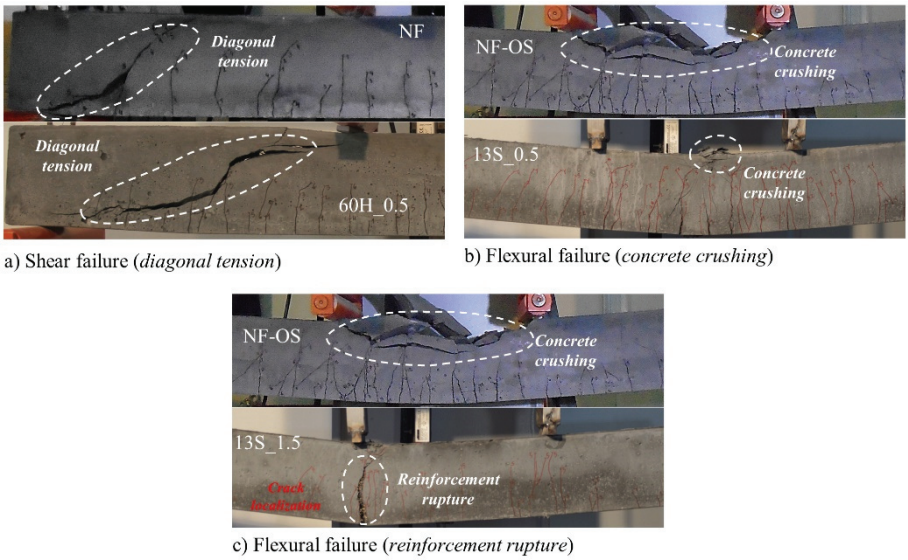

a) Shear failure (*diagonal tension*)

b) Flexural failure (*concrete crushing*)

c) Flexural failure (*reinforcement rupture*)

Figure 6 - Typical collapse modes for the test beams

Whereas the reference beam NF was designed to fail by shear, the reference beam NF_OS, which had the minimum shear reinforcement ratio, exhibited full flexural behavior resulting the concrete crushing (CC) along a wide region at the constant moment zone, as shown in Figures 6b-6c. The catastrophic collapse with the CC occurred in the compression zone when the critical section of beam reached their flexural capacity. When it comes to the UHPFRC beams without stirrup having an adequate fiber content in the concrete matrix, the test beams showed well enough stable behavior from the beginning to the end of tests through the deformation ability provided by the steel fibers. In this regard, the fibers prevented the formation of diagonal cracks therefore, well-distributed flexural cracks propagated towards to the compression zone with further load increments, as shown in Figure 5.

The beams containing the straight fiber of 6 mm as well as the beams 13S_0.5, 30H_1.5 and 60H_1.5 failed by the concrete crushing (CC) as such in the reference beam NF_OS rather than the non-ductile shear failure (Figure 6b). While the CC occurred in the UHPFRC beams, the deformation stayed at a limited region since the steel fibers produced a kind of confinement effect in comparison with the NF_OS. For the beams 13S_1.0 and 13S_1.5, flexural behavior was terminated by the reinforcement rupture (RR). In the UHPFRC beams

with flexural failure, a large crack formed at a single point adjacent to the beam midpoint. As shown in Figure 6c, the related crack width intensely enlarged as against others and dominated the beams' collapse mode. This response of UHPFRC is widely defined as the crack localization [44, 48-51]. It should be noted that even though the crack localization phenomenon occurred in all UHPFRC beams, only the beams 13S_1.0 and 1.5 failed by RR. This outcome indicates that the use of 13 mm straight steel fiber pointedly increased the compressive deformation capacity of the UHPFRC more than other fiber types. Despite the increased deformation, the concrete did not crush and eventually the RR occurred. Regarding the crack localization phenomenon, while the research by others [2, 13, 30, 45, 52] reported the RR for only the 13 mm straight fiber, Yoo and Yoon [46] declared that the rupturing failure was inevitable under low reinforcement ratio regardless of the fiber type. Sturm et al. [52] also pointed out that the reinforcement ratio had particular importance on the collapse condition. The authors' previous study [13] confirmed this outcome since very high strength and deformation capacity of the UHPFRC could allow the use of excessive tensile reinforcements.

It can be deduced from these tests that the use of short-straight fiber in the UHPFRC beams, even at very low volume fractions of 0.5 percent, changed the collapse mode to flexure resulting the ductile behavior without placing the stirrups. However, the hooked fiber inclusion by 1.5 vol percent at least is needed to guarantee the flexural behavior regardless of hooked or multi hooked-end form. The test results also revealed that the short-straight fibers showed much better performance in terms of the limitation of diagonal cracks as against the hooked fiber types. This is related to the fact that number of the hooked fibers in per unit volume is lower than the straight fibers due to their longer length. Beside this, the dispersion and orientation of longer fibers became poor because of the blocking effect of longitudinal reinforcement.

3.3. Deflection Ductilities

For the UHPFRC beams exhibiting the flexure behavior with the help of some fiber contents, the ductility responses were evaluated by the peak load deflection ductility $\mu_{\Delta p}$ and ultimate deflection ductility $\mu_{\Delta u}$. Firstly, the ductility corresponding to the peak load can be determined by proportioning the deflection at the peak load Δ_p to the yield deflection Δ_y. Secondly, the deflection ductility capacity can be calculated by considering the ultimate deflection Δ_u instead of the Δ_p for the beams continued to sustain loads well beyond the peak load, just as the UHPFRC beams. Both ductility indexes calculated for the corresponding UHPFRC beams as well as the reference NF_OS beam are compared in Figure 7. It can be noted that the test beams that failed by the shear were left out of the flexural assessments.

Referring the Figure 7 and Table 3, while the ductility levels at the peak loads of the beams 6S_0.5 and 13S_0.5 nearly corresponded to that of the reference beam NF_OS, regardless of the fiber length, the ductility level provided by the stirrups couldn't be ensured for higher fiber amounts. The reason of this is that as the fiber volume fraction increased in the concrete matrix, its restriction ability on the crack formations was enhanced. Thus, the beam deflections before the peak load decreased by a certain amount in comparison to the non-fiber stirrup configuration. This circumstance led to a decrease in the peak load ductility with the increase of fiber amounts. Figure 7 also allows to compare the effect of fiber length for

1.5 vol percent. Accordingly, longer fiber use slightly increased the deflection ductility due to fibers' low efficiency in the pre-peak area where the crack widths were too small.

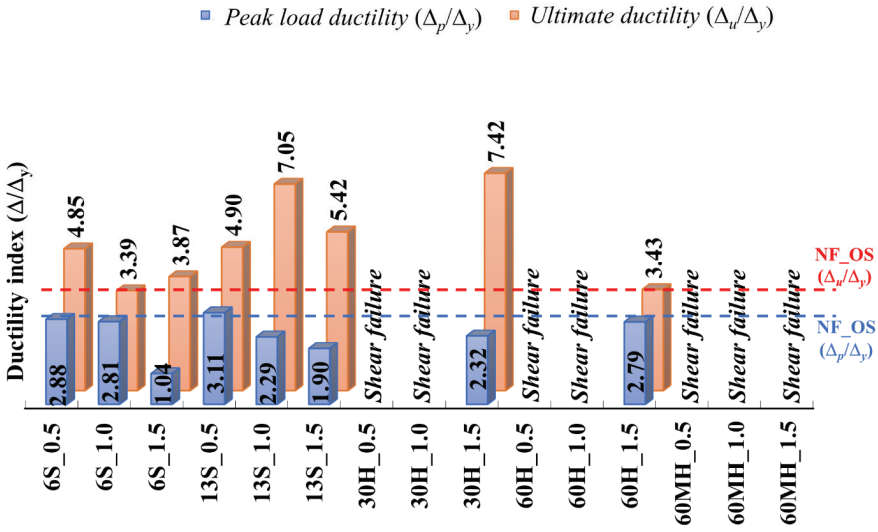

Figure 7 - Ductility indexes at the peak load and ultimate deflection

From the point of the ultimate deflection ductility $\mu_{\Delta u}$, as shown in Figure 7, fully replacement of stirrups by the straight fibers of 6 mm and 13 mm is feasible for the considered volume fractions. Moreover, these UHPFRC beams showed more ductile behavior up to 2.1 times compared to NF_OS. It can be pointed out that the minimum 1.5 vol percent needed to get the same ductility level by the hooked fiber (Figure 7). Here, the ductility performance of hooked-end fiber 30H was better than the 60H and 60DH. While the ductility ratio obtained for the beam 30H_1.5 was greater 2.2 times than that of the beam NF_OS, the beam 60H_1.5 exhibited the same ductility level. But the multi hooked-end fiber use, even at 1.5 vol percent, could not change the collapse condition to the flexure. However, there was no apparent trend between the considered fiber types and amounts from the point of the ultimate ductility (Figure 7). It can be also understood that while the fiber length relating to the straight fiber did not affect the ductility ratio for the lowest volume fraction, it became an important variable to be considered for additional volume ratios. Unfortunately, it is not easy to support this outcome for the UHPFRC beams with the hooked or multi hooked-end fiber types because the most of them failed by shear. Regarding this issue, Yoo and Yoon [48] and Singh et al. [45] reported that higher flexural ductility could be achieved as the fiber length increases in the UHPFRC matrix. From the point of ductility definitions, it can be clearly deduced that the most effective fiber type was the 13 mm straight fiber (Figure 7). This fiber type not only had a great potential to change the structural behavior of shear dominant UHPFRC beams, but also provided the stipulated ductility by means of the stirrups in design codes.

3.4. Shear and Flexural Capacities

In the shear dominant UHPFRC beams exhibiting the brittle failure even when higher amount of steel fiber was used for the certain fiber types, the ultimate shear strengths V_u of UHPFRC and non-fiber reference beam are presented together in Figure 8 in order to show how the fiber content influenced the behavior. It can be added that the test beams displaying flexural collapse were left out in the discussions related to the shear strengths.

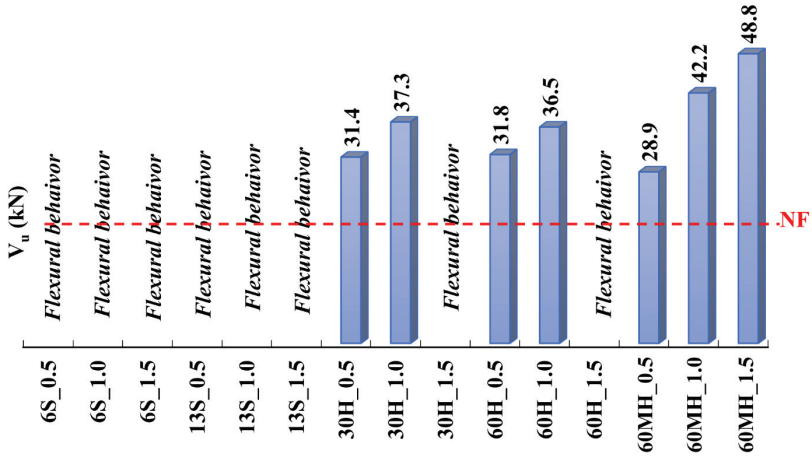

Figure 8 - Influences of fiber type and amount on the shear strength of UHPFRC beams

Referring the Figure 8 and Table 3, the strength of shear dominant beams were much higher than those of the non-fiber configuration. Besides, an increase in the volume fraction of fibers uniformly enhanced the shear strength, regardless of the fiber type for both 0.5 vol percent and 1.0 vol percent. However, the steel fibers increased the shear strength in ratios varying between 22 percent and 106 percent depending on whether the fiber type is hooked or multi hooked-end (Table 3). As a side note, an increment of 0.5 percent in the fiber amount gained significant strength varying between 15 percent and 46 percent.

While various investigations [7, 15-25] generally accepted the view that the steel fibers enhance the shear strength, the provided strength increase was more apparent for the fiber amounts higher than 1.0 vol percent according to Pansuk et al. [53] and Meszöly and Randl [31]. For the same fiber amount (1.0 vol percent), Meszöly and Randl [31] obtained roughly four times higher capacity than non-fiber condition. However, the authors' previous study [7] revealed that the fiber contribution on shear strength remained very limited below 0.5 vol percent for the straight, hooked and multi hooked-end fibers.

Figure 8 also indicates that the fiber type does not have an importance on the ultimate strength of shear dominant UHPFRC beams. Besides that, the choice of hooked or multi hooked-end fiber type did not affect the shear behavior distinctively. Although the largest capacity enhancement among the test beams was obtained for the beam 60DH_1.5, this fiber type could not transform the collapse mode to the flexure in contrast to other UHPFRC beams having 1.5 vol percent. On the other hand, the nominal moment capacities M_p corresponding

to peak load of the experimental load-deflection relationships with respect to the UHPFRC beams transferring the flexure by steel fibers as well as the non-fiber beam with the minimum transverse reinforcement are presented for each volume fraction in Figure 9. Parallel to the shear strength, the test beams failed by shear were left out in the discussions. For the UHPFRC beams exhibiting flexural behavior, a small increment in the fiber amount provided notable contribution to the capacity in a positive manner. So, the moments were enhanced up to 27 percent depending on the fiber amount in the concrete matrix (Table 3). However, the fiber type had a particular influence on the moment capacity unlike the shear behavior. In this sense, longer fiber length resulted in an apparent capacity increase for the straight fiber type since the fibers' crack-bridging ability improved across the crack width. The moment capacities of beams 13S_0.5, 1.0 and 1.5 were greater by 18 percent, 13 percent and 9 percent than those of the 6S_0.5, 1.0 and 1.5, respectively.

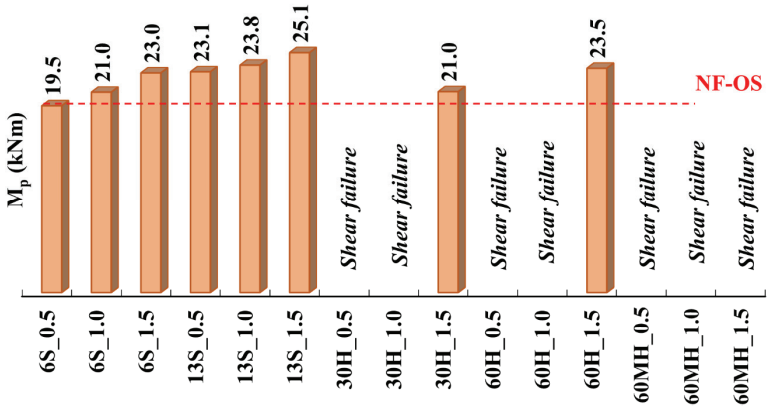

Figure 9 - Influences of fiber type and amount on the moment capacity of UHPFRC beams

Considering both straight fiber types, whereas the 0.5 vol percent for the fiber 6S almost corresponded to the minimum transverse reinforcement, as shown in Figure 9, the hooked fiber inclusion by 1.5 vol percent at least was required to guarantee the flexural behavior. For others, the 30 mm and 60 mm hooked fibers for the related fiber amount could improve the moment capacity by 7 percent and 19 percent when compared with NF_OS, respectively. As in the straight fibers, it is perceived that the variation of moment capacity will be in an increasing tendency as the length of hooked fiber increases to the further amounts such as 2.0 vol percent and 2.5 vol percent. The best performance from the point of the moment capacity was obtained once again for the beam 13S_1.5 (Figure 9). These results indicated that the use of straight fibers in place of the stirrups in UHPFRC beams not only transformed the collapse mode from the shear behavior, but also provided additional flexural capacity even for the lowest volume fraction considered (0.5 vol percent). It should be also noted that these findings are based on the considered UHPFRC matrix and steel fiber content used in this study. It is necessary to emphasize that this ratio is far below the ACI 318 criteria [28], in which the minimum amount of steel fiber by 0.75 vol percent is needed for the stirrup replacement in the structural members produced by the normal strength fibrous concrete.

4. CONCLUSIONS

In the present study, the impacts of different fiber contents on the shear dominant UHPFRC beams as well as the feasibility of fully replacement of stirrups by the steel fibers were investigated. In this framework, the total of fifteen UHPFRC beams containing five different fiber types and three volume ratios were prepared without transverse reinforcement and were loaded until collapse failure. The following findings can be drawn from the experimental investigations:

- All the *P*–Δ relationships of UHPFRC beams showed linear elastic response until the first cracking points. Beyond this level, all *P*–Δ relationships were divided into two groups according to their collapse modes as shear or flexure.
- Regarding UHPFRC beams that failed in the form of diagonal tension, the steel fiber use substantially increased the post-cracking stiffness and load capacity in comparison with the non-fiber reference configuration because of the crack-bridging ability which allowed smaller deflections even at higher load levels. However, the fiber type did not have an important influence on the shear failure. As in the existing shear investigations, the shear strengths of UHPFRC beams were much higher than that of the non-fiber configuration. However, an increase in the volume fraction of fibers uniformly enhanced the shear strength, regardless of the fiber type.
- On the other hand, the UHPFRC beams, in which an adequate fiber content was ensured without stirrup, showed well enough stable behavior through the deformation ability provided by the steel fibers. The fibers prevented the formation of diagonal cracks for further load increments and thus, well-disturbed vertical cracks propagated towards to the uppermost compression face. Accordingly, the test beams with the straight fiber of 6 mm as well as the 13S_0.5, 30H_1.5 and 60H_1.5 failed by the concrete crushing. Differently, the beams 13S_1.0 and 1.5 showed more deformation ability than other beams and failed by the reinforcement rupture due to the crack localization phenomenon.
- A small increase of the fiber amount provided notable contribution to the moment capacity in a positive manner. So, the moments increased up to 27 percent depending on the fiber amount in the concrete matrix. Unlike the shear behavior, the fiber type has also a particular influence on the moment capacity.
- It can be drawn from the conducted tests that the use of straight fiber in the UHPFRC beams, even at very low volume fraction of 0.5 percent, changed the collapse condition to flexure resulting the ductile behavior without placing the stirrups. It is important to note that this ratio is far below the ACI 318 requirements regarding stirrup replacement in the structural members. However, the hooked fiber inclusion by 1.5 vol percent at least is needed to guarantee the flexural behavior regardless of hooked or multi hooked-end form.
- Referring to the ultimate deflection ductility, the full replacement of stirrups by the straight fibers of 6 mm and 13 mm is feasible for fiber amounts by 0.5 percent-1.5 percent by volume. These beams showed more ductile behavior up to 2.1 times in proportion to the non-fiber configuration with the stirrups. But the 1.5 vol percent

at least is needed to get same ductility level by the hooked fiber because of less homogenous dispersion and less numbers per unit volume.

The primarily results of this study revealed that the fiber type and amount significantly affects the shear and flexural behaviors of the UHPFRC members. It should be also noted that these findings are based on the considered UHPFRC matrix and steel fiber content used in this study. Similar studies incorporating other parameters such as fiber contents, shear span-to-depth ratios, reinforcement ratios, and loading conditions, will play an important role on the preparing of specific code and standard regarding the UHPFRC.

Acknowledgement:

This research was funded by the Scientific Research Projects' Foundation of Balikesir University (Project No: 2018/151).

References

[1] Graybeal BA. Flexural behavior of an ultrahigh-performance concrete I-girder. J Bridge Eng 2008;13(6):602-10. https://doi.org/10.1061/(ASCE)1084-0702(2008)13:6(602).

[2] Turker K, Hasgul U, Birol T, Yavas A, Yazici H. Hybrid fiber use on flexural behavior of ultra high performance fiber reinforced concrete beams. Compos Struct 2019;229,111400.https://doi.org/10.1016/j.compstruct.2019.111400.

[3] Yoo DY, Kang ST, Lee JH, Yoon YS. Effect of shrinkage reducing admixture on tensile and flexural behaviors of UHPFRC considering fiber distribution characteristics. Cem Concr Res 2013;54:180-190. https://doi.org/10.1016/j.cemconres.2013.09.006.

[4] Kusumawardaningsih Y, Fehling E, Ismail M, Aboubakr AAM. Tensile strength behavior of UHPC and UHPFRC. Procedia Eng 2015;125:1081-1086. https://doi.org/10.1016/j.proeng.2015.11.166.

[5] ACI PRC-239-18. Ultra-high-performance concrete: An emerging technology report. American Concrete Institute, Farmington Hills, MI, USA, 2018.

[6] Yavas A, Birol T, Turker K, Hasgul U, Yazici H. Improvement of flexural performance of UHPFRC with hybrid steel fiber. Tech J 2020;31(6):10379-10397. https://doi.org/10.18400/tekderg.485565.

[7] Yavas A, Hasgul U, Turker K, Birol T. Effective fiber type investigation on the shear behavior of ultrahigh-performance fiber-reinforced concrete beams. Adv Struc Eng 2019;22(7):1591-1605. https://doi.org/10.1177/1369433218820788.

[8] Park JJ, Kang ST, Koh KT, Kim SW. Influence of the Ingredients on the Compressive Strength of UHPC as A Fundamental Study to Optimize the Mixing Proportion. In Proceedings of the Second International Symposium on Ultra High Performance Concrete, Kassel, Germany, 5-7 March 2008:105–112.

[9] Yoo DY, Lee JH, Yoon YS. Effect of fiber content on mechanical and fracture properties of ultra high performance fiber reinforced cementitious composites. Compos Struct 2013;106:742-753. https://doi.org/10.1016/j.compstruct.2013.07.033.

[10] Meng W, Valipour M, Khayat KH. Optimization and performance of cost-effective ultra-high performance concrete. Mater Struct 2017;50:1-16. https://doi.org/10.1617/s11527-016-0896-3

[11] Banthia N, Majdzadeh F, Wu J, Bindiganavile V. Fiber synergy in hybrid fiber reinforced concrete (HyFRC) in flexure and direct shear. Cem Concr Compos 2014;48:91-7. https://doi.org/10.1016/j.cemconcomp.2013.10.018.

[12] Yoo DY, Banthia N, Yoon YS. Flexural behavior of ultra-high-performance fiber-reinforced concrete beams reinforced with GFRP and steel rebars. Eng Struct 2016;111:246-262. https://doi.org/10.1016/j.engstruct.2015.12.003.

[13] Hasgul U, Turker K, Birol T, Yavas A. Flexural behavior of ultra-high-performance fiber reinforced concrete beams with low and high reinforcement ratios. Struct Conc 2018;19(6):1577-1590. https://doi.org/10.1002/suco.201700089.

[14] Turker K, Birol T, Yavas A, Hasgul U. Effective steel fiber type investigation on ultra high performance fiber reinforced concrete beams. Afyon Kocatepe Univ J Sci Eng 2016;16: 776-785 (in Turkish). https://doi.org/10.5578/fmbd.39342.

[15] Baby F, Marchand P, Toutlemonde F. Shear behavior of ultra high performance fiber-reinforced concrete beams. I: experimental investigation. J Struct Eng 2014;140(5). https://doi.org/10.1061/(ASCE)ST.1943-541X.0000907.

[16] El-Dieb AS, El-Maaddawy TA, Al-Rawashdah O. Shear behavior of ultra-high-strength steel fiberreinforced self-compacting concrete beams. In: Proceedings of the construction materials and structures (eds SO Ekolu, M Dundu, X Gao), Johannesburg, South Africa, 24–26 November 2014:972–979.

[17] Qi JN, Ma ZJ, Wang JQ, Liu TX. Post-cracking shear strength and deformability of HSS-UHPFRC beams. Struct Conc 2016;17(6):1033-1046. https://doi.org/10.1002/suco.201500191.

[18] Voo YL, Poon WK, Foster SJ. Shear strength of steel fiber-reinforced ultra high-performance concrete beams without stirrups. J Struct Eng 2010;136(11):1393-1400. https://doi.org/10.1061/(ASCE)ST.1943-541X.0000234.

[19] Ngo TT, Park JK, Pyo S, Kim DJ. Shear resistance of ultra-high-performance fiber-reinforced concrete. Constr Build Mater 2017;151:246-257. https://doi.org/10.1016/j.conbuildmat.2017.06.079.

[20] Lim WY, Hong SG. Shear tests for ultra-high performance fiber reinforced concrete (UHPFRC) beams with shear reinforcement. Int J Concr Struct M 2016;10(2):177-188. https://doi.org/10.1007/s40069-016-0145-8.

[21] Yang IH, Kim BS, Joh C. Shear behaviour of ultra-high performance fibre-reinforced concrete beams without stirrups. Mag Concr Res 2012;64(11):979-993. https://doi.org/10.1680/macr.11.00153.

[22] Hegger J, Bertram G. Shear Carrying Capacity of Ultra-High Performance Concrete Beams. Tailor Made Concrete Structures; Walraven JC, Stoelhorst D. Eds.; Taylor & Francis Group: London, UK, 2008:341–347.

[23] Ciprian T, Dan B, Victor V, Cornelia. Ultra high performance fiber reinforced concrete I beams subjected to shear action. ACTA Technica Napocensis: Civ Eng Arch 2011;55(2):121-126.

[24] Kamal MM, Safan MA, Etman ZA, Salama RA. Behavior and strength of beams cast with ultra high strength concrete containing different types of fibers. HBRC J 2014;10:55-63. https://doi.org/10.1016/j.hbrcj.2013.09.008.

[25] Ahmad S, Bahij S, Al-Osta MA, Adekunle SK, Al-Dulaijan SU. Shear behavior of ultra-high-performance concrete beams reinforced with high-strength steel bars. ACI Struct J 2019;116(4):3-14. https://doi.org/10.14359/51714484.

[26] Voo YL, Foster SJ, Gilbert RI. Shear strength of fiber reinforced reactive powder concrete prestressed girders without stirrups. J Adv Concr Technol 2006; 4(1):123-132.

[27] Yavas A, Goker, CO. Impact of reinforcement ratio on shear behavior of I-shaped UHPC beams with and without fiber shear reinforcement. Mater 2020;13(7),1575. https://doi.org/10.3390/ma13071525.

[28] ACI 318-19. Building Code Requirements for Structural Concrete, American Concrete Institute, Farmington Hills, MI, USA, 2019.

[29] Zagon R., Matthys S., Kiss Z. Shear behaviour of SFR-UHPC I-shaped beams, Constr Build Mater 2016;124:258-268. http://dx.doi.org/10.1016/j.conbuildmat.2016.07.075.

[30] Yoo DY, Yuan T, Yang JM, Yoon YS, Feasibility of replacing minimum shear reinforcement with steel fibers for sustainable high-strength concrete beams, Eng Struct 2017;147:207–222. http://dx.doi.org/10.1016/j.engstruct.2017.06.004.

[31] Mészöly T, Randl N. Shear behavior of fiber-reinforced ultra-high performance concrete beams Eng Struct 2018;168:119-127. https://doi.org/10.1016/j.engstruct.2018.04.075.

[32] EN 12390-1. Testing hardened concrete - Part 1: Shape, dimensions and other requirements for specimens and moulds. European Committee for Standardization, Brussels, Belgium, 2021.

[33] EN 12390-3. Testing hardened concrete. Part 3: Compressive strength of test specimens. European Committee for Standardization, Brussels, Belgium, 2019.

[34] Yoo DY, Shin HO, Yang JM, Yoon YS. Material bond properties of ultra high performance fiber reinforced concrete with micro steel fibers. Compos B Eng 2014;58:122-133. http://dx.doi.org/10.1016/j.compositesb.2013.10.081.

[35] Yu R, Spiesz P, Brouwers HJH. Development of Ultra-High Performance Fibre Reinforced Concrete (UHPFRC): Towards an efficient utilization of binders and fibres. Constr Build Mater 2015;79:273-282. http://dx.doi.org/10.1016/j.conbuildmat.2015.01.050.

[36] Ren GM, Wu H, Fang Q, Liu JZ. Effects of steel fiber content and type on static mechanical properties of UHPCC. Constr Build Mater 2018;163:826-839. https://doi.org/10.1016/j.conbuildmat.2017.12.184.

[37] TS 500. Requirements for Design and Construction of Reinforced Concrete Structures, Ankara, Turkish Standards Institution, 2000 (*in Turkish*).

[38] ACI 318-11. Building Code Requirements for Structural Concrete, American Concrete Institute, Farmington Hills, MI, USA, 2011.

[39] ACI 318-14. Building Code Requirements for Structural Concrete, American Concrete Institute, Farmington Hills, MI, USA, 2014.

[40] Park R. Evaluation of ductility of structures and structural assemblages from laboratory testing. Bull New Zealand Natl Soc Earthq Eng 1989;22(3):155-166.

[41] Park YJ, Ang AHS. Mechanistic seismic damage model for reinforced concrete, J Struct Eng 1985;3(4):722–739.

[42] Shin S, Ghosh SH, Moreno J. Flexural ductility of ultra-high strength concrete members, ACI Struct J 1989;8(4):394–400.

[43] Hadi MN, Elbasha N. Effects of tensile reinforcement ratio and compressive strength on the behaviour of over-reinforced helically confined HSC beams. Constr Build Mater 2007;21(2):269–76. http://dx.doi.org/10.1016/J.CONBUILDMAT.2005.08.020.

[44] Yoo DY, Banthia N, Yoon YS. Experimental and numerical study on flexural behavior of UHPFRC beams with low reinforcement ratios. Can J Civ Eng 2017;44(1):18-28. https://doi.org/10.1139/cjce-2015-0384.

[45] Singh M, Sheikh AH, Ali MSM, Visintin P, Griffith MC. Experimental and numerical study of the flexural behaviour of ultra-high performance fibre reinforced concrete beams. Constr Build Mater 2017;138:12-25. https://doi.org/10.1016/j.conbuildmat.2017.02.002.

[46] Qi J, Wang J, Ma ZJ. Flexural response of high-strength steel-ultra-high-performance fiber reinforced concrete beams based on a mesoscale constitutive model: Experiment and theory. Struct Conc 2018;19(3):719-734. https://doi.org/10.1002/suco.201700043.

[47] Biolzi L, Cattaneo S. Response of steel fiber reinforced high strength concrete beams: Experiments and code predictions. Cem Concr Compos 2017;77:1-13. https://doi.org/10.1016/j.cemconcomp.2016.12.002.

[48] Yoo DY, Yoon YS. Structural performance of ultra-high-performance concrete beams with different steel fibers. Eng Struct 2015;102: 409-423. https://doi.org/10.1016/j.engstruct.2015.08.029.

[49] Dancygier AN, Savir Z. Flexural behavior of HSFRC with low reinforcement ratios. Eng Struct 2006;28:1503–12. https://doi.org/10.1016/j.engstruct.2006.02.005.

[50] Dancygier AN, Berkover E. Cracking localization and reduced ductility in fiber-reinforced concrete beams with low reinforcement ratios. Eng Struct 2016;111:411–24. http://dx.doi.org/10.1016/j.engstruct.2015.11.046.

[51] Deluce JR, Vecchio FJ. Cracking behavior of steel fiber-reinforced concrete members containing conventional reinforcement. ACI Struct J 2013;110(3):481–90. http://dx.doi.org/10.14359/51685605.

[52] Sturm AB, Visintin P, Oehlers DJ. Blending fibres to enhance the flexural properties of UHPFRC beams. Constr Build Mater 2020;244,118328. https://doi.org/10.1016/j.conbuildmat.2020.118328.

[53] Pansuk W, Nguyen TN, Sato Y, Uijl JAD, Walraven JC. Shear capacity of high performance fiber reinforced concrete I-beam. Constr Build Mater 2017;157:182-193. https://doi.org/10.1016/j.conbuildmat.2017.09.057.

Turkish Journal of Civil Engineering, 2023 125-143, Paper 728, ***Research Article***

Finite Element Analysis and Investigation of Critical Impact Point of Steel Guardrails Affecting Safety and Structural Performance

Sedat OZCANAN[1]

ABSTRACT

After the guardrails are designed, the structural adequacy and safety criteria are determined by the relevant standards and full-scale crash tests. One of the widely used standards is European Norm 1317 (EN1317). Guardrail systems generally consist of rails and posts. The guardrails are more rigid around the posts, which are mounted on the ground or embedded in soil at certain intervals. Therefore, it is important for driver/passenger and roadside safety to determine the most critical point in terms of structural and safety performance and design according to the most unfavourable situation. With this motivation, in this study, the effect of different impact points on the structural and safety performance of the H1W4 guardrail was investigated by finite element (FE) analysis. For this purpose, first of all, the finite element models of the H1W4-A system were calibrated and validated with real crash test data. Then, with the help of the validated models, analyses were completed for different impact points as 0.5, 1.0, 1.5 and 2.0 meters with a half-meter difference for the standard 2-meter post spacing. In the light of the measured safety parameters such as Acceleration Severity Index (ASI), Theoretical Head Impact Velocity (THIV) and structural performance criteria such as working width (W) and exit angle (α), the critical impact point for the guardrail was determined. Contrary to what is generally known, crashing vehicles into flexible points (0.5 and 1.0 m) rather than impacting rigid points (1.5 and 2.0 m) creates a more negative situation in crash tests.

Keywords: Guardrail, EN1317, ASI, THIV, finite element analysis.

1. INTRODUCTION

Guardrails are passive protective systems built on the roadside parallel to the road that keep errant vehicles on the road after an accident. Guardrails are classified into three main groups according to their deformation characteristics. Flexible, semi-rigid and rigid systems.

Note:
- This paper was received on July 2, 2022 and accepted for publication by the Editorial Board on January 17, 2023.
- Discussions on this paper will be accepted by May 31, 2023.
- https://doi.org/10.18400/tjce.1238657

1 Department of Civil Engineering, Sirnak University, Şırnak, Türkiye
sozcanan@sirnak.edu.tr - https://orcid.org/0000-0002-8504-7611

Systems with 3 meters of lateral deformation during impact are defined as flexible, systems with 0.2-1.5 meters of lateral deformation as semi-rigid, and systems with 0-0.2 meters of lateral deformation are defined as rigid systems. As given in Figure 1, (a) concrete barriers are rigid, (b) steel guardrails are semi-rigid and (c) cable guardrails are examples of flexible systems.

Guardrails used in roadside safety as passive protective systems go through various structural and safety adequacy standards before being applied. The most common of these safety standards are EN1317 [1] and MASH [2]. These standards make performance analysis in two aspects. The first is the performance of the barrier in terms of driver and passenger safety, and the second is the structural performance of the barrier. Before applying the designed roadside safety systems, their safety and structural performances are tested in crash test centers. Systems that pass the tests are certified and approved for application.

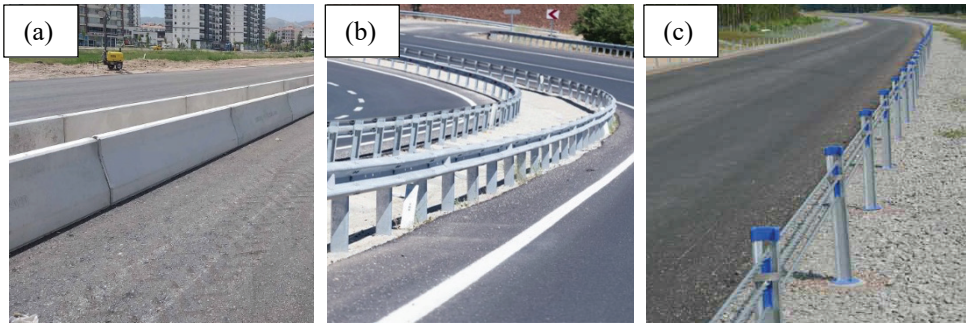

Figure 1 - (a) Concrete barriers (rigid), (b) Steel guardrails (semi-rigid), (c) Cable guardrails (flexible)

Instruments that provide roadside safety are required to provide the highest level of driver and passenger safety. The ASI value used to determine driver and passenger safety in EN1317 is evaluated in 3 classes. Class A (ASI≤1) is defined as safe, class B as potentially hazardous (ASI≤1.4), and class C as dangerous (ASI≤1.9). Class A ASI values are generally obtained for guardrails designed mostly from steel and flexible material, while class B-C ASI values are obtained for rigid concrete barriers. In this sense, it can be said that steel barriers are safer than concrete barriers in terms of driver and passenger safety [3]. There are many studies conducted to improve the ASI values of currently used or newly designed roadside safety systems. Teng et al. [4] conducted a study on the effect of guardrail height and post spacing criteria on the ASI value of W rail type steel guardrails. In the study, it was understood that these two criteria affect the ASI value. Again, Teng et al. [5] investigated the reliability of W-rail type steel guardrails formed with different post types (I profile, C profile, U profile, and Sigma profile) based on factors such as ASI, THIV, and working width (W). As a result, it is stated that the most reliable and best performing post type is the Sigma profile, and the worst- performing and least energy-absorbing post type is the I profile. Wilde et al. [6] made a finite element analysis in their study, and determined that the transition regions of steel guardrails to different levels are the most critical regions in terms of ASI-THIV values. In studies on concrete barriers, Borkowski et al. [7] simulated TB11 and TB32 tests separately for ground-fixed and non-fixed concrete barrier types using the LS-DYNA

program, and it was stated that the unfixed barrier was safer than the fixed one in terms of ASI. Ozcanan and Atahan [8], in their optimization to improve the ASI value of the NJ type concrete barrier, stated that the ASI value after the optimal design was improved by 14.1% compared to the original design, and in the case that the optimal barrier was not fixed to the ground, the ASI value obtained was 23.5% better than the original design value. Other than steel guardrails and concrete barriers mentioned above, there are studies related to roadside safety. Yumrutas et al. [9] made a performance analysis of the newly developed hybrid barrier, and compared the results to the conventional roadside barriers. It was stated that the developed hybrid barrier could be used as an alternative to the commonly used barriers. In the study for the development of bollard systems used to protect the infrastructure facilities used in the city [10], the weaknesses of the existing bollard systems were identified and suggestions were made for their improvement. In the study conducted by Yilmaz et al. [11], the motorcyclist protection barrier system was optimized, and as a result safer and more economical sections were obtained. Moreover, other investigators considered the problem of improving crash cushion systems that provide road safety [12], ASI value of cable barrier for different speeds [13], determining the danger levels of obstacles such as traffic lights, trees, lighting poles, rocks, ditches, etc. that threaten roadside safety [14], and comparing the ASI-THIV values and AIS-HIC values [15][16][17]. These studies were carried out with the help of real crash tests and FE analyses.

It is inevitable to use the finite element method (FEM) in roadside safety analysis. Because the full-size tests of the developed systems are expensive in terms of cost and time. Especially performing more than one experiment can make the situation much more difficult. Therefore, the use of finite element analysis provides great advantages in full-size modelling of real crash tests. In this sense, any number of analysis can be performed with FEM and variations can be tried for different parameters and variables. Ray [18] stated that nonlinear FE analysis has become a useful part of the roadside safety hardware design and evaluation process. Ren and Vesenjak [19], in their study aimed to compare FE and experimental crash analyses for roadside safety, concluded that the results of numerical and experimental crash tests are very close, and that nonlinear dynamic FE analysis can be performed instead of performing many costly and laborious real crash tests. Borovinsek et al. [20], in their studies investigating the reliability of FE simulations for roadside safety, error values of less than 8% were obtained between FE simulation values and real collision values, and it was argued that FE simulations could be used in this sense. Borkowski et al. [21] compared the TB11 test with the real crash test and LS-DYNA FE simulation according to some criteria within the scope of EN 1317 standard and emphasized that the LS-DYNA FE model can be used. Niezgoda et al. [22] in their studies on the use of computer-assisted software in modelling and simulation of crash tests, it was recommended that numerical and experimental tests largely confirm each other, and the use of computer-aided software in crash tests would be convenient. Pachocki and Wilde [23] stated in their study that the H2W5-B type steel barrier was successfully designed and tested with LS-DYNA non-linear FE program. It has been seen that the common FE program used in the road restraint system (RRS) research is LS-DYNA. Therefore, LS-DYNA [24] was used for FE analysis in this study.

The two basic elements of steel guardrails are rail and posts. Posts are mounted on the ground or embedded in soil with certain distances. The system is more rigid, especially in areas close to the posts. Knowing the most critical impact point of guardrail in terms of design is important for driver/passenger and road safety. The aim of this study is to investigate the

effect of the impact point on the structural and safety performance of the steel guardrails using a finite element analysis. For this, a H1W4-A class guardrail was chosen as an example. FE models were calibrated and validated using prioritized impact tests data. Then, using the validated models, the impact points on the guardrail system were determined as 0.5, 1.0, 1.5, 2.0 meters for the system with a standard post width of 2 meters, and analyses were made. In the light of the analysis made, the critical impact point was determined in terms of guardrails and the results were shared below. This study makes this research unique as it investigates the FE analysis of the effect of the impact point on the structural and safety performance of the steel guardrails. Calculation of the ASI, THIV, working width (W), and exit angle (α) parameters are determined through the TB11 and TB42 test of the EN1317 standard for H1W4-A system.

2. EUROPEAN NORMS (EN1317-16303), GUARDRAIL, AND FE TECHNIQUES AND VALIDATION

2.1. EN1317 safety and Performance Criteria

The EN1317 standard expresses the severity of injury with 2 parameters that known as safety criteria. These are the acceleration (injury) severity index (ASI) and the theoretical head impact velocity (THIV). The injury parameter ASI takes into account the effect of occupant restraint systems such as seat belts. It is determined according to ASI Equation (1),

$$ASI(t) = \sqrt{\left(\frac{a_x}{\hat{a}_x}\right)^2 + \left(\frac{a_y}{\hat{a}_y}\right)^2 + \left(\frac{a_z}{\hat{a}_z}\right)^2} \quad (1)$$

Here, the components a_x, a_y, a_z contain the vehicle acceleration values in the Ox, Oy, Oz axes, respectively, and the components in the denominator represent the threshold values applied according to the standard, which are respectively: $\hat{a}_x = 12g, \hat{a}_y = 9g, \hat{a}_z = 10g$. The g is the gravitational acceleration. The calculated value of ASI is the scalar value expressed by Equation (2).

$$ASI = \max[ASI(t)] \quad (2)$$

The second parameter specified by the EN 1317 standard is the theoretical head impact velocity (THIV). In this parameter, it is assumed that possible injuries to the vehicle occupant are directly related to the occupant's collision with the interior of the vehicle. The THIV value can be calculated with Equation (3) assuming that the head speed of the driver/passenger inside the vehicle is equal to the vehicle speed in the horizontal plane.

$$THIV = \left[{V_{head\,x}}^2(T) + {V_{head\,y}}^2(T)\right]^{0.5} \quad (3)$$

Here, $V_{head\,x}, V_{head\,y}$, are the values of the head velocity in the longitudinal and lateral directions relative to the vehicle axis passing through its center, respectively. T is when the theoretical passenger head moves 600 mm in the O_x axis direction or 300 mm in the O_y axis direction.

Limit values of ASI and THIV safety parameters are given in Table 1.

Table 1 - Impact severity levels [1]

Impact severity level	Index values		
A	ASI ≤ 1.0		
B	ASI ≤ 1.4	and	THIV ≤ 33 km/h
C	ASI ≤ 1.9		

In Figure 2 are the positions of the accelerometer and dummy used in the vehicle while measuring ASI and THIV during the TB11 crash test.

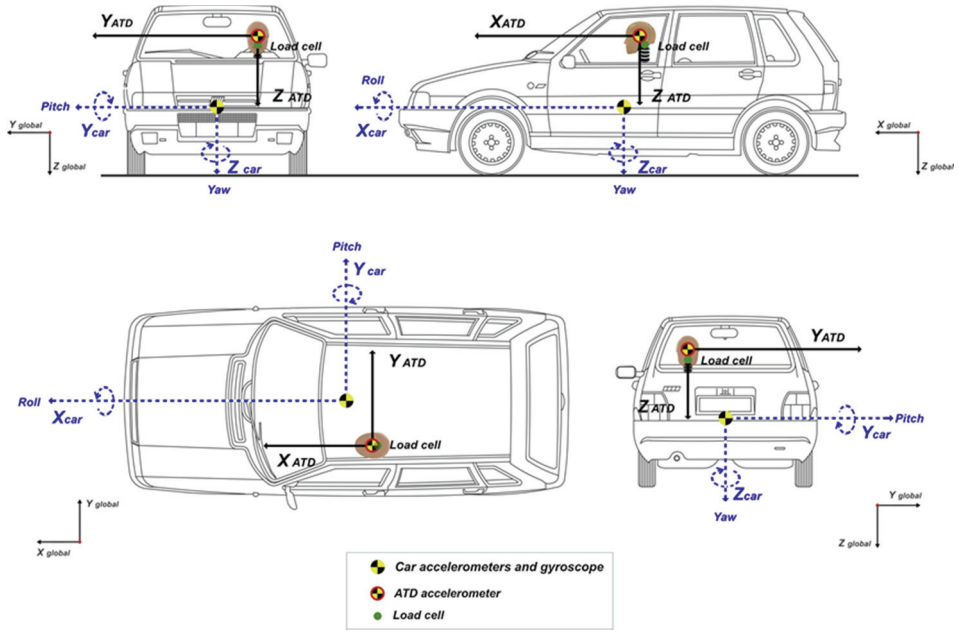

Figure 2 - Accelerometer and dummy positions for ASI and THIV calculation [25]

Table 2 gives the performance evaluation criteria of H1W4-A barrier system. Figure 3 shows the test case according to EN1317 standards. As can be seen from the figure, the working width (W) is the greatest displacement of the guardrail during an impact. After a vehicle has impacted into the guardrail, it leaves the guardrail from an exit point. Exit box can be designed as a rectangular shaped box, calculated from the beginning of the vehicle exit point, the width (A) and length (B) of the impacting vehicle. One of the evaluation criteria of a crash test according to EN1317 is that a vehicle must remain inside the short edge of the exit

box when exiting the barrier. The aim here is to prevent vehicles entering the traffic after an accident. Hence, calculation of the exit angle of a vehicle is of importance in terms of test acceptance.

The maximum acceptable lateral displacement or working width (W) is 1.3 m which is upper limit of W4 level. Also, for the test conditions of TB11, and TB42 the maximum exit angle (α) is no more than 19° in reference to guardrail.

Table 2 - *EN1317 test evaluation criteria for H1 guardrail systems*

System Type	Test	Working width (W) (m)	Exit box (width(A) x length(B)) (m)*	Exit angle (α) (°)**
H1W4A	TB11	≤1.3	4.4x10	≤19
	TB42	≤1.3	8.22x20	≤17

*Calculated based on EN1317/2

**Calculated based on exit box length

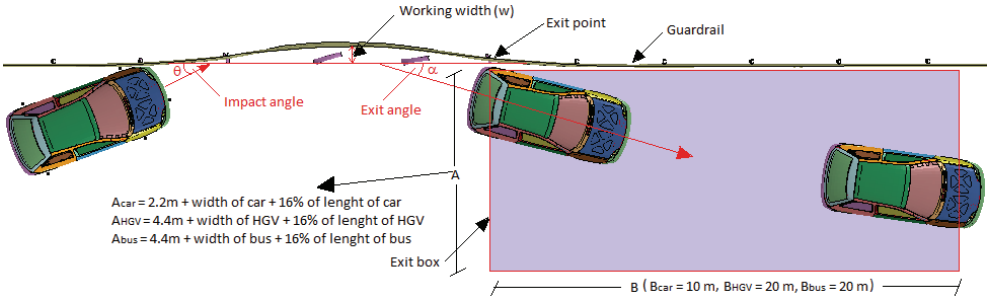

Figure 3 - Illustration of crash test condition of EN1317 and exit box calculation [26]

The evaluation of the road safety designs in Turkey is performed in accordance with the EN1317 standards. The test acceptance criteria that is specified in EN1317 for H1 containment level, is given in Table 3. Detail on vehicle crash test descriptions and containment levels are given in EN1317 part 2 [1].

Table 3 - EN1317 test acceptance criteria for H1 guardrail systems [1]

System type	Test	Impact speed (km/h)	Impact angle (Θ) (°)	Total mass (kg)	Type of vehicle
H1	TB11	100	20	900	Car
	TB42	70	15	10000	Rigid HGV*

*Heavy Goods Vehicle

2.2. Virtual Testing Tolerance in European Norm (EN) 16303

Validation and calibration are required in order to be able to analyze with numerical models of crash tests conducted within the scope of EN1317. For this, there are acceptance criteria and error tolerances specified in EN16303 [28]. Allowable tolerances regarding safety and performance parameters are given in Table 4. In the quantitative comparison of the numerical models made with the real models, the allowed error tolerances must remain within the given deviation values.

Table 4 - EN 16303 virtual test tolerance for validation process

Parameter	Tolerance
ASI	±0.1
THIV (km/h)	±3
W (m)	±0.1
Exit angle (α)	*

* Calculation and acceptance criterion are given in EN1317. Limit values are given in Table 2.

2.3. The Details and FE Models of H1W4-A Guardrail System

In this study, crash test data related to the H1W4-A barrier system were used. H1W4-A represents one most widely used barrier systems in general. The main components of the

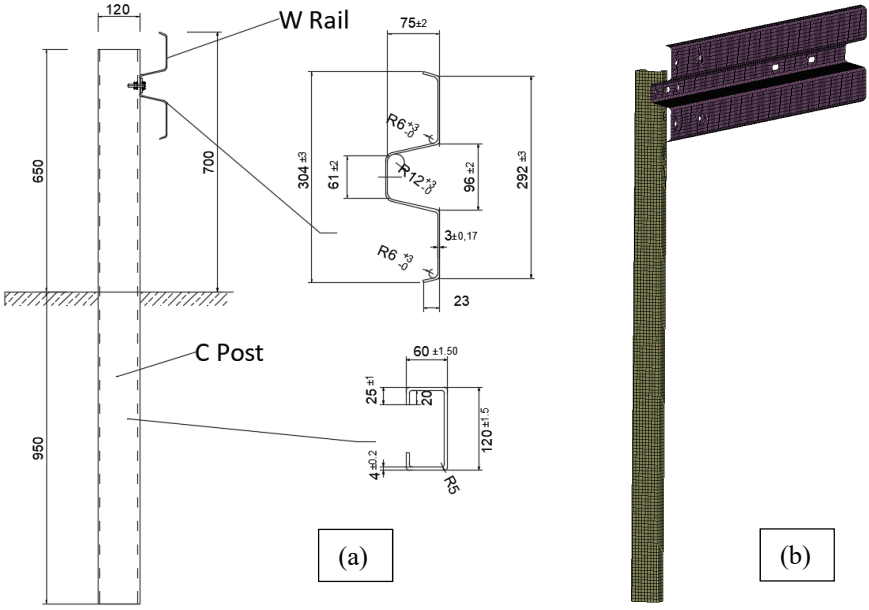

Figure 4 - (a) H1W4 guardrail system details and (b) FE model of the design

guardrail are the W-beam rail and the C-type post. The guardrail consists of S235JR graded steel material. In Figure 4 geometric details and FE model of the H1W4-A system are given. In the LS-DYNA model, the rail and post section are 'Shell' modelled, and the 'MAT24' is used as the material for both. Bolt connections between rail and post are defined as 'Beam'. Materials and models validated from previous studies [8], [26], [29] were used in this research.

Figure 5 shows the meanings of the symbols which are forming the name of the guardrail system that is classified according to EN 1317 standards.

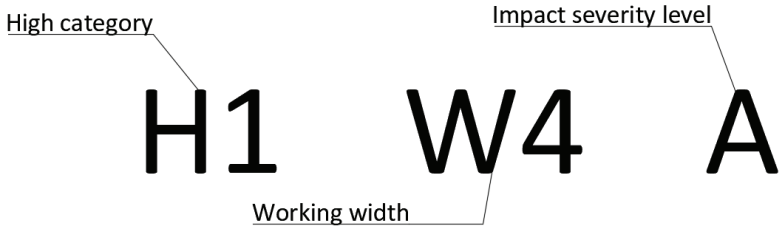

Figure 5 - Symbol meanings of H1W4-A system

Commonly used materials and technical specifications of H1W4A system are given in Table 5.

Table 5 - Technical details of guardrail systems used in this study

Guardrail system type	Rail	Post	Material	Rail thickness (mm)	Post thickness (mm)
H1W4A	W	C120X60X20	S235JR	3.0	4.0

2.4. FE Analysis Techniques

Figure 6 shows technical details and the FE models of the vehicles used in the TB11 and TB42 tests. The FE vehicles used here were not modelled for this study. The vehicles are models shared and validated by the National Crash Analysis Center [27]. These models have been developed for free use in safety assessment and crash tests. In the FE model created for this study, only the guardrail part is modelled and the vehicles were used as ready-made.

Since the crash tests are dynamic tests, the FE analysis is run explicitly. Termination time was calculated as 0.4 s for TB11 and 1.5 s for TB42. Time Step is selected by default. The ASCI card was opened for outputs such as acceleration and displacement, and the plot time interval was defined as 0.01 s. The "LS-Manager" interface was used for analysis. In this interface, analyses were made for a total of 8 cores, 4 real and 4 virtual, and MEMORY=400 000 000.

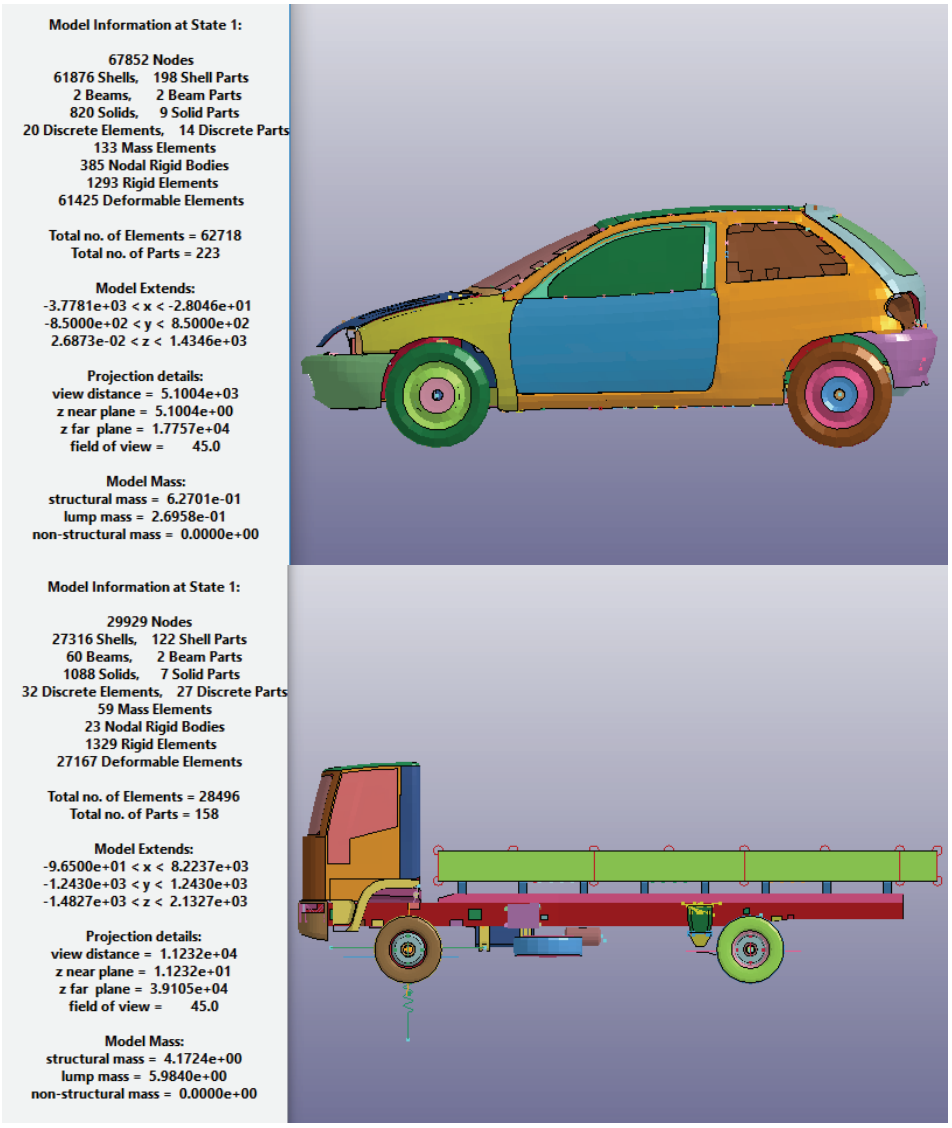

Figure 6 - Technical details and the FE models of vehicles used in TB11 (car) and TB42 (HGV) tests [27]

2.5. Validation of the FE Models

In the above section, the tests to be performed for H1 system is given in Table 2. Previous studies have included actual test data for TB11, and TB42 tests. Based on these tests, full-scale finite element models of H1 system was created using LS-DYNA software. The validity of these models created in the FE environment was compared against the actual crash test

Table 6 - Comparison of data obtained from real tests and FE models

Tests	Parameters	Real crash tests	FE models	Tolerance	Inside limits?
TB11	ASI	0.86	0.79	±0.1	Yes
	THIV (km/h)	22	21	±3	Yes
TB42	W (m)	1.12	1.20	±0.1	Yes
	α (°)	8	10	≤19	Yes

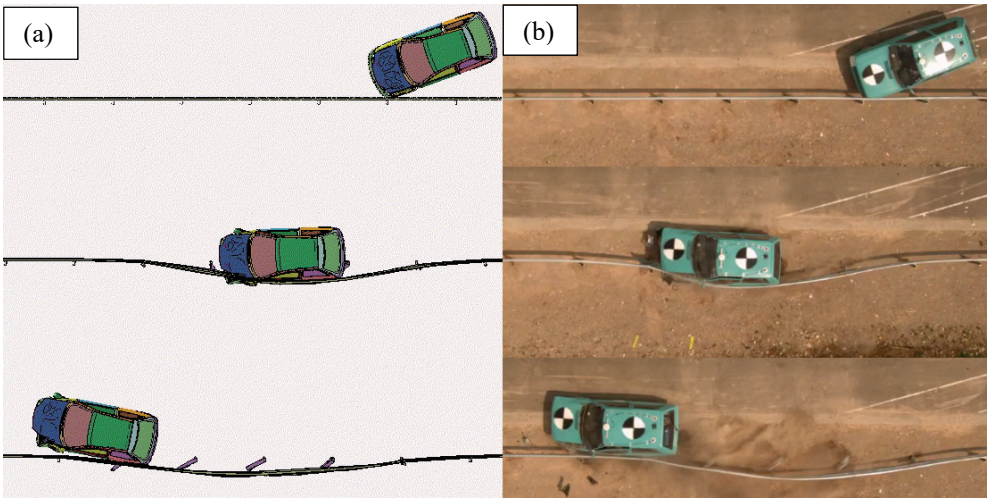

Figure 7 - (a) FE model of TB11 (b) Real test of TB11 (CSI 2017 [30]) [26]

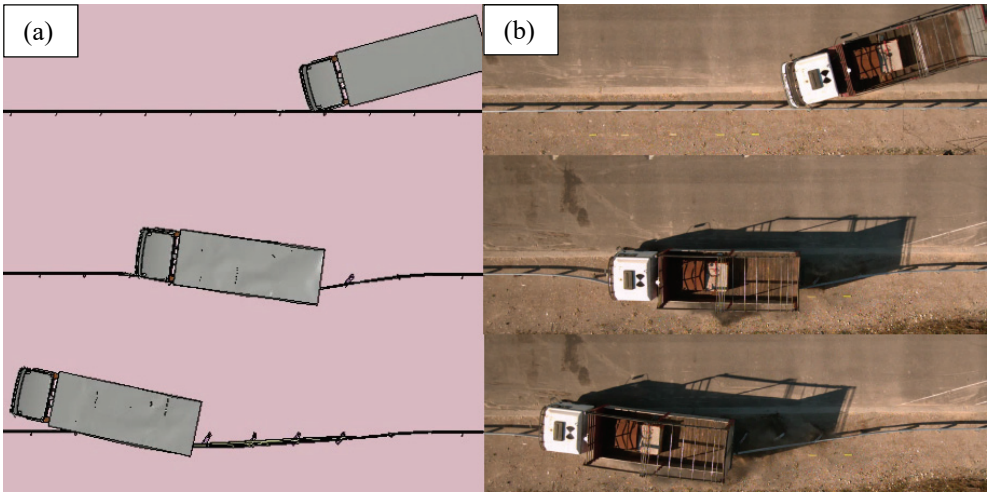

Figure 8 - (a) FE model of TB42 (b) Real test of TB42 (CSI 2017 [30]) [26]

data. The quantitative comparison of the FE model and the crash test is given in Table 6. The difference between the ASI, THIV, W and α values obtained for the FE model and the crash test as a result of the TB11 and TB42 tests remains within the limits specified in the EN16303 and EN1317 standards. In addition, the qualitative comparison of FE model and crash test is given in Figures 7-8. As shown in Figures 7-8, results obtained from the FE models and the real crash tests show good agreement. As a result of the validation, it was understood that the FE model could be used in this study.

3. FINITE ELEMENT TEST SETUP AND ANALYSIS

3.1. Finite Element Test Setup

Studies conducted in America and Europe have shown that the crash angles in accidents are between 30º-34º with a 90% probability [31]. The impact angles taken in EN1317 remain lower. However, it is obvious that as the impact angle and impact speed increase, the impact intensity and acceleration increase. There are studies evaluating impact velocity and angle conditions for EN1317 barrier tests [31][32]. Therefore, in this study, the critical impact point, which is not mentioned in the literature, was investigated for steel guardrails, rather than the impact angle and speed. For this, first of all, the FE model of H1W4 guardrail has been calibrated and validated with crash test data. As a result of the validation, it was deemed appropriate to use the guardrail FE model with acceptable error values in this engineering problem. Different impact points were determined on the validated FE model, and tests were created with validated vehicles. The determined impact points are given in Figure 9. Considered the standard 2 m spacing, the impact points were determined as 0.5 m, 1.0 m, 1.5 m and 2.0 m points. In crash test centers, the vehicles are usually crashed into the posts (2.0 m point) as the most unfavourable point, as can be seen from the crash test images in Figures 6-7. It is known that the system behaves more rigidly around the posts. However, it is not clear whether the impact point should be chosen for just upon the post or before-after the post. In this study, research was carried out for 4 points immediately after the post (0.5m), in the middle of the two posts (1.0m), just before the post (1.5m) and upon the post (2.0m). For analysis, 900 kg vehicles under TB11 and 10 000 kg HGV vehicles within the scope of TB42 test were hit at the points determined on the H1W4 system.

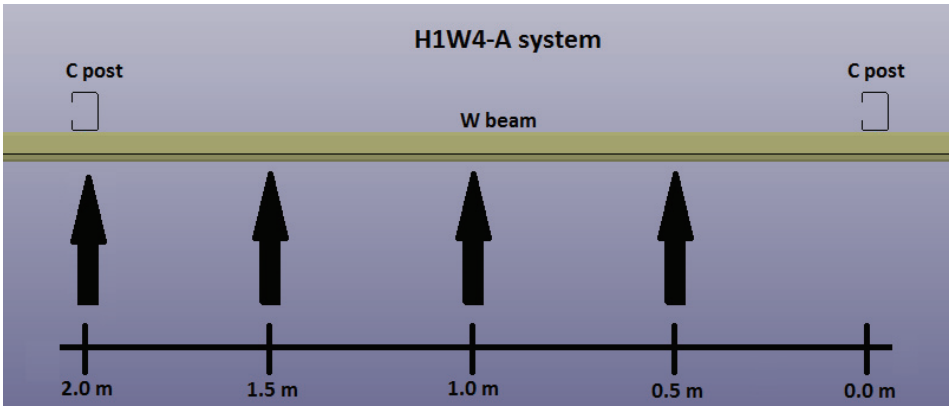

Figure 9 - Vehicles impact points of H1W4-A system

3.2. Analysis and Results

Totally, 8 analyses were made, including 4 TB11 and 4 TB42 subject to determined impact points. The outcomes obtained for TB11 (ASI, THIV) and TB42 (W, α) as a consequence of the analysis are given in Table 7. As can be seen from the table, the highest values in terms of safety and structural performance are seen at 0.5 and 1.0 m points. The smallest values occurred at 1.5 m and 2.0 m points. As can be seen from Figures 6-7 in crash tests, vehicles are usually crash into the post (2.0 m point). Assuming that this point is more rigid in the guardrail system, the worst situation is expected. However, the 2.0 m point, which was expected as the most negative point, turned out to be the safest point in terms of impact, just like the 1.5 m point. In addition, it can be seen that different behaviours occur at all 4 different impact points in the ASI graphs given in Figure 10. The most important reason for this is that the rigidity of the steel guardrails is not the same at every point.

Table 7 - Quantitative comparison of data obtained from TB11 and TB42 tests

Tests	Parameters	Impact points			
		0.5 m	1.0 m	1.5 m	2.0 m
TB11	ASI	**0.85**	0.84	0.78	0.79
	THIV (km/h)	**24**	24	21	21
TB42	W (m)	1.22	**1.24**	1.17	1.20
	α (°)	**32**	27	5	10

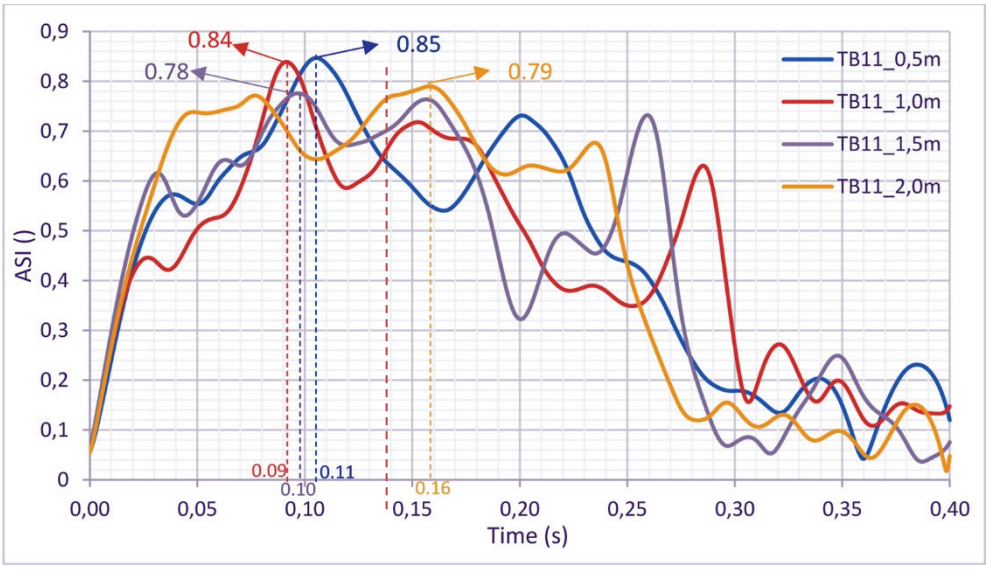

Figure 10 - ASI comparison for different impact points

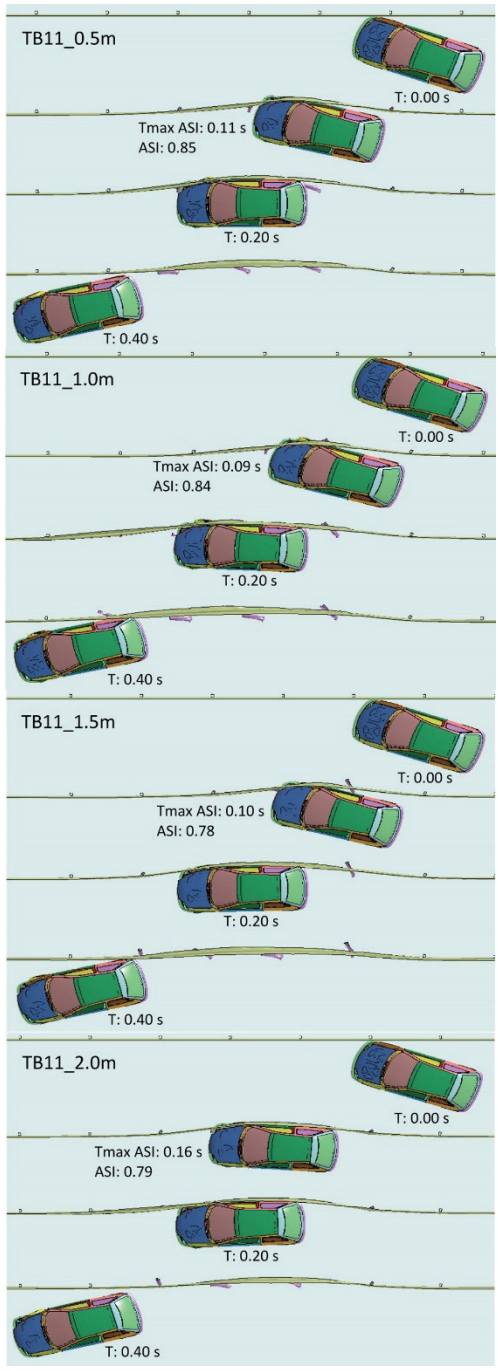

Figure 11 - Qualitative comparison of TB11 test for different impact points

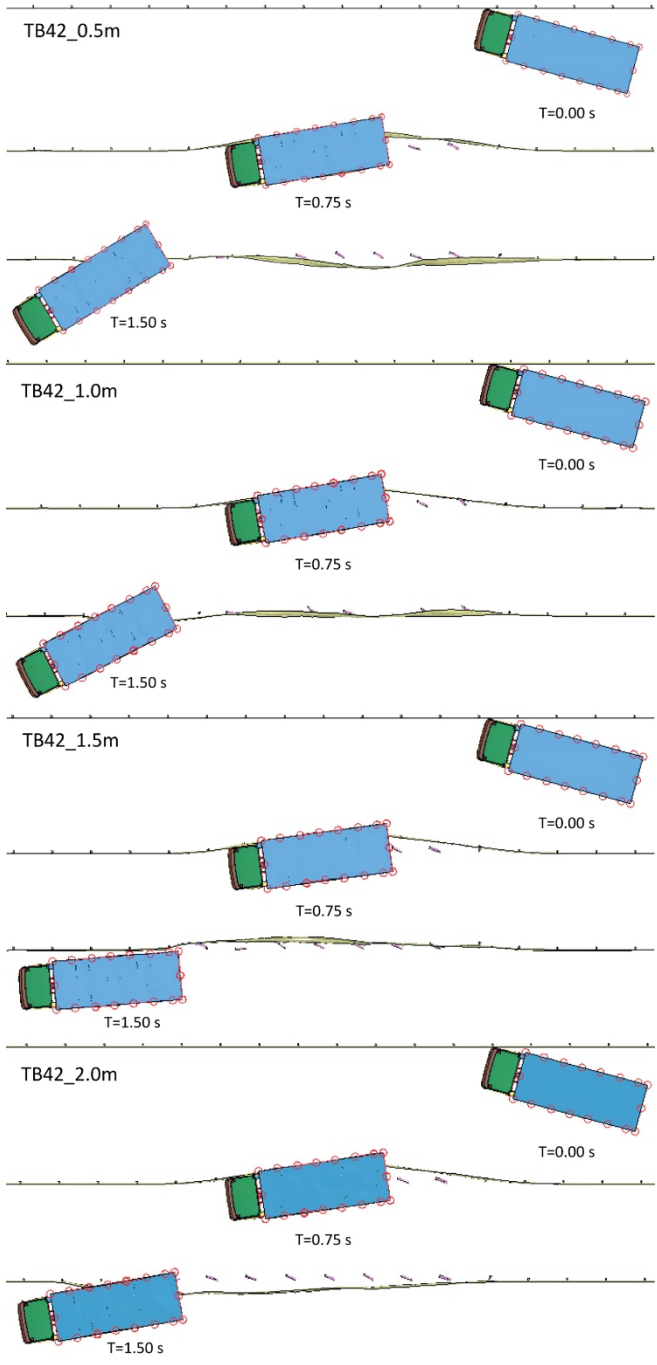

Figure 12 - Qualitative comparison of TB42 test for different impact points

If we look at the differences of the parameters in Table 7 at different points as significant, the difference between the largest ASI value and the smallest value is approximately 8-9%. Again, the THIV value is within the tolerance limit of ±3 given in EN16303. The exit angle (α) differences are more than 6 times between the largest value and the smallest value. In addition, these values at 0.5 and 1.0 m points exceed the limit values given in Table 2. Therefore, these differences are too large to be neglected.

If we interpret our results with the help of the qualitative comparisons of different impact points given in Figure 11-12 for TB11 and TB42; the reason why ASI, THIV, W and α values are higher at 0.5 m and 1.0 m points is due to the higher penetration amount in vehicles impacting these points. Because these points are far from the post or because the post does not come immediately after the impact, these are the points where the vehicles act more flexible and, hence, penetrate more. It is known that the surrounding of the post is more rigid, so the penetration amount is less at the points that vehicle crash into the post (2.0 m point) or the post come to immediately after impacting (1.5 m point). This can be observed for cases TB11 and TB42 in Figures 10-11. In Figure 11, it can be seen that the impacting part of the vehicle passes the guardrail for 0.5 and 1.0 m points, but not at 1.5 and 2.0 m points, and the resulting displacements of the 1.5 and 2.0 m points are less than the 0.5 and 1.0 m points. The same is true for Figure 12. In addition, as given in Table 7, the W value at 0.5 and 1.0 m points is greater than the other two points, thus confirming the penetration status in TB11. Since the penetration is higher in hitting the flexible points, the vehicle's contact with the guardrail and acceleration values are greater and, hence, the ASI, THIV and W values are greater. Again, α values of points with higher penetration and W values are also higher. In fact, the α values obtained at 0.5 and 1.0 m points exceed the limit values calculated in the scope of EN1317 and given in Table 2. Therefore, in the light of the results given above, contrary to what is generally known, crashing vehicles into flexible points rather than impacting rigid points creates a more negative situation in crash tests.

4. DISCUSSION AND CONCLUSION

Generally, in crash tests, vehicles are crashed into posts that will produce the most negative results. As can be seen from the Figures 6-7 used for the validation of the FE model above, vehicles are crashed into the post, assuming that the post is the point that will give the most negative result in the crash tests. The general view is that the post surroundings will behave more rigidly. But in reality, it is anticipated that the situation may be different. Because rail and post behaviour work as a system in guardrails. In this study, the effects of the impact point on safety and structural performance of guardrails were investigated with finite element method. For this, the FE model was calibrated and validated using the crash test data of the H1W4-A system made within the scope of EN1317. Then, 4 different collision points (0.5, 1.0, 1.5 and 2.0 m) were determined on the validated models and analysis were done. From the analysis results, it can be concluded:

- This study brings novelty to the literature in terms of determining the most critical point in crash tests and creating an idea for determining the safety criteria of guardrails according to the most unfavourable situation.
- It has been seen that, contrary to what is generally known, during the crash tests, impacting the more flexible points (0.5 and 1.0 m) rather than the rigid points (1.5 and

2.0 m) has more negative results. The reason for this is that the vehicles are more penetrating and their contact with the guardrail and acceleration values increase when hitting flexible points.

- Guardrail manufacturers can distribute the rigidity, which formed around post, to the entire system by choosing the rail to be thicker and the steel material more resistant than the rail. Or vice versa to extend flexibility throughout the system. With more uniform rigidity or flexibility, critical impact points can be tolerated.
- It is stated in En1317 that vehicles should hit the most rigid points of guardrails in crash tests. However, as it is understood from the outputs of this study, the most rigid point may not give the most critical safety result, since the guardrail works as a system. The most rigid point may vary in different guardrail designs. Instead of such a general statement, specifying a specific point for the relevant guardrail in the standards in line with the recommendations of this and similar academic research will lead to safer designs and results.
- Since steel guardrail systems generally consist of rails and posts, the results obtained for this study can be generalized for H2, H3, and H4 guardrail systems.
- In future studies, confirming the results obtained with the validated numerical analysis in this study with full-size crash tests will support the implementation of the results.

References

[1] EN1317-2, Road restraint systems - Part 2: Performance classes, impact test acceptance criteria and test methods for safety barriers including vehicle parapets Dispositifs. 2010.

[2] American Association of State Highway and Transportation Officials, Manual for assessing safety hardware, 2009. 2009, p. 259.

[3] R. R. Neves, H. Fransplass, M. Langseth, L. Driemeier, and M. Alves, “Performance of some basic types of road barriers subjected to the collision of a light vehicle,” Journal of the Brazilian Society of Mechanical Sciences and Engineering, vol. 40, no. 6, pp. 1–14, 2018, doi: 10.1007/s40430-018-1201-x.

[4] T. L. Teng, C. C. Liang, and T. T. Tran, “Effect of various W-beam guardrail post spacings and rail heights on safety performance,” Advances in Mechanical Engineering, vol. 7, no. 11, pp. 1–16, 2015, doi: 10.1177/1687814015615544.

[5] T.-L. Teng, C. Liang, C. Hsu, C. Shih, and T. Tran, “Impact Performance of W-beam Guardrail Supported by Different Shaped Posts,” International Journal of Mechanical Engineering and Applications, vol. 4, no. 2, p. 59, 2016, doi: 10.11648/j.ijmea.20160402.14.

[6] K. Wilde, S. Burzyński, D. Bruski, J. Chróścielewski, and ..., “TB11 test for short w-beam road barrier,” 2017, [Online]. Available: https://mostwiedzy.pl/pl/publication/tb11-test-for-short-w-beam-road-barrier,141616-1%0Ahttps://mostwiedzy.pl/pl/publication/download/1/tb11-test-for-short-w-beam-road-barrier_8832.pdf

[7] W. Borkowski, Z. Hryciów, P. Rybak, and J. Wysocki, “Numerical Simulation of the Standard Tb11 and Tb32 Tests for a Concrete Safety Barrier,” Journal of KONES Powertrain and Transport, vol. 17, no. 4, 2010.

[8] S. Ozcanan and A. O. Atahan, “Minimization of Accident Severity Index in concrete barrier designs using an ensemble of radial basis function metamodel-based optimization,” Optimization and Engineering, vol. 22, no. 1, pp. 485–519, Mar. 2021, doi: 10.1007/s11081-020-09522-x.

[9] H. I. Yumrutas, S. Ozcanan, and M. Y. Apak, “Experimental and numerical comparative crashworthiness analysis of innovative renewable hybrid barrier with conventional roadside barriers,” International Journal of Crashworthiness, vol. 0, no. 0, pp. 1–17, 2022, doi: 10.1080/13588265.2022.2075124.

[10] M. Y. Apak et al., “Finite element simulation and failure analysis of fixed bollard system according to the PAS 68:2013 standard,” Engineering Failure Analysis, vol. 135, no. February, p. 106151, 2022, doi: 10.1016/j.engfailanal.2022.106151.

[11] İ. Yılmaz, İ. Yelek, S. Özcanan, A. O. Atahan, and J. M. Hiekmann, “Artificial neural network metamodeling-based design optimization of a continuous motorcyclists protection barrier system,” Structural and Multidisciplinary Optimization, vol. 64, no. 6, pp. 4305–4323, 2021, doi: 10.1007/s00158-021-03080-1.

[12] M. Büyük, A. O. Atahan, and K. Kurucuoğlu, “Impact performance evaluation of a crash cushion design using finite element simulation and full-scale crash testing,” Safety, vol. 4, no. 4, 2018, doi: 10.3390/safety4040048.

[13] D. Bruski and W. Witkowski, “Numerical studies on the influence of selected construction features and road conditions on the performance of road cable barriers,” MATEC Web of Conferences, vol. 231, 2018, doi: 10.1051/matecconf/201823101003.

[14] K. Long, Z. Gao, Q. Yuan, W. Xiang, and W. Hao, “Safety evaluation for roadside crashes by vehicle–object collision simulation,” Advances in Mechanical Engineering, vol. 10, no. 10, pp. 1–12, 2018, doi: 10.1177/1687814018805581.

[15] R. Sturt and C. Fell, “The relationship of injury risk to accident severity in impacts with roadside barriers,” International Journal of Crashworthiness, vol. 14, no. 2, pp. 165–172, 2009, doi: 10.1080/13588260802614365.

[16] A. O. Atahan, J. M. Hiekmann, J. Himpe, and J. Marra, “Development of a continuous motorcycle protection barrier system using computer simulation and full-scale crash testing,” Accident Analysis and Prevention, vol. 116, no. December 2016, pp. 103–115, 2018, doi: 10.1016/j.aap.2017.04.005.

[17] K. Wilde, A. Tilsen, S. Burzyński, and W. Witkowski, “On estimation of occupant safety in vehicular crashes into roadside obstacles using non-linear dynamic analysis,” MATEC Web of Conferences, vol. 285, p. 00022, 2019, doi: 10.1051/matecconf/201928500022.

[18] M. H. Ray, "Repeatability of Full-Scale Crash Tests and Criteria for Validating Simulation Results," Transportation Research Record: Journal of the Transportation Research Board, vol. 1528, no. 1, pp. 155–160, 1996, doi: 10.1177/0361198196152800117.

[19] Z. Ren and M. Vesenjak, "Computational and experimental crash analysis of the road safety barrier," Engineering Failure Analysis, vol. 12, no. 6 SPEC. ISS., pp. 963–973, 2005, doi: 10.1016/j.engfailanal.2004.12.033.

[20] M. Borovinšek, M. Vesenjak, M. Ulbin, and Z. Ren, "Simulation of crash tests for high containment levels of road safety barriers," Engineering Failure Analysis, vol. 14, no. 8 SPEC. ISS., pp. 1711–1718, 2007, doi: 10.1016/j.engfailanal.2006.11.068.

[21] W. Borkowski, Z. Hryciów, P. Rybak, and J. Wysocki, "The researches of effectiveness of road restraint systems," Journal of Konbin, vol. 13, no. 1, pp. 53–64, 2010, doi: 10.2478/v10040-008-0136-1.

[22] T. Niezgoda, W. Barnat, P. Dziewulski, and A. Kiczko, "Numerical modelling and simulation of road crash tests with the use of advanced CAD/CAE systems," Journal of Konbin, vol. 23, no. 1, pp. 95–108, 2012, doi: 10.2478/jok-2013-0041.

[23] L. Pachocki and K. Wilde, "Numerical simulation of the influence of the selected factors on the performance of a concrete road barrier H2/W5/B," MATEC Web of Conferences, vol. 231, 2018, doi: 10.1051/matecconf/201823101014.

[24] LSTC, "LS-DYNA Keyword User's Manual Volume," vol. I, no. February. 2018.

[25] J. Chell, C. E. Brandani, S. Fraschetti, J. Chakraverty, and V. Camomilla, "Limitations of the European barrier crash testing regulation relating to occupant safety," Accident Analysis and Prevention, vol. 133, no. July, p. 105239, 2019, doi: 10.1016/j.aap.2019.07.015.

[26] S. Ozcanan and A. O. Atahan, "RBF surrogate model and EN1317 collision safety-based optimization of two guardrails," Structural and Multidisciplinary Optimization, vol. 60, no. 1, pp. 343–362, Jul. 2019, doi: 10.1007/s00158-019-02203-z.

[27] NCAC (2008) Finite element model archive, George Washington University FHWA/NHTSA National Crash Analysis Center, http:// www.ncac.gwu.edu/vml/models.html, Virginia (Accessed 2008)

[28] Europan Norm, "BS EN 16303:2020 BSI Standards Publication Road restraint systems — Validation and verification process for the use of virtual testing in crash testing against vehicle restraint system," 2020.

[29] S. Ozcanan and A. O. Atahan, "Radial basis function surrogate model-based optimization of guardrail post embedment depth in different soil conditions," Proceedings of the Institution of Mechanical Engineers, Part D: Journal of Automobile Engineering, vol. 234, no. 2–3, pp. 739–761, Feb. 2020, doi: 10.1177/0954407019848548.

[30] CSI (2017) Crash testing of H1 and H2 guardrails systems. 0021\ME\HRB\17, Bollate, Italy

[31] N. Abraham, B. Ghosh, C. Simms, R. Thomson, and G. Amato, “Assessment of the impact speed and angle conditions for the EN1317 barrier tests,” Int. J. Crashworthiness, vol. 21, no. 3, pp. 211–221, 2016, doi: 10.1080/13588265.2016.1164444.

[32] C. Jurewicz, A. Sobhani, J. Woolley, J. Dutschke, and B. Corben, “Exploration of Vehicle Impact Speed - Injury Severity Relationships for Application in Safer Road Design,” Transp. Res. Procedia, vol. 14, pp. 4247–4256, 2016, doi: 10.1016/j.trpro.2016.05.396.

Turkish Journal of Civil Engineering, 2023 145-172, Yazı 729, ***Araştırma Makalesi***

Kohezyonsuz Zeminde Kazık Aralığının Belirlenmesi ve Temel Davranışının Deneysel İncelenmesi

Ercan Egemen BAŞAR[1]
İlyas Devran ÇELİK[2]
Münire FINDIK[3]
Soner UZUNDURUKAN[4]

ÖZ

Bu çalışmada, %50 ve %85 olmak üzere, iki farklı rölatif sıkılığa sahip kum zeminde 40 adet model test deneyi yapılmıştır. Model temel sistemleri; uygulanan yükün, sadece radyeye, sadece kazıklara ve kazıklı radye temel sistemine taşıtıldığı durumlar dikkate alınarak oluşturulmuştur. Kazıklı radye temeller radyenin zemine gömülü olduğu ve zemine gömülü olmadığı iki farklı durum için irdelenmiştir. Eksenel statik artımsal yükler altında analiz edilen modellerde; optimum kazık aralığının radyenin gömülü olmadığı durumda daha küçük, gömülü olduğu durumda ise daha büyük S/D oranına sahip olduğu belirlenmiştir. Optimum kazık aralığı, orta sıkı zeminde, 1.5D ile 4D, çok sıkı zeminde 4.5D ile 6D arasında bulunmuştur.

Anahtar Kelimeler: Yapı zemin etkileşimi, kazıklı radye temel, optimum kazık aralığı, kazık tasarım parametreleri, model test.

ABSTRACT

Experimental Investigation on Foundation Behaviour and Optimum Pile Spacing in Cohesionless Soil

In this study, 40 model test were conducted with cohesionless soil in two different relative density of 50 % and 85 %. The model tests were categorized into 3 different configurations as only raft, only pile and piled raft foundation. Also the model tests of the piled rafts were

Note:
- Yayın Kurulu'na 17 Mart 2022 günü ulaşmıştır. 24 Ocak 2023 günü yayımlanmak üzere kabul edilmiştir.
- 31 Mayıs 2023 gününe kadar tartışmaya açıktır.
- https://doi.org/10.18400/tjce.1244594

1 Süleyman Demirel Üniversitesi, İnşaat Mühendisliği Bölümü, Isparta, Türkiye
basarercan1@gmail.com - https://orcid.org/0000-0001-8175-6923

2 Süleyman Demirel Üniversitesi, İnşaat Mühendisliği Bölümü, Isparta, Türkiye
devrancelik@sdu.edu.tr - https://orcid.org/0000-0001-9011-4041

3 Süleyman Demirel Üniversitesi, İnşaat Mühendisliği Bölümü, Isparta, Türkiye
mnr.dikmen@gmail.com - https://orcid.org/0000-0001-7333-8713

4 Süleyman Demirel Üniversitesi, İnşaat Mühendisliği Bölümü, Isparta, Türkiye
soneruzundurukan@sdu.edu.tr - https://orcid.org/0000-0003-4080-6642

configured as shallow and surface. During the tests vertical loads were incrementally applied. The results demonstrate that the optimum pile spacing is smaller in the surface case compared to the shallow case. The study demonstrated experimentally that optimum pile spacing is to be between 1.5D to 4D, for 50 % relative density, whereas the optimum pile spacing for 85 % relative density is 4.5D to 6D.

Keywords: Soil-Structure Interaction, Piled Raft Foundation, Optimum Pile Spacing, Pile Designing Parameters, Model Test

1. GİRİŞ

Kazıklı radye temeller, taşıma gücü sınır değerinin yeterli olmadığı veya izin verilen oturma miktarının aşıldığı durumlarda uygulanmaktadır. Kazıklı radye temel sistemlerinde üstyapı yükü kazık ve radye tarafından beraber taşınarak zemine aktarılmakta, bu aşamada zemin-kazık-temel-üstyapı sistemleri birbiriyle etkileşim içerisinde bulunmaktadır. Kazıklı radye temel sistemleri ekonomik açıdan mümkün olan en az kazık sayısıyla üstyapı yükünü taşımayı amaçlamaktadır. Üstyapı yükü altında çalışmaya başlayan kazıklı radye temel sisteminde; kazık ve radye plağı arasındaki yük paylaşım oranları, temel sisteminin zemin ile olan etkileşimine göre şekil almaktadır. Bu noktada; özellikle sürtünme kazıklı sistemlerde üst yapı yüküne maruz temel sistemlerinde ilk mobilizasyon yada ilk oturma başlayıncaya kadar; üst yapıdan gelen yük, büyük oranda kazıklar tarafından taşınmaktadır. İlk mobilizasyonun tamamlanmasıyla, kazık ucu kotunda yükün büyük bir kısmı zemine transfer olmuş olacak ve temelin oturma değerleri minimize olacaktır. Tam bu noktada kazıklar maksimum taşıma gücüne ulaşacak ve yük, plak temel tarafından da karşılanmaya başlayacaktır. Belirtildiği gibi söz konusu bu sistemin zemin-kazık-radye-üstyapı etkileşimi dahilinde sistemin çalışma mekanizmasını irdelemek, sistemin ekonomik ve güvenli dizayn kriterlerinin belirlenmesine katkı sağlayacaktır [1, 2].

Son yıllarda kazıklı radye temellerin davranışının, farklı yöntemler kullanılarak incelendiği çalışmalarla sıkça karşılaşılmaktadır. Konuyla ilgili çalışmalarda kullanılan yöntemler genel olarak; analitik yöntemler, nümerik yöntemler, analitik-nümerik yöntemler, küçük ölçekli laboratuvar model testleri, saha vaka analizleri şeklinde gruplandırılabilmektedir [3, 4, 5]. Krisnanto ve diğ. [5], bu yöntemler arasında olan küçük ölçekli laboratuvar model testlerinin, özellikle ön tasarım aşamasında nihai yük ve oturma davranışının belirlenmesinde etkili olduğunu belirtmiştir.

Kazıklı radye temel sistemlerinin geleneksel tasarımında temel plağının taşıma kapasitesine katkısı gözardı edilerek sadece kazıkların yük taşıdığı dikkate alınmaktadır. Bununla birlikte bu tip sistemlerde radye plağının taşıma kapasitesine artan yönde, oturmalarda azalan yönde katkı sağladığı bilinmektedir. Kuwabara [6] ve Sharafkhah ve Shooshpasha [7], düşey yüklenmiş kazıklı radye temellerin davranışlarının elastik teoriye dayanan sınır eleman yöntemiyle analiz edildiği çalışmalarda kazık başlığının zemine temas etmediği, sadece kazıkların yük alabildiği temel sistemleri ile kazıklı radye temellerin davranışı karşılaştırmıştır. Kazıklı radyelerde, düşey yükün %20-40 arasındaki kısmının radye tarafından ve kalan %60-80 arasındaki kısmının ise kazıklar tarafından taşınacağı bu çalışmalarda ifade edilmiştir.

Kazıklı radye temel davranışının incelendiği model testlerde kazık çapı, kazık uzunluğu ve zemin sıkılığı gibi parametreleri değişken kabul ederek, kazıklı radye temellerde plağın

taşıma gücüne katkısının ve optimum kazık aralığının incelendiği çalışmalar mevcuttur [8, 9, 10]. Bu çalışmalarda sınır koşullarının test sonuçlarına etkisinin minimize edilmesi amacıyla tank boyutları için minimum derinlik ve genişlik tavsiyeleri bulunmaktadır [11]. Nihai taşıma gücünün artmasında kazık uzunluğu, kazık çapı, rölatif sıkılık ve kazıklar arası mesafe v.b. parametreler etkili olmakla birlikte, kohezyonsuz zeminde kazık çapı, kazık uzunluğu, kazıklar arası mesafenin değişken olarak incelendiği bir çalışmada kazıklı radye temellerin sadece radye temele göre gevşek kum zeminlerde %42-129 oranında, sıkı zeminlerde ise %74-124 daha fazla taşıma gücüne sahip olduğu belirtilmiştir [12].

Raut ve Diğ. [13] saha gözlemleriyle kazık uzunluğu, kazık çapı ve temel boyutlarının, kazık radye yük paylaşım oranını nasıl etkilediğini inceleyen bu çalışmada aynı kazık uzunluğunda (L_P), kazık çapındaki (D) artışın kazıklar tarafından karşılanan yükte artışa neden olduğu bulunmuştur. Diğer yandan L_P/D oranının artmasıyla aynı yük altında aynı kazık aralığındaki kazıklı temel tasarımları düşey yük altında daha az oturmaktadır [13,14]. Model testlerde L_P/D oranı ve kazık sayısı arttıkça kazıklı radye temellerin aynı oturma mertebesinde radye temellere göre daha fazla yük aldığı analiz edilmiştir [15]. Ancak üstyapı yükü kaynaklı eksantirisitenin mevcut olduğu durumlarda uzun kazık kullanımının yapı üzerindeki riski büyüteceği yapılan çalışmada belirtilmiştir. Bu tür durumlarda uzun kazıkların zemindeki oturmayı azaltmasına rağmen kısa kazıklı radye temelin kullanımının uygun olacağı da ifade edilmiştir [16]. Kazık başlığının rijit, yarı rijit veya esnek olması durumu göz önüne alındığında temel sistemlerinde kazık başlığı rijitliği ve yatay yönde oluşan gerilme artışlarının oturma davranışlarını artırdığı belirlenmiştir [17].

Kazık yerleşim aralığı dikkate alındığında kazık başının zemine gömülü olduğu veya olmadığı durumda kazıklar arası mesafenin nihai taşıma gücüne etkisi üzerine yapılan çalışmalarla incelenmiştir. Kazık başının zemine gömülü olmadığı durumda, kazıklar arası mesafenin 4D 'den daha büyük olmasının nihai taşıma kapasitesinde azalmaya neden olduğu, kazık başının gömülü olduğu durumda ise kazıklar arası mesafenin 4D değerinden büyük olması durumunda dahi nihai taşıma kapasitesinde artışın devam ettiği görülmüştür. Kazıklar arası mesafe artsa bile kazık ve temel birlikte çalışmaya devam ettiği için taşıma gücü açısından katkı ortaya koymaktadır. Ancak 1D ve 2D gibi mesafe aralığında kazıklar arasında zeminde gerilme girişimleri oluşmaktadır. [18]. Tekil kazık, kazık grubu, sadece radye ve kazıklı radye temel yüklemesinde optimum kazık aralığı 3D olarak kazıklı radye temel sistemi için elde edilmiştir [19]. Deneysel ve sayısal olarak yapılan analizlerde kazık yerleşim aralığı/kazık çapı oranlarının incelenmesi dışında kazık aralığı/temel genişliği (S/B) oranı dikkate alındığında bu oranın % 0.7 olduğu durumda kazıklı radye sisteminin üstyapı yüküne karşı en yüksek taşıma kapasitesinde olduğu literatürde ifade edilmiştir[1]. Saha çalışmaları ve kazıklı radye temeller için Clancy ve Randolph [20] tarafından önerilen formüllerden elde edilen veriler karşılaştırmalı dikkate alındığında aynı yük altında oturma değeri açısından saha çalışmaları ve formüller arasında % 23'e varan farklar çıkmaktadır [21]. Bu amaçla ön tasarım yaparken model deneyleri dikkate almak bize yol gösterici olmaktadır.

Bu çalışmada, model testlerle optimum kazık yerleşimine, L_P/D oranı, temel ve kazık geometrisi, zemin elastisite modülü v.b. değişkenlerin etkisi araştırılmıştır. Aynı zemin koşulları, sadece radye, sadece kazık, radyenin zemine gömülü olduğu ve olmadığı durumda kazıklı radye temel olarak 4 farklı koşul altında analiz edilmiştir. 0.5-1.0 mm dane çapı dağılımına sahip iki farklı sıkılıktaki kum zeminde artan statik yük altında testler yapılmıştır. Çalışmada kazıklı radye temel sistemlerinde, ilk mobilizasyon kaynaklı yük paylaşım

mekanizmasını ayrıştırabilmek için temel plağı zemine gömülü ve plak tabanı zemin kotunda yani temelin gömülü olmadığı durumda olmak üzere iki aşamada değerlendirilmiştir. Model testlerde iki farklı temel boyutu, iki farklı kazık çapı, 1.5D, 2D, 3D, 4.5D ve 6D kazık aralığı için oluşturulan numuneler, çok sıkı ve orta sıkı zemin koşullarında test edilmiştir. Deneyler sonucunda elde edilen veriler kullanılarak, kazık uzunluğu/çap oranı, temel ve kazık geometrisi, zemin sıkılığı, üstyapı yükü, oturmalar v.b. kazıklı radye temel sisteminin taşıma gücü üzerinde etkisi bulunan yapı-zemin unsurlarının katkıları değerlendirilmiş ve bu değerlendirmeler ışığında kazık radye yük paylaşım oranı, optimum kazık aralığı v.b. tasarım parametreleri hakkında literatüre katkı sağlanmıştır.

2. MATERYAL VE METOT

2.1. Model Testlerde Kullanılan Zeminin Mühendislik Özellikleri

Bu çalışmada kullanılan zemin Kocaeli ilinden temin edilmiş olan kötü derecelenmiş (SP) kuvars kumudur. İki farklı rölatif sıkılıkta (% 50 ve % 85) hazırlanan kum zemin üzerinde model deneyleri yapılmıştır. Model testlerde kullanılan zeminin indeks özelliklerinin belirlenmesi için ASTM D6913 [22] standardıyla elek analizi, ASTM D854-14 [23] Standartıyla Piknometre, ASTM D4253-16 [24] standardıyla maksimum ve minimum boşluk oranı, ASTM D3080 [25] Standardıyla direkt kesme kutusu deneyleri yapılmıştır. İlgili zemin deneylerinin sonuçları Şekil 1 ve Tablo 1,2 ve 3'te verilmiştir.

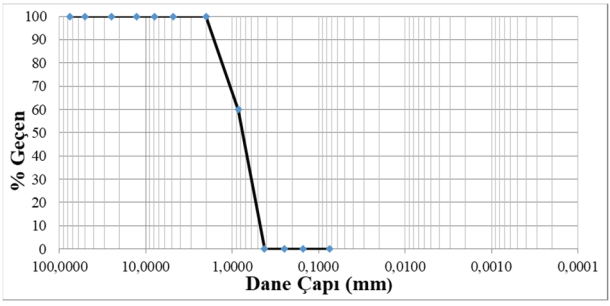

a) Kum Zemin Dane Çapı Dağılımı

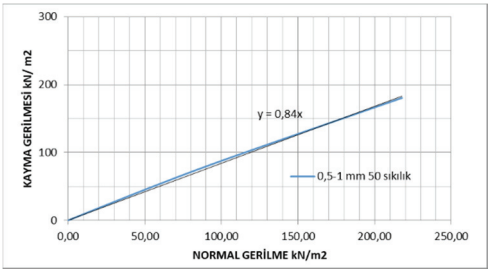

b) % 50 Sıkılıkta Kesme Kutusu Kayma Gerilmesi Normal Gerilme Değerleri

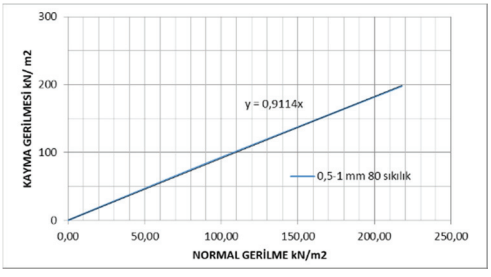

c) % 85 Sıkılıkta Kesme Kutusu Kayma Gerilmesi- Normal Gerilme Değerleri

Şekil 1 - Zemin Dane Çapı Dağılımı ve Direkt Kesme Kutusu Kayma-Normal Gerilme Grafikleri

Tablo 1 - Kumun Fiziksel Özellikleri

Granülometri Parametreleri	Birim	Değer
Kaba Kum Yüzdesi	%	0
Orta Kum Yüzdesi	%	100
İnce Kum Yüzdesi	%	0
D_{10}	mm	0.48
D_{30}	mm	0.65
D_{60}	mm	0.85
D_{50}	mm	0.75
Üniformluk Katsayısı C_u	-	1.77
Derecelenme Katsayısı C_c	-	1.03
Zemin Sınıfı	-	SP

Tablo 2 ve 3'te kum zemine ait sıkılık özellikleri verilmiş olup, % 50 ve % 85 sıkılıkta model test tankına yerleşimi için gerekli mühendislik parametreleri belirlenmiştir.

Tablo 2 - Kum Zemine Ait Sıkılık Değerleri

Rölatif Sıkılık Parametreleri	Birim	Değer
Dane Birim Hacim Ağırlığı	kN/m^3	26.8
Maksimum Boşluk Oranı(e_{maks})	-	0.85
Minimum Boşluk Oranı(e_{min})	-	0.51
γ_{kmaks}	kN/m^3	17.41
γ_{kmin}	kN/m^3	14.21

Tablo 3 - Kum Zeminin Çok Sıkı ve Orta Sıkı Durumdaki Malzeme Özellikleri

	%85 Sıkılık	%50 Sıkılık
$\gamma_{kuru}(kN/m^3)$	17	15.8
$E(kN/m^2)$	36010	21060
v	0.3	0.3
$G(kN/m^2)$	13850	8100
$\phi(°)$	42	38
$c(kN/m^2)$	0	0

Tablo 3'te yer alan elastisite, kayma modülü ve Poisson oranı Şekil 1 b ve c'de yer alan başlangıç aşamasındaki direkt kesme kutusu deneylerinden elde edilen kayma gerilmesi yatay birim şekil değiştirme oranlanarak kayma modülü elde edilmiş buna göre literatürde Noonan ve ark. [26] ve Çetin [27]'de yer alan formüllerden yararlanılarak elastisite modülü ve Poisson oranı hesaplanıp, Tablo 3 oluşturulmuştur.

2.2. Model Test Deneylerinde Kullanılan Temel ve Kazıklara Ait Özellikler

Model deneylerde kullanılan temel plakları ve kazıklar çelik malzemeden imal edilmiştir. Çalışmada, uzunlukları aynı olan iki farklı çapa sahip kazık tipi, kalınlıkları aynı olan iki farklı boyuttaki temel tipi kullanılmıştır. Temel plaklarının cidar kalınlığı 20 mm dir. Kazıklara ve temellere ait malzeme özellikleri ve boyutsal parametreler Şekil 2 ve Tablo 4'te verilmiştir.

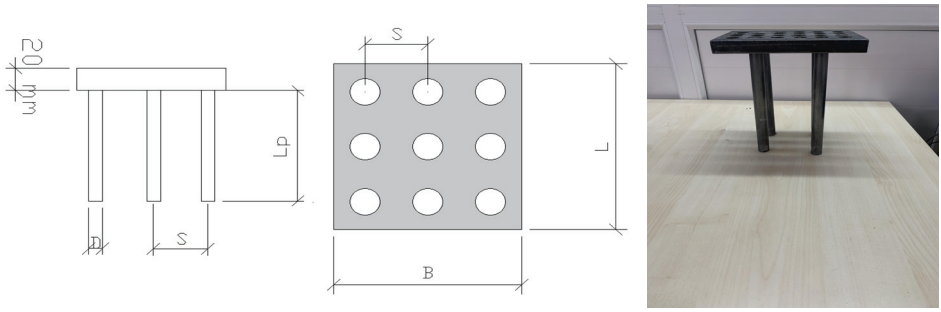

Şekil 2 - Temel plağı ve kazık elemanların boyutsal parametreleri

Şekil 2'de temel genişliği (B), temel uzunluğu (L) ve kazık uzunluğu (Lp) ve kazık çapı (D) görsel olarak yer almaktadır.

Tablo 4. Temel ve Kazık Geometrik Ölçüleri ve Kazık Malzeme Özellikleri

Malzeme Cinsi	Malzeme Niteliği	B(mm.)	L(mm.)	D(mm.)	L_P(mm.)	L_P/D	γ(kN/m³)	E(kN/m²)	ν
Çelik	Birinci Temel	120	120	-	-		77	$2*10^8$	0.30
	İkinci Temel	200	160	-	-		77	$2*10^8$	0.30
	Birinci Temel Kazığı	-	-	7.5	230	30.7	77	$2*10^8$	0.30
	İkinci Temel Kazığı	-	-	20	210	10.5	77	$2*10^8$	0.30

Çalışmada kullanılan tanklar çelik levhalar kullanılarak tasarlanmış, tank duvarında yeterli rijitliği sağlayabilmek için tankın yarı kotunda (250mm'de) kuşaklama yapılmıştır. Yükleme esnasında zemin tabakasında sıkışmaya bağlı olarak meydana gelebilecek hareketliliğin gözlemlenebilmesi amacıyla model test tankının cam kaplamalı gözlem boşlukları bulunmaktadır ve Şekil 10'da görülmektedir. Statik yükleme koşullarındaki model testlerde, sınır koşullarının test sonuçlarına etkilerini değerlendirmek amacıyla 500 mm derinliğe

sahip, 500x500 mm ve 500x750 mm boyutlarında iki farklı kum tankı üzerinde referans model test deneyleri yapılmıştır. Referans deneylerden elde edilen sonuçlar birbirleriyle ve Plaxis 3D sonlu elemanlar programı sonuçları ile karşılaştırılmıştır. Sınır koşulları etkisi bir sonraki bölümde değerlendirilmiştir.

2.3. Sınır Koşulları Etkisi

Statik yüklemeye tabi tutulan model testlerde, sınır koşullarının test sonuçlarına etkilerini inceleyebilmek için derinlikleri 50 cm sabit kalmak kaydı ile yatay ölçüleri 50x50 cm ve 50x75 cm boyutlarındaki iki adet kum tankında referans model testler (Şekil 9, Durum 1) yapılmıştır. Durum 1 ve Durum 2 (Şekil 3 a ve b) için iki farklı temel boyutunda (12*12 cm ve 20*16 cm) Tablo 2 ve Tablo 3'te bulunan rijitlik parametreleri kullanılarak Plaxis 3D programında sayısal modeller oluşturulmuştur. Sayısal analizlerde sınır koşullarının sonuçlara olan etkisini irdeleyebilmek amacıyla, sonlu modeller 50x50x50cm(Şekil 3c), 50x75x50cm(Şekil 3d) ve saha koşulları (Şekil 3e) için tekrarlanmıştır. Literatürde de yer aldığı gibi [12], yapılan referans deneylerden elde edilen sonuçlar birbirleri ve Plaxis 3D sonlu elemanlar programı ile karşılaştırılmıştır. Her üç durumda da oturma ve taşıma kapasitesi sonuçlarının birbiri ile benzer olması sebebi ile çalışmada kullanılan tankların deney sonuçları için yeterli olduğu anlaşılmıştır.

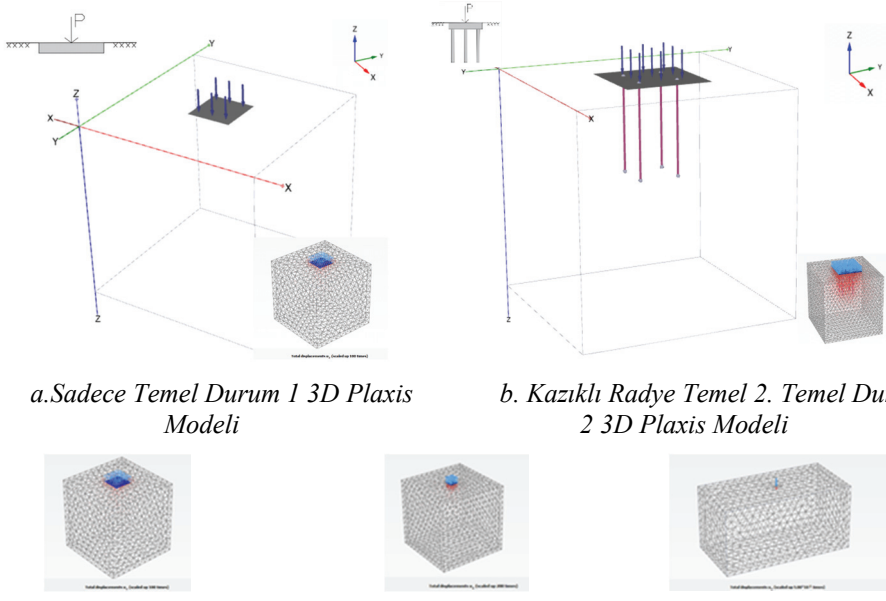

a.Sadece Temel Durum 1 3D Plaxis Modeli

b. Kazıklı Radye Temel 2. Temel Durum 2 3D Plaxis Modeli

*c.(x,y,z)50*50*50 cm.*

*d. (x,y,z)50*75*50 cm*

*e. (x,y,z)10*20*10 m.*

Şekil 3 - Plaxis 3D Sayısal Modelleri Genel Görünümü ve Tank Boyutları

Çalışmada tablo 5'te yer alan E1,E8,E15,E18,E22,E25 model test deneyleri ve Şekil 3 c,d,e'de yer alan 3 farklı sınır koşuluna göre yapılan tüm Plaxis 3D sonlu elemanlar

analizlerinde elde edilen yük-oturma davranışlarının örtüşmekte olduğu Şekil 4 ve Şekil 5'te görülmektedir.

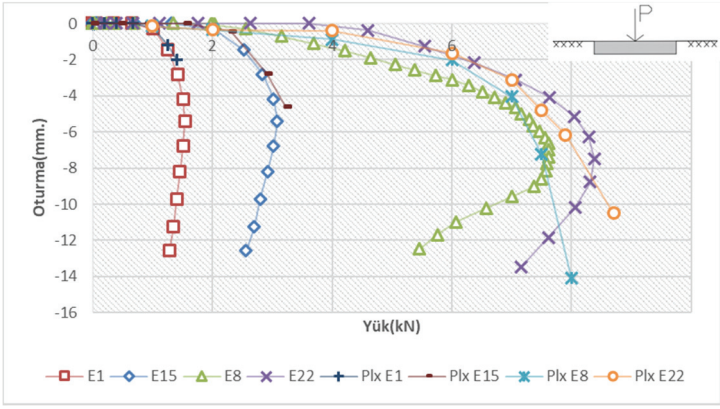

Şekil 4 - E1,E8,E15,E22 Durum 1 için yapılan Deneysel ve Sonlu Elemanlar Karşılaştırma Grafikleri

Bu çalışmadaki model testler arasında en yüksek taşıma kapasitesine ulaşan 2. Temel boyutlarında ve 4.5D kazık aralığına sahip E18 (orta sıkı kum) ve E25 (çok sıkı kum) deneyleri sonlu eleman analizi ve model test deneyi grafiği Şekil 5'te sunulmuştur.

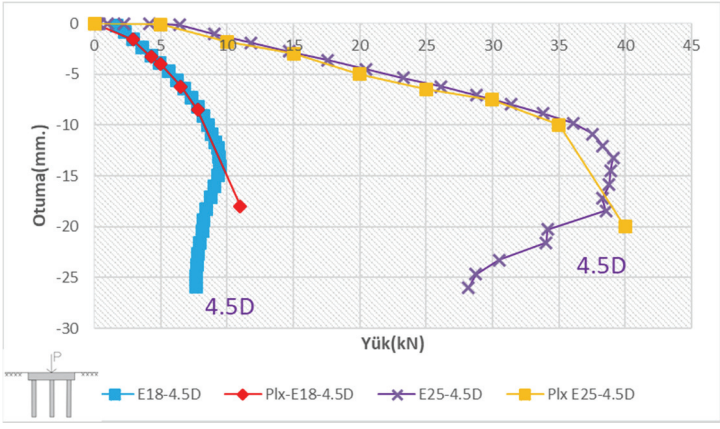

Şekil 5 - E18,E25 Durum 2 4.5D Kazık Aralıklı Kazıklı Temel İçin Deneysel ve Sonlu Elemanlar Karşılaştırma Grafikleri

Şekil 5'ten görüleceği üzere bahsedilen tank boyutlarında, sonlu eleman analizleri ve model test sonuçları birbiri ile uyum içerisindedir. Elde edilen bu sonuçlar çalışmada kullanılan 50x50x50 cm boyutlarına sahip tank ile yapılan deneylerin sınır koşullarından etkilenmeyeceğini göstermiştir. Bu nedenle model test çalışmalarında ve analizlere 50x50x50 cm boyutlarındaki tank kullanılarak devam edilmiştir.

2.4. Model Test Deneylerinin Uygulaması ve Test Programı

Farklı boyutsal parametrelerin mevcut olduğu model testlerin sonuçlarının aynı düzlemde değerlendirilebilmesi, tekrarlanabilirlik ve sonuç olarak çalışmanın etkinliği açısından, yükleme hızı, sınır koşulları ve özellikle zemin koşullarının standart hale getirilmesi oldukça önemlidir. Bu nedenle, zeminin kum tankına doldurulması esnasında azami özen gösterilmiştir. Kum zeminin tanka doldurulması için bir yağmurlama kulesi kullanılmış ve zemin danelerinin tankın içine aynı yükseklikten serbestçe düşürülmesi sağlanmıştır. Tankın yağmurlama kulesinden yükleme ünitesine taşınması sırasında olası sarsıntıların zemin sıkılığını değiştirmesini engellemek amacıyla kayar vinç hattı tasarlanmıştır. Şekil 6'da gösterilen düzenek sayesinde kum tankı içindeki zemin tabakasının yağmurlama hattından yükleme ünitesine istenilen koşula en yakın durumda olacak şekilde geçişi sağlanmıştır.

(a) Model Testin Hazırlanışındaki İlk Aşama *(b)Model Testin İkinci Aşaması*

Şekil 6 - Model Testlerin Hazırlanış ve Yapılma Görseli

Şekil 6a'da yer alan yağmurlama kulesinden düşen kum, boru içinde hızlanarak boru ağzında model tankının içine 5 cm yükseklikten düşmektedir. Bu doğal akış ile kum tankındaki zemin tabakasının % 50 rölatif sıkılıkta yerleşmesi sağlanmaktadır. Tankın 500mm olan derinliği, 50mm kalınlığında 10 zemin tabakası halinde yerleştirilmiştir. Tankın alt ve üst kısmına yerleştirilen 30mm çapında 20mm derinliğinde numune alma kapları yardımıyla her dolumda iki defa olmak üzere rölatif sıkılık kontrolü yapılmıştır [12, 28, 29].

Çalışmada dikkate alınan ikinci sıkılık değeri olan %85 rölatif sıkılığa ulaşabilmek için vibrasyonla sıkıştırma tekniği kullanılmıştır [28, 29]. Sıkıştırma işlemi yukarıda bahsedilen her 50 mm'lik serim işlemi gerçekleştirildikten sonra uygulanmıştır. Şekil 7'de bu

uygulamaya ait genel görünüm verilmiştir. Vibrasyon işleminin zemin granülometrisinde olası etkilerini değerlendirebilmek açısından sıkıştırma işlemi öncesi ve sonrasında yapılan elek analizleri vibrasyonla sıkıştırmanın zemin granülometrisinde kayda değer bir değişime neden olmadığı işlem öncesi ve sonrası her iki elek analizi sonuçlarının çok yakın çıkmasından dolayı göstermiştir.

Şekil 7 - Kohezyonsuz Zemini İstenilen Rölatif Sıkılığa Getirmek için Titreşim Cihazı

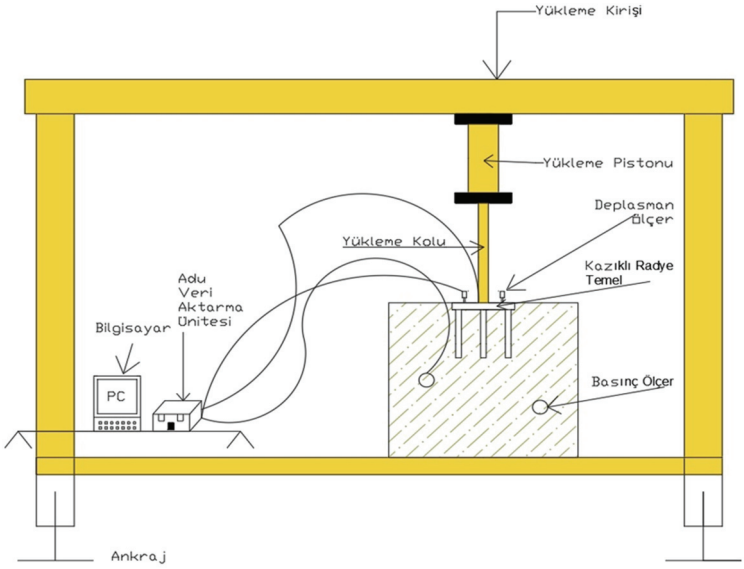

Şekil 8 - Deney Düzeneğinin Şematik Olarak Gösterimi

Şekil 8'de deney düzeneğinin genel şeması yer almaktadır. Düzenekte; yükleme kirişi, yükleme pistonu, yükleme kolu, deplasman ölçer, kazıklı radye temel, basınç ölçer, veri

aktarma ünitesi ve bilgisayar yer almaktadır. Yükleme pistonu 20 ton kapasiteli olup 0.5 mm/dk'lık yükleme hızına sahiptir. Yükleme kolunun içinde 5 tonluk 0.01 kN hassasiyetinde yük hücresi bulunmaktadır. Deplasman ölçerler 50 mm'ye kadar 0.01 mm hassasiyetinde ölçüm alabilmektedir. Buna göre Şekil 8'den görüleceği üzere kazıklı radye temel kum tankının içine 0.5 mm/dk'lık hız ile yerleştirilmekte daha sonra yük oturma eğrileri bu sistemler yardımıyla oluşturulabilmektedir. Şekil 8'de görülen basınç ölçerler sayesinde kazıklı temelin alt bölgesinde, diğer bir deyişle literatürde [11, 30, 31] eşdeğer radye olarak tanımlanan bölgede basınç değerleri ölçülebilmektedir. Bu sistem ve değerleri belirtildiği gibi literatürde yer alan çalışmalara [32,33] hassasiyet ve yükleme hızı olarak uyum sağlamaktadır. Diğer yandan bu standartlar dışına çıkılması halinde kazıkların yerinde dökme veya çakma kazık olarak davranması söz konusudur, bu durumlar için de benzer biçimde yerleştirme ve yükleme standartları bulunmaktadır [32, 33]. Çalışmada kullanılan radye temel ve kazıklı temel sistemleri dört farklı durumda incelenmiştir. Şekil 9'da model testlerde dikkate alınan başlangıç koşulları gösterilmiştir. Buna göre Durum 1'de sadece radye temel, Durum 2'de kazıklı radye (radye plağının zemine gömülü olduğu durum), Durum 3'te sadece kazık temel (kazık başlığının zemin üst kotundan 25 mm. yüksekte bulunduğu durum), Durum 4'te plak tabanı zemine (radye temelin gömülü olmadığı durum) temaslı kazıklı radye dikkate alınarak yükleme testlerine tabi tutulmuştur.

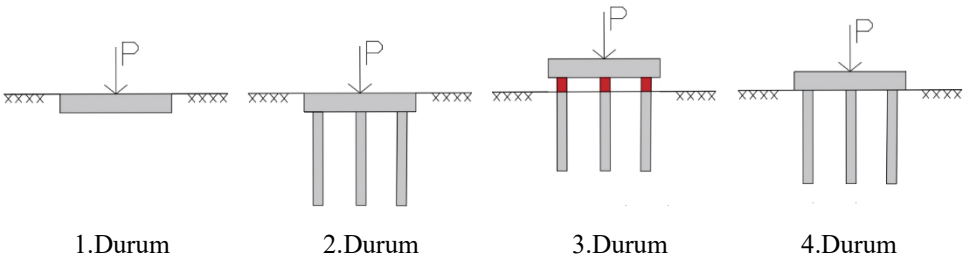

Şekil 9 - Model Testlere Yerleştirilen Temel Sistemlerinin Gösterimi

Testlerde kullanılan temel, kazık ve zemin sıkılık varyasyonlarına bağlı olarak parametre sayısının artırıldığı bu çalışmada, oluşturulan deney düzeneklerinin isimleri ve dikkate alınan parametrelerin değerleri Tablo 5'te gösterilmiştir. Tabloda boyutsal açılımları ve zemin durumları ifade edilen toplam 40 adet model test deneyi yapılmıştır. Çalışmada dikkate alınan temel sistemi durumlarına ait test görüntüleri Şekil 10'da verilmiştir.

Tablo 5 - Deney Programı

*G Orta Sıkı *S Sıkı Durum		Deney No	B(mm.)	L(mm.)	Lp(mm)	d(mm)	Lp/D	S
Durum 1	G	E1	120	120	-	-	-	-
	S	E8	120	120	-	-	-	-
	G	E15	200	160	-	-	-	-
	S	E22	200	160	-	-	-	-

Tablo 5 - Deney Programı (devam)

*G Orta Sıkı *S Sıkı Durum		Deney No	B(mm.)	L(mm.)	Lp(mm)	d(mm)	Lp/D	S
Durum 2	G	E2,E3,E4	120	120	230	7,5	30,7	2D, 4D, 6D
	S	E9,E10,E11	120	120	230	7,5	30,7	2D, 4D, 6D
	G	E16,E17,E18	200	160	210	20	10,5	1.5D, 3D, 4.5D
	S	E23,E24,E25	200	160	210	20	10,5	1.5D, 3D, 4.5D
Durum 3	G	E5,E6,E7	-	-	230	7,5	30,7	2D, 4D, 6D
	S	E12,E13,E14	-	-	230	7,5	30,7	2D, 4D, 6D
	G	E19,E20,E21	-	-	210	20	10,5	1.5D, 3D, 4.5D
	S	E26,E27,E28	-	-	210	20	10,5	1.5D, 3D, 4.5D
Durum 4	G	E29,E30,E31	120	120	230	7,5	30,7	2D, 4D, 6D
	S	E32,E33,E34	120	120	230	7,5	30,7	2D, 4D, 6D
	G	E35,E36,E37	200	160	210	20	10,5	1.5D, 3D, 4.5D
	S	E38,E39,E40	200	160	210	20	10,5	1.5D, 3D, 4.5D

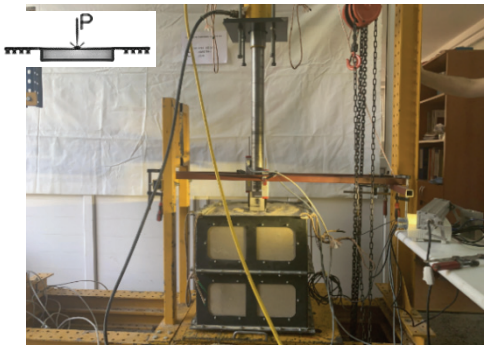

a)Durum 1 E8 Deney Düzeneği

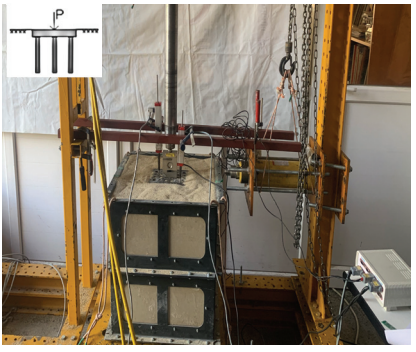

b)Durum 2 E23 Kazıklı Radye Temel Deney Fotoğrafı

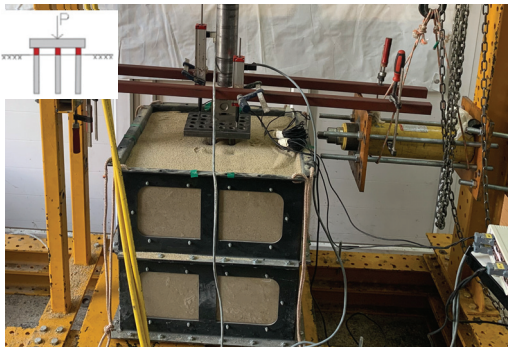

c)Durum 3 E26 Deney Fotoğrafı

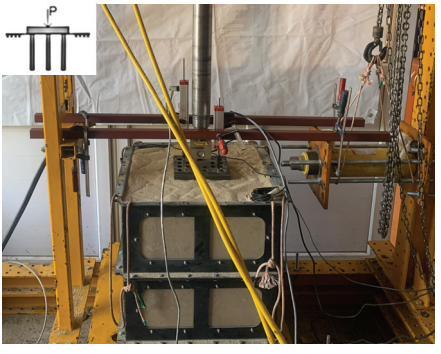

d)Durum 4 E29 Deney Fotoğrafı

Şekil 10 - Durum 1,2,3,4 gösteren model test deneyleri

Şekil 10'da çalışmada temel sistemi test durumlarına ait örnek görünümler verilmiştir. Model test kutusunun üzerine yerleştirilen cam kaplamalı gözlem boşlukları sayesinde deney esnasında zemin tabakasında sıkışmaya bağlı hareketlilik gözlemlenmiştir.

3. BULGULAR VE TARTIŞMA

Kazıklı radye temellerin davranışının deneysel olarak incelendiği bu çalışmada, orta sıkı ve çok sıkı olmak üzere iki farklı sıkılıkta hazırlanan kötü derecelenmiş kum zemin için model deneyler yapılmıştır. Deneylerde kazık çapı, kazık uzunluğu, kazıklar arası mesafe ve temel boyutları değişken olarak seçilmiştir. Kazık-temel plak etkileşiminin daha net olarak

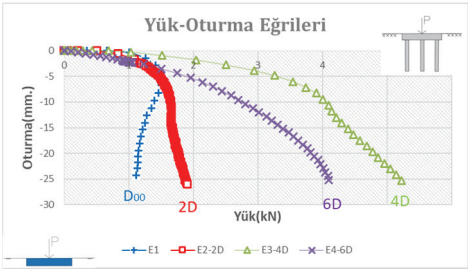

a) %50 Rölatif Sıkılık Durum 1-Durum 2 Karşılaştırması

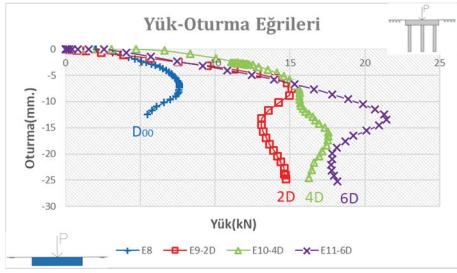

b) %85 Rölatif Sıkılık Durum 1-Durum 2 Karşılaştırması

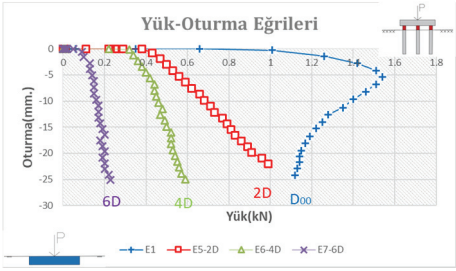

c) %50 Rölatif Sıkılık Durum 1-Durum 3 Karşılaştırması

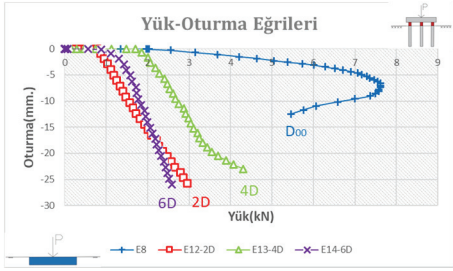

d) %85 Rölatif Sıkılık Durum 1-Durum 3 Karşılaştırması

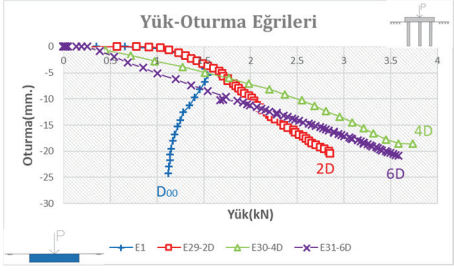

e) %50 Rölatif Sıkılık Durum 1-Durum 4 Karşılaştırması

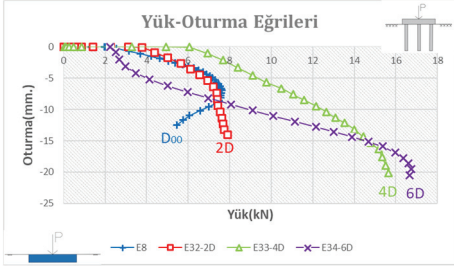

f) %85 Rölatif Sıkılık Durum 1-Durum 4 Karşılaştırması

Şekil 11 - 120x120x20mm plak, D7,5 mm kazık çapı durumuna ait model test sonuçları

anlaşılabilmesi için deneyler, Şekil 9'da gösterilen dört farklı durum için aynı koşullarda tekrarlanmıştır. Bu kapsamda yapılan model testlerden elde edilen yük oturma değerleri grafiklendirilmiştir. Grafiklerde iki farklı boyuttaki temel geometrisi, orta sıkı ve çok sıkı zemin koşulunda dört farklı başlangıç durumu için elde edilen sonuçlar ayrı ayrı olarak sunulmuştur. Şekil 11'de 120x120x20 mm boyutlarındaki birinci temel durumuna ait sonuçlar gösterilmiştir. Şekilde kazıklı radye temel durumlarını (Durum 2, 4) ve sadece kazık temel (Durum 3) temsil eden sonuçlar, sadece radye temel (1. Durum) için elde edilen referans değer ile karşılaştırmalı olarak sunulmuştur. Şekil 11'de sol sütunda yer alan grafikler zeminin %50 rölatif sıkılık değerindeki orta sıkı yerleşimine, sağ sütundaki grafikler %85 rölatif sıkılıktaki çok sıkı yerleşime aittir.

Tablo 6 - 1. Temel İçin Durum 1,2 ve 4 Kendi İçinde Kazık Temel Yük Paylaşma Oranları

Referans Deney		Karşılaştırma Deneyi			
Deney No	Temel Nihai Taşıma Kapasitesi(kN)	Deney No(S)	Kazıklı Temel Nihai Taşıma Kapasitesi(kN)	Kazık Taşıma Yüzdesi(%)	Temel Taşıma Yüzdesi(%)
E1	1.5	E3(4D)	5.2	71.15	28.84
E8	7.62	E11(6D)	21.44	64.45	35.54
E1	1.5	E30(4D)	3.73	60	40
E8	7.62	E34(6D)	16.61	54.12	45.87

Tablo 6'da Durum 1, 2 ve 4'ün kazık ve temelin yük paylaşma oranları yer almaktadır. 1.durum radye temelin göçme anındaki nihai yük diğer kazıklı radye temelin birlikte çalıştığı durum 2 ve 4'ün nihai taşıma kapasitelerine bölünerek kazık radye yük paylaşım oranları yüzde olarak tabloda verilmiştir.

$$Temel\ Taşıma\ Yüzdesi = \frac{Temel\ taşıma\ kapasitesi}{Kazıklı\ temel\ Taşıma\ Kapasitesi} * 100 \quad (1)$$

Birinci temel tipi için yapılan model testlere ait sonuçların verildiği Şekil 11 incelendiğinde; orta sıkı ve çok sıkı zemin koşullarında kazık aralıklarının, temel sisteminin düşey deplasmanları ve nihai taşıma kapasiteleri üzerinde belirleyici sonuçları olduğu görülmektedir. Şekil 11a'da orta sıkı kumda referans deney yani sadece radye temelin nihai durumu olan 1,5 kN taşıma kapasitesi dikkate alınarak, Durum 2 için kazık-radye yük paylaşım oranları karşılaştırılmıştır. Kazıklar arası mesafenin 4D olduğu E3 no'lu kazıklı temel sistemi, -25 mm düşey deplasman değerinde 5,2 kN nihai taşıma kapasitesine ulaşmıştır. Bu değer, E1 nolu referans deneyde elde edilen kapasite değerinin (1,5 kN) 3,46 katına karşılık gelmektedir. Bu deney için sisteme eklenen kazıkların etkili olduğu nihai durum dikkate alındığında temel sistemine gelen yükün %71.15 oranında kazıklarca karşılandığı hesaplanmıştır. 6D aralığındaki E4 nolu deneydeki kazıklı temel sisteminde 4 kN nihai kapasite değeri elde edilmiş, bu durum için kazıklar %62.5 oranında yükü üstlenmiştir. 2D aralığındaki E2 nolu deney için elde edilen sonuçlar incelendiğinde; orta sıkı zemin durumu için radye ve kazıklı radye taşıma kapasiteleri açısından belirgin bir farklılığın olmadığı görülmektedir. Kumdaki kazıklı temelllerde kazıklar arası mesafe için önerilen sınır

değerlerin altında kalındığı bu durumda, literatürde belirtilen gerilme girişiminin [20, 30, 31, 34], gelişmesiyle temel sisteminin taşıma kapasitesi düşmüştür ve referans deney(durum 1) ile neredeyse aynı değerde nihai yük dayanım değeriyle karşılaşılmıştır Sadece 4D aralıktaki E3 deneyinde kazıkların yük paylaşımına %71.15 oranında katkı sağladığı, diğer kazık yerleşimlerinde sürtünme direncinin yeterli seviyede mobilize olamaması nedeniyle bu oturma değerinde kazıkların yük paylaşımına katkı sağlayamadığı gözlenmektedir [30]. İlerleyen yükleme aşamalarında nihai sınırda 6D aralıktaki E4 deneyinde kazıkların yük paylaşımına olan katkısı %62.5 mertebesine ulaşmaktadır. Ancak 2D aralığındaki E2 deneyinde kazık-zemin etkileşim bölgesinde gerilme girişimi[6, 35, 36, 37, 38], nedeniyle taşıma gücü azalırken, kazıklar arası mesafenin oldukça fazla olduğu 6D durumunda blok davranış söz konusu olamamış, 4D durumunda ise kazık grubu blok olarak davrandığından taşıma gücü daha yüksek çıkmış diğer bir deyişle kazıklar en etkin şekilde çalışmıştır.

Şekil 11b'de %85 rölatif sıkılık değerinde hazırlanan kumda Durum 2 için yapılan model test sonuçları sunulmuştur. Şekil 11a ve 11b karşılaştırıldığında tüm kazık aralıkları için zemin sıkılığındaki artışa paralel olarak taşıma kapasitelerinde artış olduğu görülmektedir. Bu sıkılık durumunda, referans deneyinin nihai taşıma kapasitesinin elde edildiği oturma değerinde (-7.5mm) tüm kazık yerleşimleri için kazıklı radyenin taşıma kapasitesinin radye temelin 2 katı mertebesinde olduğu görülmektedir. Kazıklı radye temellerin nihai kapasiteleri dikkate alındığında kazık yük paylaşım oranları 2D ve 4D için %50, 6D durumu için %70 olarak hesaplanmıştır. Bu sonuçlar, kazıklar arası mesafenin kazıklı radye performansı üzerinde önemli etkiye sahip olduğunu ve optimum aralığının zemin sıkılığından önemli ölçüde etkilendiğini göstermektedir. Bu nedenle zemin sıkılığına bağlı olan optimum kazık aralığına sahip kazıklı radye temellerde, etkileşimde bulunan kazık-zemin bölgesinde sürtünme ve uç direncini artırıcı yönde kazanımlar geliştiği ve temel sisteminin taşıma kapasitesinde kayda değer artışlar meydana geldiği görülmektedir. Bu bulgular Poulos [30] ve Nyugen vd. [32] tarafından elde edilen bulgularla örtüşmekte ve geleneksel oturmadan bağımsız temel taşıma ve sadece kazıkların yük taşıma kapasitesini sürtünme ve uç direncince hesaplayan söz konusu formüllerin literatürde[38] gelişmesi gerektiğini göstermektedir.

Çalışmada Durum 3 olarak tanımlanan ve sadece kazıkların sürtünme ve uç direncinin sistem davranışına olan etkisinin ayrıştırılması amacıyla oluşturulan model testlere ait sonuçlar Şekil 11 c ve d'de gösterilmiştir. Bu bölüm 120x120x20 mm boyutlarındaki temel sistemi ve 7,5mm çapındaki kazık aralığına ait sonuçları kapsamaktadır. Deneylerde temel tabanı, zemin üst kotundan 25 mm yukarıda yerleştirilmiştir (Şekil 11c). Bu duruma ait deneylerde uygulanan yük; plak tabanı ve zemin arasında temas sağlanıncaya kadar, kazık yüzey alanı boyunca sürtünme direnci ve kazık alt ucunda uç direnci tarafından karşılanmıştır. Sonuçlar incelendiğinde, kazık taşıma kapasitelerinin referans deneyin çok altında kaldığı görülmektedir. Kazık aralığı sistemin yük oturma davranışını doğrudan etkilemektedir. Orta sıkı kumda 6D aralığındaki E7 nolu deneyde yükleme boyunca 0,2 kN nihai kapasite değerine ulaşıldıktan sonra sistem yük alamamıştır. Orta sıkı durumda kazıklar arasındaki mesafe azaldıkça, kazıkların etkileşime zorlandığı, kazık-zemin sisteminin blok davranışa geçerek nihai kapasiteye pozitif yönde katkı sağladığı görülmektedir. Bu bulgular Nyugen vd. [32] ve Reese vd. [36] tarafından elde edilen bulgularla örtüşmektedir.

Bununla birlikte sırasıyla 2D ve 4D kazık aralıklarının incelendiği E5 ve E6 deneylerinde temel sistemi oturmadaki artışla yük almaya devam etmiş ancak temel zemine temas edene kadar referans deney taşıma kapasitesine ulaşılamamıştır.

Şekil 11d'de %85 rölatif sıkılığa sahip kumda Durum 3 için yapılan deneylerin sonuçları sunulmuştur. Zemin sıkılığındaki artış, bekleneceği üzere, hem referans deneyde hem de Durum 3'e ait deneylerde yük taşıma kapasitesine artışa neden olmuştur. Çok sıkı kumda kazık sürtünmesinden kaynaklanan düşey yük kapasite kazanımı, orta sıkı kuma göre ortalama 4 kat artmıştır. Ancak hiçbir kazık aralığı için referans deneyin nihai taşıma kapasitesine ulaşılamamıştır. Çok sıkı kumda, orta sıkı kumdan farklı olarak en büyük kazanım 4D aralık olan E13 için sağlanmıştır, maksimum sürtünme direncine 2 kN yükleme mertebesinde ulaşıldığı görülmektedir. 2D ve 6D aralıklarda ise 1,12k N ve 1,35 kN mertebesindeki yüklemenin ardından mobilizasyona geçilmiştir. Sonuç olarak orta sıkı zeminde optimum kazık aralığı çok sıkı zemine göre daha düşük çıkmıştır. Buna göre çok sıkı durumda mobilizasyon daha geç başlamıştır. Bu bulgular, Hadi vd. [2] tarafından elde edilen araştırma bulgularıyla örtüşmektedir. Optimum kazık aralıkları, Durum 3'te Durum 2'ye kıyasla hem sıkı hem de orta sıkı durumda daha az çıkmıştır. Benzer biçimde El Samee [18] kazık başlıklarının gömülü olmadığı, sadece kazıkların çalıştığı durumda optimum kazık aralığının, kazık başlığının gömülü olması durumuna göre daha yakın yani daha az olduğunu gözlemlemişlerdir. Radye temelin dahil olması (Durum 4) ve kazık başlıklarının gömülmesi (Durum 2) durumlarında yapılan deneylerde nihai yük taşıma kapasitesini kazık başlıklarının gömülü olmadığı yani sadece kazıkların çalıştığı duruma (Durum 3) göre daha yüksek bulmuştur.

Çalışmada Durum 4 olarak tanımlanan radye plağının zemin üst kotuna temas ettiği duruma ait deneyler Şekil 11 e ve f'de sunulmuştur. Durum 4'ü Durum 2'den ayıran temel fark, temel plağı düşey yerdeğiştirmeye başladığında, kazık-radye yük paylaşımının başlayacak olmasıdır. Orta sıkı durum için yapılan test sonuçları incelendiğinde; 2D aralığına sahip E29 nolu deneyde, plak yük paylaşımına yükleme başından itibaren dahil olmuştur. E29 yük oturma grafiği referans deney yani E1 ile örtüşmektedir. Referans deneyde olduğu gibi zeminde belirgin bir oturma meydana gelmeksizin temel sistemi bir miktar yük alabilmiştir. Bununla birlikte E29 modelinde temel sistemi referans deney nihai kapasite sınırını takiben yük almaya devam etmiş ve düşey yük kapasite kazanımı E1'e göre 1,86 katına çıkmıştır. Bu sınır durum için kazık radye yük paylasım oranı kazıklar için %49 mertebesindedir. 4D ve 6D aralığına ait E30 ve E31 nolu deneylerde başlangıç kısmında referans deneye göre daha büyük deplasmanların gerçekleştiği görülmektedir. Referans deneyin nihai taşıma kapasitesinde meydana gelmiş olan oturma değerleri dikkate alınarak şekil 11e incelendiğinde; E30 ve E31 için daha yüksek oturma değerleri kayda alınmıştır. Oturma sınırını, kazıklar sayesinde temelin gömülü olduğu duruma göre daha üst seviyeye çekebilmiştir. Yükleme devam ettirildiğinde nihai kapasite E30 deneyi için -18mm düşey yerdeğiştirmede 3,5kN ve E31 deneyi için -20mm düşey yer değiştirmede 3,4kN olarak gerçekleşmiştir. Yükleme başlangıcında radye plak tabanı referans deneyde olduğu gibi zemin ile temas halinde olmasına rağmen, E30 ve E31 deneylerinde daha düşük yük değerlerinde referans deneye kıyasla büyük oturmalar meydana gelmiştir. Ayrıca yerdeğiştirme direncinin özellikle ilk oturma değerleri diğer bir deyişle mobilizasyon başlangıcında durum 2'ye göre farklı olduğu görülmektedir. Bu durum sistemin ilk mobilizasyonunun kazık aralığı ve radye plak derinliğinden etkilendiğini göstermektedir.

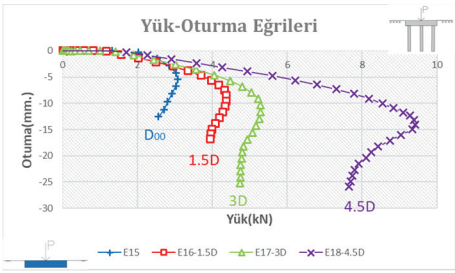

a) %50 Rölatif Sıkılık Durum 1-Durum 2 Karşılaştırması

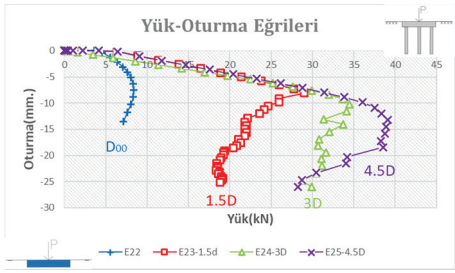

b) %85 Rölatif Sıkılık Durum 1-Durum 2 Karşılaştırması

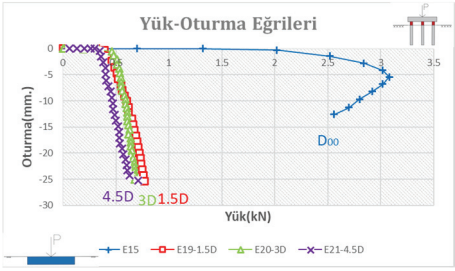

c) %50 Rölatif Sıkılık Durum 1-Durum 3 Karşılaştırması

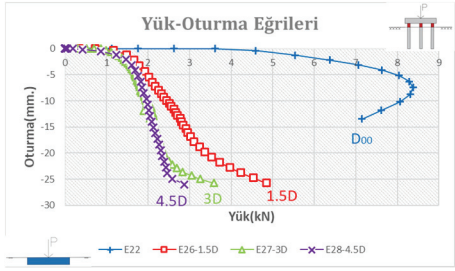

d) %85 Rölatif Sıkılık Durum 1-Durum 3 Karşılaştırması

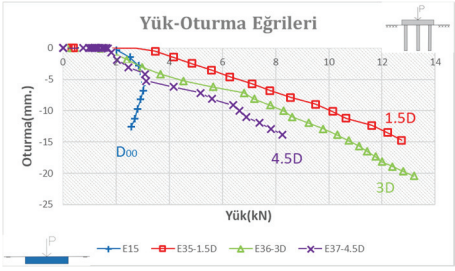

e) %50 Rölatif Sıkılık Durum 1-Durum 4 Karşılaştırması

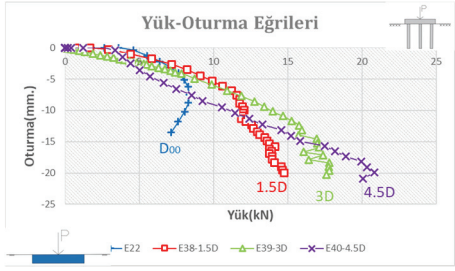

f) %85 Rölatif Sıkılık Durum 1-Durum 4 Karşılaştırması

Şekil 12 - 200x160x20mm plak, D20mm. kazık çapı durumuna ait model test sonuçları

Çok sıkı zemindeki 2D aralığına sahip E32 deneyinde yük oturma davranışı E8 deneyinde gözlenen davranışı ile örtüşmektedir. Orta sıkı zemindeki aynı aralığa sahip E29 deneyinde olduğu gibi referans deneyin nihai taşıma kapasitesine ulaşılana kadar referans deneyin yük oturma davranışını takip etmiştir. bununla birlikte referans deneyin nihai taşıma kapasitesi aşıldıktan sonra E29 ile E32 deneyinin davranışı farklılaşmıştır. E32 deneyinde referans deneyin nihai taşıma kapasitesi aşıldıktan sonra temel sisteminde oturmalar devam etmesine rağmen kayda değer bir yük kazanımı gözlenmemiştir.. Kazıklar arası mesafenin 4D olduğu E33 deneyinde ise optimum davranış gözlenmiştir. Bu deneyde, referans deney olan E8 deneyindeki nihai kapasite değeri 7,5 kN yük değerine daha küçük oturma seviyelerinde

ulaşmıştır. E33'de -7,5 mm oturma seviyesinde 12,5 kN yük değeri için kazıklar %39.04 oranında yük almıştır. E33 deneyinde temel sistemindeki oturma artıkça referans deneyde gözlenen nihai değerin üzerine çıkan taşıma kapasiteleri gerçekleşmiştir. Bu, radye temelin gömülü derinliğinin daha az olması veya hiç olmaması durumunda kazıklı temel sisteminin daha yüksek oturma değerlerinde nihai yüke daha geç ulaşacağı anlamına gelmektedir. Benzer şekilde sadece kazık temel durumunda oturmadaki artışla sistem göçmeden yük almaya devam etmiştir. Bu nedenle kazıklar vasıtasıyla, zeminde göçme oluşmaksızın daha büyük oturma mertebelerine karşı konulduğu görülmektedir. Çalışmada en yüksek kazık aralığı aralığına sahip E34 nolu deneyde, referans deney nihai taşıma kapasitesine daha büyük bir oturma değerinde ulaşılırken, E34 deneyinin nihai yük taşıma değeri E33'ten daha yüksek çıkmıştır. E33 ve E34 nihai durumu dikkate alındığında kazıkların yük paylaşımına %54.12 oranında katkı sağladıkları hesaplanmıştır.Daha önce de bahsedildiği gibi radyenin altında kalan bölgede temel derinliği yada kazıkların sık aralıkta küçük oturma mertebelerinde daha fazla yük taşıyabilmekte ancak nihai durumda daha büyük kazık aralığında daha büyük kapasite değerleri çıkmaktadır. Bu durum, Poulos [30] tarafından da belirtildiği üzere eşdeğer radye bölgesinde oluşan kazık-temel-zemin etkileşimine bağlı oturma davranışının tasarımda dikkate alınması gerektiğini göstermekte ve oturma değerlerinden bağımsız bir taşıma kapasitesinin gerçekten uzak olduğunu söz konusu bu çalışmalar ifade etmektedir.

Tablo 7 - 2. Temel İçin Durum 1,2 ve 4 kendi içinde kazık temel yük paylaşma oranları

Referans Deney		Karşılaştırma Deneyi			
Deney No	Temel Nihai Taşıma Kapasitesi(kN)	Deney No(S)	Kazıklı Temel Nihai Taşıma Kapasitesi(kN)	Kazık Taşıma Yüzdesi(%)	Temel Taşıma Yüzdesi(%)
E15	3.08	E18(4.5D)	9.42	67.3	32.7
E22	8.38	E25(4.5D)	38.9	78.45	21.54
E15	3.08	E35(1.5D)	12.74	75.82	24.17
E22	8.38	E40(4.5D)	20.85	59.81	40.19

Tablo 7'de Durum 1,2 ve 4'ün kazık ve temelin yük paylaşma oranları yer almaktadır. 1.durum radye temelin göçme anındaki nihai yük diğer kazıklı radye temelin birlikte çalıştığı durum 2 ve 4'ün nihai taşıma kapasitelerine bölünerek kazık radye yük paylaşım oranları yüzde olarak tabloda verilmiştir.

İkinci temel tipi kullanılarak yapılan model deneylerinin sonuçları Şekil 12'de verilmiştir. Bu deneylerde radye plağının boyutları 200X160X20 mm, kazık boyu 210 mm ve kazık çapı 20 mm dir. Burada Lp kazık uzunluğu, birinci temel ile neredeyse aynı kalırken kazık çapı 7.5 mm'den 20 mm'ye çıkmış, 2.66 kat büyümüştür. Şekil 12 incelendiğinde; orta sıkı ve çok sıkı zemin koşullarında kazık aralıklarının, temel sistemi nihai taşıma kapasitesi ve oturma rijitliği üzerinde birinci temelle benzer ve belirleyici etkileri olduğu görülmektedir. Ancak Lp/D oranının 10,5 olması nedeniyle eşdeğer radye bölgesinde [31, 37] zemin-kazık etkileşiminde farklılıklar bulunmaktadır. Şekil 12a'da orta sıkı kumda Durum 2 için elde edilen sonuçlar, referans değer olan 1. Durum (E 15) ile kıyaslandığında maksimum düşey

yük taşıma kapasitesine 4,5D kazık aralığına sahip E18 nolu kazıklı temel sisteminde ulaşıldığı görülmektedir. Kazık çapının 7,5 mm olduğu birinci temel tipinin kullanıldığı E3 deneyinde 25 mm düşey deplasman değerinde 4.5 kN nihai taşıma kapasitesine ulaşılırken, 20 mm kazık çapının kullanıldığı E18 deneyinde 15 mm düşey deplasman değerinde 8,65 kN taşıma kapasitesi değerine ulaşılmıştır. Bu değer E15 nolu referans deney için elde edilen düşey yük kapasite değerinin (3,08 kN) 2,80 katıdır. Bu nedenle E18 nolu model için nihai yük taşıma kapasitesi dikkate alındığında yükün %67.30 oranında kazıklarca karşılandığı hesaplanmıştır. 3D aralığındaki E17 deneyinde 5,5 kN nihai yük değeri elde edilmiş, bu durum için kazıklar %44 oranında yükü üstlenmiştir. Bu deney için en düşük kapasite değerine ulaşan 1.5D aralığında E17 nolu deneyde 7,5mm kazık çapındaki temsil model olan E2 deneyi kadar sistem mobilize olmamış, 4,8 kN'da nihai taşıma kapasitine ulaşmıştır. Bu deneyde %35.83 oranında kazıklarca yük paylaşımı sağlanmıştır. Diğer yandan aslında kazıklı radye temel sistemlerinde Tomlinson [38] tarafından ifade edildiği gibi geleneksel yöntemde temellerin yük almadığı varsayılarak tasarım yapıldığında güvenli tarafta kalınmakta ancak sahadaki gerçek olan durum bu olmamaktadır.

İkinci temel boyutu nihai oturma değeri referans alınarak grafikler incelendiğinde (5mm oturma için 3,1 kN kapasite değeri) E16 deneyinde aynı oturma miktarı için aynı yük taşıma kapasitesine, E17 deneyi 3,7 kN'da , E18 deneyi 4,8 kN'da ulaşmıştır. E16 ve E17 nolu deneyler 10mm düşey yer değiştirmede göçme durumuna geçerken optimum sonuç olan E18 nolu deney aynı yer değiştirmede en yakın sonuca göre 1,5 kat fazla düşey yük alabilme kapasitesi göstermiştir. Bu sonuçlar optimum kazık aralığındaki aralığında, sistemin yükleme başından itibaren oturma rijitliği sergilediğini, diğer kazıkların oturma artışı ile referans deney sınırını aştıklarını göstermektedir.

Şekil 12b'de ikinci temel, 2. Durum, %85 rölatif sıkılık değeri için yapılan model test sonuçları sunulmuştur. Şekil incelendiğinde birinci temel tipinde olduğu gibi tüm deneylerde zemin sıkılığındaki artışa paralel olarak taşıma kapasitelerinde artış görülmektedir. Bu sıkılık durumu için 1,5D, 3D ve 4,5D aralığındaki tüm deneylerde, referans deneyin nihai durumu için elde edilen oturma miktarı -4 mm. civarı dikkate alındığında; düşey yük kapasite kazanımı 2,5 katı mertebesindedir. Bu kazanım için kazık yük paylaşım oranları tüm deneylerde %58 olarak hesaplanmıştır. Bu temel sisteminde birinci temele göre, farklı kazık aralıklarına sahip tüm deney düzenekleri nihai sınırlarına kadar aynı rijitlikte yük oturma davranışına devam etmiştir. Modeller sadece nihai kapasite olarak birbirinden ayrışmıştır. Bu kapsamda 4,5D aralığındaki E25 deneyinde 38.9 kN, 3D aralıktaki E24 deneyinde 34 kN, 1,5D aralıktaki E23 deneyinde 28 kN nihai taşıma kapasitesine ulaşılmıştır. Nihai durumdaki kazık-radye yük paylaşımı dikkate alındığında E25 deneyinde %78.45, E24 deneyinde %75 ve E23 deneyinde %70 oranında yük kazıklar tarafından karşılanmıştır. Benzer biçimde El Samee [18] 2. Durum yüklemesi olan kazık başlığı ve radye temelin sisteme dahil olması durumunda sistemin optimum kazık aralığının büyüyeceği ve yük oturma davranışının belli bir sınırda göçmeye maruz kalacağını belirtmiştir.

Kazıkların kazık temel sistemine sıkı zeminlerde kazandırdığı en önemli özellik optimum aralığın oturma değerini diğer aralıklara göre daha üst sınıra çekebilmesidir. Çok sıkı zeminde birinci temel deneylerinde E9,E10,E11'de olduğu gibi neredeyse tüm kazık aralıklarında yük oturma davranışı benzer trend izlemiş ancak nihai dayanıma yakın bölgelerde kazık aralığındaki artış yük taşıma kapasitene olumlu katkı sağlamıştır [16, 18, 34].

Çalışmada Durum 3 olarak tanımlanan ve sadece kazıkların sürtünme direncinin sistem davranışına olan etkisinin ayrıştırılması amacıyla ikinci temel tipi ve 20 mm çapında kazıklar için oluşturulan model testlere ait sonuçlar Şekil 11c ve d'de gösterilmiştir. Şekil 12 c'de %50 rölatif sıkılık, şekil 12 d'de ise %85 rölatif sıkılık değeri için sonuçlar sunulmuştur. Sonuçlar incelendiğinde hem orta sıkı kum hemde çok sıkı kumda kazık taşıma kapasitelerinin birinci temel tipinde olduğu gibi referans deneyin çok altında kaldığı görülmektedir. Bu temel tipinde orta sıkı zeminde yapılan deneylerde çalışmada kullanılan kazık aralığının deplasman rijitliği üzerine bir fark ortaya koymadığı görülmektedir.

İlk yükleme direnci olan 0,5 kN aşıldıktan sonra tüm kazıklarda mobilizasyon gerçekleşmiştir. Çok sıkı zemin durumunda tüm kazık aralıkları için ilk yükleme direnci 1,5 kN olarak sağlanmıştır. Bunu takip eden yüklemede, tüm kazık durumları mobilize olmuştur. Deneylerde etkili sürtünme direnci 23mm mertebesinde devreye girmiştir. Temel tabanının, 25mm yerdeğiştirme sonucunda zeminle teması sağlanmış buna bağlı yükleme direncindeki artış sonuçlara yansımıştır. Durum 3 çok sıkı durum için yapılan model testlerde 4,5D ve 3D dizlimdeki E28 ve E27 nolu modeller aynı ötelenme rijitliği sergilerken, 1,5D lik aralığındaki E26 nolu model 5mm düşey yerdeğiştirmeden itibaren diğer modellerden rijitlik kazanımı yönünde ayrışmıştır.

Durum 4 yükleme koşullarındaki deneyler şekil 12 e ve f'de sunulmuştur. Orta sıkı durum için yapılan test sonuçları incelendiğinde; birinci temel tipinde olduğu gibi bu deneylerde de en küçük kazık aralığına sahip 1,5D dizilmi E35 nolu deneyde, referans deneyle aynı oturma rijitliği referans deney nihai kapasitesine kadar sergilemiştir. Bunu takip eden yüklemelerde oturma ile birlikte artan zemin etkileşimi bu aralıkta yük-oturma rijitliğinde artış yönünde katkı sağlamıştır. E35 nolu deney 15mm düşey yerdeğiştirme için 12.74 kN kapasite değerine ulaşmıştır. Kazıklar, bu değer için %75.82 oranında yük paylaşımında rol üstlenmiştir. 3D ve 4,5D aralığındaki E36 ve E37 nolu deneyler 1,5 kN ötelenme rijtliğini takiben, mobilize olmuş, referans deney ve E35 nolu model testten ayrışmıştır. E36 nolu test 7,5mm oturmada, E35 nolu test oturma rijitliğine yaklaşırken, E37 nolu deney rijitlik kazanımı 20mm yer değiştime için sağlanmıştır. Çok sıkı durum için elde edilen sonuçlar incelendiğinde referans deney nihai taşıma kapasitesi orta sıkı duruma göre 2 kat artış sağlamıştır. Sıkı durumda 1,5D ve 3D aralığındaki modeller referans deney ile aynı rijitlik ile yüklemeye tepki vermiş, oturma arttıkça kazık yük paylaşımı pozitif yönde sisteme katkı sağlamıştır. Bu sebeple referans değer nihai taşıma kapasitesinin ölçüldüğü 7,5mm oturma değerinde 1,5D ve 3D aralığındaki modeller 1,6 kat düşey yük kapasite kazanımı sergilemişlerdir. 1,5D aralığındaki E38 nolu deney 20mm oturma değerinde 14 kN nihai taşıma kapasitesine, 3D aralığındaki E39 nolu deney18mm oturma için 17,5 kN taşıma kapasitesine kadar yük almıştır. 4,5D dizlimdeki E40 nolu model 3,5 kN ilk ötelenme rijitliğine kadar referans deneyi sağlarken, bu değere müteakip mobilize olmuştur. 15mm oturma miktarına kadar diğer modellerin altında kalmasına rağmen, en büyük nihai düşey yük değeri olan 21 kN'a ulaşmıştır.

İki farklı temel boyutu, iki farklı kazık boyutundaki model test düzeneklerinin orta sıkı ve çok sıkı zemin durumlarında, dört farklı başlangıç durumu için yapılan yük-oturma analizlerinin yapıldığı bu çalışmada; Şekil 13'de tüm durumların maksimum kapasite değerlerinin elde edildiği test sonuçları karşılaştırmalı olarak sunulmuştur. Şekil 13 a ve b'de birinci temel sisteminde orta sıkı ve sıkı duruma ait sonuçlar, Şekil 13 c ve d'de ikinci temel sisteminde orta sıkı ve çok sıkı duruma ait sonuçlar sunulmuştur.

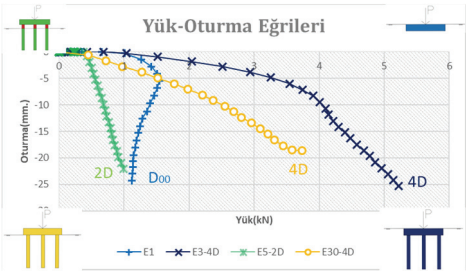

a. % 50 Rölatif Sıkılık 1. Temel

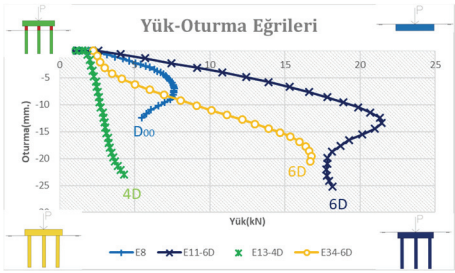

b.% 85 Rölatif Sıkılık 1. Temel

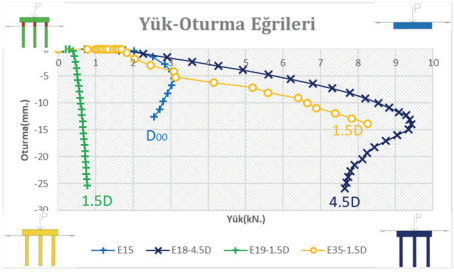

c.% 50 Rölatif Sıkılık 2. Temel

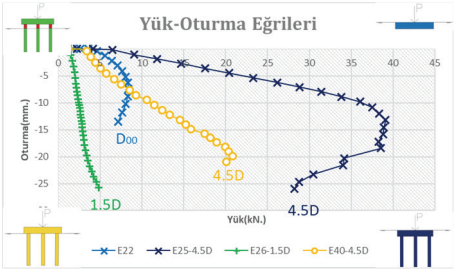

d. % 85 Rölatif Sıkılık 2. Temel

Şekil 13 - Dört Durumun Karşılaştırması

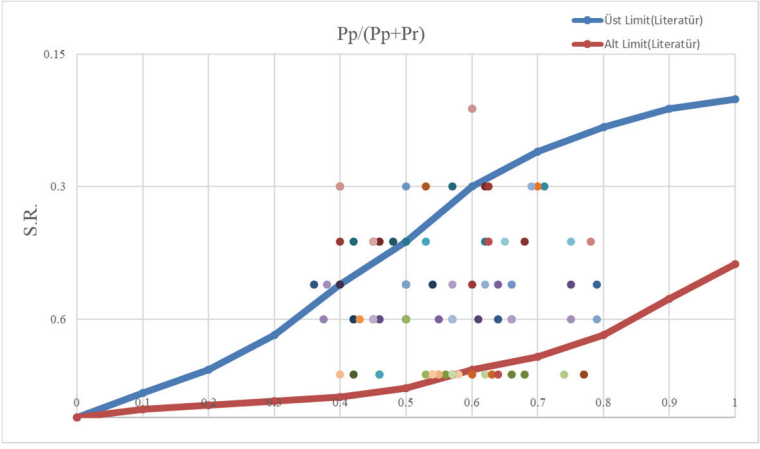

Şekil 14 - 25mm. Sınır Değer için Oturma-Sistemdeki Kazık Yük Taşıma Oranı

Maksimum kapasite değerlerinin karşılaştırıldığı bu grafiklerde; sadece radye sisteminin olduğu referans durumlar karşılaştırma düzlemi seçildiğinde; Durum 2 ve Durum 4'te kazık kapasitesinin artan oturma ile birlikte taşıma kapasitesine olan pozitif katkısı açıkça görülmektedir. Birinci temel sisteminde Durum 2 ve Durum 4 için orta sıkı zemin durumunda

4D kazık aralıkları en yüksek nihai yük değerini verirken, sıkı zeminde 6D kazık aralığı en yüksek nihai yük sonucunu vermiştir. İkinci temel sisteminde aynı durum orta sıkı zeminde 1,5D aralığı için, çok sıkı zeminde 4,5D aralık için optimum sonucu vermiştir. Bu durum orta sıkı zeminde; düşük kazık aralığının etkili olduğunu, sıkı zeminde ise daha geniş kazık aralığının etkili olduğu göstermektedir. Kazıklı radye temel durumunda gevşek ve sıkı zemin için yapılan testlerde, ilk oturma rijitliğince daha iyi olan, hatta referans deneyin üzerinde kalan, yani deney başından itibaren kazık yük paylaşımının etkili olduğu test sonuçları genellikle plağın zemine gömülü olduğu Durum 2 için elde edilmiştir. Ancak Durum 4 için nihai yük taşıma değeri söz konusu olduğunda, sistem ilk başlarda oturma yaparak mobilize olsa da, artan oturma ile birlikte daha büyük taşıma kapasitelerinin elde edilmektedir. Ayrıca plağın gömülü olduğu Durum 2'ye nihai yük olarak orta sıkı durumda yaklaşılmaktadır.

$$S.R. = \frac{Düşey Deplasman Değeri}{25mm.} \tag{2}$$

Şekil 14'te S.R. oturma oranını, $\frac{Pp}{(Pp + \Pr)}$, kazıklı radye temel sistemlerinde kazıkların yük taşıma yüzdesini temsil etmekte ve literatürde yer alan[15] 25 mm sınırına göre bu grafik oluşturulmuştur. Oturma oranı, kazıkların yük taşıma yüzdesi grafiği, literatürde yer alan saha çalışmalarına [15, 39, 40, 41] göre karşılaştırma grafiği olarak Şekil 14'te sunulmuş bu saha çalışmaları grafiklerde üst limit ve alt limit olarak yer almaktadır. Buna göre saha çalışmalarının neredeyse tamamı yük oturma grafiğinin değersel olarak güvenli kalan bölgelerinden alınan rakamlarla dizayn edilmiş, diğer bir ifadeyle yük oturma grafiğinin göçme veya mobilizasyon başlangıcı bölgelerinden uzak kalan, kazıklı radye temelin güvenli bir biçimde oturma aldığı bölgelerde dizayn ve uygulaması gerçekleşmiştir. Kazıklı radye temellerin oturma oranı-kazık yük taşıma oranı grafiği kazıklı radye temellerin ön tasarım aşamasında kullanılabilir[33, 35]. Sharafkakh ve Shooshpasha [7]'e göre kazıklı radye temelin nihai ve izin verilebilir yani nihai yükten güvenlik sayısıyla üç kat azaltılmış yükle yapılan dizaynlarda kazıklı radye temellerin kazık veya radyesinden yeterince verim alınamamakta buna göre ekonomik dizayn olmamaktadır. Diğer bir deyişle kazıklı radye temellerde kazık ve radye üstyapı yüküne beraber karşı koymakta ve bu durum oturma değerine bağlı olarak, zemin,kazık,temel geometrisi ve özelliklerine bağlı olarak değişmekte buna göre ekonomik tasarımlar yapılmalıdır. Diğer yandan literatürde, Ateş ve Şadoğlu [12] iyi derecelenmiş ve dane çapı dağılımı 1-5 mm arasında değişen kum ile beton kazıklar ile bu çalışmaya benzer kazık çapı,uzunluğu ve radye temel ölçülerinde deneyler yapmıştır. Bu çalışmada ise 0.5-1.0 mm aralığında kötü derecelenmiş kum zemin ile çelik kazık ve radye ile çalışılmıştır. Ateş ve Şadoğlunun'da [12] değindiği üzere literatürde optimum kazık aralığı çok geniş bir aralıkta olup 2D ile 12D arasında değişmektedir. Bu çalışmada ise Optimum kazık aralığı orta sıkı zeminde 1.5D ile 4D arasında çıkmış, çok sıkı zeminlerde ise 4.5D ve 6D arasında çıkmıştır. Diğer yandan orta sıkı zeminde kazıklı radye temel, radye temele göre optimum kazık aralığında % 233-300 arasında yük taşımada artışa çok sıkı zeminde ise optimum kazık aralığında kazıklı radye temel radye temele göre yük taşıma kapasitesinde % 275-400 artışa sebep olmuştur. Diğer bir deyişle kazıklı radye sistemlerinde radye temel derinliği olmasa dahi radyenin taşıyabileceği yüzde bu çalışmada yer alan tüm sistemler için nihai yükleme sınırlarında %21.54 ile %60 arasında kalmaktadır. Benzer biçimde El-Wakil ve Azzam [1] yapmış olduğu çalışmada kazıklı temellerde radyelerin

sisteme katkısını genel olarak % 30 civarında bulmuş ve % 55'in üzerine çıkamayacağını belirtmiş ancak çalışmada temel kalınlığına dair bir parametre bulunmadığı için bu yüzdeleri sonuç olarak vermiştir. Bulgular ve tartışma kısmında bahsedildiği üzere radye kalınlığı parametresi bu sonuçları etkileyebilmekte ve kazıklı radye temel sistemlerinde temelinde taşıma gücüne katkısı aşikardır.

4. **SONUÇLAR VE ÖNERİLER**

Bu çalışmada kazıklı radye temellerin yük oturma davranışları, nihai taşıma kapasitesi ve her bir temel elemanının (kazık,radye ve radye gömülü derinliğinin) zemin ile etkileşimi araştırılmıştır. Toplam 40 adet model test deneyi yapılmıştır. Model testlerde % 50 ve % 85 sıkılıkta kumda sadece radye temel, sadece kazık temel, kazıklı radye temel sistemleri için deneysel analizler yapılmıştır. Çalışmada kazıklı radye temel sistemi, plağın zemine gömülü olduğu ve plak tabanının zemine temaslı olduğu iki farklı başlangıç durumu için incelenmiştir. Yük-oturma davranışı, kazık radye yük paylaşım oranı, optimum kazık aralığı, rölatif sıkılığın etkisi irdelenmiştir. Buna göre yapılan deneysel çalışmalarla elde edilen sonuçlar aşağıda yer almaktadır.

Optimum kazık aralığı 2. Durum deneylerinde 1. Temel boyutları için çok sıkı zeminde 6D, orta sıkı zeminde 4D olarak 2. Temel boyutları içinse orta sıkı zeminde 1.5D çok sıkı zeminde 4.5D olarak bulunmuştur. Radyenin zemine gömülü olmadığı 4. Durum içinde analizlerde optimum kazık aralığının sıkılık azaldıkça azaldığı analizlerde görülmüştür. Diğer bir deyişle zemin sıkılaştıkça optimum kazık aralığı artmakta ancak yük oturma davranışı daha geniş bir sahanlıkta seyretmektedir.

1.5D'den başlayarak 6D'ye kadar artan kazık aralıklarında, kazıklı radye temellerin yük oturma davranışı başlangıçta benzer gitsede özellikle sıkı zeminlerde daha geniş aralıklarda davranış daha fazla nihai yük taşıma kapasitesiyle sonuçlanmıştır. Burada oturma değerlerine göre optimum kazık aralığı bulunmalı veya sistemin en performanslı çalıştığı oturma değerleri baz alınarak tasarım yapılmalıdır. Diğer bir deyişle güvenlik faktörü katsayısına bölünerek ve oturma değerlerinden bağımsız olarak tasarıma giden geleneksel yöntemler, ekonomi açısından ve sahadaki kazıklı radye temellerin davranışından uzak kalabilmektedir.

Bu çalışmada yer alan tüm model testler için, kazıklı radye sistemlerinde, radyenin yük paylaşım oranı, nihai yükleme sınırlarında %21.54 ile %60 arasında kalmaktadır. Kazıklı radye temeller nihai yük taşıma kapasitesinde sadece radye temellere göre orta sıkı kum zeminlerde % 233-300 arasında, çok sıkı kum zeminlerde ise % 275-400 arasında artışa sebep olmaktadır. Kazıklı radye temeller, radye temellerle kıyaslandığında nihai taşıma kapasitesinde artış sağlarken, oturma sınırlarını da daha yüksek yük seviyelerinde ulaşmıştır. Çok sıkı zeminlerde radye plağının zemine gömülü olmadığı durumda, plağın gömülü olduğu duruma göre daha yüksek oturma değerlerinde daha düşük taşıma kapasiteleri gözlenmiştir.

Optimum kazık aralığı kavramı literatürde 1.5D ile 12D arasında yer almaktadır. Bu kavramın çakma kazık, yerinde dökme kazık, betonarme kazık, beton kazık, çelik kazık, ahşap kazık v.b. ve zeminin tipine göre kadar bu yapı malzemeleriyle etkileşimi değerlendirilebilir. Çünkü kazıklı radye temel uygulanan zemin artık sade zemin davranışı olmaktan çıkmakta kazıklar ve temelle birlikte kompozit malzemeye dönüşmekte ve kazıklı

radye temelin altında kalan bölge(eşdeğer radye bölgesi), zemin ile yapının beraber çalıştığı davranıştan oluşagelmektedir.

Model test sonuçları incelendiğinde, literatürde yer alan [1, 12] optimum kazık aralığı yaklaşımının sabit olmadığı, aslında yük başlangıcında ve sistemin taşıyabileceği nihai yük değerine yakın olduğu durumda değiştiğini göstermektedir. Kazıklı radye temel sistemlerinde mobilizasyonun toplam düşey oturmaya yansıyan optimum bir seviyesi bulunmakta ve bu seviyede sistem ekonomik ve yüksek perofromanslı çalışmaktadır. Burada oturma değerlerine göre optimum kazık aralığı bulunmalı veya sistemin en performanslı çalıştığı oturma değerleri baz alınarak tasarım yapılmalıdır. Diğer bir deyişle güvenlik faktörü katsayısına bölünerek ve oturma değerlerinden bağımsız olarak tasarıma giden geleneksel yöntemler, ekonomik ve sahadaki kazıklı radye temellerin davranışından uzak kalabilmektedir

Sonuç olarak, orta sıkı zeminlerde düşük kazık aralığında, kazık-zemin etkileşimi arttıkça, oturma rijitliğinde pozitif yönde kazanım sağlanmaktadır. Ancak sıkı zeminlerde ise kısa kazık aralığı durumu zaten yeter sıkılıkta olan zemin tanelerinin, kazık yerdeğiştirmesi ile birlikte göçme sınırına getirmesi süreci kapasite ve davranışta belirleyicidir. Bu durumun kazık taşıma gücü problemlerinde önemli etkisi olduğu bilinen genleşme davranışı ile ilişkili olduğu düşünülebilir. Sıkı zeminlerde düşük kazık aralığındaki sistemler, oturma artıkça, ilk başlarda daha büyük kapasite değerlerine ulaşmakta ancak bu durum zeminin daha önce göçmesine sebep olmaktadır. Geniş dizilimli kazık aralıklarında ise zemindeki sıkışma kaynaklı göçme durumu, daha büyük oturma değerlerinde gerçekleşmektedir. Bu durum başlarda daha düşük oturma rijitliğine sahip kazıkların daha büyük nihai kapasiteye ulşamasını sağlamakta, söz konusu bu dört durumun özellikle radye temelin dahil olup olmamasına göre oturma yaparak düşey yük alma kabiliyetine yansımaktadır. Bu sonuç; oturma sınırları daha üst değerlere ulaşmasına izin verilen tasarımlarda kapasite bazlı yaklaşım yerine oturma bazlı yaklaşım izlenerek nihai kapasite limitlerinin belirlenmesinde kullanılabilir. Kazık aralığının aynı zeminde sık olması veya daha aralıklı olması temelin altında kalan literatürde[30, 31] eşdeğer radye denilen bölgede, zeminle-yapı elemanlarının etkileşimi burada kompozit bir davranış durumu oluşturmaktadır. Bu nedenle kazıklı radye temellerin daha güvenli ve ekonomik tasarımı için araştırmaların eşdeğer radye bölgesindeki sistem davranışı üzerine odaklanması literatür ve mühendislik uygulamaları açısından faydalı olacak ve bu çalışmada davranış bu nedenle sadece radye, kazıklı radye ve sadece kazık gibi yapı elemanlarına parçalanarak model test deneyleri ve bunların birbirleri ile olan mukayesesi açıklanmıştır.

Semboller

ϕ	İçsel Sürtünme Açısı
γ_{kmaks}	Maksimum Birim Hacim Ağırlık
γ_{kmin}	Minimum Birim Hacim Ağırlık
V	Poisson Oran
B	Temel Genişliği
C	Kohezyon

C_c	Derecelenme Katsayısı
C_u	Üniformluk Katsayısı
D	Kazık Çapı
dk	Dakika
D_{10}	%10'a Karşılık Gelen Çap
D_{30}	%30'a Karşılık Gelen Çap
D_{50}	%50'a Karşılık Gelen Çap
D_{60}	%60'a Karşılık Gelen Çap
E	Elastisite Modülü
E_{min}	Minimum Boşluk Oranı
E_{maks}	Maksimum Boşluk Oranı
G	Kayma Modülü
H	Eşdeğer Radye Bölgesinin Yüzeyden İtibaren Düşey Yönde Etki Ettiği Son Derinlik
kN	Kilonewton
L	Temel Genişliği
Lp	Kazık Uzunluğu
P	Düşey Yük
Pp	Kazıkların Taşıdığı Yük
Pr	Radyenin Taşıdığı Yük
S	Kazıklar Arası Mesafe
S/D	Kazık Aralığı
SP	Kötü Derecelenmiş Kum
S.R.	Oturma Yüzdesi

Teşekkür

Bu çalışma S.D.Ü Bap birimi tarafından Yök 100/2000 öncelikli alanlar kapsamında FDK-7456 numaralı proje olarak desteklenmiştir. Yök 100/2000 ve S.D.Ü bap biriminin değerli çalışanlarına katkılarından dolayı teşekkür ederiz.

Kaynaklar

[1] Elwakil, A., Azzam, W., Experimental And Numerical Study Of Piled Raft System. Alexandria Engineering Journal. 55. 10.1016/j.aej.2015.10.001, 2015.

[2] Hadi, Dheyaa & Fattah, Mohammed & Waheed, Mohanned. Effect of Pile's Number on the Behavior of Piled Raft Foundation. 39. 1080-1091. 10.30684/etj.v39i7.1795 2021.

[3] Hamderi, M., Kazıklı Radye Temellerin Oturma Tahmini İçin Yeni Bir Yöntem, Dicle Üniversitesi Mühendislik Fakültesi Mühendislik Dergisi, c. 9, sayı. 2, ss. 881-893, 2018.

[4] Hamderi, M., New Approach to Group Pile Load Estimation. International Journal of Geomechanics. 04019013-1. 10.1061/(ASCE)GM.1943-5622.0001374, 2019.

[5] Krisnanto, S., Sengara, I., Adelina, F., Advancement of Bearing Capacity and Settlement Analyses of Piled Raft Foundation, Proceeding SEAGC 3rd AGSSEA Conference in conjuction with 22nd Annual Indonesian National Conference on Geotechnical Engineering. Indonesia, 81-84,2018.

[6] Kuwabara, F., An Elastic Analysis for Piled Raft Foundations in Homogeneous Soils, Soils and Foundations, Vol. 29, No:1, pp. 82-92, 1989.

[7] Sharafkhah, M., Shooshpasha, I., Physical Modeling Of Behaviors Of Cast-In-Place Concrete Piled Raft Compared To Free-Standing Pile Group In Sand. Journal of Rock Mechanics Geotechnical Engineering, 10:703–16 2018, https://doi.org/10.1016/j.jrmge.2017.12.007.

[8] Ersoy, Ç. Ö., Yıldırım, S., Experimental Investigation of Piles Behavior Subjected to Lateral Soil Movement. Teknik Dergi 25, 2014.

[9] Al-Neami, M., & Rahil, F., A., K., Effect of Relative Density on Behavior of Single Pile and Piles Groups Embedded with Different Lengths in Sand. Engineering Technology. 34. 1206 2015 .

[10] Hama, S., Soran S., Nihad, N., D., Optimum design of steel piles in different sandy soil configurations. Geomechanics and Geoengineering. 17. 1-11. 10.1080/17486025.2020.1755461 2020.

[11] Babagiray, G., Akbaş, S. O., Sığ Rijit Tabaka Üzerinde Yer Alan Kohezyonsuz Zeminlerdeki Yüzeysel Temellerin Taşıma Gücü Hakkında Sayısal Modelleme Esaslı Parametrik Bir Çalışma. Teknik Dergi 29 8185-8198, 2018.

[12] Ateş, B., Şadoglu, Erol., Kum Zeminlerdeki Kazıklı Radye Temellerin Optimum Kazık Aralığının Deneysel Olarak İncelenmesi. Teknik Dergi, 10.18400/tekderg.644885, 2021.

[13] Raut, J., Khadeshwar, S., Bajad, S., Kadu, M., Simplified Design Method for Piled Raft Foundations. Geotechnical Special Publication. 462-471. 10.1061/9780784413425.047, 2014.

[14] Butterfield, R., and Banerjee, P. K., The Problem of Pile Group-Pile Cap Interaction, Géotechnique,Volume 21, No:2, pp. 135-142, 1971.

[15] El Garhy, B., Galil, A. A., Youssef A. F., Raia, M. A., Behaviour Of Raft On Settlement Reducing Piles Experimental Model Study. J Rock Mech Geotech Eng 389–99, 2013 .

[16] El Sawwaf, M., Experimental Study of Eccentrically Loaded Raft with Connected and Unconnected Short Piles. Journal of Geotechnical and Geoenvironmental Engineering 136. 10.1061/(ASCE)GT.1943-5606.0000341 2010.

[17] Dung N.T., Chung S.G., Kim S.R.,. Settlement of large-scale piled foundations using equivalent raft approach, ICE Proceedings Geotechnical Engineering, 163 2010.

[18] Abd Elsamee, W., Analysis Of Pile- Raft Foundations Non- Rested And Directly Rested On Soil. International Journal of Civil Engineering and Technology. 9. 418-439, 2018.

[19] Lee, S. H., and Chung, C. K., An Experimental Study Of The Interaction Of Vertically Loaded Pile Groups İn Sand, Canadian Geotechnical Journal, 42, 1485–93, 2005.

[20] Clancy, P., and Randolph, M., F., Simple Design Tools For Piled Raft Foundations, Geotechnique 46, No.2, 313-328. 1996.

[21] Yamashita, K., Tanikawa, T., Hamada, J., Applicability Of Simple Method To Piled Raft Analysis In Comparison With Field Measurements. Geotechnical Engineering Journal of the SEAGS & AGSSEA. 46. 43-53, 2015.

[22] A.S.T.M., Standard Test Methods for Particle-Size Distribution (Gradation) of Soils Using Sieve Analysis, D-6913, American Society for Testing and Materials,West Conshohocken, 34, 2017.

[23] A.S.T.M., Standard Test Methods for Specific Gravity of Soil Solids by Water Pycnometer, D-854, American Society for Testing and Materials, West Conshohocken, 8, 2006.

[24] ASTM D4253-16, Standard Test Methods for Maximum Index Density and Unit Weight of Soils Using a Vibratory Table, ASTM International, West Conshohocken, PA, www.astm.org, 2016.

[25] ASTM D3080 / D3080M-11, Standard Test Method for Direct Shear Test of Soils Under Consolidated Drained Conditions, ASTM International, West Conshohocken, PA, www.astm.org, 2011.

[26] Noonan, D. K. J., Nixon, J., F., The Determination of Young's Modulus from the Direct Shear Test. Canadian Geotechnical Journal, 9(4), 504–507. doi:10.1139/t72-049 1972.

[27] Çetin, K.,Ö., Geoteknik ve Sayısal Modelleme, İmo Meslek İçi Eğitim Kursu Raporu, 2018.

[28] Tabaroei, A., Abrishami, S., Seyedi H., Ehsan., Comparison between Two Different Pluviation Setups of Sand Specimens. Journal of Materials in Civil Engineering. 29. 10.1061/(ASCE)MT.1943-5533.0001985, 2017 .

[29] Hariprasad, C., Mekala, R., Umashankar, B., Preparation of Uniform Sand Specimens Using Stationary Pluviation and Vibratory Methods. Geotechnical and Geological Engineering. 34. 10.1007/s10706-016-0064-0, 2016.

[30] Poulos, H., Piled Raft Foundations Design And Applications. Geotechnique. 51. 95-113. 10.1680/geot..51.2.95 2001.

[31] Poulos, H., Randolph, M., Pile Group Analysis A Study of Two Methods. Journal of Geotechnical Engineering. 109. 10.1061/(ASCE)0733-9410109:3(355) 1983.

[32] Nguyen, D. D. C., Jo, S. B., and Kim, D. S., Design Method Of Piled-Raft Foundations Under Vertical Load Considering İnteraction Effects, Computers and Geotechnics, 47, 16-27, 2013.

[33] Bajad, S., P., and Sahu, R., B., An Experimental Study On The Behavior Of Vertically Loaded Piled Raft On Soft Clay, The 12th Intl. Conf. Of International Association for Computer Methods and Advances in Geomechanics (IACMAG), 84–90. 2008.

[34] Birand, A. A., Kazıklı Temeller Teknik Yayınevi Ankara, 2007.

[35] Nguyen, T., Chung, S., Kim, S., R., Settlement Of Piled Foundations Using Equivalent Raft Approach. ICE Proceedings Geotechnical Engineering, 163. 65-81. 10.1680/geng.2010.163.2.65, 2010.

[36] Reese, L. C., William, M. I., Shin, T. W., Analysis and Design of Shallow and Deep Foundations, John Wiley Sons, Inc 2006.

[37] Bowles, J.E., Foundation Analysis and Design. 5th Edition, McGraw-Hill, New York, 2001,

[38] Tomlinson, M., J., Pile Design and Construction Practice, Chapman and Hall, London, UK, 2004.

[39] Phung, L., Piled Raft A Cost-Effective Foundation Method For High-Rises. Geotechnical Engineering Journal of the SEAGS AGSSEA. 41. 1-12. 2010.

[40] Schmitt, A. J., Turek, R. K., Reducing The Costs For Deep Foundations Of High–Rise Buildings By Advanced Numerical Modeling, Arı The Bulletin of the Istanbul Technical University, 35 (2), pp. 81-87, 2003.

[41] El-Mossallamy Y., , Lutz, T. B., Richter Innovative Application Of Piled Raft Foundation To Optimize The Design Of High-Rise Buildings And Bridge Foundations In: Proc. 10th Intl. Conf. on Piling and Deep Foundations, Amsterdam 2006.

Turkish Journal of Civil Engineering, 2023 173-195, Paper 730, ***Research Article***

Strengthening System Effects on the Out-Of-Plane Mechanisms Activation of Masonry Walls under Tsunami Loads

Stefano BELLIAZZI[1]
Gian Piero LIGNOLA[2]
Andrea PROTA[3]

ABSTRACT

The vulnerability of masonry structures against tsunami loads is a highly debated topic in the research community due to the impact in the risk evaluation. The main aim of this paper is to examine the structural response of masonry walls against tsunami loads in terms of out-of-plane local mechanism activation. Furthermore, a critical discussion is proposed about the influence of strengthening system parameters on the out-of-plane response of the masonry wall. Results of parametric analyses are shown in dimensionless form to analyse the effects of main parameters, both for masonry walls and tsunami waves, on the structural response. The analyses results are the bases to design strengthening systems with fiber-reinforced composite materials in order to reduce the vulnerability of masonry structures under tsunami loads.

Keywords: Tsunami, masonry structures, strengthening systems.

1. INTRODUCTION

Tsunami risk assessment ([1], [2], [3]) has become an important research theme due to the high reconstruction costs and human casualties associated with the events of the last decades, such as the 2004 Great Indian Ocean Tsunami [4], the 2010 Chile Tsunami [5], and the 2011 Great East Japan Tsunami [6]. A tsunami is a complex phenomenon based on the wave propagation theory; it can be triggered by several different phenomena including earthquakes

Note:
- This paper was received on August 25, 2022 and accepted for publication by the Editorial Board on January 27, 2023.
- Discussions on this paper will be accepted by May 31, 2023.
- https://doi.org/10.18400/tjce.1247194

1 University of Naples "Federico II", Department of Structures, Napoli, Italy
stefano.belliazzi@unina.it - https://orcid.org/0000-0002-0471-3601

2 University of Naples "Federico II", Department of Structures, Napoli, Italy
glignola@unina.it - https://orcid.org/0000-0001-6027-9291

3 University of Naples "Federico II", Department of Structures, Napoli, Italy
andrea.prota@unina.it - https://orcid.org/0000-0003-3820-663X

or submarine landslides. To assess the tsunami risk of a specific area, a multi-hazard approach should be considered to capture complex scenarios.

A key component in tsunami risk assessment [7] is the vulnerability assessment of buildings under tsunami loads. International building codes, standards, and guidelines provide different approaches to design tsunami-resistant structures.

The ASCE 7-22 [8] proposes an advanced approach to analyse several effects of the tsunami wave impact on the structures; impact of debris, horizontal and vertical load components are modelled on the structure. Furthermore, several coefficients are defined to analyse the effects of the wave direction on the structures. The wave parameters (e.g. inundation depth, wave velocity, moment of flux) are evaluated by the Energy Grade Line analysis where the tsunami flux is modelled as a unidirectional flow.

However, simplified models are available, too, as the Japanese guideline proposal [9] where the tsunami effects on the structure are modelled by an equivalent hydrostatic load distribution. In this model, the expected inundation depth is amplified in order to indirectly analyse the hydrodynamic effects. The Japanese guidelines are based on previous research activities conducted by Asakura et al. [10] and Okada et al. [11].

Furthermore, tsunami wave effects on structures have been analysed by an experimental program with scaled specimens [12] in order to retrieve empirical equations.

The vulnerability of structures under tsunami loads is completely different from the seismic load due to the different type of loads. In fact, seismic forces arise from inertia effects that excite the entire structure, while tsunami loads are predominantly characterized by surface forces over the inundated elements. As a result, the behaviour of buildings under tsunami loading differs from the response to seismic actions. However, both types of loads will have a combined effect on the gravity and lateral force resisting systems for the components at or below the inundation level. In addition, the modelling of tsunami effects on buildings is characterized by a high degree of uncertainty due to wave parameters and topographic information required to quantify tsunami loads [11].

In literature, the available reports on behaviour of masonry structures after a tsunami event show a high vulnerability of masonry structures to tsunami loads; the main collapse mechanisms are related to geotechnical failure (e.g. liquefaction) or local mechanisms activation (e.g. out-of-plane local mechanisms) ([13], [14]).

Preliminary mechanical analyses and studies focalize the attention on the local-mechanisms activation for both in-plane (IP) and out-of-plane (OOP) mechanisms [15] due to the high stresses at the ground floor [16] in terms of bending moment and shear. The vulnerability of the masonry structures is highly influenced by the geometrical characteristics of the masonry wall in terms of wall length and wall thickness [17].

The vulnerability assessment is the main step to develop risk mitigation techniques like as strengthening of strategic structures ([18], [19]), early warning systems or evacuation buildings.

2. RESEARCH SIGNIFICANCE

The goal of this paper is to analyse the vulnerability of masonry walls under tsunami loads in terms of out-of-plane local mechanisms activation.

Belliazzi et al. [20] analysed the effects of the strengthening systems with composite material (e.g. Fiber Reinforced Polymer, FRP, or Fiber Reinforced Cementitious Matrix, FRCM) in tension on the vulnerability of masonry walls under tsunami loads and preliminary results were provided assuming a simplified model for the tsunami loads.

The aim of this work is to improve the basis of the previous analyses [20] assuming a more refined model for the tsunami loads. Equations in dimensionless form are proposed to provide results applicable to any masonry cross-section. However, it is worth noting that masonry suffering for premature disaggregation (e.g. stone masonry walls made of weak mortar, irregular small blocks, and non-connected wall leaves) is not able to develop local mechanisms [21], hence are out of the present investigation.

In addition, parametric analyses have been performed to analyse the effects of the main parameters and coefficients of the proposed equation.

The overall results of these analyses allow to increase confidence on the design of strengthening systems with fiber-reinforced composite materials in tension in order to reduce the vulnerability of masonry structures under tsunami loads.

3. TSUNAMI LOAD MODEL

In the current literature, several approaches are available to model tsunami inundation forces on buildings due to the high degree of uncertainties in the fluid mechanics modelling.

The ASCE 7-22 proposes an advanced model where hydrostatic and hydrodynamic effects are defined separately and several parameters are required to model the tsunami forces. The Japanese guidelines propose a conservative approach where the tsunami loads are modelled by one equivalent hydrostatic distribution and the expected inundation depth is amplified in order to consider the hydrodynamic effects.

Therefore, the ASCE 7-22 requires a high knowledge of the structure and of the wave characteristics. The Japanese guideline is easier to use than the ASCE 7-22, but the tsunami force on the structure is usually overestimated. It is clear that the Japanese approach is recommended if a low knowledge level is achievable, e.g. in large-scale analysis [22].

In this paper, Foster et al. [12] approach is assumed to describe the tsunami inundation forces on the structure. The method allows to consider hydrostatic and hydrodynamic loads depending on the inundation depth and the flow velocity. In particular, the flow velocity depends on the Froud number, Fr (a dimensionless value that describes different flow regimes). An empirically equation for hydrodynamic loads is provided, dependent upon the Froude number of the flow and blocking fraction (the ratio between the structure width and the flow width), based on experimental results [12]. In the experimental activity, the water waves were generated by a tsunami simulator and the structures have been realized by means of scaled specimens.

Therefore, the equation for the hydrostatic load (Eq. 1 - F_s represents the resultant of the hydrostatic load distribution) is related to a linear distribution while the equations for the hydrodynamic load (Eq. 2 and Eq. 3 - F_d represent the resultant of the hydrodynamic load distribution) are related to a uniform distribution depending on the flow regime.

$$F_s = 0.5 \cdot \rho_s \cdot g \cdot L \cdot h^2 \quad (1)$$

If $F_r < 1$ (subcritical regime):

$$F_d = 0.5 \cdot C_D \cdot \rho_s \cdot L \cdot u^2 \cdot h \quad (2)$$

If $F_r \geq 1$ (choked regime):

$$F_d = \lambda \cdot \rho_s \cdot L \cdot \sqrt[3]{g} \cdot \sqrt[3]{(u \cdot h)^4} \quad (3)$$

Where ρ_s is the flow density, g is the gravitational acceleration constant, h is the expected inundation depth, u is the flow velocity, L is the wall length exposed to the tsunami wave, C_D is the drag coefficient and λ is an empirical coefficient.

$$C_D = 1.9 \cdot (1 + 1.9 \cdot (b/w)/2)^2 \quad (4)$$

$$\lambda = 0.73 + 1.2 \cdot (b/w) + 1.1 \cdot (b/w)^2 \quad (5)$$

Where b is the width of the structure, w is the channel width and the ratio b/w is named blocking fraction [23]. The blocking fraction generates high instability in hydraulic calculation: higher blocking fractions increase the tendency of the flow regime to change from subcritical to choked [24].

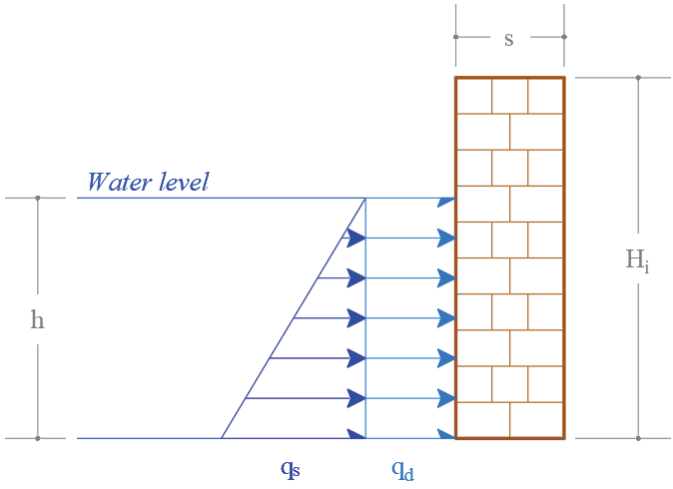

Figure 1 - Tsunami inundation forces model (s is the wall thickness, H_i is the interstorey height, q_s is the maximum hydrostatic load, q_d is the uniform hydrodynamic load)

The flow velocity u and the Froude number F_r are dependent on Eq. 6.

$$u = \frac{F_r}{\sqrt{g \cdot h}} \tag{6}$$

In addition, an opening ratio coefficient α is assumed (variable between 0.7 and 1) to consider the effects of the wall openings, according to ASCE 7-22 [8]. The wall opening coefficient is defined as one minus the ratio between the openings area and the gross wall area.

The structure is loaded by a trapezoidal load pattern equal to the sum of the hydrostatic and the hydrodynamic components (Figure 1).

4. MATERIAL CONSTITUTIVE MODEL

Several stress-strain relationships are proposed in international codes and guidelines to model the non-linear mechanical response of masonry and strengthening systems.

Different failure modes could be reached as masonry crushing or strengthening system failure in tension depending on material properties combination.

The compressive behaviour of masonry is modelled by rectangular stress-block model (Figure 2.a) according to Eurocode 6 [25]. The stress-block model is characterized by effective height ψ, effective depth of compression zone centre λ_m and the compressive strength f_m. ψ and λ_m are equal to 0.8 and 0.4, respectively, based on parabolic-rectangular stress strain relationship assuming the end of parabola at strain ε_{m0} equal to 2‰ and ultimate strain ε_{mu} equal to 3.5‰ according to Eurocode 6 [25]. These stress-block parameters are reasonable if the masonry crushing failure mode is reached.

The stress-block model is assumed as constitutive model in compression of masonry due to simplification in the calculation in order to retrieve equations in dimensionless form coherently with the goal of the paper.

Strengthening system behaviour in tension and failure modes are influenced by combination of matrix and fibers in terms of individual material properties and thicknesses. Main experimental programs show that the mechanical behaviour in tension is approximated by linear, bilinear or trilinear behaviour [26].

Furthermore, the fibers have a linear behaviour while the inorganic matrix influences the response at low strain values with its tension stiffening. In the following cross-section analysis, a linear tensile behaviour (Figure 2.b) is assumed in tension for composite strengthening systems with organic matrix (e.g. FRP) according to Italian guideline CNR-DT 200R1/2013 [27] or due to the assumptions that the inorganic matrix (e.g. FRCM) is cracked as shown in Italian guideline CNR-DT 215/2018 [28]. In particular, the linear behaviour is defined by ultimate tensile strength f_{fu}, an elastic modulus E_f and an ultimate strengthening system strain ε_{fu}, either due to fiber rupture or debonding failure ([26], [29]).

The compressive behaviour of composite strengthening systems is neglected according to Italian guidelines CNR-DT 200 R1/2013 [27] and CNR DT 215/2018 [28].

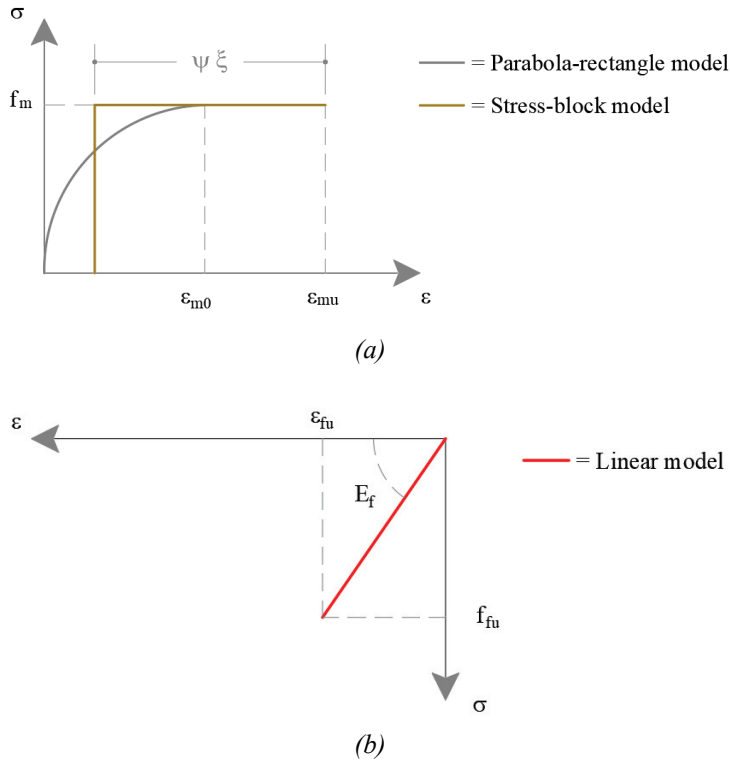

Figure 2 - Constitutive model of masonry in compression (a) and strengthening system in traction (b)

5. CROSS-SECTION ANALYSIS

Cross-section analysis is performed in order to analyse the activation of OOP local mechanisms and the effects of the strengthening system on the flexural capacity.

The cross-section analysis is performed at the ultimate limit state considering the following basic assumptions according to Italian CNR guidelines (CNR-DT 200R1/2013 [27] and CNR-DT 215/2018 [28]):

- Conservation of plain sections allow to assume linear strain diagrams, also known as the Bernoulli-Navier assumption;
- The shear deformability is neglected according to the Bernoulli assumption;
- Tensile behaviour of masonry is negligible;
- Strengthening system is effective only in traction and never in compression due to composite slenderness, as basic assumption;
- Perfect bond between strengthening system and masonry that allows to consider strengthening system strain ε_f equal to surrounding masonry strain ε_m (Eq. 7) without slip phenomena;

- The ultimate condition of the cross-section is related to compressed masonry crushing or tensile failure of the composite system depending on composite mechanical characteristics as shown in the following.

$$\varepsilon_m = \varepsilon_f \tag{7}$$

The proposed dimensionless equations are based on equilibrium equations [30] (Figure 3).

The axial forces are divided by the cross-section width, b_m, the cross-section height, s, and the compressive strength, f_m, while the bending moment is divided by $b_m\, s^2\, f_m$.

The dimensionless bending capacity equation $m_{R,0}$ (Eq. 9) of the unreinforced masonry structure (URM) cross-section is easily retrieved in the case of cross-section without strengthening system. It depends on the dimensionless external vertical axial load, n_0, (Eq. 8), the wall thickness, s, and the interstorey height, H_i; in particular, the ratio between the wall thickness s and the interstorey height H_i represents the geometrical vertical slenderness, H_i/s, of the masonry wall.

$$n_0 = 0.8 \cdot \xi \tag{8}$$

$$m_{R,0} = 0.5 \cdot n_0 \cdot \frac{s}{H_i} \cdot (1 - n_0) \tag{9}$$

Where ξ represents the dimensionless neutral axis depth; the neutral axis, x, is divided by the cross-section height, s.

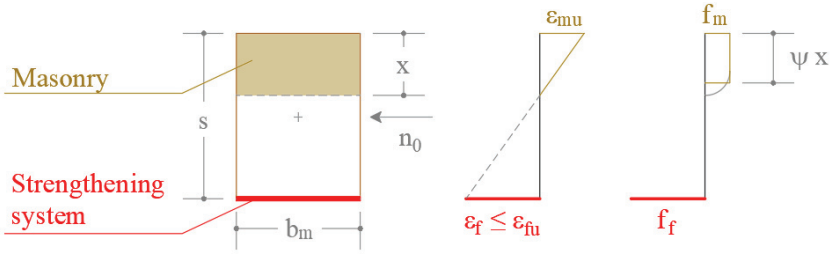

Figure 3 - Cross-section model

In the case of strengthening system applied to masonry cross-section, the dimensionless bending capacity equation $m_{R,\omega}$ (Eq. 11) is retrieved by a rotational equilibrium between the compressive masonry resultant and the tensile strengthening system resultant and it depends on the dimensionless external axial load, n_ω, (Eq. 10), the geometrical vertical slenderness, H_i/s, of the wall and the composite mechanical ratio, ω.

$$n_\omega = 0.8 \cdot \xi - \frac{1-\xi}{\xi} \cdot \omega \tag{10}$$

$$m_{R,\omega} = 0.4 \cdot \xi \cdot \frac{s}{H_i} \cdot (1 - 0.8\,\xi) + \frac{0.8 - n_\omega}{n_\omega} \cdot \frac{\omega}{2} \cdot \frac{s}{H_i} \quad (11)$$

It is worth noting that the external axial loads n_0 and n_ω depend on the wall self-weight and the effect of upper storeys.

The composite mechanical coefficient, ω, (Eq. 13) is function of different masonry and strengthening system properties according to the dimensionless approach; furthermore, a ratio between the elastic moduli of the two materials can be detected if it is assumed that the elastic modulus of masonry E_m depends on f_m (Eq. 12) [31] according to Eurocode 6 [25] definition.

$$E_m = 10^3 \cdot f_m \quad (12)$$

$$\omega = \frac{t_f}{s} \cdot \frac{\varepsilon_{mu}}{f_m} \cdot E_f = 10^3 \cdot \frac{t_f}{s} \cdot \frac{E_f}{E_m} \cdot \varepsilon_{mu} \quad (13)$$

Where t_f represents the fiber equivalent dry thickness.

The composite mechanical ratio ω allows to define the strengthening system with respect to wall composition in terms of both geometrical and mechanical properties.

6. OUT-OF-PLANE LOCAL MECHANISM

The local mechanism activation is a key aspect of the vulnerability of masonry structures. It depends on several factors as the material properties, the geometry of the wall, the boundary conditions and the connections between structural elements.

Several numerical methods have been employed to assess the OOP behaviour of URM structures. Finite element macro-modelling approaches are the most famous methods to analyse the OOP mechanisms activation even though the high degree of uncertainties may provide a non-realistic result in terms of crack pattern. Another criterion is to discretize the masonry wall in rigid blocks; D'Ayala and Speranza [32] proposed several configurations.

The main OOP local mechanisms are the vertical and the horizontal [27], [33] bending mechanisms (Figure 4), while shear mechanism are usually negligible with commonly slender walls (i.e. high H_i/s ratio). The horizontal bending mechanisms are activated when the external load exceeds the capacity of the cross-section in terms of axial load ([34]). The masonry wall thrust of the internal arch mechanism equilibrates the external load. In this paper, the horizontal bending mechanism [35] is not analysed because it requires a masonry wall without openings for the internal arch mechanism development. Vertical bending mechanism is typical in masonry walls with openings (common for structures in front of the seaside).

The strengthening configuration is based on main fibers applied along the vertical direction over the internal side of the walls (tensile side) with fibers anchored at least at the bottom of the structure. Typical composite mechanical ratio values, mechanical properties, materials, application schemes and few photographs are available in many references and a valuable outline is provided in both Italian CNR guidelines (CNR-DT 200R1/2013 [27] and CNR-DT 215/2018 [28]).

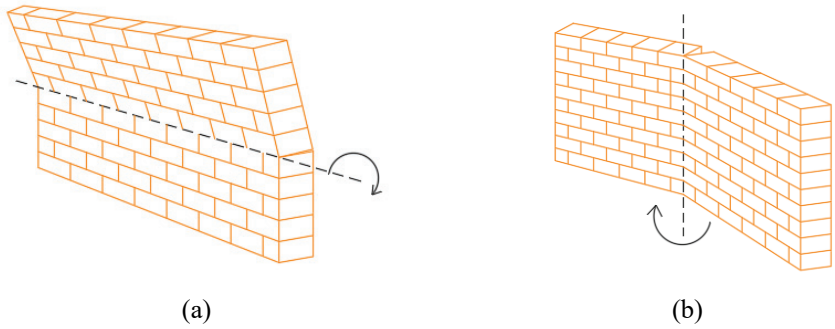

Figure 4 - Vertical (a) and horizontal (b) bending mechanisms

Therefore, the vertical bending [36] OOP mechanism activation is reached when the cross-section capacity is equal to the maximum external load in terms of bending moment.

Linear analyses are performed considering a simply supported beam with a trapezoidal load pattern changing the inundation depth and the Froude number; the Froude number changes in the range between 0.7 and 2.0 [37]. The simply supported beam length is equal to the interstorey height, H_i.

A concentrated external axial load, n, is considered on the top for modelling the wall self-weight and the effect of upper storeys. Therefore, a normalized external axial load on the cross-section is considered, variable in a range from zero up to about 35% of the ultimate axial load capacity of the masonry walls. As it will be seen later, this is an upper axial load threshold, beyond which, the effects of strengthening are negligible [30].

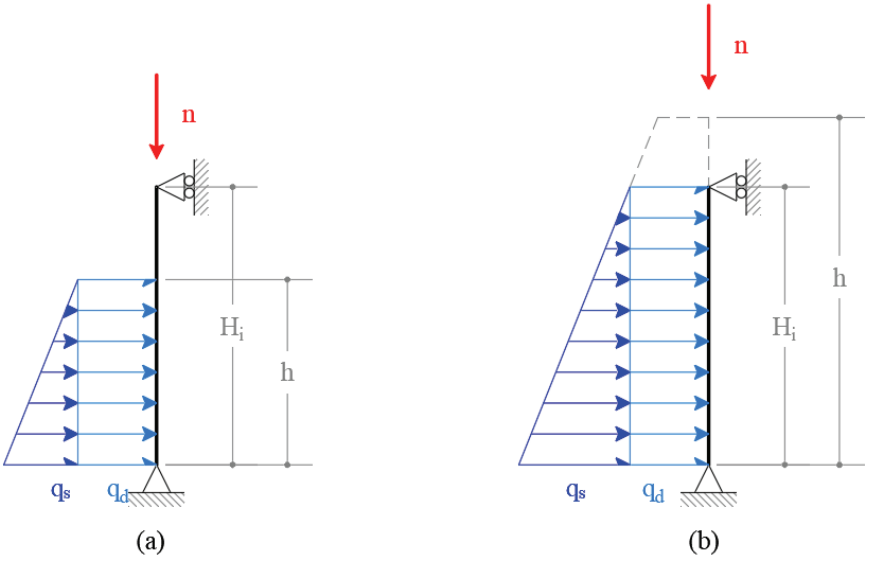

Figure 5 - Static model for $h < H_i$ (a) and $h \geq H_i$ (a)

The maximum bending moment function is simple to derive, considering the static model shown in Figures 5a and 5b.

The masonry wall is loaded with a hydrostatic load q_s and a hydrodynamic load q_d according to Foster et al. [12]:

$$q_s = \gamma_w \cdot L \cdot h \cdot \alpha \tag{14}$$

$$q_d = \beta \cdot \gamma_w \cdot L \cdot h \cdot \alpha \tag{15}$$

Where γ_w is the specific weight of the water, while β is a coefficient depending on the Froud number, if the flow regime is a subcritical regime or chocked regime:

$$\gamma_w = \rho_s \cdot g \tag{16}$$

$$\text{if } F_r < 1, \quad \beta = 0.5 \cdot C_d \cdot F_r^2 \tag{17}$$

$$\text{if } F_r \geq 1, \quad \beta = \lambda \cdot F_r^{4/3} \tag{18}$$

Therefore, equations in dimensionless form of the maximum bending moment are derived depending on the ratio between the inundation depth and the interstorey height.

If $h/H_i < 1$:

$$m_{s,1} = k_1 \cdot \left(\frac{h}{H_i}\right)^3 \cdot [-3 \cdot (\alpha + \beta) + k_2] \cdot \begin{bmatrix} 2 \cdot \frac{h}{H_i} \cdot \alpha \cdot (\alpha + 3\,\beta) + \\ + 3 \cdot (\beta^2 - 2\,\beta\,\alpha - \alpha^2) - (\alpha + \beta) \cdot k_2 \end{bmatrix} \tag{19}$$

If $h/H_i \geq 1$:

$$m_{s,2} = -k_1 \cdot k_3 \left\{-2 \cdot \alpha^2 + 6 \cdot \frac{h}{H_i} \cdot \alpha \cdot (\alpha + \beta) + (\alpha + \beta) \cdot \frac{h}{H_i} \cdot k_3\right\} \tag{20}$$

Where four numerical coefficients k_1, k_2, k_3 and k are defined to simplify the Eqs. 19 and 20:

$$k_1 = \frac{1}{54 \cdot \alpha^2} \cdot k \cdot \left(\frac{H_i}{s}\right)^2 \tag{21}$$

$$k_2 = \sqrt{9 \cdot \beta^2 + 3 \cdot \frac{h}{H_i} \cdot \alpha \cdot (\alpha + 3\,\beta)} \tag{22}$$

$$k_3 = \left[-3 \cdot \frac{h}{H_i} \cdot (\alpha + \beta) + \sqrt{3 \cdot \alpha^2 - 9 \cdot \frac{h}{H_i} \cdot \alpha \cdot (\alpha + \beta) + 9 \cdot \left(\frac{h}{H_i}\right)^2 \cdot (\alpha + \beta)^2}\right] \tag{23}$$

$$k = \frac{\gamma_w \cdot H_i}{f_m} \tag{24}$$

7. PARAMETRIC ANALYSES

Several parametric analyses have been performed to analyse the sensibility of the main parameters of the dimensionless equations.

The tsunami loads depend on the expected inundation depth h and Froude number Fr. Therefore, 3D charts are plotted using Mathworks Matlab where on the x-axis and y-axis are shown the inundation depth h/H_i (in dimensionless form) and the Froude number F_r while on the z-axis is shown the dimensionless bending moment, m_s.

The investigated main parameters are: the external axial load, n, the blocking fraction, b/w, the drag coefficient, C_D, the empirical coefficient, λ, the wall openings coefficient, α, the vertical geometrical slenderness of the wall, H_i/s, the composite mechanical percentage, ω, and the k numerical coefficient.

Each parameter changes in specific range as shown in Table 1 and Table 2. The blocking fraction is assumed equal to 0.1 and 0.6, as representative of different flow regimes [12], [23], [24]. The empirical parameter λ and the drag coefficient C_D are evaluated depending on the blocking fraction coefficient (Table 1). Masonry wall parameters in Table 2 are usual values for masonry buildings in front of the seaside (e.g. in Italy [22]).

The composite mechanical percentage ω is assumed equal to 0.00, 0.01, 0.02, 0.03, and 0.04 in order to consider the URM cross-section and the effects of the strengthening system on the cross-section capacity in terms of ultimate bending moment.

The external axial load n changes among 0.05, 0.15, 0.20, and 0.35.

Table 1 - Wave parameters evaluated depending on blocking fraction b/w

b/w	λ	C_D
0.1	0.86	2.28
0.6	1.85	4.68

Table 2 - Min, mean and max values of the vertical geometrical slenderness of the wall H_i/s, the wall openings coefficient α and the k numerical coefficient

Parameter	Min	Mean	max
H_i/s	2.50	9.58	16.67
α	0.70	0.85	1.00
k	0.003	0.029	0.055

In Figure 6, the effects of the blocking fraction b/w parameter are shown for n equal to 0.05 while the values assumed for the main parameters are shown Table 3. In addition, the representation of the effects of the blocking fraction b/w parameter and of the composite mechanical percentage ω in one figure allow to analyse the combined influence in terms of

external loads (depending on b/w) and cross-section capacity (plane horizontal surfaces depending on ω), respectively.

It is worth noting that at the Froud number value of one, a discontinuity on the maximum bending moment surface is shown due to the abrupt change of the flow regime.

In addition, it is possible to appreciate the effects of the strengthening system on the masonry wall changing the composite mechanical ratio ω. The bending moment capacity of the cross-section does not depend on the inundation depth and the Froude number; therefore, a horizontal plane represents the bending moment capacity.

The scale of the chart does not allow to appreciate the effects of the strengthening systems on the masonry cross-section due to the high values of the external bending moment while increasing the inundation depth (h/H_i); capacity is clearly lower than demand at $h/H_i>0.5$. The dimensionless inundation depth h/H_i allows to clearly define the shift between Eq. 19 or Eq. 20.

Table 3 - Values of the parameters assumed to describe the maximum bending moment surfaces in Figure 6

Parameter	Maximum bending moment - Surface 1	Maximum bending moment - Surface 2
b/w	0.1	0.6
C_D	2.28	4.68
λ	0.86	1.85
α	0.7	0.7
k	0.029	0.029
H_i/s	9.58	9.58

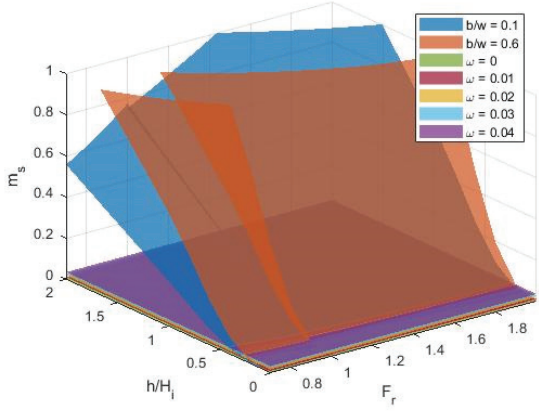

Figure 6 - Effects of the blocking fraction b/w parameter with n = 0.05

Therefore, in Figure 7, the effects of the blocking fraction b/w parameter are shown, for n equal to 0.05, 0.15, 0.20 and 0.35, with a reduced scale in order to understand the effects of the strengthening system and to analyse reasonable values of the external bending moment.

The 3D charts are shown for several external axial load values to investigate the strengthening system effects; in fact, the ultimate bending moment of the cross-section depends on the external axial load parameter while the external bending moment is not affected.

Increasing the external axial load, the effects of the strengthening systems are minimal due to the increase of the neutral axis depth and consequentially, due to the lower strain of the composite. Low composite mechanical values provide yet huge percentage effects in terms of bending moment capacity due to tensile behaviour added to URM cross-section.

For values of the external axial load n higher than 0.05, the composite mechanical ratio ω is limited only to 0.02 and 0.04 because the plan surfaces are almost overlapped.

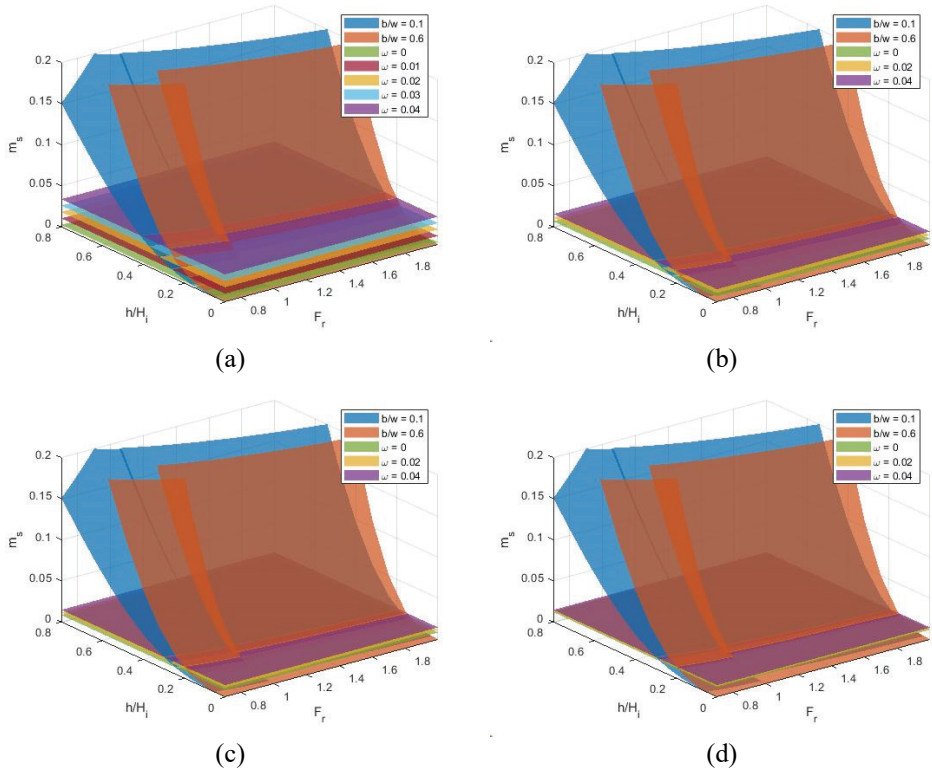

Figure 7 - Effects of the blocking fraction b/w parameter for n equal to 0.05 (a), 0.15 (b), 0.20 (c) and 0.35 (d)

The strengthening system effects become negligible for external load n value higher than 0.35. A masonry wall with higher external axial loads requires other types of strengthening

strategy as the composite reinforced mortar (CRM) ([38], [39]) in order to carry high compression loads, too.

The blocking fraction b/w has high effects on the structural response and it is strictly related to the flow regime. In particular, the vulnerability of the masonry wall increases with the b/w coefficient.

In Figure 8, the effects of the wall openings α parameter are investigated and the values assumed for the main parameters are shown in Table 4.

Table 4 - Values of the parameters assumed to describe the maximum bending moment surfaces in Figure 8

Parameter	Maximum bending moment - Surface 1	Maximum bending moment - Surface 2
b/w	0.1	0.1
C_D	2.28	2.28
λ	0.86	0.86
α	0.7	1
k	0.029	0.029
H_i/s	9.58	9.58

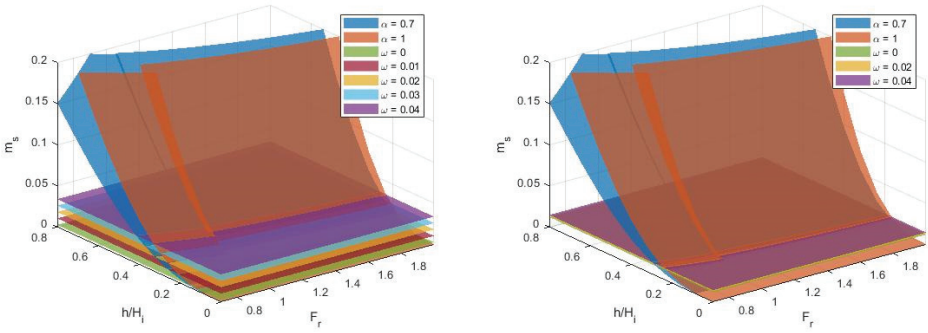

(a) (b)

Figure 8 - Effects of the wall openings α parameter for n equal to 0.05 (a), 0.35 (b)

As expected, the wall openings have a high influence on the vulnerability of masonry wall for several reasons. In fact, the openings reduce the load bearing area of the wall and consequentially, the tsunami forces, hence the influence is in terms of external loads.

In Figure 9, the effects of the geometrical vertical slenderness H_i/s parameter are investigated and the values assumed for the main parameters are shown in Table 5. The strengthening

system effects (different capacity horizontal planes) in terms of composite mechanical ratio ω are not plotted here to focus on H_i/s.

Table 5 - Values of the parameters assumed to describe the maximum bending moment surfaces in Figure 9

Parameter	Maximum bending moment - Surface 1	Maximum bending moment - Surface 2	Maximum bending moment - Surface 3
b/w	0.1 - 0.6	0.1 - 0.6	0.1 - 0.6
C_D	2.28 - 4.68	2.28 - 4.68	2.28 - 4.68
λ	0.86 - 1.85	0.86 - 1.85	0.86 - 1.85
α	0.85	0.85	0.85
k	0.029	0.029	0.029
H_i/s	2.50	9.58	16.67

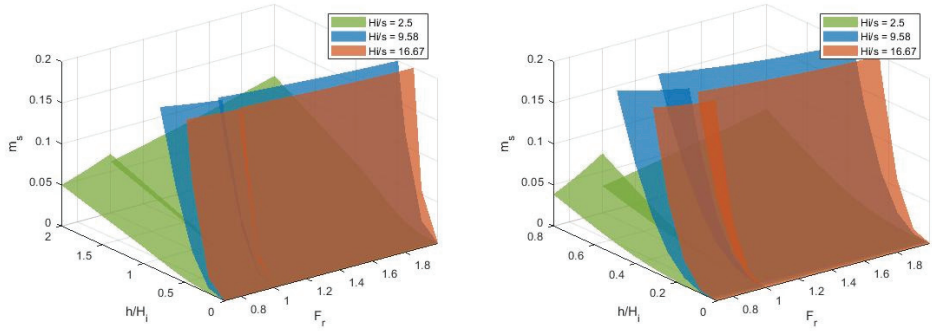

(a) (b)

Figure 9 - Effects of the geometrical vertical slenderness H_i/s parameter for b/w equal to 0.1 (a) and 0.6 (b)

The geometrical vertical slenderness of the masonry wall affects the vertical bending mechanisms activation, as expected. The vertical bending mechanism is a flexural mechanism and the activation is triggered when the external bending moment equals the flexural capacity of the cross-section, not depending on H_i/s. Therefore, slender elements (high value of H_i/s parameter) compared to squat elements are more vulnerable to flexural mechanisms. The friction block affects mainly the discontinuity of the surfaces while changing the flow regime.

In Figure 10, the effects of the numerical coefficient k are investigated and the values assumed for the main parameters are shown in Table 6.

Table 6 - Values of the parameters assumed to describe the maximum bending moment surfaces in Figure 10

Parameter	Maximum bending moment - Surface 1	Maximum bending moment - Surface 2	Maximum bending moment - Surface 3
b/w	0.6	0.6	0.6
C_D	4.68	4.68	4.68
λ	1.85	1.85	1.85
α	0.85	0.85	0.85
k	0.003	0.029	0.055
H_i/s	9.58	9.58	9.58

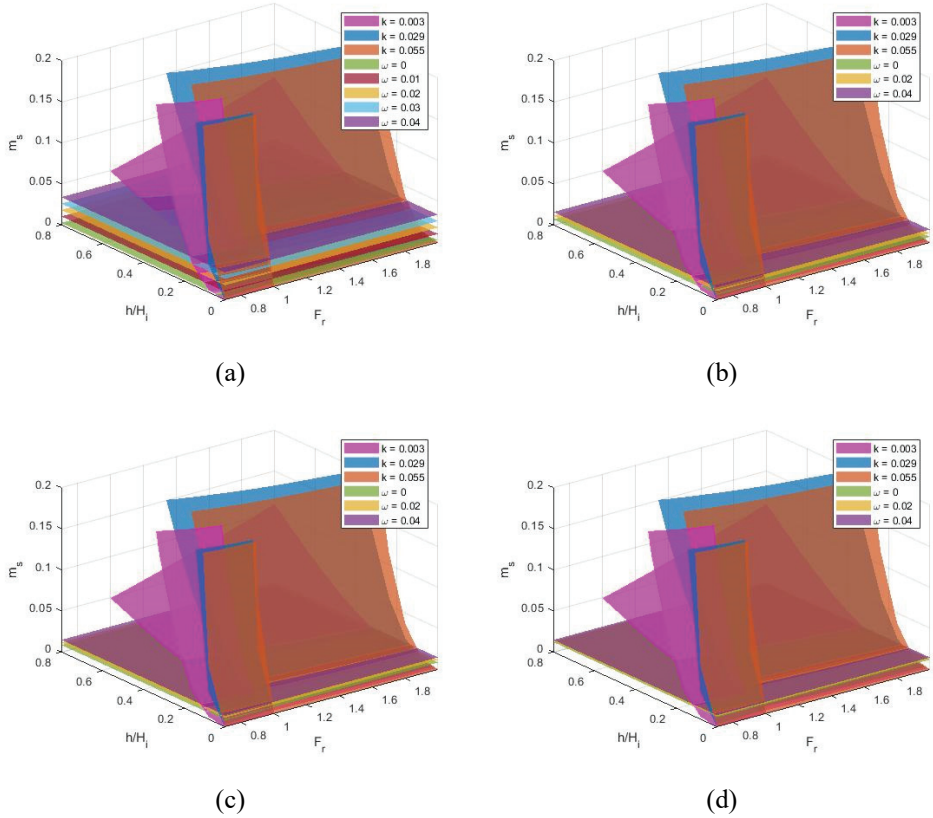

Figure 10 - Effects of the numerical coefficient k for n equal to 0.05 (a), 0.15 (b), 0.20 (c) and 0.35 (d)

The numerical coefficient k depends on the specific weight of water, γ_w, the interstorey height, H_i, and the compressive strength of masonry, f_m. The specific weight of water is approximately constant (effects of debris and sediment in the case of tsunami can be expected); the numerical coefficient k allows to investigate indirectly the effects of the interstorey height H_i. The vulnerability is high for high values of the k coefficient because the slenderness of the wall is increasing.

8. CONCLUSIONS

The main aim of this paper is to analyse the behaviour of masonry walls under tsunami loads in terms of out-of-plane (OOP) local mechanisms activation and the benefits of strengthening systems.

Strengthening systems with composite material represent an important innovation in the civil engineering techniques to retrofit existing buildings because it is not invasive on the structure, in terms of mass, stiffness and dynamic response, and it is recommended to preserve safety of cultural heritage in the case of FRCM or CRM where resin matrix is substituted by mortar.

The vertical bending mechanisms activation is investigated as main OOP local mechanism of the masonry wall under tsunami loads.

The tsunami load is modelled by the Foster et al. [12] model where the external loads are modelled by a hydrostatic plus a hydrodynamic load pattern.

Linear analyses are performed considering a simply supported beam as static model assuming a safety criterion to analyse the bending moment trend. In addition, an external axial load is modelled to simulate the wall self-weight and the effect of upper storeys due to the effects of the external axial load on the cross-section capacity.

Equations in dimensionless form are provided to describe the maximum external bending moment trend and the cross-section capacity in terms of bending moment in order to provide generalizable results applicable to any masonry wall cross-section and tsunami, but excluding masonry suffering for premature disaggregation.

Several parametric analyses are performed and the results are shown in terms of 3D charts in order to analyse the effects of the main parameters on the external bending moment trend and on the strengthening system. The inundation depth, the Froude number and the bending moment are shown on the axes. The inundation depth and the Froude number are the main parameters related to the hydrostatic and the hydrodynamic load.

The investigated main parameters are the external axial load n, the blocking fraction b/w, the wall openings coefficient, the vertical geometrical slenderness of the wall and the composite mechanical percentage.

Low composite mechanical values provide huge percentage effects in terms of bending moment capacity due to tensile behaviour added to unreinforced masonry cross-section, while benefits of high composite mechanical ratio could be negligible. This is due to the fact that increasing the external axial load, the effects of the strengthening systems are minimal due to the increasing of the neutral axis depth and consequentially, the lower strain of the composite.

The blocking fraction parameter has a high impact on the vulnerability of the masonry wall because it affects the flow regime and therefore, the external bending moment trend; the vulnerability of the masonry wall increases with the b/w coefficient. The wall openings have a high influence on the behaviour of masonry because the openings affect the load bearing area of the wall and the activation of the OOP local mechanism.

The geometrical vertical slenderness of the masonry wall affects the vertical bending mechanisms activation. In fact, the vertical bending mechanism is a flexural mechanism and the activation is triggered when the external bending moment equals the flexural capacity of the cross-section. Therefore, slender elements are more vulnerable to flexural mechanisms than squat elements.

Furthermore, the showed charts and the dimensionless equations are the bases of design tools for strengthening systems applied on masonry walls under tsunami loads to prevent the OOP vertical bending mechanism activation. The main parameters are the mechanical and geometrical parameters of masonry wall and composite system; safety factor has to be properly considered in the evaluation of the materials mechanical properties and external loads. In particular, it is important to balance properly such mechanical and geometrical parameters in order to design optimal strengthening systems, characterized by the best mechanical performance without economic waste.

Future work will take into account advanced constitutive behaviour of composites depending on specific assumed fiber and matrix. In addition, other local mechanisms will be taken into account as in-plane and out-of-plane local mechanisms in terms of bending and shear capacity.

Symbols

b = width of the structure;

b_m = width of the cross-section;

b/w = blocking fraction;

C_D = drag coefficient;

F_d = resultant of the hydrodynamic load distribution;

F_r = Froude number;

F_s = resultant of the hydrostatic load distribution;

f_f = tensile strength of strengthening system;

f_{fu} = ultimate tensile strength of strengthening system;

f_m = compressive strength of masonry;

g = gravitational acceleration constant;

E_f = elastic modulus of strengthening system;

E_m = elastic modulus of masonry;

k = numerical coefficient;

k_1 = numerical coefficient;

k_2 = numerical coefficient;

k_3 = numerical coefficient;

L = wall length;

$m_{s,1}$ = dimensionless bending moment equation for $h < H_i$;

$m_{s,2}$ = dimensionless bending moment equation for $h \geq H_i$;

$m_{R,0}$ = dimensionless ultimate bending moment of URM;

$m_{R,\omega}$ = dimensionless ultimate bending moment of strengthened cross-section;

n = dimensionless external axial load;

n_0 = dimensionless axial load of URM;

n_ω = dimensionless axial load of strengthened cross-section;

H_i = interstorey height;

h = expected inundation depth;

q_s = hydrostatic load;

q_d = hydrodynamic load;

s = thickness of masonry wall;

s/H_i = geometrical vertical slenderness of masonry wall;

t_f = equivalent thickness of fiber;

u = flow velocity;

w = channel width;

x = neutral axis depth;

α = opening ratio coefficient;

β = coefficient depending on the Froud number;

ε = generic strain;

ε_f = generic strain of strengthening system;

ε_m = generic strain of masonry;

ε_{m0} = peak strain of masonry;

ε_{mu} = ultimate strain of masonry;

ε_{fu} = ultimate strengthening system strain;

λ = empirical coefficient;

λ_m.= effective depth of compression zone centre of stress-block model;

γ_w = specific weight of water;

ψ_m = effective height of stress-block model;

ρ_s = flow density;

σ = generic strength;

ξ = dimensionless neutral axis depth;

ω = composite mechanical ratio.

References

[1] Strunz, G., Post, J., Zosseder, K., Wegscheider, T., et al. Tsunami risk assessment in Indonesia. Natural Hazards and Earth System Sciences, 11, 67-82, 2011. https://doi.org/10.5194/nhess-11-67-2011

[2] Behrens, J., Løvholt, F., Jalayer, F., et al. Probabilistic tsunami hazard and risk analysis: a review of research gaps. Frontiers in Earth Science, 9-114, 2021. http://doi.org/10.3389/feart.2021.628772

[3] Rafliana, I., Jalayer, F., Cerase, A., et al. Tsunami risk communication and management: Contemporary gaps and challenges. International Journal of Disaster Risk Reduction, 102771, 2022. http://doi.org/10.1016/j.ijdrr.2021.102771

[4] Athukorala, P.C., Resosudarmo, B.P. The Indian Ocean tsunami: Economic impact, disaster management, and lessons. Asian economic papers, 4(1), 1-39, 2005. https://doi.org/10.1162/asep.2005.4.1.1

[5] Palermo, D., Nistor, I., Saatcioglu, M., Ghobarah, A. Impact and damage to structures during the 27 February 2010 Chile tsunami. Canadian Journal of Civil Engineering, 40(8), 750-758, 2013. https://doi.org/10.1139/cjce-2012-0553

[6] Suppasri, A., Shuto, N., Imamura, F., et al. Lessons learned from the 2011 Great East Japan tsunami: Performance of tsunami countermeasures, coastal buildings, and tsunami evacuation in Japan. Pure and Applied Geophysics, 170(6-8), 993-1018, 2013. https://doi.org/10.1007/s00024-012-0511-7.

[7] Lorito, S., Behrens, J., Løvholt, F., et al. From Tsunami Science to Hazard and Risk Assessment: Methods and Models, Front. Earth Sci. 9:764922, 2021. https://doi.org/10.3389/feart.2021.764922.

[8] ASCE/SEI 7-22 Minimum Design Loads and Associated Criteria for Buildings and Other Structures, Reston, Virginia; 2021. https://doi.org/10.1061/9780784415788

[9] Fukuyama, H., Kato, H., Ishihara, T., et al. Structural design requirement on the tsunami evacuation buildings. US-Japan Cooperative Program in Natural Resources (UJNR), Tokyo; 2011.

[10] Asakura, R., Iwase, K., Ikeya, T., et al. An Experimental Study on Wave Force Acting on On-Shore Structures due to Overflowing Tsunamis. In Proceedings of Coastal Engineering Japan Society of Civil Engineers, Japan, 911-915, 2000.

[11] Okada, T., Sugano, T., Ishikawa, T., et al. Structural Design Method of Buildings for Tsunami Resistance. The Building Center of Japan, Japan, 2005

[12] Foster, A., Rossetto, T., Allsop, W. An experimentally validated approach for evaluating tsunami inundation forces on rectangular buildings. Coastal Engineering, 128, 44-57, 2017. https://doi.org/10.1016/j.coastaleng.2017.07.006

[13] Peiris, N., Pomonis, A. Decembre 26, 2004 Indian Ocean Tsunami: vulnerability functions for loss estimation in Sri Lanka. In Proceedings of the Geotechnical Engineering for Disaster Mitigation and Rehabilitation, Singapore, 2005.

[14] Mallawaarachchi, R.S., Jayasinghe, C. The effects of cyclones, tsunami and earthquakes on built environments and strategies for reduced damage. Journal of the National Science Foundation of Sri Lanka, 36, 03-14, 2008.

[15] Vlachakis, G., Cervera, M., Barbat, G. B., Saloustros, S. Out-of-plane seismic response and failure mechanism of masonry structures using finite elements with enhanced strain accuracy. Engineering Failure Analysis, 97, 534-555, 2019. https://doi.org/10.1016/j.engfailanal.2019.01.017

[16] Belliazzi, S., Lignola, G.P., Prota, A. Simplified approach to assess the vulnerability of masonry buildings under tsunami loads. Proceedings of the Institution of Civil Engineers-Structures and Buildings, 1-13, 2020. https://doi.org/10.1680/jstbu.20.00147

[17] Belliazzi, S., Lignola, G.P., Prota, A. Textile Reinforced Mortars systems: a sustainable way to retrofit structural masonry walls under tsunami loads. International Journal of Masonry Research and Innovation, 3(3), 200-222, 2018. https://doi.org/10.1504/IJMRI.2018.093484

[18] Ai, F., Comfort, L. K., Dong, Y., Znati, T. A dynamic decision support system based on geographical information and mobile social networks: A model for tsunami risk mitigation in Padang, Indonesia. Safety science, 90, 62-74, 2016. https://doi.org/10.1016/j.ssci.2015.09.022

[19] Fabbrocino, F., Belliazzi, S., Ramaglia, G., Lignola, G.P., Prota, A. Masonry walls retrofitted with natural fibers under tsunami loads. Materials and Structures, 54(3), 1-15, 2021. http://doi.org/10.1617/s11527-021-01707-9

[20] Belliazzi, S., Lignola, G.P., & Prota, A. Retrofit of Masonry Walls with Composites to Reduce Vulnerability to Tsunami Loads. In Proceedings of International Conference on Fibre-Reinforced Polymer (FRP) Composites in Civil Engineering, Istanbul, Turkey, 2021.

[21] Borri, A.; Corradi, M.; De Maria, A. The Failure of Masonry Walls by Disaggregation and the Masonry Quality Index. Heritage, 3, 1162-1198, 2020. https://doi.org/10.3390/heritage3040065

[22] Belliazzi, S., Lignola, G.P., Di Ludovico, M., Prota, A. Preliminary tsunami analytical fragility functions proposal for Italian coastal residential masonry buildings. Structures, 31, 68-79, 2021. https://doi.org/10.1016/j.istruc.2021.01.059

[23] Lloyd, T. O. An experimental investigation of tsunami forces on coastal structures (Doctoral dissertation, UCL (University College London)), 2016.

[24] Qi, Z.X., Eames, I., Johnson, E.R. Force acting on a square cylinder fixed in a free-surface channel flow. Journal of Fluid Mechanics, 756, 716-727, 2014. https://doi.org/10.1017/jfm.2014.455

[25] Eurocode 6 - Design of Masonry Structures; EN 1996. Design of Masonry Structures, part 1.1: General Rules for Reinforced and Unreinforced Masonry Structures, Brussels, Belgium. 2006.

[26] de Felice, G., Aiello, M.A., Caggegi, C., et al. Recommendation of RILEM Technical Committee 250-CSM: Test method for Textile Reinforced Mortar to substrate bond characterization. Materials and Structures, 51 (4), 95, 2018. https://doi.org/10.1617/s11527-018-1216-x

[27] CNR DT 200R1/2013 Guide for the Design and Construction of Externally Bonded FRP Systems for Strengthening Existing Structures, Rome, Italy. 2014.

[28] CNR DT 215/2018 Guide for the Design and Construction of Externally Bonded Fibre Reinforced Inorganic Matrix Systems for Strengthening Existing Structures, Rome, Italy. 2020.

[29] Zinno, A., Lignola, G.P., Prota, A., et al. Influence of free edge stress concentration on effectiveness of FRP confinement. Composites Part B: Engineering, 41(7), 523-532, 2010. https://doi.org/10.1016/j.compositesb.2010.07.003

[30] Belliazzi, S., Ramaglia, G., Lignola, G.P., Prota, A. Out-of-plane retrofit of masonry with fiber-reinforced polymer and fiber-reinforced cementitious matrix systems: normalized interaction diagrams and effects on mechanisms activation. Journal of Composites for Construction, 04020081, 25 (1), 2021. http://doi.org/10.1061/(ASCE)CC.1943-5614.0001093

[31] Priestley, M. J. N., Seible, F. Design of seismic retrofit measures for concrete and masonry structures. Construction and Building Materials, 9(6), 365-377, 1995. https://doi.org/10.1016/0950-0618(95)00049-6

[32] D'Ayala, D., Speranza, E. Definition of collapse mechanisms and seismic vulnerability of historic masonry buildings. Earthquake Spectra, 19(3), 479-509, 2003. https://doi.org/10.1193%2F1.1599896

[33] Milano, G., Lourenço, P., Tralli, A. Homogenization Approach for the Limit Analysis of Out-of-Plane Loaded Masonry Walls. Journal of Structural Engineering. 132 (10), 1650-1663, 2006. https://doi.org/10.1061/(ASCE)0733-9445(2006)132:10(1650)

[34] De Lorenzis, L. Strengthening of masonry structures with fibre-reinforced polymer (FRP) composites. Strengthening and Rehabilitation of Civil Infrastructures Using Fibre-Reinforced Polymer (FRP) Composites. Woodhead Publishing, eds Hollaway LC and Teng JG: 235-266, 2008. https://doi.org/10.1533/9781845694890.235

[35] Guadagnuolo, M., Faella, G. The friction in the out-of-plane failure mechanisms of masonry walls. In: Proceedings of the 14th International Brick and Block Masonry Conference. Sydney: Cracow University of Technology, Silesian University of Technology and Wroclaw University of Technology, 2008

[36] D'Altri, A. M., De Miranda, S., Castellazzi, G., Sarhosis, V. A 3D detailed micro-model for the in-plane and out-of-plane numerical analysis of masonry panels. Computers and Structures, 18-30, 206, 2016. https://doi.org/10.1016/j.compstruc.2018.06.007

[37] Harish, S., Sriram, V., Schüttrumpf, H., Sannasiraj, S. A. Tsunami-like flow induced forces on the structure: Dependence of the hydrodynamic force coefficients on Froude number and flow channel width in quasi-steady flow phase. Coastal Engineering, 168, 103938, 2021. https://doi.org/10.1016/j.coastaleng.2021.103938

[38] D'Antino, T., Calabrese, A. S., Poggi, C. Experimental procedures for the mechanical characterization of composite reinforced mortar (CRM) systems for retrofitting of masonry structures. Materials and Structures, 53(4), 1-18, 2020. https://doi.org/10.1617/s11527-020-01529-1

[39] de Santis, S., de Felice, G., Di Noia, G. L., Meriggi, P., Volpe, M. Shake table tests on a masonry structure retrofitted with composite reinforced mortar. Key Engineering Materials, 817, 342-349, 2019. https://doi.org/10.4028/www.scientific.net/KEM.817.342

Turkish Journal of Civil Engineering (formerly Teknik Dergi)
Manuscript Drafting Rules

1. The whole manuscript (text, charts, equations, drawings etc.) should be arranged in Word and submitted in ready to print format. The article should be typed on A4 (210 x 297 mm) size paper using 10 pt (main title 15 pt) Times New Roman font, single spacing. Margins should be 40 mm on the left and right sides and 52.5 mm at the top and bottom of the page.
2. Including drawings and tables, articles should not exceed 25 pages, technical notes 10 pages.
3. Your contributed manuscript must be sent over the DergiPark system. (http://dergipark.gov.tr/tekderg)
4. The text must be written in a clear and understandable language, conform to the grammar rules. Third singular person and passive tense must be used, and no inverted sentences should be contained.
5. Title must be short (10 words maximum) and clear, and reflect the content of the paper.
6. Sections should be arranged as: (i) abstract and keywords, (ii) title, abstract and keywords in the other language, (iii) main text, (iv) symbols, (v) acknowledgements (if required) and (vi) references.
7. Both abstracts should briefly describe the object, scope, method and conclusions of the work and should not exceed 100 words. If necessary, abstracts may be re-written without consulting the author. At least three keywords must be given. Titles, abstracts and keywords must be fitted in the first page leaving ten line space at the bottom of the first page and the main text must start in the second page.
8. Section and sub-section titles must be numbered complying with the standard TS1212.
9. Symbols must conform to the international rules; each symbol must be defined where it appears first, additionally, a list of symbols must be given in alphabetic order (first Latin, then Greek alphabets) at the end of the text (before References).
10. Equations must be numbered and these numbers must be shown in brackets at the end of the line.
11. Tables, drawings and photographs must be placed inside the text, each one should have a number and title and titles should be written above the tables and below the drawings and photographs.
12. Only SI units must be used in the manuscripts.
13. Quotes must be given in inverted commas and the source must be indicated with a reference number.
14. Acknowledgement must be short and mention the people/ institutions contributed or assisted the study.
15. References must be numbered (in brackets) in the text referring to the reference list arranged in the order of appearance in the text. References must include the following information:

    If the reference is an article: Author's surname, his/her initials, other authors, full title of the article, name of the journal, volume, issue, starting and ending pages, year of publication.

    Example : Naghdi, P. M., Kalnins, A., On Vibrations of Elastic Spherical Shells. J. Appl. Mech., 29, 65-72, 1962.

    If the reference is a book: Author's surname, his/her initials, other authors, title of the book, volume number, editor if available, place of publication, year of publication.

    Example : Kraus. H., Thin Elastic Shells, New York. Wiley, 1967.

    If the reference is a conference paper: Author's surname, his/her initials, other authors, title of the paper, title of the conference, location and year.

    If the source is a thesis: Author's surname, his/her initials, thesis title, level, university, year.

    If the source is a report: Author's surname, his/her initials, other authors, title of the report, type, number, institution it is submitted to, publication place, year.
16. Discussions to an article published in Turkish Journal of Civil Engineering (formerly Teknik Dergi) should not exceed two pages, must briefly express the addressed points, must criticize the content, not the author and must be written in a polite language. Authors' closing remarks must also follow the above rules.
17. A separate note should accompany the manuscript. The note should include, (i) authors' names, business and home addresses and phone numbers, (ii) brief resumes of the authors and (iii) a statement "I declare in honesty that this article is the product of a genuinely original study and that a similar version of the article has not been previously published anywhere else" signed by all authors.
18. Copyright has to be transferred to UCTEA Turkish Chamber of Civil Engineers. The standard copyright form signed by the authorised author should therefore be submitted together with the manuscript.

UCTEA Turkish Chamber of Civil Engineers
TMMOB İnşaat Mühendisleri Odası
Necatibey St. No: 57, Kızılay, Ankara / Türkiye
Tel: +90.312.294 30 00 - Faks: 294 30 88
www.imo.org.tr